ANL-6561
Reactor Technology
(TID-4500, 17th Ed.)
AEC Research and
Development Report

ARGONNE NATIONAL LABORATORY
9700 South Cass Avenue
Argonne, Illinois

BOILING WATER REACTOR TECHNOLOGY
STATUS OF THE ART REPORT

VOLUME I. HEAT TRANSFER AND HYDRAULICS

by

P. A. Lottes
Associate Editors: R. P. Anderson,
B. M. Hoglund, J. F. Marchaterre,
M. Petrick, G. F. Popper,
and R. J. Weatherhead

Reactor Engineering Division

The final draft of this volume was completed
in August 1959. Some revision was made during editing
in 1961 but essentially the volume remains the same.

February 1962

Operated by The University of Chicago
under
Contract W-31-109-eng-38

DISCLAIMER

FOREWORD

The Boiling Water Reactor Technology Status of the Art Report consists of four volumes that treat respectively the following major areas of boiling water reactor design:

Vol. I - Heat Transfer and Hydraulics (ANL-6561)
Vol. II - Physics — Never published
Vol. III - Water Chemistry and Corrosion (Became Vol. II)(ANL-6562)
Vol. IV - Engineering Design - probably never to be published

The objective is to provide the reader with information pertinent to the design and operation of boiling water reactor power plants. Nuclear instrumentation and reactor control are not covered in this Status of the Art Report as this subject is adequately covered in J. M. Harrer's book, "Nuclear Reactor Control Engineering" which had its genesis in parallel efforts to this volume. Radioisotope hazards analysis and safeguards are also not included since these and other related disciplines are the subject of timely, single-volume documents available in the open literature.

In compiling and evaluating the material in each volume, the authors also have been confronted with the problem of timeliness of data. It is anticipated that subsequent editions of each volume shall be published periodically, consistent with the degree of technological advance in the status of the art of boiling water reactors. Accordingly the attention of the reader is directed to the terminal date for compilation of data which appear in the front matter of each volume.

The writers wish to acknowledge the cooperation of the leading commercial developers of boiling water nuclear power plants - Allis-Chalmers Manufacturing Company, General Electric Company, and General Nuclear Engineering Company, - for providing technical details on their respective power plants. Grateful recognition is also given to Mr. B. Dieter and members of the Technical Information Division of Argonne National Laboratory in assisting the Reactor Engineering Division staff in the final preparation of these four volumes.

C. Victor Pearson
Editor
February 13, 1962

TABLE OF CONTENTS

VOLUME I: HEAT TRANSFER AND HYDRAULICS

TABLE OF CONTENTS

TABLE OF CONTENTS

LIST OF FIGURES

LIST OF FIGURES

LIST OF FIGURES

LIST OF FIGURES

LIST OF FIGURES

VOLUME I

HEAT TRANSFER AND HYDRAULICS

by

P. A. Lottes, R. P. Anderson, B. M. Hoglund, J. F. Marchaterre, M. Petrick, G. F. Popper, and R. J. Weatherhead

1. INTRODUCTION

The water-moderated and -cooled reactors, both pressurized and boiling, have demonstrated performance characteristics which make them attractive as possible producers of heat which can be converted to low cost electrical power. An extensive research and development program has been carried on under AEC sponsorship for the purpose of exploiting this potential. An important part of the effort is an intensive research program to obtain basic data on natural and forced circulation boiling water reactor systems. The results of this work are also applicable in many instances to pressurized water systems. However, the major amount of data developed, analyzed, and discussed herein is concerned with the boiling water reactor concept.

This section is divided into the following areas of discussion:

1. Heat Transfer
2. Two-Phase Density Studies
3. Two-Phase Pressure Drop
4. Critical Heat Flux and Burnout
5. Boiling Stability
6. Calculation Procedures for Boiling Systems
7. Thermal-Hydraulic Design Procedures for Boiling Water Reactors

The information discussed represents primarily the work carried on at Argonne National Laboratory. The presentation represents the opinions of the authors as to the applicability of available data which can be used for engineering applications.

No effort has been made to include all the available information on any specific subject or area. However, where possible, references have been made to the great amount of data available in published literature. This additional information is obviously required by anyone interested in making an intensive investigation on any of the subjects.

2. HEAT TRANSFER

2.1. Basic Ideas and Concepts in Boiling Heat Transfer

The process of boiling is defined as the heat transfer of energy to a liquid from a solid surface in contact with the liquid causing a change in phase from liquid to vapor. The means by which energy is transferred from a solid heat transfer surface to vapor is not easily understood. A few facts about the process have been determined by experiment.

It is true that for an equilibrium condition, a change in phase from liquid to vapor occurs at constant temperature. In forming a bubble of vapor, the liquid-vapor interface is supposed to remain at a constant temperature. In reality, the formation of a bubble takes place in a violent manner and may be considered as a minor underwater explosion.

A force balance on a bubble shows that the vapor pressure inside the bubble is greater than the liquid pressure outside the bubble, and the difference in pressure, ΔP, is related to the liquid surface tension, σ, and the bubble radius, r, according to the equation

$$\Delta P = 2\sigma/r \quad . \tag{2.1}$$

As r approaches zero, the required pressure difference approaches infinity. Since fluids have as one of their thermodynamic properties an increase in boiling point with pressure, it now becomes necessary to have a "superheated" liquid before boiling can occur. Assume, for example, that a bubble is present with radius "r." For an equilibrium condition without heat transfer, the bubble vapor temperature will be equal to the surrounding liquid temperature. Due to surface tension, the bubble pressure will be higher than the surrounding liquid pressure. For the bubble to exist at all, the vapor temperature must be equal to or higher than the saturation temperature corresponding to the bubble pressure. The liquid will therefore be at this same temperature and will be at a temperature higher than the saturation temperature corresponding to the liquid pressure. This state of the liquid is referred to as liquid superheat.

The presence of liquid superheat has been demonstrated in the laboratory. B. R. Mead[1] and others at UCLA measured liquid superheats as high as 145°F at one atmosphere. Bubble pressures at the onset of boiling could well have reached 145 psia.

The sudden explosive growth of bubbles in superheated liquid causes a very high turbulence level in the liquid. It is this turbulence or violent mixing and agitation of the liquid that accounts for the high heat transfer rates. The effect of boiling from a heated solid surface is that

the layers of liquid near the solid surface are disrupted by the mixing action of the bubbles.[2] This in effect causes the bulk of the liquid to move in next to solid surface. The over-all result is a very efficient scouring action of the liquid upon the surface, causing a high heat transfer coefficient.

There are several types of boiling heat transfer to be considered. These types may be classified as follows:

1. Local boiling, or surface boiling as it is sometimes called, occurs when the hot solid surface is above the liquid saturation temperature, while the liquid is below saturation temperature.

2. Net boiling, or nucleate boiling, occurs when the liquid is at or above saturation temperature.

3. Film boiling occurs when the hot surface is completely covered with a blanket of vapor, and the heat is transferred by conduction through and radiation across the vapor blanket.

4. Transition boiling is a combination of 2 and 3 above.

Local boiling has the unique condition that there is no net formation of vapor. The bubbles may or may not leave the hot surface. If they do leave, they are very quickly condensed. Bubble lifetimes range from a few microseconds to several seconds, depending on the amount of subcooling in the liquid phase. The higher the subcooling, the shorter the lifetime.[3]

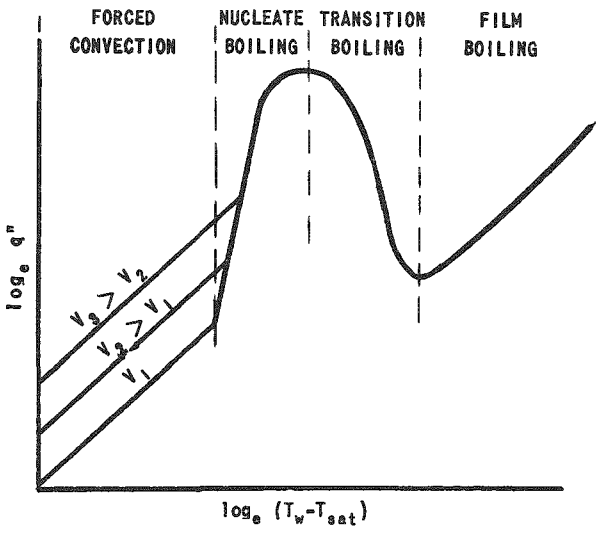

Fig. 2.1

Boiling Regions

Figure 2.1 shows the various types of boiling that can occur. It is also worthy to note that the effect of velocity on boiling heat transfer is negligible, even though forced convection heat transfer coefficients vary as the 0.8 power of the liquid velocity, V. The reason for the independence of boiling heat transfer coefficients from flow rate is due to the "turbulence promoter" action of the bubbles. The turbulence level is relatively unaffected by flow rate and therefore the heat transfer coefficient is relatively unaffected.

It is also of interest to notice that (a) the temperature differences between surface and liquid are rather small for nucleate boiling and (b) rather large for film boiling. The part of the curve of Fig. 2.1 that has zero slope is the maximum point for nucleate boiling. It is this value which is of greatest concern to designers in the boiling field. In a boiling reactor, for example, this value is the maximum value that would occur just before the element jumps into film boiling. The onset of film boiling at a heat flux equal to the maximum in the nucleate boiling range almost always means that the temperature of the solid surface will rise to the melting point of the material. This condition is referred to as "burnout."

2.2 Boiling Heat Transfer Equations

In general, the evaluation of the heat transfer characteristics during steady-state boiling in a reactor is not of great importance. The reasons will be shown by an example in a later section of this chapter. It is of interest to list at this point the various equations that may be used to calculate boiling heat transfer, together with references for those who wish to pursue the subject in detail.

(1) McAdams,[4] for pool boiling (saturated water):

$$q/A = a_1 (T_w - T_{sat})^n \tag{2.2}$$

where q/A or q'' is the heat flux in Btu/hr ft^2; where the value of a_1 depends upon the liquid, surface condition, and pressure, while the value of n ranges from 3 to 4.

(2) Rohsenow,[5] for pool boiling (saturated water):

$$\frac{C_p T_x}{h_{fg}} = C_{sf}\left(\frac{q/A}{\mu_f h_{fg}}\sqrt{\frac{g_c \sigma}{g(\rho_l - \rho_v)}}\right)^{0.33}\left(\frac{C_p \mu_f}{k_f}\right)^{1.7} \tag{2.3}$$

where the values of C_{sf} are as follows:

Fluid-heating surface	C_{sf}
Water-platinum	0.013
Benzene-chromium	0.010
Ethyl alcohol-chromium	0.0027
n-pentane-chromium	0.015
Water-brass	0.006

(3) Forster-Zuber,[6] pool boiling (saturated water):

$$h = \frac{0.0012\ \Delta T^{0.24}(P_v - P_l)^{0.75} C_p^{0.45} \rho_f^{0.49} k_f^{0.79}}{\sigma^{0.5} h_{fg}^{0.24} \mu^{0.29} \rho_v^{0.24}} \quad . \tag{2.4}$$

This form of the equation is presented and discussed by Perkins and Westwater.[7] Comparisons are also given to the Rohsenow equation and to experimental data with a boiling methanol system.

(4) Jens-Lottes,[8] subcooled boiling (subcooled water):

$$\Delta T = 1.9\,(q/A)^{0.25}/e^{P/900} \tag{2.5}$$

for pressures of 100 to 2500 psia, water temperatures from 229 to 636°F, mass flow rates from 0.008 $(10)^6$ to 7.7 $(10)^6$ lb/hr ft^2, and heat fluxes to 4 $(10)^6$ Btu/hr ft^2.

(5) Mumm,[9] forced circulation of boiling saturated water inside tubes:

$$\frac{h D_e}{k} = 4.3 + 5.0\,(10)^{-4}\left(\frac{v_{fg}}{v_f}\right)^{1.64}\left(\frac{q/A}{G h_{fg}}\right)^{0.464}\left(\frac{G D_e}{\mu_f}\right) \tag{2.6}$$

for pressures of 45 to 200 psia, heat fluxes from 50,000 to 250,000 Btu/hr ft^2, and mass flow rates from 70 to 280 lb/hr ft^2.

(6) Bromley,[10] film boiling:

$$h = 0.62\left[\frac{k_v^3 \rho_v (\rho_l - \rho_v) h_{fg}}{\mu_v D_0 \Delta T}\right]^{0.25} . \tag{2.7}$$

In addition to the above heat transfer equations there are a number of burnout equations in the literature for various types of heated channels. McAdams[4] summarizes and discusses the equations. It is sufficient at this time to mention that the range of heat flux for burnout under most design conditions is from 500,000 to 1,500,000 Btu/hr ft^2.

The calculation of temperature drop during boiling in a nuclear reactor is of secondary importance. The accurate evaluation of heat transfer coefficients in evaporator-condenser units may also be unnecessary. An example will illustrate the two cases.

Case I - Boiling Reactor Heat Transfer

Let us suppose that it is desired to evaluate the fuel plate surface temperature at design conditions such that system pressure is 600 psia and average heat flux is 100,000 Btu/hr ft^2.

Using Eq. (2.5) the film drop is calculated to be 17°F. Since the film drop is proportional to the 0.25 power of the heat flux, we may note that even if the heat flux were as high as 1,000,000 Btu/hr ft^2, the film drop under these conditions would only be $\Delta T = 17\,(10)^{0.25} = 30$°F.

Accordingly, the surface temperature at 100,000 Btu/hr ft^2 would be $T_w = T_{sat} + 17 = 503°F$, while the surface temperature at 1,000,000 Btu/hr ft^2 would be $T_w = T_{sat} + 30 = 516°F$. It is evident, therefore, that in a system where heat flux is the independent variable the calculation of surface temperature does not require great accuracy. Equation (2.5) is recommended for general use, since it can be evaluated quite easily. Figure 2.2 shows a comparison of Eqs. (2.3), (2.4), and (2.5) at 600 psia.

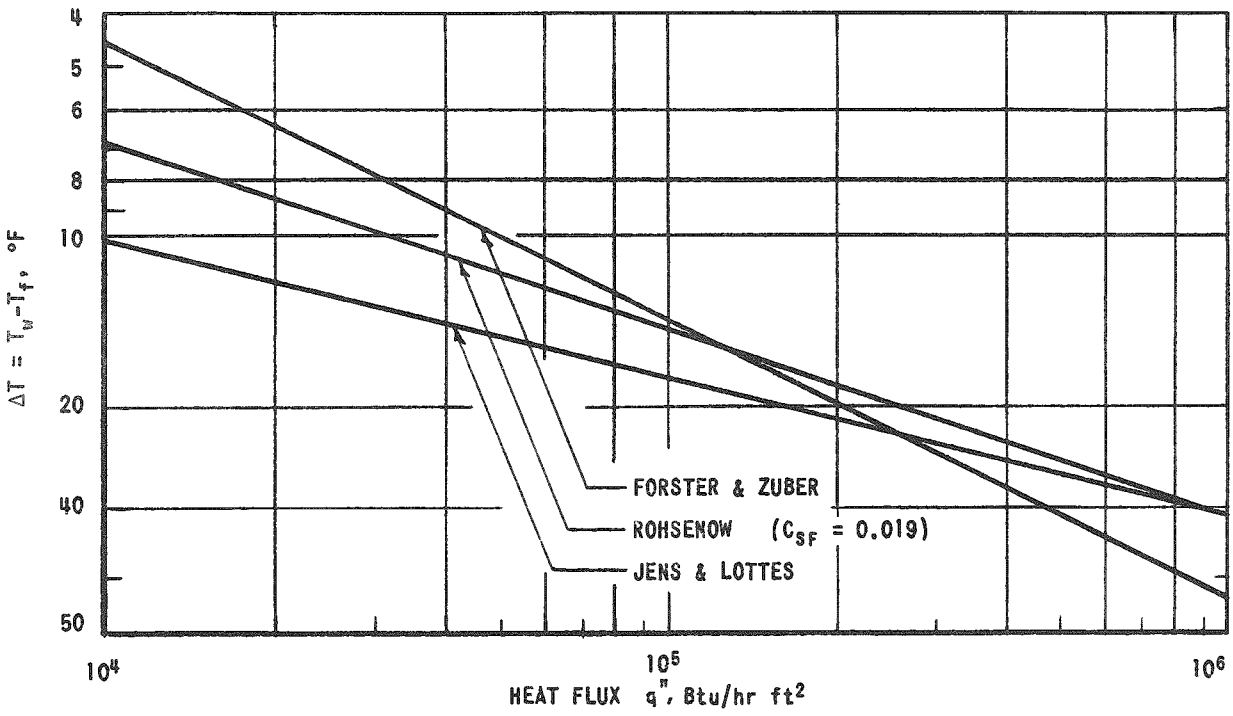

Fig. 2.2

Comparison of Boiling Heat Transfer Equations at 600 psia

Referring to the same temperature drops listed on preceding page, it is important to notice that in a system where temperature is the controlled variable, an increase in surface temperature from 503°F to 516°F will cause an increase in heat flux by a factor of 10. This increase may not occur if there are other resistances to heat flow in the system. The following example will show these effects.

Case II - Evaporator-Condenser Heat Transfer

In this case, we are faced with determining the size of an exchanger to transfer a given or predetermined amount of power. Unlike the reactor where power was an independent variable, we now have the over-all temperature difference as the independent variable. For this case, we may write a heat balance on the element of heat exchanger surface such as is shown in Fig. 2.3.

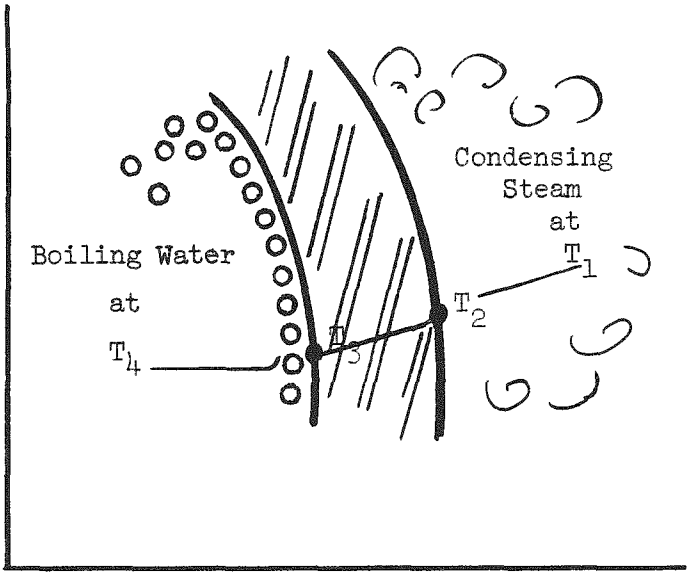

Fig. 2.3

Temperature Gradient through Heat Exchanger Tube

Ignoring scale resistances to heat flow for this example, and assuming that the inner and outer tube areas are very nearly equal, we may write

$$q/A = h_c(T_1 - T_2) = (k/\Delta x)(T_2 - T_3) = h_b(T_3 - T_4) \qquad (2.8)$$

where T_1 is the steam condensing temperature, T_2 the outer tube wall temperature, T_3 the inner tube wall temperature, T_4 the boiling fluid temperature, and x the tube wall thickness. Rearranging the above equation and solving for the required area (for this example, it is sufficient to neglect the tube curvature),

$$A = \left[\frac{1}{h_c} + \frac{\Delta x}{k} + \frac{1}{h_b}\right]\frac{q}{(T_1 - T_4)} \quad . \qquad (2.9)$$

Suppose it is given that $(T_1 - T_4)$ is 50°F and that the over-all power or heat transfer, q, is 50,000,000 Btu/hr. We must now evaluate A to determine the size or capacity of a heat exchanger that will perform the required job. We are faced with the problem of selecting an exchanger that is adequate, but not oversized by too great an amount. It may be noticed from Eq. (2.9) that a given per cent error in the bracket term will cause the same per cent error in A. Now, let us select an example to show the relative size of these errors.

Let: $h_c = 5000$ Btu/hr ft^2,

$k = 30$ Btu/hr ft °F,

$\Delta x = \frac{1}{16}$ in. $= 0.0052$ ft,

$P = 600$ psia.

Let us first assume that $h_b = 5000$ Btu/hr ft^2 °F.

$$A = \left[\frac{1}{5000} + \frac{0.0052}{30} + \frac{1}{5000}\right]\frac{50(10)^6}{50} = 573 \text{ ft}^2 \quad .$$

From Eq. (2.5) and from the definition of h_b,

$$h_b = \frac{q}{A\Delta T} = \left(\frac{q}{A}\right)^{0.75}\frac{e^{P/900}}{1.9} \quad . \tag{2.10}$$

Combining Eq. (2.9) and (2.10),

$$A = \left[\frac{1}{h_c} + \frac{\Delta x}{k} + \frac{1.9\ A^{0.75}}{(q)^{0.75}\ e^{P/900}}\right]\frac{q}{T_1 - T_4} \quad . \tag{2.11}$$

Solving this by trial and error, the correct value of A is 551 ft^2.

The correct value of h_b is 5,370 Btu/hr ft^2 °F, the correct $(T_3 - T_4)$ is 16.9°F and the average heat flux is 90,600 Btu/hr ft^2. Our first calculation based on $h_b = 5000$ gave a value of $(T_3 - T_4)$ equal to 16.7°F Our error in boiling coefficient was

$$\frac{5370 - 5000}{5370} \times 100 = 6.9\% \quad .$$

The error in $(T_3 - T_4)$ was

$$\frac{16.9 - 16.7}{16.9} \times 100 = 1.2\% \quad .$$

However, the error in the area was small:

$$\frac{573 - 551}{551} \times 100\% = 4\% \quad .$$

The error in area is directly related to the error in boiling coefficient from Eq. (2.9). Assuming no scale resistance,

$$dA = d\left(\frac{1}{h_b}\right)\frac{q}{(T_1 - T_4)} \quad ,$$

or

$$\left(\frac{dA}{A}\right) = \frac{d\left(\frac{1}{h_b}\right)}{\frac{1}{h_c} + \frac{\Delta x}{k} + \frac{1}{h_b}} \quad .$$

Assume, for example,

$$\frac{1}{h_c} = 0.0002 \quad (h_c = 5000 \text{ Btu/hr ft}^2 \text{ F}) \quad ,$$

$$\frac{\Delta x}{k} = 0.0002 \left(\frac{k}{\Delta x} = 5000 \text{ Btu/hr ft}^2 \text{ F}\right) \quad ,$$

$$\frac{1}{h_b} = 0.0001 \quad (h_b = 10{,}000 \text{ Btu/hr ft}^2\text{F}) \quad .$$

Since

$$d\left(\frac{1}{h_b}\right) = -\frac{1}{h_b}\left(\frac{d\,h_b}{h_b}\right) \quad ,$$

then

$$\frac{dA}{A} = \frac{-\left(\frac{d\,h_b}{h_b}\right)}{h_b\left(\frac{1}{h_c} + \frac{\Delta x}{k} + \frac{1}{h_b}\right)} = \frac{-\frac{d\,h_b}{h_b}}{10{,}000\ (0.0002 + 0.0002 + 0.0001)}$$

$$= -0.2\left(\frac{d\,h_b}{h_b}\right) \quad .$$

The error in the area determination is only 20% of the error in the boiling heat transfer coefficient.

If a scale resistance of 0.001 (h = 1000) is included on both sides of the heat exchanger tube, the errors are still less, and may be shown to be

$$\left(\frac{dA}{A}\right) = 0.04\left(\frac{d\,h_b}{h_b}\right) \quad .$$

2.3 Fuel Element Heat Transfer

Case 1 - Fuel Plate

The heat transfer from the clad surface to the coolant has already been described in the previous section.

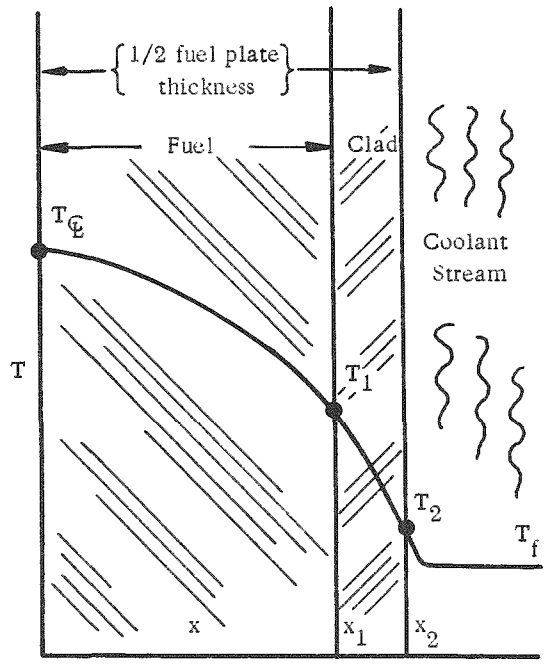

Fig. 2.4

Temperature Gradient in Plate-type Fuel Element

The temperature drop in the cladding is (see Fig. 2.4)

$$T_1 - T_2 = q''(x_2 - x_1)/k_{clad} \quad . \quad (2.12)$$

For uniform heat generation in the fuel and constant thermal conductivity, the fuel temperature drop is

$$T_{\mathbb{C}} - T_1 = q''(x_1)/2\,k_{fuel} \quad . \quad (2.13)$$

It may be noticed that the temperature distribution through the fuel is parabolic and that the temperature difference is exactly one-half of the value obtained for the case where all of the heat generated is passed through a slab of equal thickness.

In the case of variable thermal conductivity, the temperature difference can be found as follows from Fig. 2.5:

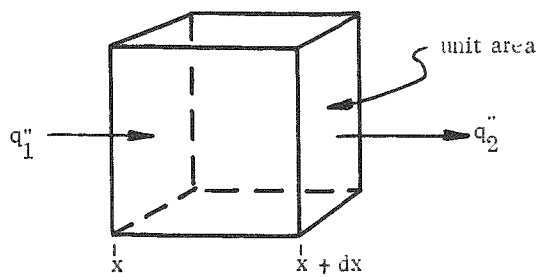

Fig. 2.5

Element of Fuel Plate

$$q_1'' A + q''' A dx = q_2'' A \tag{2.14}$$

$$-kA\left(\frac{dt}{dx}\right)_x + \left(k + \frac{dk}{dx}dx\right) A \left(\frac{dt}{dx}\right)_{x+dx} + q''' A dx = 0 \quad . \tag{2.15}$$

Dividing by Adx and rearranging

$$\frac{k\left[\left(\frac{dt}{dx}\right)_{x+dx} - \left(\frac{dt}{dx}\right)_x\right]}{dx} + \frac{dk}{dx}\left(\frac{dt}{dx}\right)_{x+dx} + q''' = 0 \quad , \tag{2.16}$$

or

$$k\frac{d^2t}{dx^2} + \frac{dk}{dx}\left(\frac{dt}{dx}\right) + q''' = 0 \quad . \tag{2.17}$$

This is identical to

$$\frac{d}{dx}\left(k\frac{dt}{dx}\right) + q''' = 0 \quad . \tag{2.18}$$

For a constant value of q''', Eq. (2.18) may be integrated to give

$$\int_0^{\phi} d\left(k\frac{dt}{dx}\right) = -\int_0^x q''' dx \tag{2.19}$$

where

$$\phi = k\frac{dt}{dx} \quad .$$

Then

$$k\frac{dt}{dx} = -q'''x \quad , \tag{2.20}$$

or

$$\int_{T_{\mathbb{Q}}}^{T_1} kdt = -\int_0^{x_1} q''' xdx \quad . \tag{2.21}$$

Thus for constant k

$$k\left(T_1 - T_{\mathbb{Q}}\right) = -q'''\frac{x_1^2}{2} \quad , \tag{2.22}$$

or

$$T_{\mathbb{L}} - T_1 = q''' x_1^2/2k \quad . \tag{2.23}$$

For steady state,

$$q''' = (q'') \text{ Area/Volume} = q'' A/Ax_1 = q''/x_1 \quad . \tag{2.24}$$

Equation (2.23) becomes identical to Eq. (2.13)

$$T_{\mathbb{L}} - T_1 = q'' x_1/2k \tag{2.23a}$$

For variable k, we can usually approximate k by the expression

$$k = a + bT \quad . \tag{2.25}$$

Then Eq. (2.21) becomes

$$\int_{T_{\mathbb{L}}}^{T_1} (a + bT)\, dT = -\int_0^{x_1} q''' x dx \quad , \tag{2.26}$$

or

$$a\left(T_1 - T_{\mathbb{L}}\right) + \frac{b}{2}\left(T_1^2 - T_{\mathbb{L}}^2\right) = -q''' \frac{x_1^2}{2} \quad , \tag{2.27}$$

or

$$a\left(T_{\mathbb{L}} - T_1\right) + \frac{b}{2}\left(T_{\mathbb{L}}^2 - T_1^2\right) = q''' \frac{x_1^2}{2} \quad , \tag{2.28}$$

so that

$$\left(T_{\mathbb{L}} - T_1\right) = -\left(T_1 + \frac{a}{b}\right) \pm \sqrt{\left(T_1 + \frac{a}{b}\right)^2 + \frac{q''' x_1^2}{b}} \quad . \tag{2.29}$$

Equation (2.13) is generally used, since the effect of a variable k is not very great, as shown by the following example.

Example

$q''' = 5(10)^7$ Btu/hr ft^3

$x = 0.12$ in. $= 0.01$ ft

$T_1 = 500°F$

$k = 10 + 0.01\ T$ Btu/hr-ft-°F

The heat flux is

$$q'' = q'''x = 5(10)^7 (0.01) = 500{,}000 \text{ Btu/hr ft}^2 \quad .$$

From Eq. (2.29), with a = 10 Btu/hr-ft-°F and b = 0.01 Btu/hr ft $(°F)^2$,

$$\left(T_{\mathbb{L}} - T_1\right) = -(500 + 1000) \pm \sqrt{(1500)^2 + \frac{5(10)^7 (0.01)^2}{0.01}} = 160°F$$

If we approximate this case by assuming an average k over the interval, say k_{avg} = 15 Btu/hr-ft-°F, then from Eq. (2.13)

$$\left(T_{\mathbb{L}} - T_1\right) = \frac{(500{,}000)(0.01)}{2(15)} = 167°F \quad .$$

Therefore in flat plate elements, it is sufficient to assume constant properties for metallic fuels.

Case 2 - Fuel Rods

A heat balance on the element in Fig 2.6 gives

$$q_1'' + q''' \text{ (Volume)} = q_2'' \quad .$$

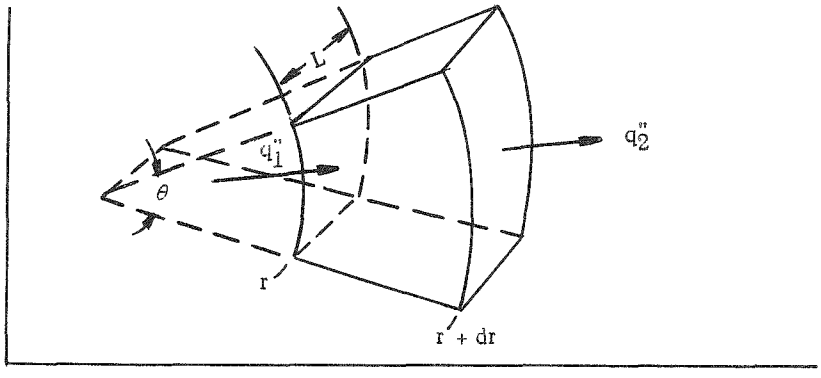

Fig. 2.6

Element of Fuel Rod

Then

$$-kr\theta L\left(\frac{dt}{dr}\right)_r + q''' r\theta L dr = -\left[k + \left(\frac{dk}{dr}\right) dr\right] (r + dr)\theta L\left(\frac{dt}{dr}\right)_{r + dr} \quad . \tag{2.30}$$

Rearranging, dividing by $r\theta L dr$, and neglecting second-order differentials,

$$\frac{k}{dr}\left[\left(\frac{dt}{dr}\right)_{r+dr} - \left(\frac{dt}{dr}\right)_{r}\right] + \frac{k}{r}\left(\frac{dt}{dr}\right)_{r+dr} + \left(\frac{dk}{dr}\right)\left(\frac{dt}{dr}\right)_{r+dr} + q''' = 0 \quad . \tag{2.31}$$

This may be written (as $dr \rightarrow 0$):

$$k\frac{d^2t}{dr^2} + \frac{k}{r}\frac{dt}{dr} + \left(\frac{dk}{dr}\right)\left(\frac{dt}{dr}\right) + q''' = 0 \quad . \tag{2.32}$$

Another, more useful form of Eq. (2.32) is

$$\frac{1}{r}\frac{d}{dr}\left(kr\frac{dt}{dr}\right) + q''' = 0 \quad . \tag{2.33}$$

Rearranging and integrating,

$$\int_0^{\phi} d\left(kr\frac{dt}{dr}\right) = -\int_0^{r} q''' r dr \tag{2.34}$$

where

$$\phi = kr\frac{dt}{dr} \quad .$$

Thus

$$kr\frac{dt}{dr} = -\frac{q''' r^2}{2} \quad . \tag{2.35}$$

Rearranging again and integrating,

$$\int_{T_{\mathcal{L}}}^{T_0} k dt = -\int_0^{r_0} \frac{q''' r dr}{2} \tag{2.36}$$

$$\int_{T_0}^{T_{\mathcal{L}}} k dt = \frac{q''' r_0^2}{4} \quad . \tag{2.37}$$

It is interesting to note that the heat generation per unit length of rod is

$$\frac{Q}{L} = \frac{q''' \pi r_0^2 L}{L} = q''' \pi r_0^2 \quad . \tag{2.38}$$

The right-hand side of Eq. (2.37) multiplied by 4π will give the heat released per unit rod length.

Although thermal conductivities of oxide fuels are difficult to determine accurately, Eq. (2.37) gives a convenient way of comparing experimental test data on rods of various diameters, enrichment, and composition. J A. L. Robertson[11] et al. show that satisfactory performance without melting was achieved with oxide fuel provided that

$$\int k\,dt \leq 39 \text{ watts/cm} \quad .$$

Oxide fuels appear to have conductivities that obey the law[12]

$$k = d/T + 460 \quad ,$$

where T is in °F and where T + 460 is degrees absolute, and where d is a constant. An example is given: Find the maximum heat generation rate and heat flux that will produce a centerline temperature of 4000°F ($T_{\mathbb{Q}}$ = 4000°F) for the following conditions:

$$r_0 = 0.24 \text{ in.} = 0.02 \text{ ft}$$

$$T_1 = 700°F$$

$$k = \frac{3300}{T + 460} \quad .$$

From Eq (2.37)

$$q''' = \frac{4}{r_0^2} \int_{700}^{4000} \left(\frac{3300}{T + 460}\right) dt = \frac{4(3300)}{(0.02)^2} \ln\left(\frac{4460}{1160}\right) = 4.45(10)^7 \text{ Btu/hr ft}^3 \quad .$$

The heat flux is

$$q'' = \frac{q'''(\text{Volume})}{(\text{Area})} = \frac{q'''\pi r_0^2 L}{2\pi r_0 L} = q''' \frac{r_0}{2} = 4.45(10)^7 \frac{(0.02)}{2}$$

$$\approx 445{,}000 \text{ Btu/hr-ft}^2 \quad .$$

The errors introduced in assuming a constant value of k can be shown as follows. Assume k = 1.17 Btu/hr ft F (value at 2350°F) and from Eq. (2.37),

$$q''' = \frac{4}{r_0^2} \int_{700}^{4000} 1.17\,dT = \frac{4(1.17)(3300)}{(0.02)^2} = 3.86(10)^7 \text{ Btu/hr ft}^3$$

and

$$q'' = 3.86(10)^7 \frac{(0.02)}{2} = 386{,}000 \text{ Btu/hr ft}^2 \quad ,$$

which is a per cent decrease of

$$\frac{445{,}000 - 386{,}000}{445{,}000} \times 100\% = 13\% \quad .$$

Conversely, if we assume a heat flux of 445,000 Btu/hr ft^2 and calculate the centerline temperature by using a constant k value,

$$T_{\mathbb{L}} = 700 + \frac{4.45(10)^7 (0.02)^2}{4(1.17)} = 700 + 3800 = 4500°F \quad ,$$

which is in error by 500°F.

2.4 Steam Heat Transfer

1. Saturated Steam

Heat transfer coefficients to flowing saturated steam are low compared to boiling coefficients, but not very much lower than the coefficients to flowing water when compared at the same mass flow rate. For either water or steam, we may write

$$\frac{hD}{k} = 0.023 \left(\frac{GD}{\mu}\right)^{0.8} \left(\frac{C_p \mu}{k}\right)^{0.4} \quad . \tag{2.39}$$

Rearranging,

$$h = 0.023 \frac{G^{0.8} C_p^{0.4} k^{0.6}}{D^{0.2} \mu^{0.4}} \quad . \tag{2.40}$$

The ratio of the heat transfer coefficient for water and steam is therefore

$$\frac{h_{steam}}{h_{water}} = \frac{\left[\left(\frac{C_p}{\mu}\right)^{0.4} k^{0.6}\right]_{steam}}{\left[\left(\frac{C_p}{\mu}\right)^{0.4} k^{0.6}\right]_{water}} \quad . \tag{2.41}$$

A comparison is given in Fig. 2.7. The minimum ratio is about 0.3 and this ratio occurs at a temperature of about 320°F.

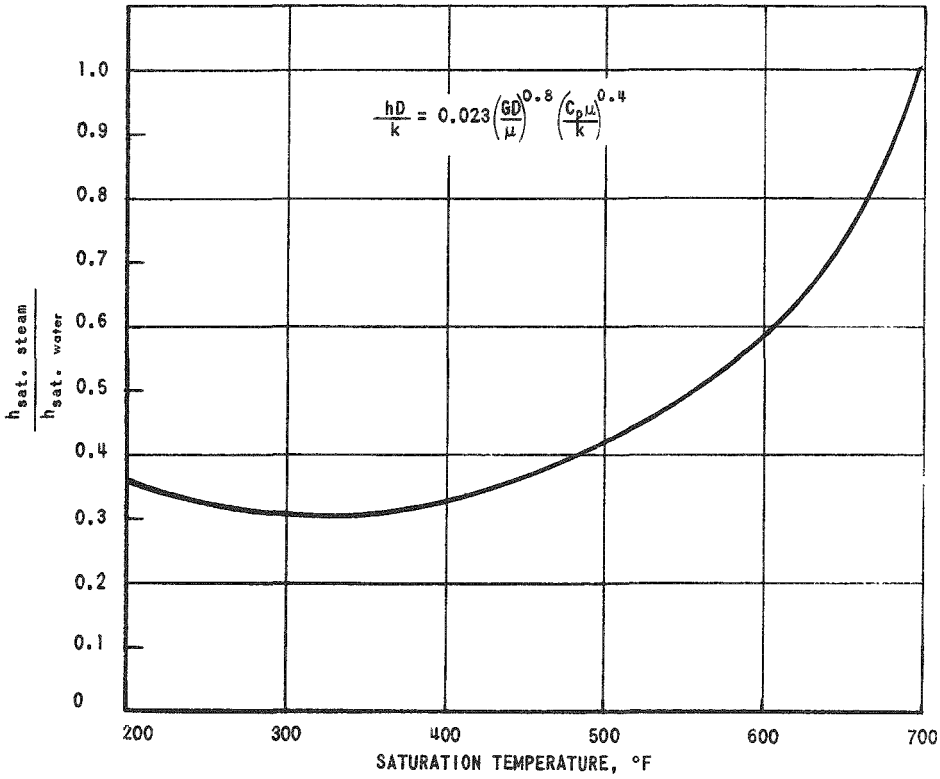

Fig. 2.7

Comparison of Steam and Water as Coolants

2. Superheated Steam

Equation (2.39) may be used to calculate the heat transfer coefficients for superheated steam. Rearranging Eq. (2.39) or Eq. (2.40),

$$h = 0.023\,(G^{0.8}/D^{0.2})\,\phi\ , \qquad (2.42)$$

where

$$\phi = \left(\frac{C_p}{\mu}\right)^{0.4} k^{0.6} \qquad (2.43)$$

This function is shown in Fig. 2.8. The values given are approximate and should not be used for design equations. Figure 2.8 is given to show the trend in the heat transfer coefficient with temperature and pressure.

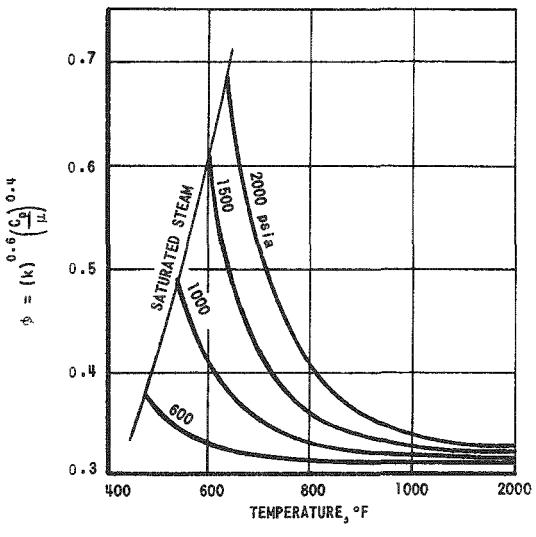

Fig. 2.8

Effect of Pressure and Temperature on Steam Heat Transfer

3. TWO-PHASE DENSITY STUDIES

3.1. Introduction

The ability to predict accurately the steam volume fractions in boiling systems is a prerequisite for a competent evaluation of the performance characteristics of such systems. This is especially true in boiling water reactors where the nuclear aspects are intimately interrelated to the two-phase flow characteristics of the system. The reactor recirculation rate, coolant-moderator density, core neutron kinetics, and reactor stability are all dependent upon the steam volume fraction.

Because of the complexity of the boiling process, the prediction of the density of steam-water mixture is of necessity almost completely empirical. As a result, considerable effort has been expended during the past few years by a number of investigators on the experimental measurement of steam volume fractions. Some of the pertinent information derived from these studies is described briefly.

Martinelli et al.[13] obtained liquid-holdup data at atmospheric pressure and correlated this data as a function of quality and a physical property parameter, x_{tt}. They also extrapolated their atmospheric pressure correlation to regions of higher pressure. Dengler[14] reported measurements of steam volume fractions at atmospheric pressure, using a radioactive tracer in the water for volume fraction measurements. Data were correlated using the Martinelli x_{tt} parameter. Isbin et al.[15-18] obtained volume fraction data for both horizontal and vertical flow over a wide pressure range and found that the velocity ratios were a function of mixture quality as well as pressure.

Lottes and Flinn,[19] Cook,[20] Petrick,[21] Richardson[22] and Marchaterre[14] have reported results from studies at ANL with air-water systems and steam-water systems. The superficial velocity and quality were found to affect the velocity ratio; significant differences between horizontal and vertical flow were also found.

Egen, Dingee and Chastain[31] have reported results from narrow rectangular channels at 2000 psi. The volume fractions were found to be heat-flux dependent well into the net quality region. The velocity ratio was independent of quality and of velocity over the range of variables tested. Hughes[23] presented volume fraction measurements obtained from large equivalent-diameter adiabatic systems at 1200, 1400, 1800, and 2400 psia. The velocity ratio and velocity difference were shown to be a function of the flow rate and quality. Recently Asyee[24] has reported results for a cosine-heated annulus over a considerable pressure range. He also found velocity ratios to be a function of pressure, quality and circulation velocity. Schwartz[25] conducted investigations in horizontal and vertical boiler tubes and observed that the volume fractions were different for the two cases.

Other investigations have been performed and the work is discussed in several extensive literature surveys on the subject of two-phase flow.[26,16,27,22]

The 600 psia multichannel boiler was built to get design information on power vs steam volume fraction for EBWR. The 600 psia single channel boiler was built to obtain information on slip ratios and boiling pressure drop. The results from these systems are shown in various figures throughout the discussion.

Since EBWR has been placed into operation, the experimental program has been directed toward obtaining more refined basic data on relative velocity of steam-water mixtures, two-phase friction factors, and hydrodynamic stability during boiling. This information is required for the design of large scale central station boiling reactors. Following is a description of the more recent data that have been taken.

3.2. Relative Velocity of Steam Water Mixtures

From a mass balance at a plane perpendicular to the flow of a steam water mixture, it may be shown that slip ratio,

$$\frac{V_g}{V_f} = \left(\frac{x}{1-x}\right)\left(\frac{1-\alpha}{\alpha}\right)\frac{\rho_f}{\rho_g} \quad . \tag{3.1}$$

The importance of this V_g/V_f is that power generation for a given value of α is proportional to x. The above equation shows that x increases as V_g/V_f increases. V_g/V_f must therefore be known to evaluate power generation in a boiling reactor.

There are presently many ways of calculating V_g/V_f and many ways of interpreting experimental information on this subject. The bibliography lists references on the subject of slip ratio. Additional equations relating the variables of interest are

$$Q_T = \rho_f A V_0 [C_p(T_f - T_i) + x h_{fg}] \tag{3.2}$$

$$V_g - V_f = V_0 \left[\frac{x}{\alpha}\frac{\rho_f}{\rho_g} - \frac{1-x}{1-\alpha}\right] \quad . \tag{3.3}$$

These equations show that $V_g - V_f$, V_0, x, Q_T, etc., are all interrelated. The correct interpretation of data and the selection of the proper variables are presently matters of personal preference. Figures 3.1, 3.2, and 3.3 show several ways of presenting the information. Figure 3.1 shows slip ratio as a function of inlet velocity. There is a separation with power density. Figure 3.2 shows slip ratios as a function of quality with pressure as a parameter.

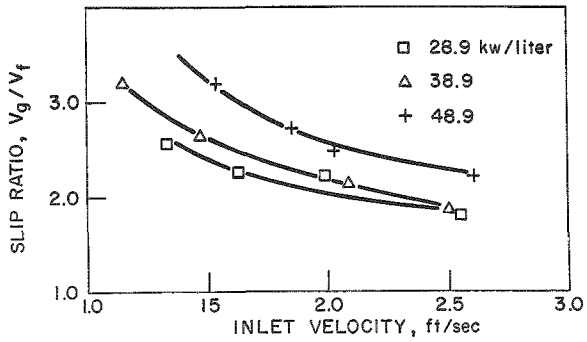

Fig. 3.1

Slip Ratio vs Inlet Velocity for a $\frac{1}{2}$ x 2 x 60-in. Channel at 600 psig
111-6850

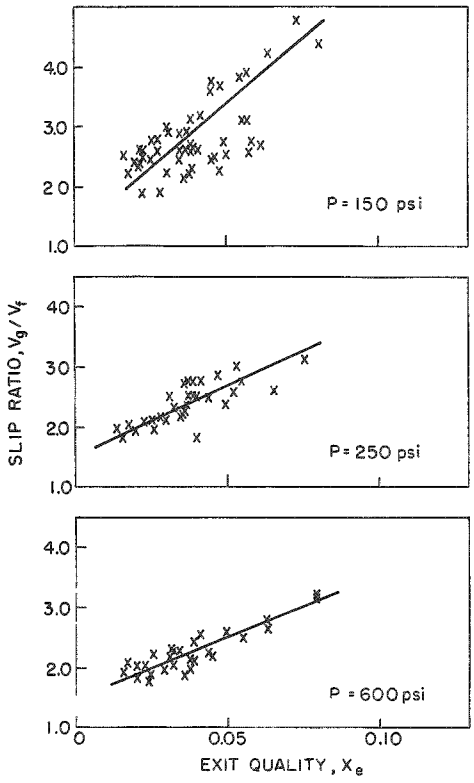

Fig. 3.2

Slip Ratio vs Exit Quality for Various Pressures
111-7207

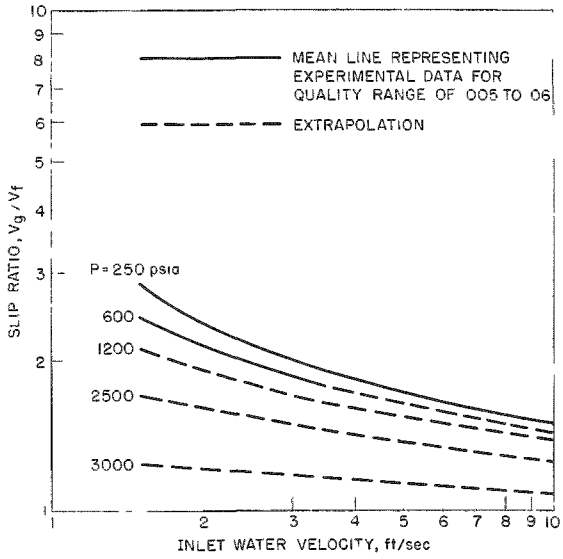

Fig. 3.3

Estimated Variation of Slip Ratios with Velocity and Pressure
111-7208

Figure 3.3 represents the authors' opinion of best available estimates of V_g/V_f shown as functions of mass flow rate and pressure. This form of showing the information was selected since it is very convenient for calculating reactor performance.

3.3. Methods of Measurement

In an analysis of a natural circulation system it is necessary to evaluate the effect of a sudden change of flow area (such as an expansion or a contraction) on the two-phase fluid density. It was difficult to predict these changes utilizing information previously available. Therefore, an experimental program was undertaken to provide adequate information on the effect of flow area changes on the two-phase fluid density and to explore further the factors which effect the relative velocity of the two phases.

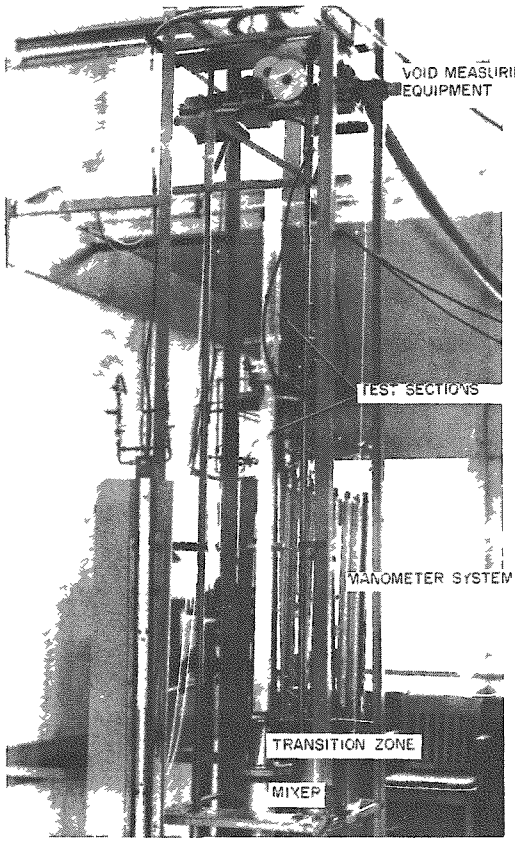

Fig. 3.4

Atmospheric Air-Water System
111-5636-A

A number of experimental systems have been used for studying the relative velocity of the phases in two-phase mixtures. Data were taken in both horizontal and vertical flow air-water systems, a 600-psi single-channel boiler, a 600-psi multichannel boiler, and a 2000-psi single-channel boiler.

The apparatus used for the vertical up-flow air-water studies is shown in Fig. 3.4. Air and demineralized water were mixed in a mixing section and the mixture then passed upwards through the test section. Five test sections of 4-ft length and 2-in. width with spacings of $\frac{1}{8}$, $\frac{1}{4}$, $\frac{1}{2}$, $\frac{3}{4}$, and 1 in. were constructed from Lucite to allow visual observations and photographic studies.

A schematic diagram of a representative boiling loop is illustrated in Fig. 3.5. Tests were run with both natural and forced circulation. Boiling took place in the active test section and the two-phase mixture flowed upwards through a riser section. Steam was separated at the steam-water interface and discharged to a condenser. The water returned through a crossover, where makeup water was added, and flowed down the downcomer to the test section inlet.

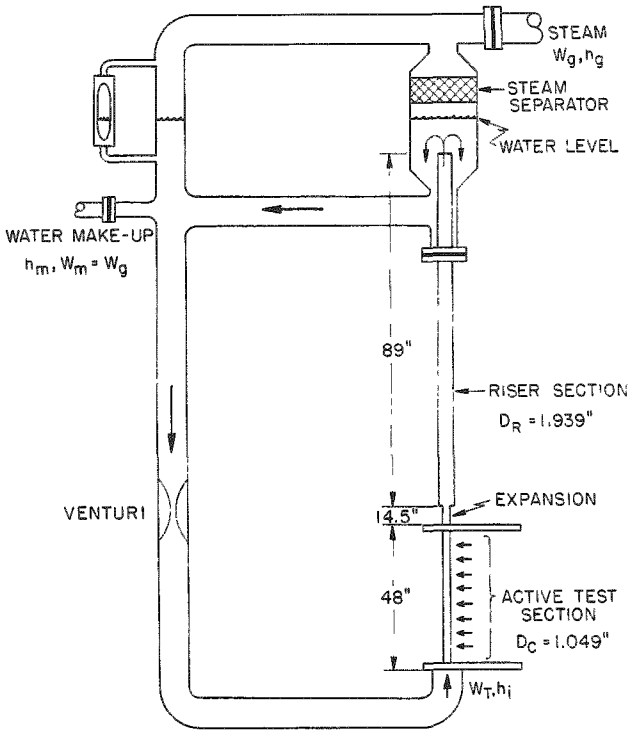

Fig. 3.5

Schematic Diagram of Typical Boiling Loop 700-436

Steam volume fractions were measured by a gamma-attenuation technique. The equipment and instrumentation consisted basically of a Tm^{170} gamma source, a scintillation-crystal photomultiplier-tube arrangement, amplifier, differential analyzer, count rate meter and recorder. The attenuation of the gamma beam passing through the steam-water mixture was measured and calibrated against the attenuation observed when the section was full of water and when it was full of steam.

Several methods of measuring the density of a two-phase mixture were considered before a final selection was made. Two types of mixtures required measurement: steam-water and air-water. These mixtures were to be enclosed in heavy wall steel containers designed to operate at 2500 psig.

Some of the properties of these mixtures which might be a function of their density include:

(1) Absorption or velocity of vibration energy;

(2) electrical or magnetic effects such as:
   (a) dielectric constant
   (b) resistivity
   (c) permeability;

(3) absorption of particles such as:
   (a) neutrons
   (b) alpha
   (c) beta
   (d) gamma;

(4) absorption of radiant energy.

The above properties were studied and evaluated as described below.

1. Absorption or Velocity of Vibration Energy

In the sonic range of frequencies the geometry and acoustical characteristics of the heat transfer apparatus would not permit precise measurements of low frequency acoustical energy absorption or velocity.

In the ultrasonic range of frequencies the absorption and scattering phenomena in the water, caused by the liquid-vapor or liquid-gas interfaces existing under boiling conditions, would make it extremely difficult to distinguish absorption or phase differences caused by finite velocity of propagation, from reflecting and scattering.

In both frequency ranges variations in absorption or velocity caused by water temperature and pressure changes also complicate the problem. Pressure waves might also affect the boiling phenomena.

2. Electrical or Magnetic Effects

The relatively high electrical conductance of the container in which the two-phase mixture is flowing and the necessity of making local density measurements were incompatible in utilizing electrical effects. The relatively high permeability of the container would make it difficult to obtain strong magnetic fields in the mixture and would completely mask the small permeability changes taking place in the mixture.

3. Particle Absorption

Measurement of absorption by the two-phase mixture of alpha or beta particles or neutrons is another possibility. Because of the heavy walls surrounding the mixture, alpha particles and all but the highest energy beta particles cannot be used. High energy beta particles would be useable, but a complex calibration procedure would be required at every point a density measurement is desired as the nature of absorption would be determined by the quantity of structural material between the source and the detector. Neutrons can also be used for density measurements. It is felt, however, that a radiant energy system would be simpler in nature for pipe walls up to one inch in thickness because of the more complex detection system needed when using neutrons.(26)

4. Radiant Energy Absorption

Various wave length regions of the radiant energy system were studied. The micro-wave, infra-red, ultra-violet and visible regions were eliminated because of the tendency of the heat transfer facility to absorb these radiations prior to transmission through the two-phase mixture zone.

Gamma and X-rays show the most promise for the measurement of a two-phase mixture density by a radiant-energy absorption system.

Commercial X-ray generators can produce high intensity radiation with the proper energy for density measurements. However, a more complex and expensive system is required as compared to a system using a radioactive source.

Radioactive material contained within the water was also considered. This system can be used when an isotope which is soluble in water and which has the proper energy spectrum is available. There are several objections to this system, including:

(1) Lack of precise knowledge of the effect of isotopic content of the water on the heat transfer characteristics.

(2) Personnel hazard in storing and handling radioactive water.

(3) Deposition of radioactive material in stagnant or inaccessible areas of the heat transfer loop.

Radioactive material located externally to the channel or container in which the two-phase mixture is located proved to be the most practical system. Sources with low energy gamma rays are available so that satisfactory density measurement is practical. However, a monoenergetic source is needed or one must be able to select only one energy level if a source with more than one energy peak is used.

After a consideration of the above properties and the physical construction of the heat transfer facility, the radiant energy absorption property had the most promise of success. With this in mind, a system was developed at Argonne utilizing a radioactive source external to the container of the two-phase mixture. The system consists of a Thulium-170 source, a scintillation crystal-photomultiplier tube assembly, a current amplifier, and a recorder. This system measures the steam void fraction from which the two-phase mixture density can be calculated.

The gamma attenuation measurement technique has been described in detail by Petrick[28] and by Hooker and Popper.[29] Figure 3.6 shows the source and photomultiplier-tube arrangement in place on a test section.

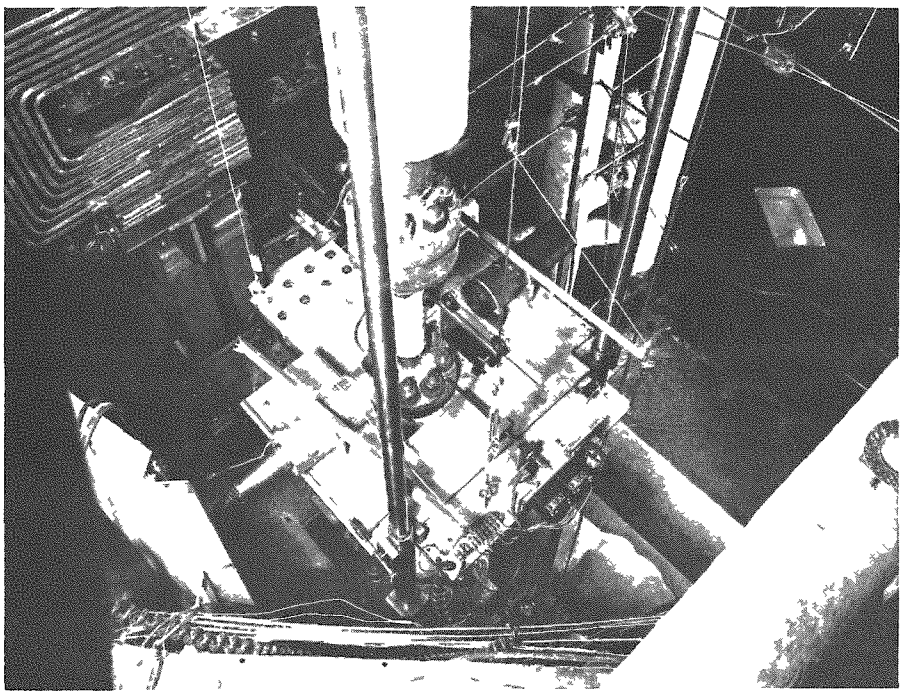

Fig. 3.6

Source and Photomultiplier Tube Arrangement for Density Studies
111-7612

3.4. Correlation of Data

In the analysis of experimental data several choices of dependent variable for correlation can be made. The steam volume fraction can be correlated directly as a function of the various parameters or may be reduced to phase velocities. A correlation of the steam volume fraction vs system parameters is perhaps the easiest to use but has the objectionable feature that extrapolation is difficult and may be misleading. For example, Martinelli's data, which was presented in this manner, predicts steam volume fractions that do not occur in vertical upflow systems, i.e., the steam velocity is less than the water velocity.

A more useful parameter is obtained by using an expression involving the velocity of each phase. The parameters most frequently used are the phase velocity difference, defined in Eq. (3.3) and repeated here:

$$V_g - V_f = V_0 \left[\frac{x}{\alpha} \frac{\rho_f}{f_g} - \frac{1-x}{1-\alpha} \right] , \qquad (3.4)$$

and the velocity ratio defined in Eq. (3.1) and repeated here:

$$V_g/V_f = \left(\frac{x}{1-x}\right)\left(\frac{1-\alpha}{\alpha}\right)\frac{\rho_f}{\rho_g} \quad . \tag{3.5}$$

These parameters have the advantage that they are more sensitive to the variation in other variables such as superficial velocity and quality. Also they have the additional advantage that they are more basic parameters, and, using them, arguments concerning postulated mechanisms can be made more readily. Since the velocity ratio is the more convenient term, it was chosen for correlation. It is recognized that this ratio represents a mean velocity for each phase and it is not necessarily the correct velocity to be used in momentum and kinetic energy terms.

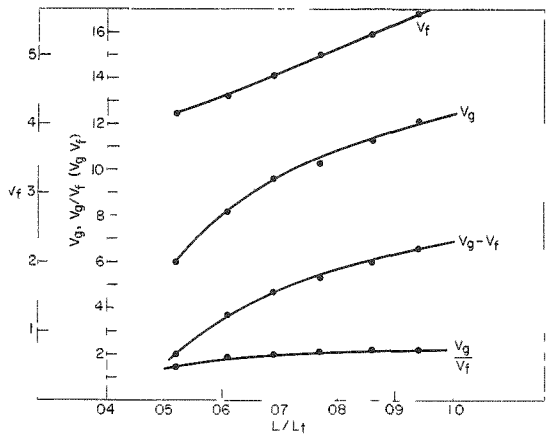

Fig. 3.7

Variation of Local Phase Velocities, Velocity Ratio, and Velocity Difference for a Typical Boiling Run
111-77

It is of interest to see how the phase velocities vary in a typical boiling channel. Figure 3.7 shows the variation of the liquid velocity, steam velocity, velocity ratio, and velocity difference for an experimental run in a $\frac{1}{4} \times 2 \times 60$ in. rectangular channel. It can be seen that both the relative velocity and the velocity ratio vary markedly with channel length and hence mixture quality.

The data of four experimental systems have been used in developing the correlations. Extensive data were taken on air-water systems to establish the effects of the various parameters at atmospheric pressure. Additional volume fraction measurements of steam-water mixtures were made on $\frac{1}{4} \times 2$, $\frac{1}{2} \times 2$ and $\frac{7}{16} \times 4$ in. rectangular channels in boiling, and 1-in. and 2-in. circular channels under adiabatic flow, conditions to extend the range of variables such as pressure, quality, etc.

3.5. Experimental Results

1. Air-Water Tests

Tests were run in both horizontal and vertical flow with atmospheric air-water systems. These results have been reported by Petrick[30] and Richardson.[22] Since the tests indicated significant

differences between horizontal and vertical flows, only the vertical flow tests will be considered here.

Figure 3.8 shows representative data for the velocity ratio as a function of the superficial velocity at a constant quality. The data show the relative velocity of the two phases is a function of both the water velocity and quality. The slope of the quality parameters changed only slightly over the range of qualities studied. The studies also indicated that geometrical arrangements may affect the phase velocities because of changing flow patterns, but that this effect is small.

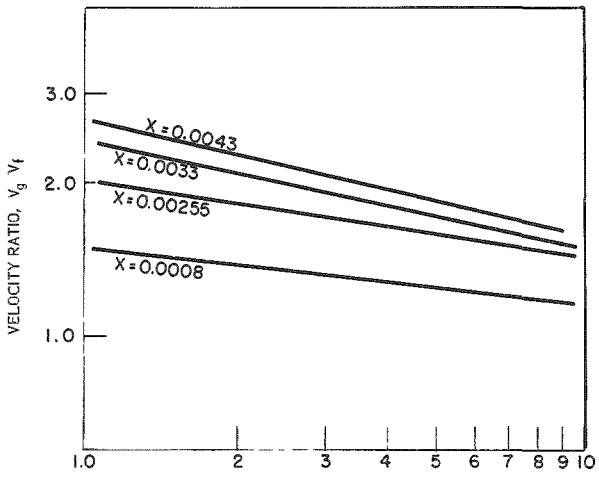

Fig. 3.8

Representative Results from Air-Water Studies

Studies were made of the distribution of the air phase in the water by traversing the channel with a narrow gamma beam. These data showed that the distribution of the air phase in the water was parabolic in nature, but that the ratio of v_{max}/v_{avg} which characterizes the distribution varied at random.

The results of these studies were used as a guide in analyzing the steam-water data at higher pressures.

2. Steam Volume Fraction Data

The steam-water volume fraction data were analyzed, using the air-water results as a guide. When the slip ratios were plotted as a function of the same parameters, similar effects of flow rate, quality, pressure and geometrical arrangement were observed (see Figs. 3.8 to 3.19).

The data shown are typical of the great quantity of data accumulated during the past few years on a number of experimental loops. It can be seen that each of the parameters by itself does not affect the velocity ratio greatly; however, several such parameters in combination could produce a substantial effect. It is possible, therefore, that the differences in results reported in the literature by the various investigators are not due as much to differences in experimental technique as they are to the aforementioned effects. Effects of this type can be found only if experimental measurements are such that the velocity ratios can be calculated to within ±10%, which is extremely difficult experimentally.

As an example, effects of channel geometry have not been clearly established. Figure 3.9 shows a representative difference between data taken on a 2-in. diameter circular channel and data taken on a 0.622-in. diameter circular channel. This is a representative trend but the effect has not been noted in all cases.

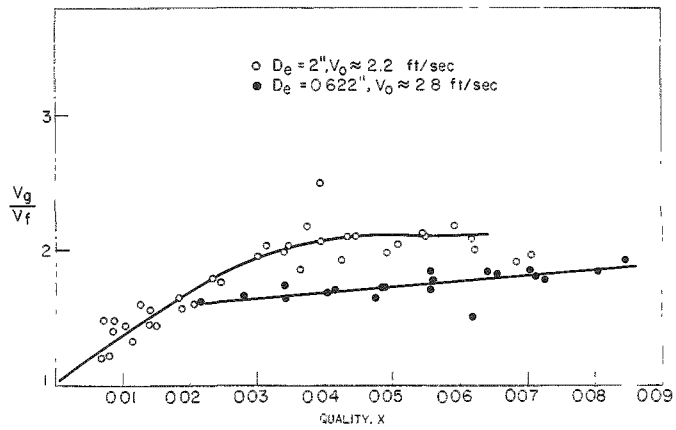

Fig. 3.9

Effect of Geometry on
Velocity Ratio at 600 psig

Since the effect cannot be predicted on the basis of present data, it has not been included in the data correlation.

3. Quality Effects

The effect of quality on the slip ratio is shown in Figs. 3.9 to 3.15. The data encompass a superficial water velocity range from 1.4 to 2.5 ft/sec (the average velocity of approximately 2 ft/sec), a pressure range from 150 to 1500 psi, and a flow channel equivalent diameter range from 0.44 to 2 in. These parameters are indicated on the figures. The lines drawn through the data represent a least squares fit of a first degree polynomial. It can be seen that the slopes of the lines, and hence effect of quality on the slip ratio, decrease with the pressure for the range of variables specified. Data of other investigators were analyzed in an analogous manner to obtain a comparison. These data are plotted in Fig. 3.16, and, as can be seen, tend to check the ANL data. The quality effects on the slip ratio also appears to diminish with increasing mass velocity. This has been observed in recent data obtained in the higher mass velocity range. However, sufficient data have not been accumulated to quantitatively establish the magnitude of effect. It appears that a family of curves of the type shown in Fig. 3.16 may be obtained.

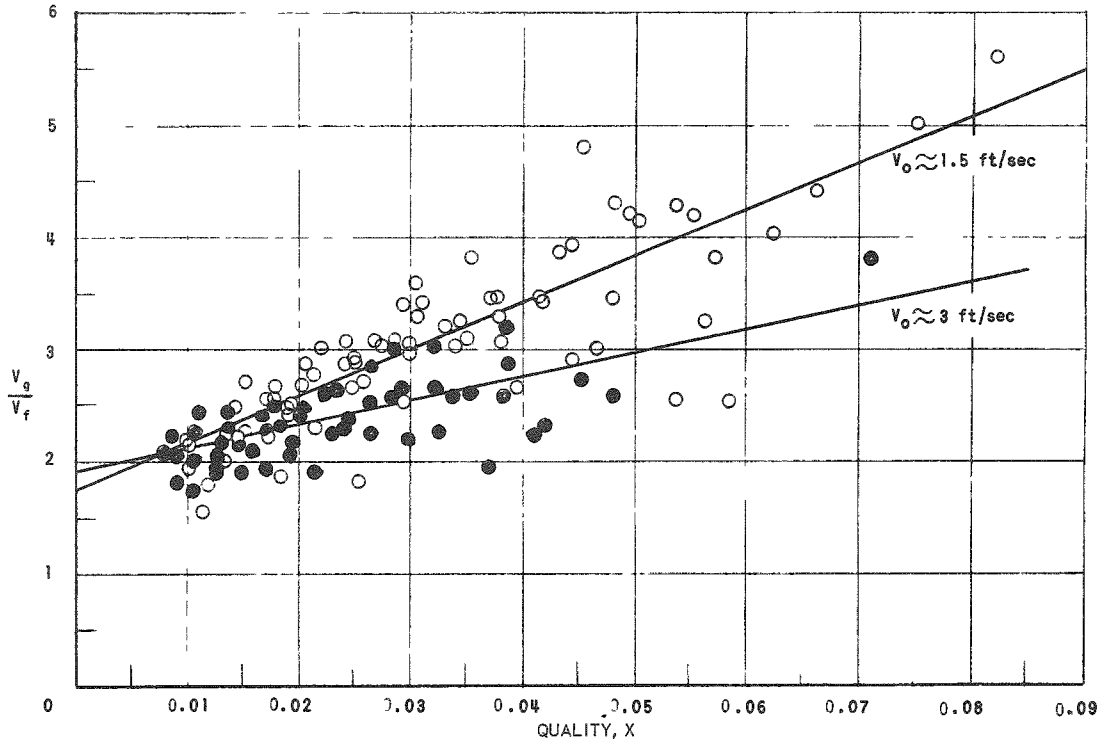

Fig. 3.10

The Effect of Quality on Velocity Ratio at 150 psig

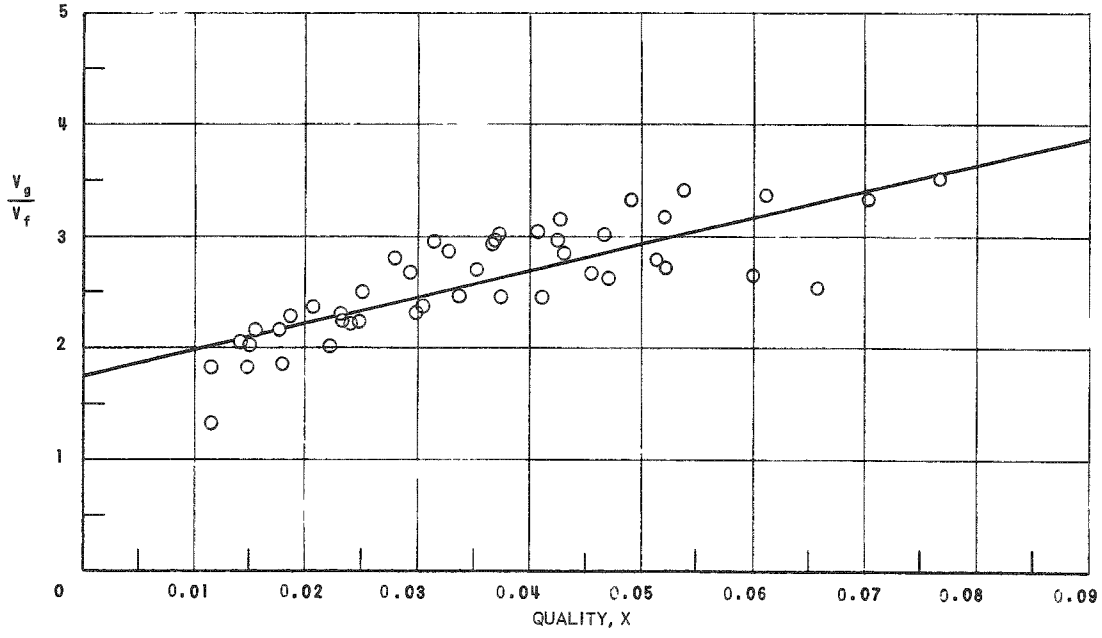

Fig. 3.11

The Effect of Quality on Velocity Ratio at 250 psi at $V_0 \approx 1.5$ ft/sec

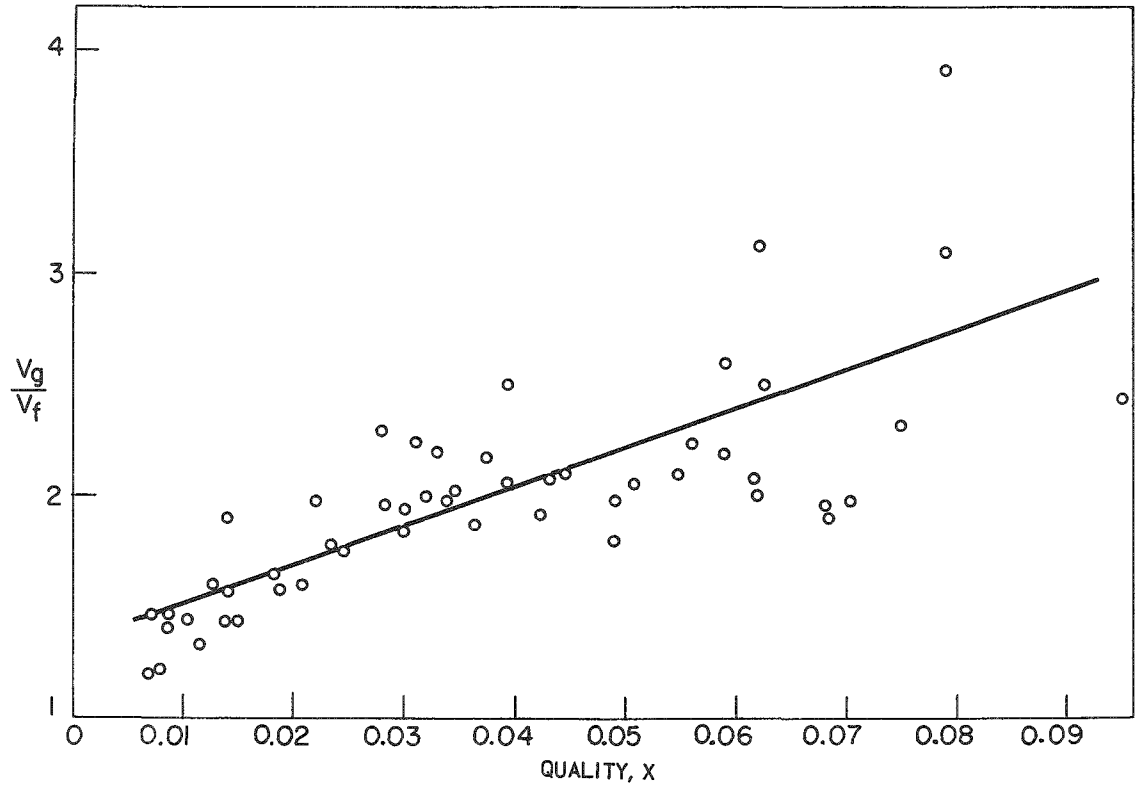

Fig. 3.12

Effect of Quality on Velocity Ratio at 600 psig at $V_0 \approx 2.2$ ft/sec

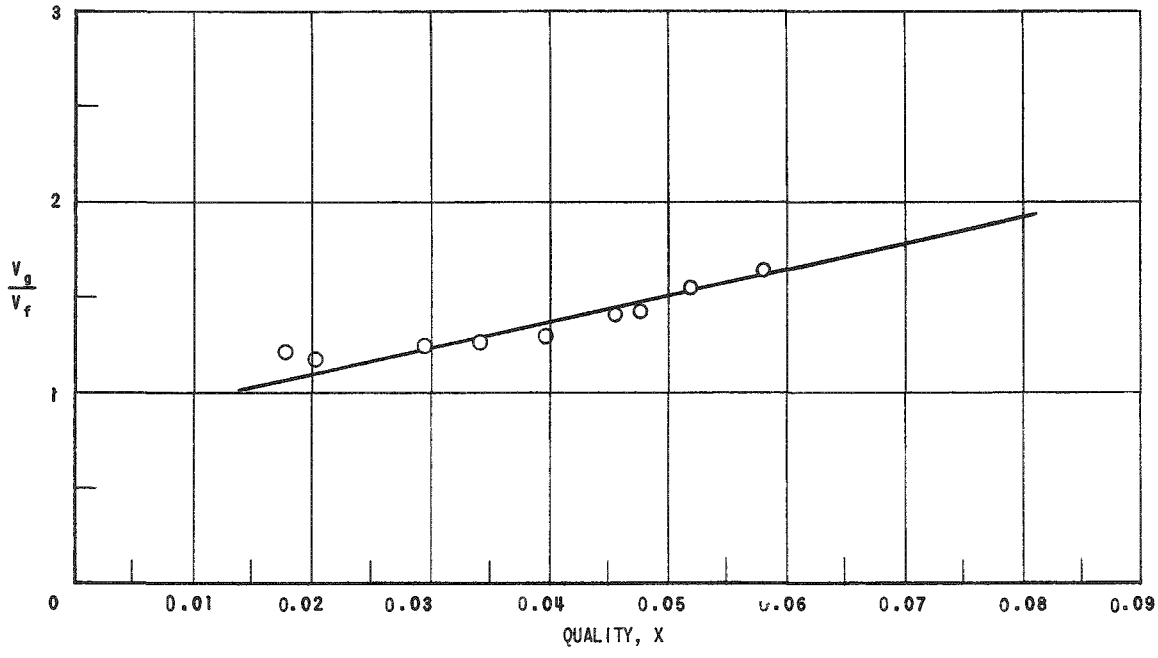

Fig.3.13

The Effect of Quality on Velocity Ratio at 1000 psi; $V_0 \approx 2.5$ ft/sec

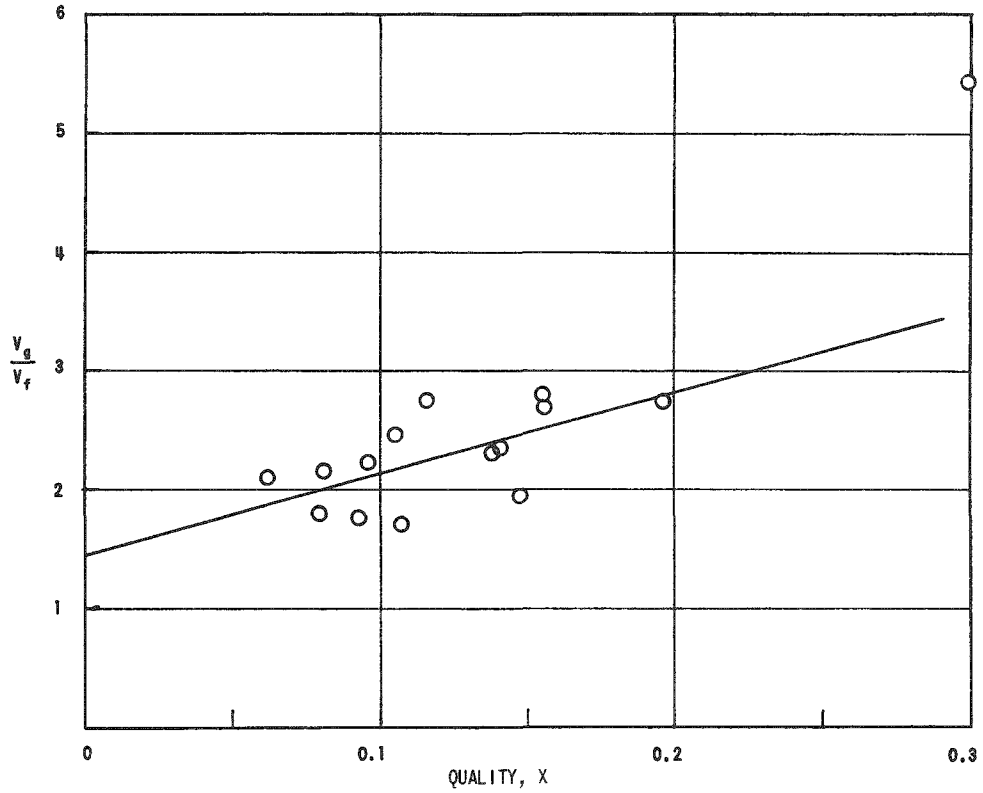

Fig. 3.14

Velocity Ratio as a Function of Quality at 1500 psig

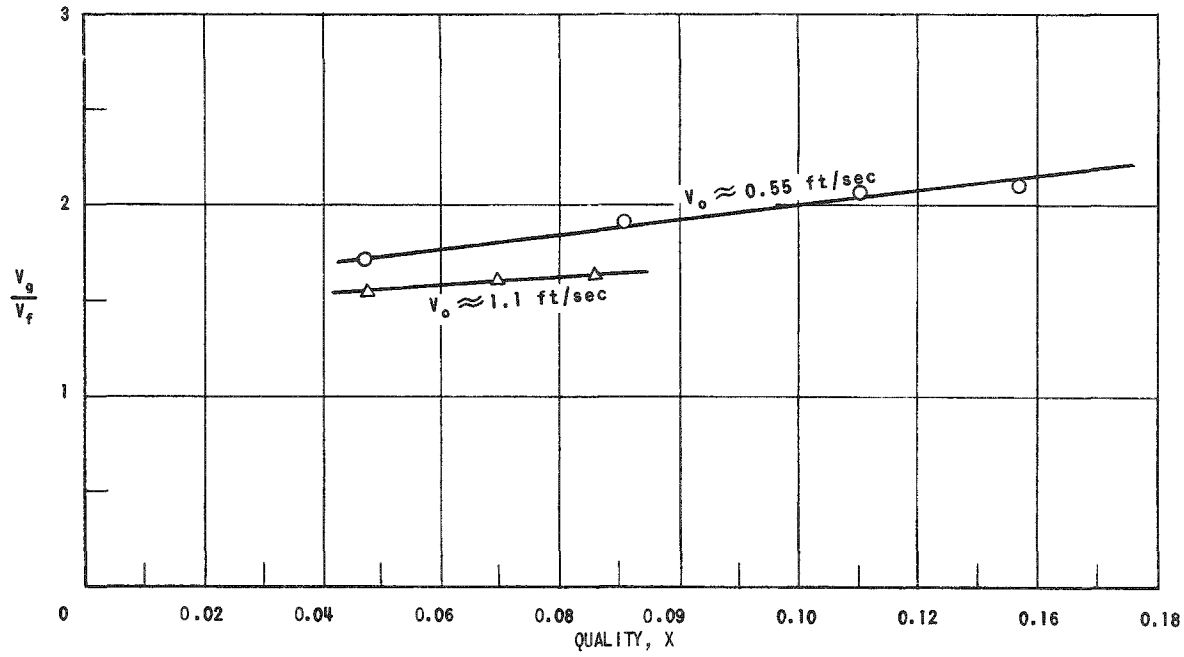

Fig. 3.15

The Effect of Superficial Velocity on Velocity Ratio at 1200 psia - Data of Hughes

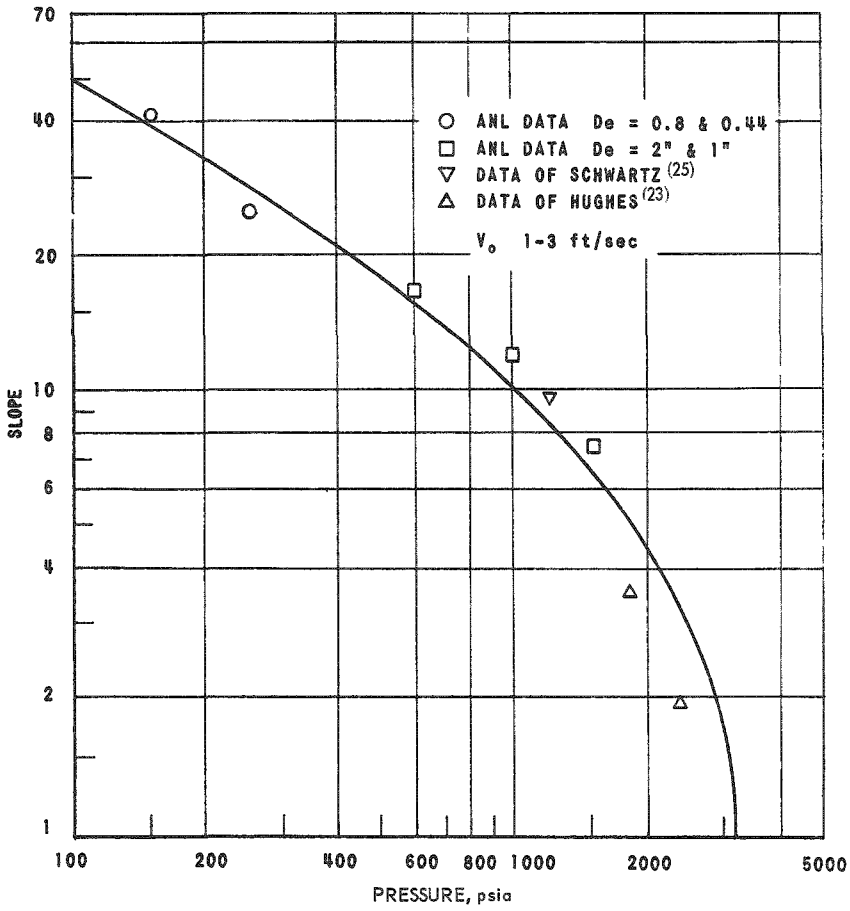

Fig. 3.16

Slope of V_g/V_f Quality Lines as a Function of Pressure
111-8425

4. Mass Velocity Effect

The magnitude of velocity effect on the slip ratio is illustrated in Figs. 3.10, 3.15 and 3.17 for a steam-water system and in Fig. 3.8 for an air-water system.

It can be seen that the slip ratio shows the same dependency on the superficial velocity for both systems. As the superficial velocity increases, the slip ratio decreases. The magnitude of the velocity effect appears to decrease with decreasing quality and increasing pressure. From Figs. 3.10 and 3.15 it can be seen that for a constant quality of the slope of the V_g/V_f vs V_0 line decreases with increasing pressure. It is interesting to note, however, that the velocity effect is greater at 150 psi than that observed at atmospheric pressure (See Figs. 3.8 and 3.17). This apparent incompatibility is probably due to the quality effect. Extrapolation of the quality range of the air-water data to coincide with the quality range of the steam-water data would make the velocity effect greater than that observed at 150 psi.

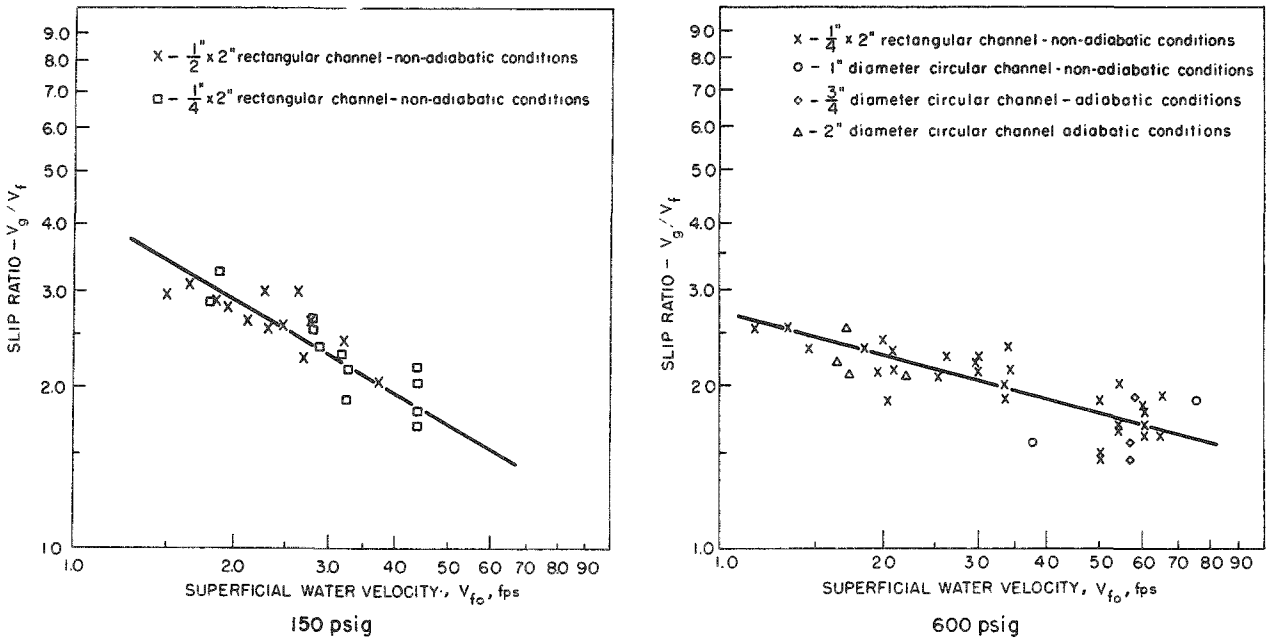

Fig. 3.17

Velocity Ratio as a Function of Superficial Velocity at 150 and 600 psig ($x \approx 0.03$)

The decrease in the velocity effect with decreasing quality can be seen in the data from ANL for 150 psi (Fig. 3.10) and from the data of Hughes[23] at 1200 psi (Fig. 3.15). The slopes of the slip ratio-quality lines increase with decreasing velocity. Thus at low mixture qualities there is very little effect of the mass flow rate on the slip ratio, whereas in the higher quality range the velocity effect is substantial. It appears that the mass velocity effect also decreases with pressure (see Figs. 3.10 and 3.15).

5. Pressure Effects

As expected, the slip ratio decreases with increasing pressure; this is illustrated in Fig. 3.18. The lines shown represent a least square fit of the data at pressures of 150, 200, 600, 1000 and 1500 psi at approximately the same superficial velocity and in similarly sized channels. The dashed line shown represents a series of data points obtained from a 1-in. pipe at 1500 psig, whereas the solid line at the same pressure represents data taken from a 2-in. pipe. No conclusive explanation can be given for the inconsistencies between the two sets of data. However, the velocity measurements for the 1-in. pipe were subject to question due to probable errors in the venturi measurement. This in turn would be reflected in the calculated slip ratio through the mixture quality. A new venturi was installed prior to running the several series of data points in the 2-in. pipe.

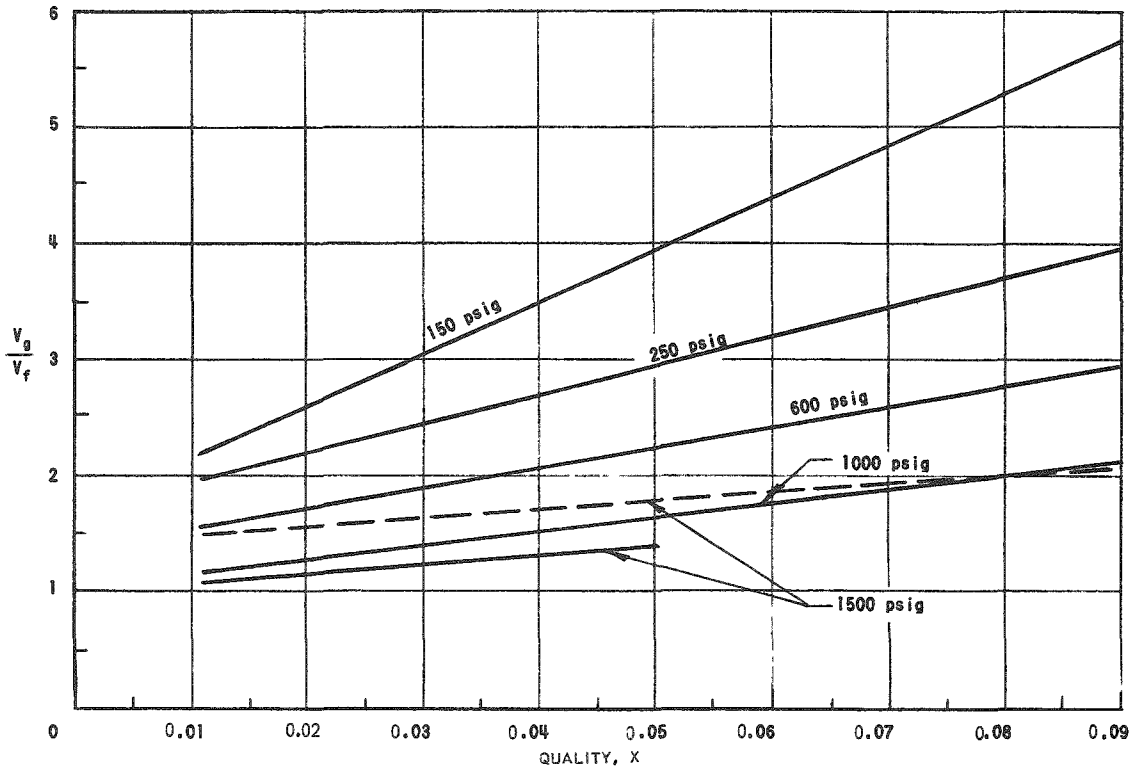

Fig. 3.18

Velocity Ratio as a Function of Quality
at Various Pressures ($V_0 \approx 1$ to 3 ft/sec)
111-8427

The pressure effect on the slip ratio is perhaps more vividly demonstrated in Fig. 3.19 for constant parameters of velocity ($V_0 \approx 1$-3 ft/sec) and quality ($x \approx 0.05$). Data of other investigators at the higher pressures are also compared with the ANL data and, as can be seen, the data check quite well. The extrapolation into the very high pressure range as indicated in the figure was based on the variation of the density difference of the two phases. The density difference is a measure of the buoyancy force which is a factor affecting the relative velocity of the two phases. The data of Hughes[23] and Egen et al.,[31] which are shown on Fig. 3.19, were also used as a guide; however, their data are subject to question. The data of Hughes may be in error since only centerline void measurements were taken and multiplied by a constant $\alpha_{max}/\alpha_{avg}$ to obtain the average voids at any cross section. Data taken at ANL[30] have indicated that this multiplier varied considerably. The data of Egen et al. were obtained from a very narrow rectangular channel (0.1 x 1 in.) and, as a result, the low slip ratio may be due to the geometrical effect as pointed out previously. Also, it should be noted that the accuracy of void measurements tends to decrease with increasing pressure, especially for small-width channels.

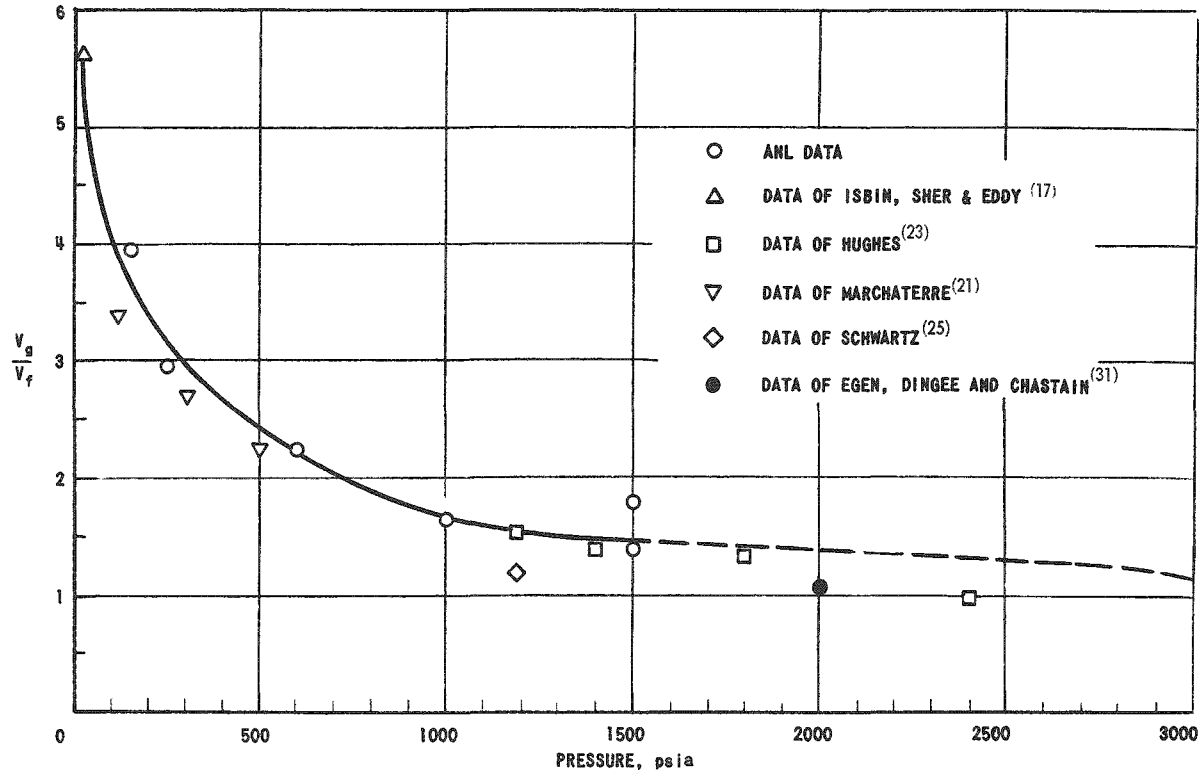

Fig. 3.19

Velocity Ratio as a Function of Pressure;
$V_0 \approx 1$ to 3 ft/sec and $x \approx 0.05$

Curves using this method of extrapolation have been drawn and are presented in Fig. 3.23 for pressures of 1000, 1500 and 2000 psia. Extrapolation beyond these quality ranges should probably not be made on a linear basis, since there are indications that over a wide quality range slip is not a linear function of quality.

6. Working Curves for the Prediction of Steam Volume Fractions

Working curves for predicting slip ratios at any pressure can be made by extrapolating the data presented. Initially, working curves were prepared at 150, 250, and 600 psig by smoothing the velocity ratio data with respect to quality and velocity at each of the pressures. These curves represent an attempt to get the best smooth fit of the data at each pressure and are shown in Figs. 3.20, 3.21 and 3.22. Comparisons of the working curves with actual data at 600 psig and various qualities are shown in Figs. 3.25 to 3.27. Also, an error plot of all the ANL data at 600 psi is shown in Fig. 3.24, which serves to demonstrate the accuracy of the working curve.

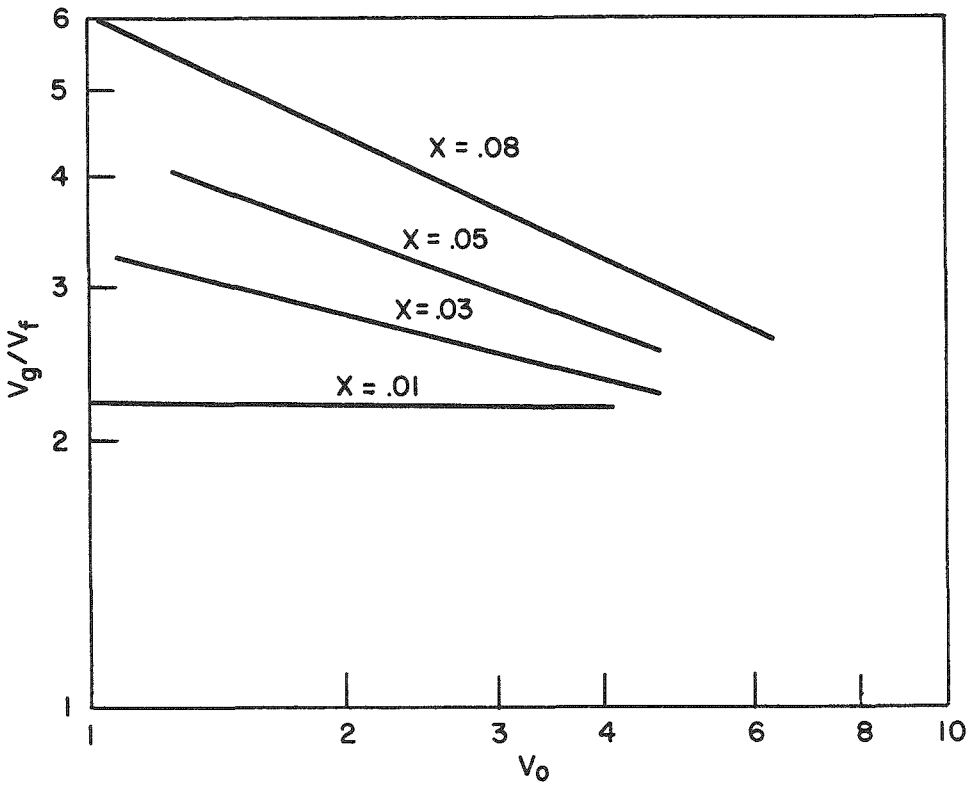

Fig. 3.20

Working Curve for Prediction of Velocity Ratios at 150 psig

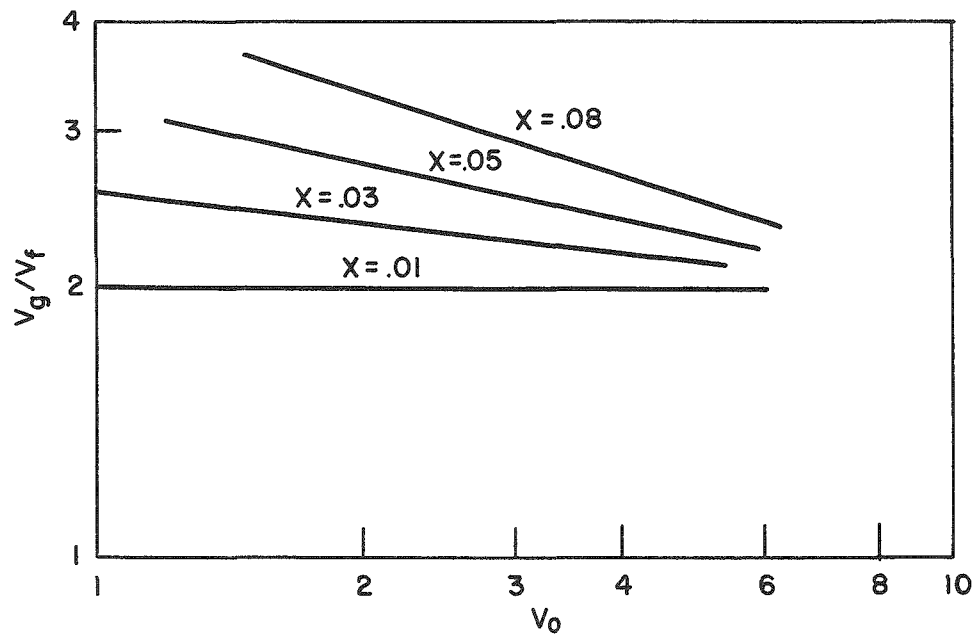

Fig. 3.21

Working Curve for Prediction of Velocity Ratios at 250 psig

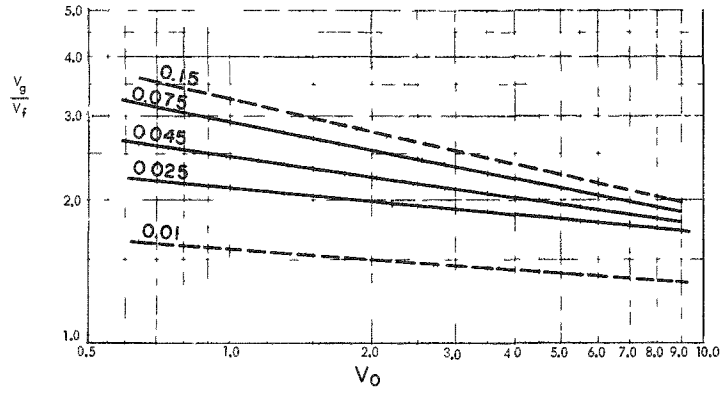

Fig. 3.22

Working Curve for the Prediction of Velocity Ratios at 600 psig

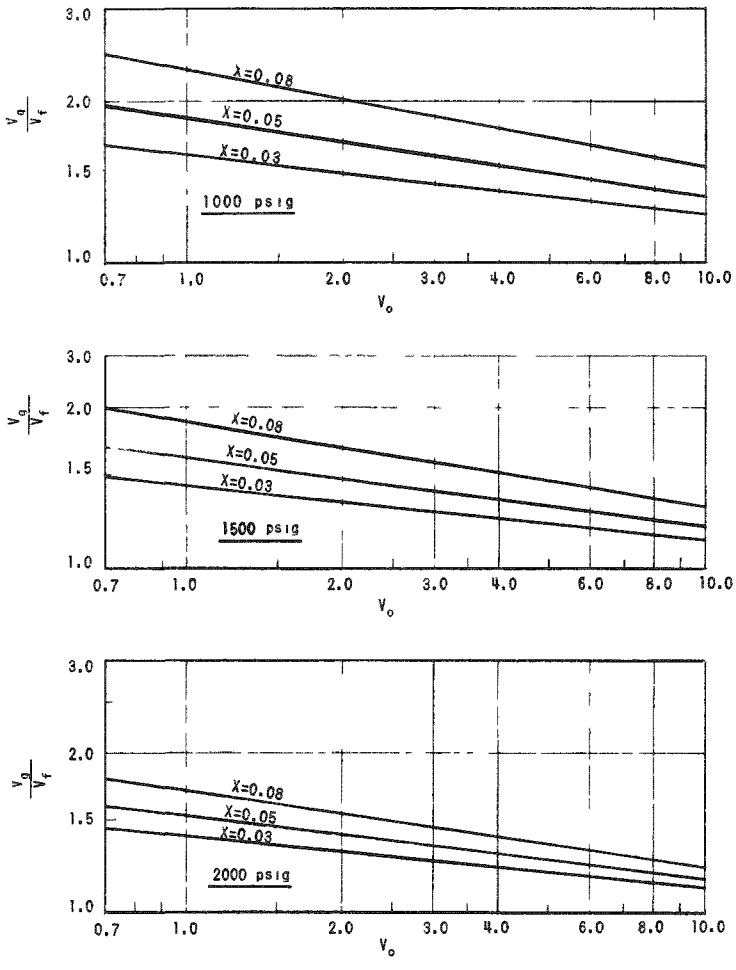

FIG. III.20

Fig. 3.23

Working Curves for the Prediction of Velocity Ratios at 1000, 1500, and 2000 psig

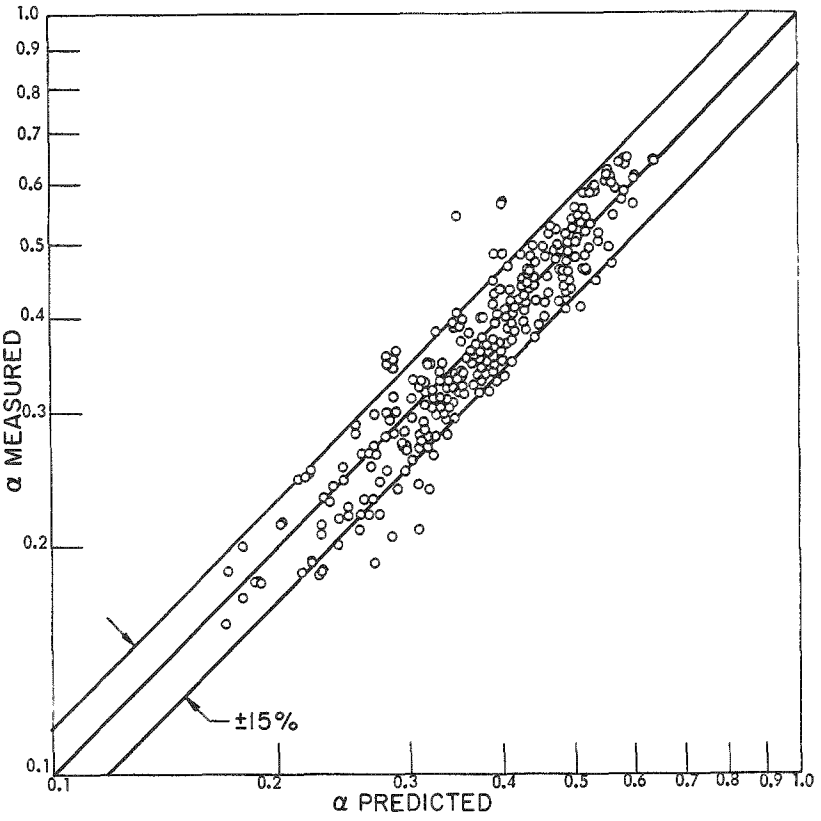

Fig. 3.24

Error Plot of Argonne 600-psig Data
Using Working Curve

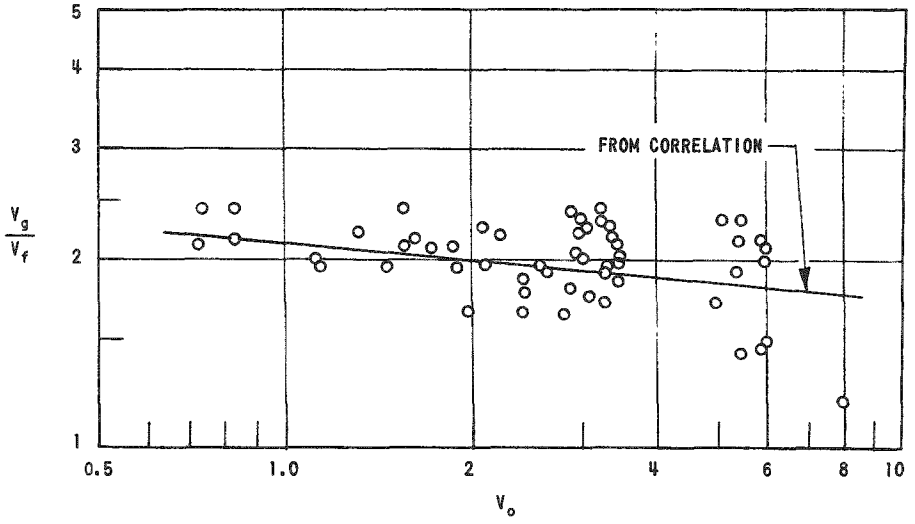

Fig. 3.25

Velocity Ratio as a Function of Superficial
Velocity at x = 0.022 at 600 psig
111-8432

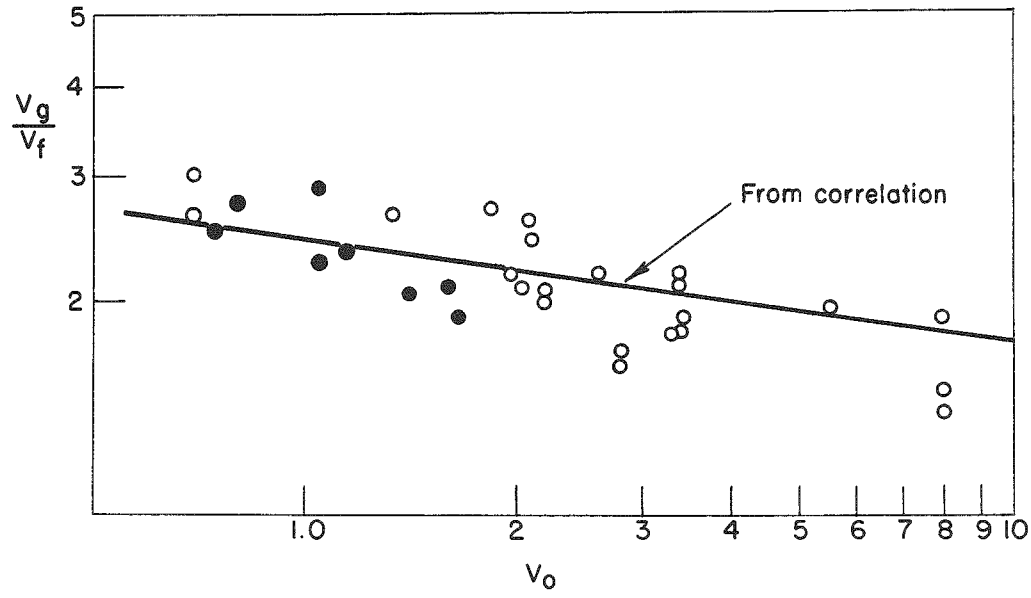

Fig. 3.26

Velocity Ratio as a Function of Superficial Velocity at 600 psig at x = 0.045

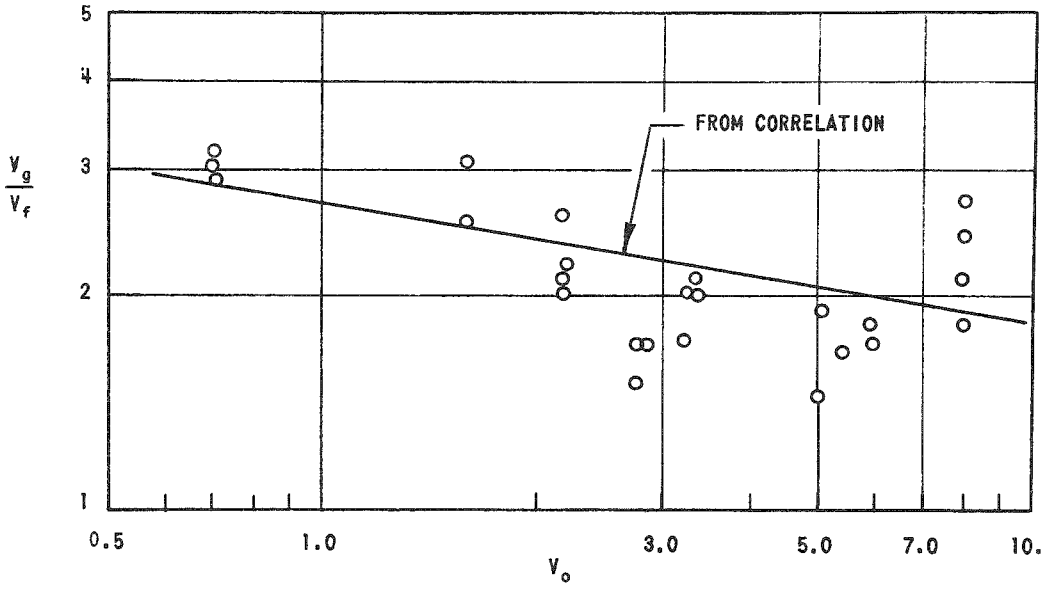

Fig. 3.27

Velocity Ratio as a Function of Superficial Velocity at x = 0.06 at 600 psig

111-8434

The 600-psig working curve (Fig. 3.22) and Fig. 3.19, which gives the variation of the velocity ratio as a function of pressure at $x \approx 0.05$ and $V_0 \approx 2$ ft/sec, can be used as a basis for predicting velocity ratios at the high pressures. From Fig. 3.19 the slip ratio is obtained at any pressure for $x \approx 0.05$ and $V_0 \approx 2$ ft/sec. This value represents the intercept of a velocity ratio-quality curve at these conditions. The slope of the curve can then be estimated from Fig. 3.16. The slope of the velocity effect can be assumed to vary with the density difference $(\rho_f - \rho_g)$ and can be extrapolated from the 600-psig data. Since the slopes are quite small (<0.25), a linear approximation may be adequate. Using extrapolated slopes for several qualities and the derived slip ratio-quality curve, a working curve at the pressure of interest can be drawn. An alternate, simpler method of drawing working curves would be possible if sufficient data were available to establish a family of curves of the type shown in Fig. 3.16.

7. Steam Volume Fractions in Subcooled Boiling

Steam volume fractions have been measured locally in the subcooled boiling region in $\frac{1}{4}$ x 2-in. and $\frac{1}{2}$ x 2-in. vertical channels. The volume fraction was found to be a function of the bulk water temperature, velocity, heat flux, pressure and channel dimensions. The effects of heat flux and velocity in a $\frac{1}{4}$-in. rectangular channel are shown in Figs 3.28 and 3.29. It can be seen that the steam volume fraction is dependent upon heat flux well into the net quality region. Because of this effect the data have been plotted as a function of $x + 0.02$ to give a continuous function through $x = 0$. Several methods of correlating the data have been attempted, but as yet no adequate correlation for the data has been found. One of the most promising is shown in Figs. 3.30 and 3.31. The steam volume fraction is correlated using $(x - x_c)$ as a parameter, where x_c is the negative quality at the inception of local boiling, defined as

$$x_c = C_p (T_f - T_i)/h_{fg} \quad .$$

These qualities were evaluated using the Jens and Lottes relation,[8]

$$\Delta T_{sat} = \frac{60(q''/10^6)^{0.25}}{e^{P/900}} \quad , \tag{3.6}$$

and the Colburn relation,

$$Nu = 0.023\, Re^{0.8}\, Pr^{0.4} \quad . \tag{3.7}$$

Missing Page
from
Original Document

Missing Page
from
Original Document

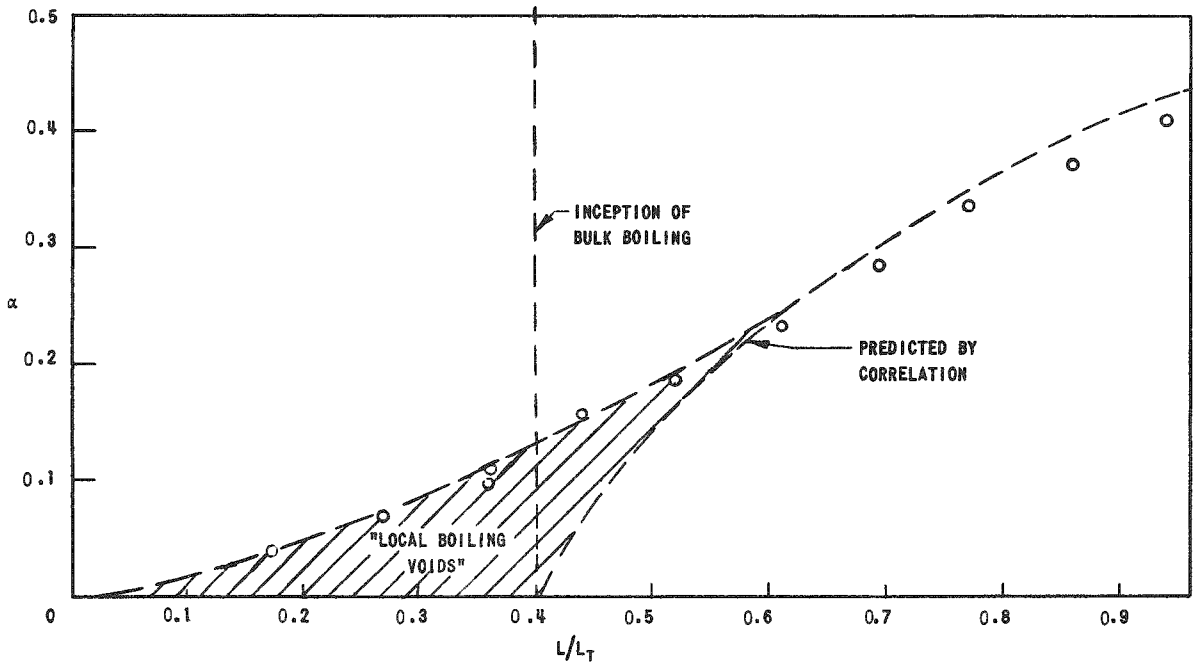

Fig. 3.32

Comparison of Predicted and Measured
Steam Volume Fractions at 600 psig
111-8439

3.7. Prediction of Average Steam Volume Fraction

The average density in a channel in which vaporization is taking place may be found as a function of pressure, slip ratio and exit steam volume fraction. For the case of a constant heat flux along the channel (if it is assumed that the slip ratio is constant along the heated length and that there is a uniform input),

$$\frac{\bar{\rho}_B}{\rho_f} = 1 - \frac{1 - \frac{\rho_g}{\rho_f}}{1 - x}\left\{1 - \left(\frac{1}{\alpha_e(1-x)} - 1\right)\left[\ln\frac{1}{1-\alpha_e(1-x)}\right]\right\} \qquad (3.9)$$

where $x = V_g \rho_g / V_f \rho_f$. For an axial cosine heat input, the average channel density ratio is

$$\frac{\bar{\rho}}{\rho_f} = 1 - \left(1 - \frac{\rho_g}{\rho_f}\right)\left[\frac{b'}{b} + \frac{a'b - ab'}{b(a^2-b^2)}\left(\frac{L_t}{L_B}\right)\left(1 - \frac{2}{\pi}\tan^{-1}\frac{\sqrt{a^2-b^2}\tan(\pi L_{NB}/2L_t)}{a+b}\right)\right] \qquad (3.10)$$

for $|a|$, $|b|$, and

$$\frac{\bar{\rho}}{\rho_f} = 1 - \left(1 - \frac{\rho_g}{\rho_f}\right)\left[\frac{b'}{b} - \frac{a'b-ab'}{\pi b\sqrt{b^2-a^2}}\left(\frac{L_t}{L_B}\right)\ln\frac{\sqrt{b^2-a^2}\tan(\pi L_{NB}/2L_t) + a+b}{\sqrt{b^2-a^2}\tan(\pi L_{NB}/2L_t) - a-b}\right] \tag{3.11}$$

for $|b| > |a|$

where

$$a = \frac{2}{\alpha_e} + b \qquad a' = 2 + b'$$

$$b = \left(1 - \frac{\rho_g V_g}{\rho_f V_f}\right)b' \qquad b' = -\frac{Q_t}{Q_B} = -\left(\frac{2}{1 - \cos\frac{\pi L_B}{L_t}}\right) .$$

These equations are shown graphically in Figs. 3.33, 3.34 and 3.35.

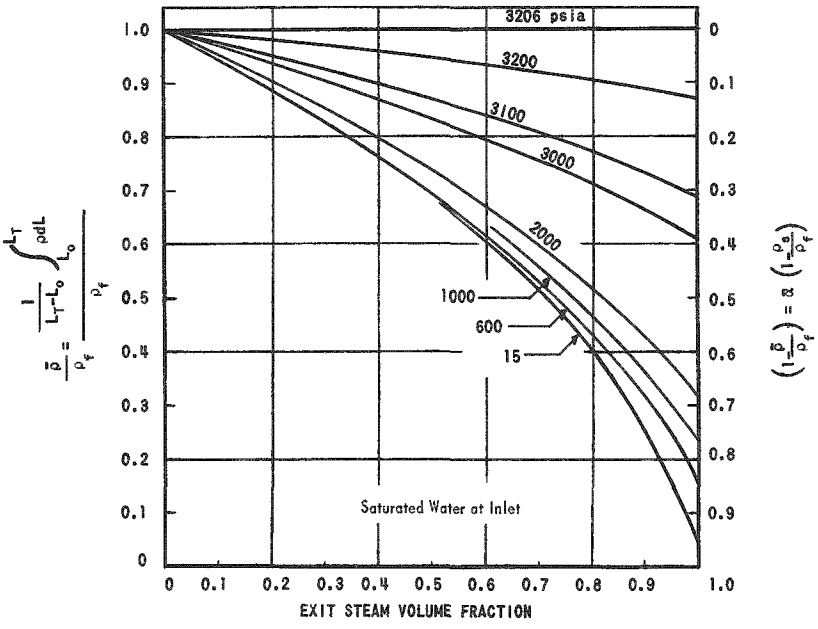

Fig. 3.33

Ratio of Mean Density in Vertical Boiling Channel to Liquid Density for Uniform Heat Generation and Slip Ratio of Unity $[(V_g/V_f) = 1]$

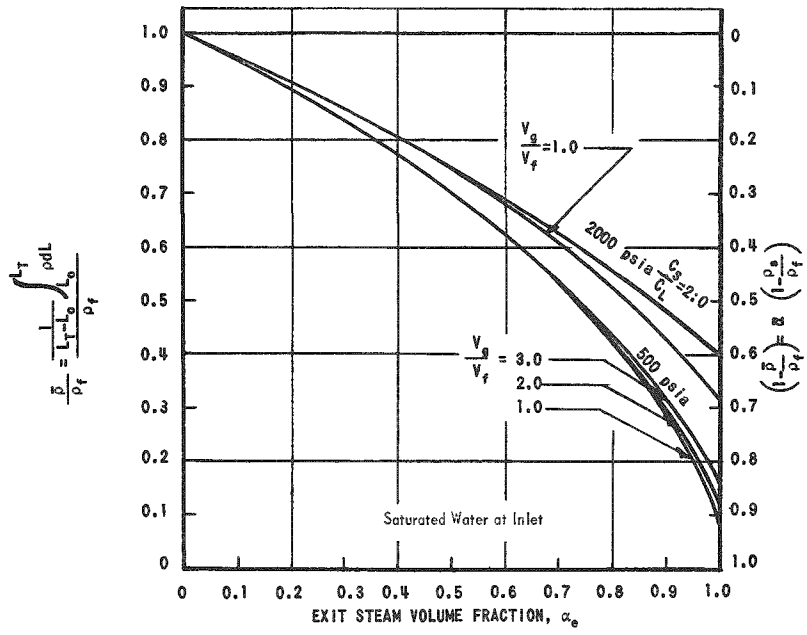

Fig. 3.34

Ratio of Mean Density in Vertical Boiling Channel to Liquid Density for Uniform Heat Generation, for Pressures of 500 and 2000 psia, slip ratio of 1 to 3

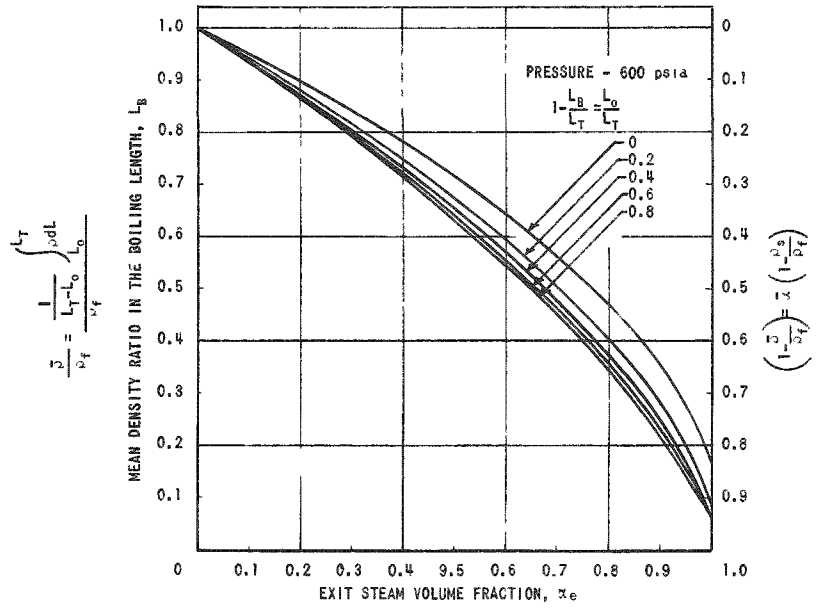

Fig. 3.35

Mean Density Ratio in Boiling Section of Vertical Channel as Function of Boiling Length Ratio for a Cosine Heat Input

Figure 3.36 shows a comparison between calculated and measured average volume fractions. These curves are slightly in error due to the assumption of a constant velocity ratio over the channel length but are adequate for design calculations, providing that the exit steam volume fraction of the boiling channel does not exceed 0.75. The exit steam volume fraction of the channel is estimated by using the working curves for velocity ratio presented in this paper, and the average steam volume fraction is then read off Figs. 3.33, 3.34 and 3.35. These curves are also in error since they neglect the volume fraction in local boiling. A more accurate density can be obtained for irregular flux distributions by calculating the steam volume fraction as length curve and graphically integrating.

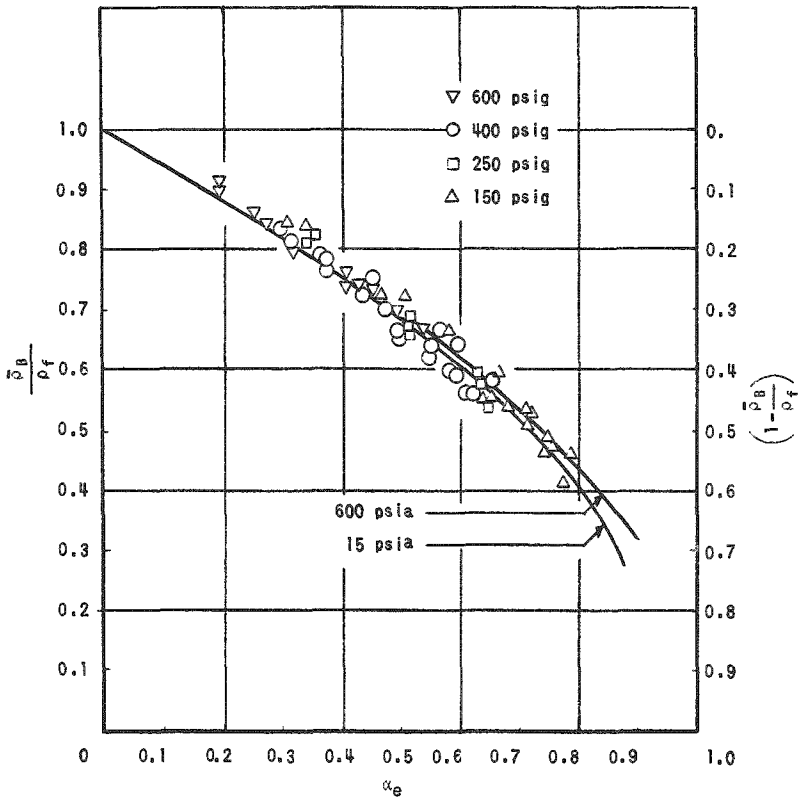

Fig. 3.36

Comparison of Calculated and Measured Average Volume Fractions

3.8. Conclusions

The conclusions from the two-phase density studies are:

(1) The working curves presented for the calculation of velocity ratios and hence steam volume fractions are adequate for engineering calculations and will predict steam volume fractions to within ±15%

(2) The curves presented, however, are derived from data taken from experiments on circular or rectangular, internally cooled channels. No significant work has been conducted on multi-rod geometries such as are of interest for current applications. Consequently there are possibilities for disagreement on the validity of interpolated results. However, it is believed that geometric differences will not affect results greater than within allowable limits of accuracy.

(3) The data presented show that slip ratio V_g/V_f is affected by mass velocity, pressure, and quality as follows:

(a) Slip ratio increases with increase in quality for any fixed pressure and mass velocity. However, the quality effect on the slip ratio appears to diminish with an increase in mass velocity.

(b) Slip ratio decreases with increase in mass velocity for any fixed pressure and quality. However, the magnitude of the velocity effect appears to decrease with decreasing quality and increasing pressure.

(c) Slip ratio decreases with increase in pressure for any fixed quality and mass velocity. The accuracy of void measurements tends to decrease with increasing pressure, especially in small width channels.

(4) Additional work is needed to determine effects of geometry, differences between adiabatic flow and boiling at high heat fluxes, and means of predicting steam volume fractions in the local boiling region.

4. TWO-PHASE PRESSURE DROP

4.1. Introduction

The reactor coolant, while flowing through the various reactor channels, will pass through several regions that are well defined by methods presently used for calculating the pressure drop. These regions are as follows:

1. Isothermal - Single Phase Region - The fluid properties are constant both across the channel and along its length.
2. Heating Region - In this region the fluid temperature is below saturation temperature. The heat transfer mechanism is that of forced convection and both the wall temperature and fluid temperature increase with length.
3. Local Boiling Region - The wall temperature remains fairly constant; the bulk liquid temperature is still below saturation temperature; the heat transfer mechanism is that of boiling in which bubbles are formed adjacent to the wall but collapse as they are swept into the subcooled liquid.
4. Bulk Boiling Region - The bulk fluid has reached saturation conditions and there is net steam generation.
5. Adiabatic Region - The two-phase mixture flows in unheated channels (fuel element extensions, risers or chimney, etc.) with negligible mass transfer between the phases.

The ability to predict the circulation rate in a boiling water reactor depends upon how accurately the pressure losses in these various regions can be evaluated. The major uncertainties are in the regions of two-phase flow.

A great deal of effort has been expended over the past fifteen years in an attempt to understand the mechanisms contributing to the pressure losses during the flow of a two-phase mixture consisting of a liquid and a gas (or vapor). A number of correlations, both theoretical and empirical, have been proposed. None, however, are general enough to provide an accurate calculation of two-phase pressure drop over a wide range of pressures, flow rates, and geometries.

As shown in Section 7, a momentum balance on the flowing mixture reveals that the total pressure drop along a channel is the sum of the hydrostatic head, the acceleration pressure drop, and the frictional losses.

$$\Delta P_t = \Delta P_H + \Delta P_{acc} + \Delta P_F \quad . \tag{4.1}$$

The frictional pressure drop term includes losses due to increased turbulence at flow expansions and contractions in addition to the usual wall shear stress losses.

Correlations providing an estimate of the frictional pressure drop in two-phase flow require experimental determination of the friction factor or friction factor multiplier (depending upon the correlation). The accuracy of these friction factors or multipliers is dependent upon subtracting the proper values for the hydrostatic head and acceleration pressure drop from the measured total pressure drop. Both the hydrostatic head and the acceleration pressure drop are dependent upon the vapor volume fraction, hereafter referred to as void fraction. Thus accurate determination of the local void fraction is essential if one is to obtain good frictional pressure drop data.

Accurate measurement of the void fraction is quite difficult and the difficulty increases with pressure. At the time of this writing very little steam-water pressure drop data[14,17,34,35] have been reported in which the void fractions were measured simultaneously with the pressure drop. Westinghouse[36] reports pressure drop data in which the void fractions were measured separately in a channel identical to the one they used for the pressure drop experiments.

A great number of investigators have successfully eliminated the void fraction variable from their two-phase pressure drop measurements by utilizing unheated, horizontal flow passages. The two phases are obtained by mixing two components, such as air-water, gas-oil, etc., or by mixing steam and saturated water. This approach eliminates the hydrostatic head and the acceleration pressure drop, so that the frictional pressure drop is measured directly. As more becomes known about two-phase pressure drop, it becomes apparent that this method leaves something to be desired. First, because of complex interaction between the two phases, it is generally admitted that the frictional losses should be a function of the two-phase flow pattern (bubble flow, plug flow, slug flow, annular flow, etc.), and since the flow patterns and relative velocity between the two phases differ somewhat in the horizontal and vertical channels, application of this data to vertical channels may be questioned. Secondly, one may question the application to boiling channels, where violent agitation exists at the walls, of two-phase pressure drop data obtained from unheated channels. The mechanisms are not understood and may be completely different. In defense of the many works that have been published to date, however, it must be admitted that the inherent experimental uncertainties encountered in two-phase pressure drop measurements have made separation of these effects extremely difficult if not impossible. Regardless of which experimental system is used, measurement of the void fraction is desirable as many investigators have found it to be an important parameter in the correlation of the frictional pressure drop data.

As mentioned previously, numerous investigations of two-phase flow phenomena have been undertaken. The significant aspects of most of these investigations have been compiled and discussed in several two-phase flow literature surveys.[16,37-40] The survey by Bennett[37] is the most recent and contains a tabulation of the authors with respect to the various phase systems, pipe size and orientation, and flow patterns. The survey by Gresham et al.[41] is the most comprehensive up to 1955, while Charvonia's survey[38] pertains mainly to annular flow of the type that would be encountered in "film cooling" of rocket motors, etc.

4.2. Status of Pressure Drop Correlations

In the following discussion the status of the pressure drop correlations for the regions listed above will be reviewed, calculational procedure will be recommended, and the areas of uncertainty that need additional investigation will be discussed.

1. Isothermal - Single Phase Region

The procedure for calculating single-phase, isothermal pressure drop is well established. The frictional pressure drop is expressed as:

$$\Delta P_F = f_{iso} \frac{L}{D_e} \frac{G^2}{\rho 2 g_c} \quad . \tag{4.2}$$

The friction factor, f_{iso}, has been determined experimentally and the most widely accepted correlation, $f_{iso} = \phi[(D_e G/\mu , \epsilon/D_e)]$ is that of Moody.[42] The hydrostatic pressure drop is equal to

$$\Delta P_H = \rho L \tag{4.3}$$

and the expansion and contraction losses are proportional to the kinetic energy

$$\Delta P_{acc} = K \frac{G^2}{\rho 2 g_c} \tag{4.4}$$

in the smallest pipe of the expansion or contraction. The proportionality constant (loss coefficient) is best presented by Kays.[45]

2. Heating Region

When a fluid is being heated, the temperature difference between the surface and fluid results in a transverse variation of the fluid properties, primarily the viscosity. This produces a friction factor that is less than the isothermal friction factor when the Reynolds Number is evaluated at the mixed mean fluid temperature. Three methods have

been proposed for correcting the isothermal friction factor for use in the heated region.

Sieder and Tate[44] suggested the following correlation as a result of heating and cooling petroleum oils:

$$f/f_{iso} = \left(\frac{\mu_w}{\mu_B}\right)^{0.14} \quad . \tag{4.5}$$

More recent work by Petukhov and Muchnik,[45] in which water and two types of oil were heated in long tubes with $3.3 \times 10^3 < Re < 2.5 \times 10^5$; $0.3 < \mu_w/\mu_B < 38$; $1.3 \quad Pr < 178$ produced the same correlation. Kreith and Summerfield[46] obtained the same correlation with an exponent of 0.13 for water flowing in a tube.

Deissler[47] approaches the problem by providing a correlation for the reference temperature, $T_B \leq T_x < T_w$, at which the viscosity in the Reynolds Number should be calculated. Curves of the isothermal friction factor are then used with this "corrected" Reynolds Number.

Sher[36] measured the heating pressure drop in 0.097 in. x 1.0 in. and 0.050 in. x 1.0 in. rectangular channels at 1100 and 2000 psia and found that the friction factor ratio was best correlated by

$$f/f_{iso} = 1 - 0.0025(\Delta T_{D-B}) \tag{4.6}$$

over the range

$$400 \leq T_B \leq 636 \ ^\circ F$$

$$0 \quad \Delta T_{D-B} \leq 100^\circ F \quad .$$

This correlation gives lower friction factor ratios (generally less than 20 per cent lower) than does Eq. (4.5). Sher's data is the only data available for pressures above 150 psia.

Considering the agreement of several independent investigators over a wide range of variables the recommended correlation for f/f_{iso} is given by Eq. (4.5) where f_{iso} is evaluated at the bulk fluid temperature. The <u>frictional</u> pressure drop across the heated region is calculated by

$$\Delta P_F = \bar{f} \frac{L}{D_e} \frac{G^2}{\rho_o g_c} \tag{4.7}$$

where $\bar{f} = f_{iso}\,(f/f_{iso})$ evaluated at the average bulk temperature for $T_B > 200°F$,

and

$$\bar{f} = \frac{I}{L}\int_0^L f_{iso}\left(\frac{f}{f_{iso}}\right)dz \qquad \text{for} \qquad T_B < 200°F \quad .$$

This correlation will provide a more conservative analysis (higher ΔP or lower circulation rate) than Eq. (4.6). While the difference between Sher's correlation and the viscosity ratio correlation is not great, additional pressure drop data for heat addition to water at higher pressures would be useful in establishing the best correlation to use for these conditions.

The hydrostatic pressure drop is evaluated from Eq. (4.3) with the density evaluated at the average bulk temperature for pressures less than 2500 psia, and

$$\bar{\rho} = \frac{1}{L}\int_0^L \rho dz$$

for pressures greater than 2500 psia.

The acceleration pressure drop in the heated region is calculated from

$$\Delta P_{acc} = \frac{G^2}{g_c}\left(\frac{1}{\rho_2} - \frac{1}{\rho_1}\right) \quad . \tag{4.8}$$

3. Local Boiling Region

The end of the heating region and beginning of the boiling region is established by the method described in Section 7. The local boiling region extends from this point to the point where a heat balance shows that the coolant has reached saturation conditions.

Very little work has been done on local boiling pressure drop. Only three correlations are known to exist. These correlations were obtained in such a way that it is virtually impossible to compare them or to extrapolate them to systems that differ from the experimental systems. There are no known theoretical investigations of local boiling pressure drop.

Reynolds[48] obtained data from a $\frac{3}{8}$ in. I.D. x 6 ft., uniformly heated, horizontal, stainless steel tube with $1.3 \times 10^5 \leq q'' \leq 3.04 \times 10^5$ Btu/hr-ft^2; $7 \leq V_0 \leq 10.6 f_{ps}$; $45 \leq P \leq 100$ psia, and exit water

temperature less than saturation temperature. The data was correlated by

$$\Delta P_{LB} = \left(\frac{dP}{dL}\right)_0 \frac{GD_e C_p (\Delta T_{sub})_0}{4aq''} \sinh\left[\frac{4aq'' L}{GD_e C_p (\Delta T_{sub})_0}\right] \qquad (4.9)$$

where $a = 1.2 + 4.6\ (q''/10^6)$.

It should be noted the correlation was obtained by measuring local pressure differentials, hence the data included not only frictional pressure drop, but also the acceleration pressure drop caused by the bubbles formed on the walls. Reynolds states that this correlation predicted the data of Buchberg et al.[49] within 50 per cent for heat fluxes up to 500,000 Btu/ft^2. Above this heat flux the correlation did not agree with the data.

Buchberg et al.[49] obtained their data from a vertical, uniformly heated, stainless steel tube, 0.226 in. I.D. x 24.6 in. long. The overall pressure drop was measured with the pressure taps located $3\frac{1}{2}$ tube diameters beyond the effective heated length. With this system there were no bubbles on the wall at the position of the pressure tap and the bubbles that had been swept into the stream would have condensed or greatly diminished in size by the time they reach the pressure tap location. Hence, the acceleration pressure drop component is not included in the overall pressure drop. This difference in the data (Reynolds' and Buchberg's) is negligible at high subcoolings but becomes increasingly important as saturation conditions are approached.

Rohde[50] correlated the data of Buchberg et al. for

$$250 \le P \le 2500 \text{ psia} \quad ; \quad q'' < 2 \times 10^6 \text{ Btu/hr-ft}^2 \quad ;$$

$$5 \le V_0 \le 30 \text{fps} \quad ; \quad 35 \le \Delta T_{sub} \le 235^\circ\text{F}$$

with a deviation of ± 40 per cent; he also correlated some Argonne National Laboratory data for P = 500 psia, $1 \times 10^6 \le q'' \le 1.5 \times 10^6$ Btu/hr-ft^2, in a uniformly heated, vertical, stainless steel tube, 0.175 in. I.D. x 24 in. long with a deviation of + 18 per cent and - 28 per cent by

$$(\Delta P/\Delta L)_{LB} \Big/ (\Delta P/\Delta L)_{HEAT} = R_q^{250/P} \quad . \qquad (4.10)$$

(Note: the local boiling pressure gradient is divided by the pressure gradient while heating rather than the isothermal pressure gradient.) The ratio, R_q, was meant to be a qualitative measure of the number of bubbles on a channel wall; i.e., the greater the ratio, the greater the number of bubbles present.

In an attempt to make his correlation applicable to channels with nonuniform heating, Rohde rederived his correlation, Eq. (4.10) in terms of an average ratio, $(R_q)_{avg}$,

$$(\Delta P/\Delta L)_{LB}/(\Delta P/\Delta L)_{HEAT} = \exp\left\{\frac{384}{P}\left[(R_q)_{avg} - 1\right]\right\} \qquad (4.11)$$

where for uniform heating

$$(R_q)_{avg} = \frac{\ln (R_q)_{exit}}{1 - 1/(R_q)_{exit}} \quad \text{for} \quad (R_q)_{in} \leq 1$$

$$= \frac{G\, D_e}{4 L h_{D-B}} \ln\left[\frac{T_w - T_{in}}{T_w - T_e}\right] \quad \text{for} \quad (R_q)_{in} > 1 \quad .$$

For nonuniform heating, the channel is to be divided into increments, local values of R_q determined, and these values integrated to obtain the average R_q which is used in Eq. (4.11). This in essence is calculating the pressure gradient ratio at an "average" position in the channel rather than calculating an average pressure gradient ratio. The use of this method for nonuniform heat input is quite difficult and time consuming and the results have never been checked against data.

Weatherhead[51] obtained local boiling pressure drop data at 600 psia in vertical, round and rectangular, nickel channels of essentially the same equivalent diameter. The pressure taps were beyond the heated length so that there was no acceleration pressure drop component. The hydrostatic head was calculated with the average liquid density. He found that Reynolds' and Rohde's correlation fitted the circular tube data equally well but that the rectangular channel was best correlated by Rohde.

Sher[36] has reported local values of the local boiling frictional pressure gradient in vertical rectangular channels, 0.097 in. x 1.0 in. x 27 in. and 0.050 in. x 1.0 in. x 27 in., at 2000 psia. Local void fractions were measured and the hydrostatic head and acceleration pressure drop were calculated assuming zero relative velocity between the phases. It was found that f/f_{iso} increased with increasing heat flux, increasing bulk temperature, decreasing static pressure, and decreasing mass velocity. He reported no significant difference for the two channel spacings. From the results of his tests, Sher concludes that if and when methods of predicting void fractions in the local boiling region become available the local boiling frictional pressure gradients may be handled in exactly the same manner as in bulk boiling. He found that at 2000 psia a plot of (f/f_{iso}) vs a fictitious quality (evaluated with the local boiling voids and an assumed slip ratio of one) gave nearly the same correlation as a similar plot of bulk boiling data.

In the absence of local boiling void data the following correlation was recommended for rectangular channels at 2000 psia.

$$f_{LB}/f_{iso} = (1-0.0025\ \Delta T^*)\left[1 + 0.76\left(\frac{G}{10^6}\right)^{2/3}\psi\right] \qquad (4.12)$$

where

$$\Delta T^* = \Delta T_f \quad \text{when} \quad \Delta T^* \leq \Delta T_f$$

$$= T_{sat} + \frac{60\,(q''/10^6)^{0.25}}{e^{P/900}} - T_B \quad \text{when} \quad \Delta T^* > \Delta T_f$$

$$\psi = 1 - \frac{\Delta T^*}{\Delta T_f}$$

$$\Delta T_f = 0.766\ q''/h_{D-B} \quad .$$

The first bracket represents the heating effect in the local boiling region and the ratio $\Delta T^*/\Delta T_f$ is a function of the single phase to the local boiling heat transfer coefficient.

It should be noted that Sher's correlation and Rohde's correlation are similar in that they both recognize a heating effect in the local boiling region and they both use parameters that are qualitative expressions of the relative agitation caused by local boiling. Rohde, however, did not report a mass velocity effect.

Costello[34] has recently reported a small amount of local boiling pressure drop data from a vertical annulus at atmospheric pressure. The local boiling void fractions were measured. No correlation was given however.

No general correlation for <u>frictional</u> pressure drop in the local boiling region can be recommended at this time. If the available data is not applicable to the system in question, the only recourse is to use this data to make an "educated" guess of the local boiling friction factor multiplier. Within the accuracy of the available data, the <u>frictional</u> pressure drop may be calculated from

$$\Delta P_{LBF} = \bar{R}_{LB}\, f_{iso} \frac{L_{LB}}{D_e} \frac{G^2}{\rho 2 g_c} \qquad (4.13)$$

where $\bar{R}_{LB}$ is an estimated average friction factor multiplier and all properties are evaluated at an average bulk temperature.

Evaluation of the <u>hydrostatic head</u> in the local boiling region presents the largest uncertainty in calculating the total local boiling pressure drop because the hydrostatic head is usually the most significant component of the total pressure drop. The uncertainty arises because of the

unknown void distribution. The usual approach has been to assume that all bubbles remain on or near the walls and that solid liquid core remains in the center. The average density of this liquid column is then used in Eq. (4.3). This assumption obviously breaks down for small channels and near the end of the local boiling region where saturation conditions are being approached. Egen et al.[31] have reported void fractions as great as 25 per cent at the saturation point at 2000 psia. Measurements at Argonne National Laboratory have shown similar void fractions at 600 psia and below, and traverses across the channel show definitely that all of the voids are not on the wall in this region. Photographs by Costello[34] give an excellent illustration of this problem. Until local boiling void fractions and their distribution can be predicted, however, the previously mentioned assumption should be used as it will result in conservative answers.

The acceleration pressure loss in the local boiling region results from, (1) the changing liquid density as the temperature increases, and (2) the formation of steam bubbles which reduce the liquid flow area. The portion resulting from changing liquid density may be calculated by Eq. (4.8), but the portion resulting from bubble formation cannot be predicted because of the inability to calculate local boiling void fractions. This inability only affects prediction of the local pressure drop. The expression used to calculate acceleration pressure drop in the bulk boiling region calculates the pressure drop due to all of the voids that have been formed, thus the pressure drop due to bubble formation in the local boiling region is considered in the overall pressure loss.

4. Bulk Boiling Region

In most boiling water reactors prediction of the frictional pressure drop in the bulk boiling region is significantly more important than in the local boiling region because the bulk boiling region usually occupies a greater portion of the heated channel and, for the same flow rate and heat flux, the pressure gradients are much larger. The various mechanisms that produce this increased pressure gradient have not been completely isolated. Many of the models that have been proposed give a qualitative correlation but quantitative agreement is presently available for only limited ranges of the parameters.

A number of investigators have observed and reported various two-phase flow patterns (bubble, plug, froth, annular, etc.) at low pressures, with and without vaporization, in both horizontal and vertical channels. Several flow pattern correlations are available for horizontal, adiabatic flow.[52-55] Kozlov[56] and Galegar et al.[57] have proposed correlations for vertical, adiabatic two-phase flow; however, no correlations are available for flow with vaporization. There is considerable disagreement among most of the correlations. The disagreement is due largely to the fact that even in adiabatic two-phase flow the flow pattern regimes are not distinct; the transition from one flow pattern to the next takes place over a range of variables. Bennett[28]

states that observations on fluids boiling in vertical channels indicate that the flow patterns are even less clearly defined than the adiabatic flow patterns due to the agitation induced by the steam generation. The prediction of flow patterns in a boiling mixture appears impossible for some time to come.

It is intuitive that the frictional pressure gradient should depend upon the two-phase flow pattern since the relative turbulence of the phases, the interfacial shear, and the momentum interchange between the phases vary with the flow pattern. A number of investigators have observed this flow pattern effect in adiabatic two-phase flow where the flow pattern persists for the entire channel length. Hoopes,[58] Dengler[14] and Sher[36] reported inflections in plots of the frictional pressure gradient vs length in boiling channels. It is believed these changing pressure gradients reflect flow pattern changes although Sher attributed it to the method used in calculating the hydrostatic head. While flow patterns have been established as an important parameter in two-phase pressure drop, the difficulty in observing and correlating these flow patterns has forced investigators to neglect them in all bulk boiling pressure drop correlations now available.

The presently available two-phase frictional pressure drop correlations differ mainly in whether the two phases are treated as a homogeneous mixture or whether the slippage (relative velocity) between the phases is recognized. Two methods of expressing the frictional pressure drop have evolved; (1) a friction factor, defined in a manner analogous to the single phase friction factor, is calculated from the two -phase pressure gradient, or (2) a dimensionless ratio is formed by dividing the two-phase pressure gradient by the liquid phase pressure gradient evaluated at the total mixture flow rate. With the exception of some of the earlier works, practically all of the boiling pressure drop correlations have used the dimensionless pressure gradient ratio.

The Martinelli-Nelson[59] pressure drop correlation, Fig. 4.1 for boiling water is the best known and probably the most widely used "general" correlation available. The correlation has been verified by a number of investigators.[35,60-62] However, one major weakness of the Martinelli-Nelson correlation is that it does not provide an apparent flow rate dependency which has been reported in several adiabatic pressure drop studies and reported also by Sher[36] for flow with vaporization

The Martinelli-Nelson boiling pressure drop correlation is an extension of a semi-empirical correlation developed by Martinelli and co-workers[63] and modified by Lockhart and Martinelli.[64] The correlation was based on data for adiabatic, two-component mixtures in horizontal flow at essentially atmospheric pressure with both phases in turbulent flow. (Turbulent flow was defined by the phase Reynolds Number

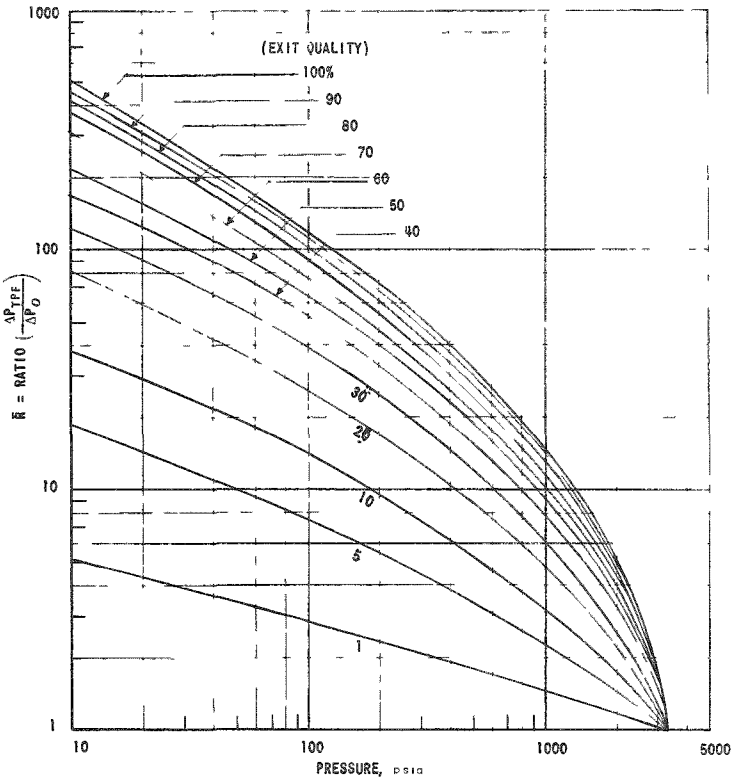

Fig. 4.1

Martinelli Average Two-Phase Friction Multiplier (Uniform Heat Input)

being greater than 2000 when the phase velocity is based on the total pipe area). The original correlation by Martinelli, for adiabatic flow, was based on two main assumptions:

1. The static pressure drop of the two phases must be equal regardless of the flow pattern.
2. The volume occupied by the liquid plus the volume occupied by the gas at any instant must be equal to the total volume of the pipe.

These assumptions infer that the flow pattern does not change with length, thus ruling out "slug" flow and stratified flows with transverse pressure gradients. Primarily it limits the correlation to annular flow. With these assumptions and their experimental data they arrived at a correlation between ϕ_{Ltt}, the square root of the ratio of the two-phase frictional pressure gradient to the frictional pressure gradient if the liquid alone were flowing in the pipe, and χ_{tt}, a nondimensional correlating parameter for turbulent-turbulent flow. The quantity χ_{tt}, may be expressed as

$$\chi_{tt} = \frac{(1 - x)}{x}\left(\frac{\rho_g}{\rho_L}\right)^{0.571}\left(\frac{\mu_f}{\mu_g}\right)^{0.143} \quad . \tag{4.14}$$

Assuming linear variation of the quality in the heated channel, Martinelli plotted the ratio of $(dP/dL)_{TPF}/(dP/dL)_0$ vs x and integrated to obtain $\Delta P_{TPF}/\Delta P_0$ for any given exit quality. Considering the limits imposed on ϕ_{Ltt} at the critical pressure, it was evident that a pressure parameter was required. Using the data of Davidson et al.[65] to obtain this pressure dependence, new curves of ϕ_{Ltt} vs χ_{tt} were obtained and integrated to give the correlation shown in Fig. 4.2. Figure 4.3 shows a comparison of this correlation with data obtained at Argonne.[35]

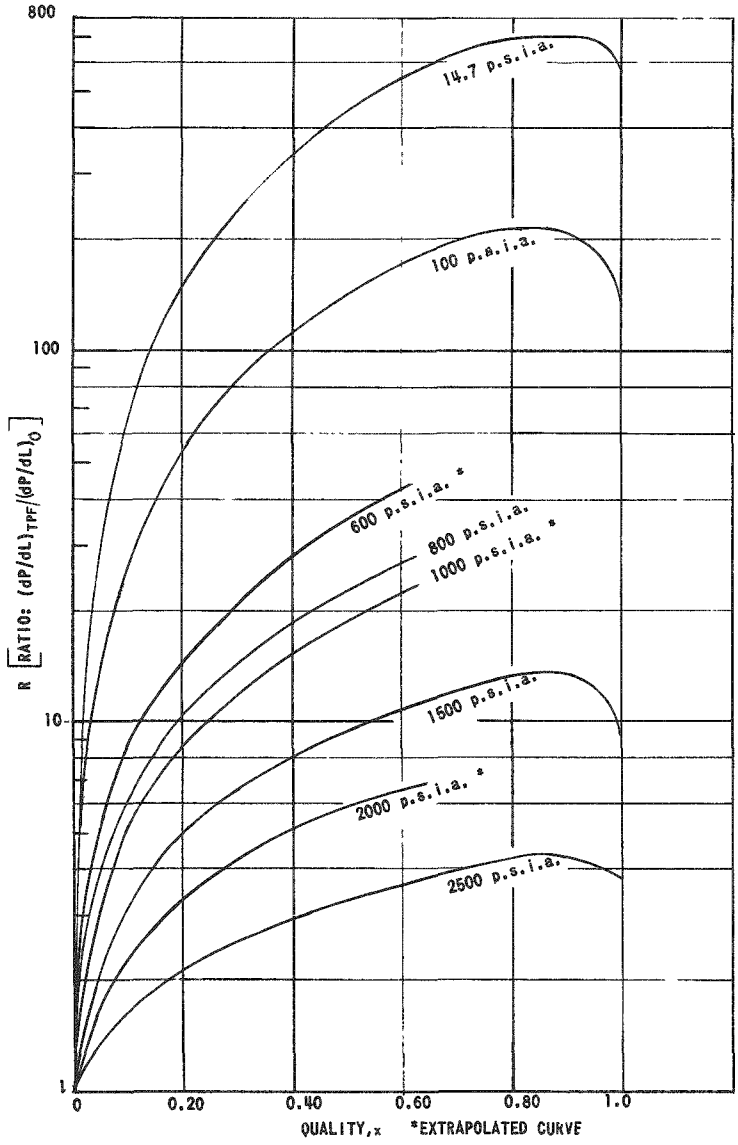

Fig. 4.2

Martinelli Local Two-Phase Friction Factor vs Quality

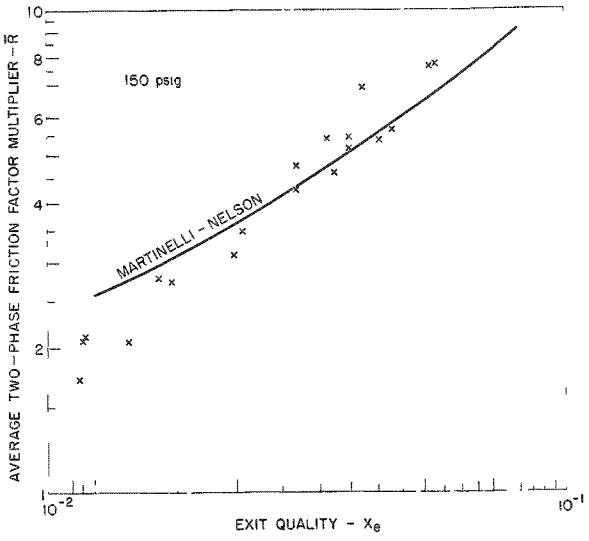

700-431-A

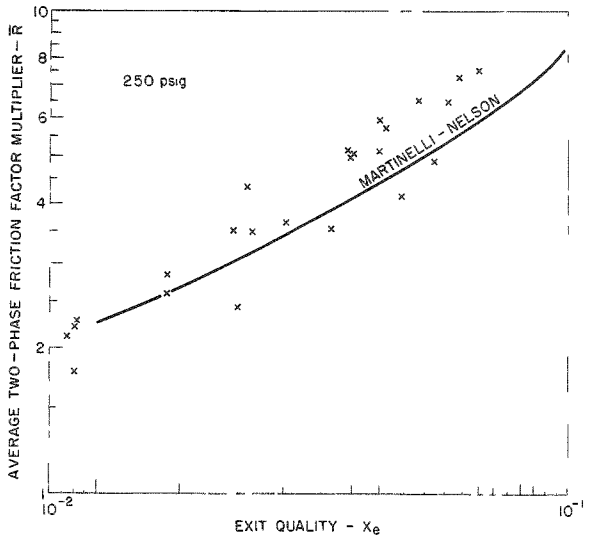

700-431-B

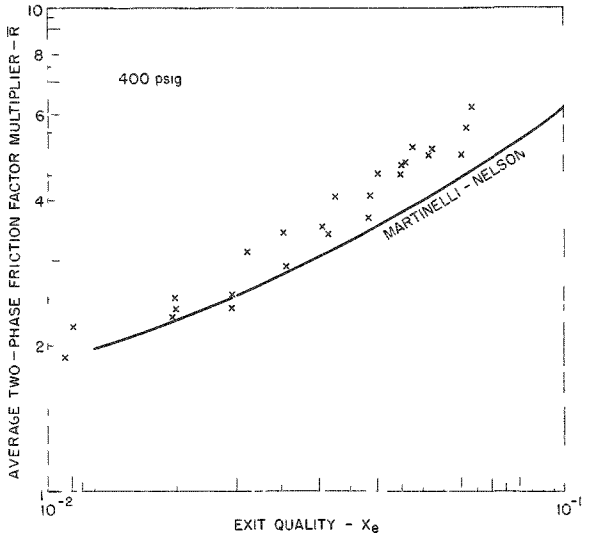

700-431-C

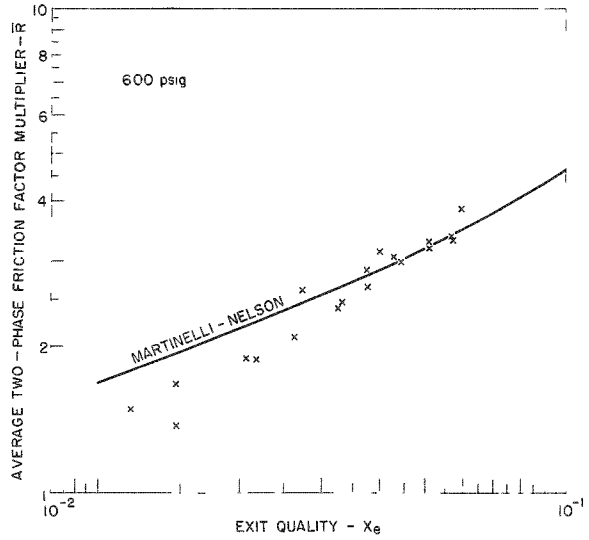

700-431-D

Fig. 4.3

Comparison of $\frac{1}{4}$ in. x 2 in. x 5 ft Vertical Channel Boiling Data with Martinelli-Nelson Correlation

Martinelli and Nelson[59] are the only investigators that have attempted to apply isothermal pressure drop data to flow with vaporization. As pointed out by Isbin,[66] the assumption of equal static pressure drop for both phases was actually equal to frictional pressure drop for both phases in the original Martinelli-Nelson derivation. Extending this correlation to flow with vaporization, where the static pressure drop for each phase would include momentum and possible head terms as well as friction, is questionable because the frictional pressure drop of the two phases could hardly be equal. It is truly amazing that the Martinelli-Nelson correlation has been so successful in view of the assumptions that were made and the data that were available at the time of its development.

Dengler,[14] Schrock and Grossman,[67] and Stein et al.[68] have obtained local two-phase frictional pressure gradients from boiling channels. Dengler's data and the data of Schrock and Grossman were obtained in vertical tubes, 0.645 in. I.D. and $\frac{1}{8}$ in. I.D., respectively. Stein's data were obtained in a vertical, 1.08 in. I.D. - 1.33 in. O.D. annulus, with downflow. These local gradients were correlated with the parameters introduced by Lockhart and Martinelli[64] and compared with the Lockhart-Martinelli correlation for horizontal, isothermal two-phase flow. The data of Schrock and Grossman agreed reasonably well while the data of Stein and Dengler tended to be higher.

Lottes and Flinn[19] proposed an annular flow model for boiling water in uniformly heated channels which was essentially the same as the Martinelli-type flow model with the exception that it was described in terms of the steam volume fraction rather than the steam weight fraction. It was proposed that the increased friction in two-phase flow was due to the increase in the local liquid velocity. The local liquid velocity was related to the inlet velocity by

$$\frac{V_f}{V_{in}} = \frac{1 - x}{1 - \alpha} \quad . \tag{4.15}$$

A mass balance shows

$$\frac{V_g}{V_f} = \left(\frac{x}{1 - x}\right)\left(\frac{1 - \alpha}{\alpha}\right)\frac{\rho_f}{\rho_g} \quad . \tag{4.16}$$

The ratio of steam to water velocities was assumed constant along the channel and the pressure and friction factors were assumed constant, thus the velocity ratio becomes a linear function of the quality

$$\frac{V_f}{V_{in}} = 1 + \left(\frac{\rho_f}{\rho_g}\,\frac{V_f}{V_g} - 1\right) x \quad . \tag{4.17}$$

The average friction factor was defined as

$$\bar{R} = \frac{1}{L_B}\int_0^{L_B} \frac{(dP/dL)_{TPF}}{(dP/dL)_0}\, dz = \frac{1}{L_B}\int_0^{L_B} \left(\frac{V_f}{V_{in}}\right)^2 dz \quad . \qquad (4.18)$$

Integrating over a uniformly heated channel gave

$$\bar{R} = \tfrac{1}{3}\left[1 + \frac{1}{1-\alpha_e(1-\phi)} + \left(\frac{1}{1-\alpha_e(1-\phi)}\right)^2\right] \qquad (4.19)$$

where

$$\phi = \left(\frac{V_g}{V_L}\right)\left(\frac{\rho_g}{\rho_L}\right) \quad .$$

For small qualities and low pressures, Eq. (4.19) reduces to

$$\bar{R} = \tfrac{1}{3}\left[1 + \frac{1}{1-\alpha_e} + \left(\frac{1}{1-\alpha_e}\right)^2\right] \quad . \qquad (4.20)$$

A comparison of this correlation with pressure drop data obtained at Argonne National Laboratory[35] in which the local void fraction was measured is shown in Fig. 4.4. The experimental data were approximately 30 per cent higher than the correlation; however, the trend of the data shows a dependence upon the void fraction for voids less than 0.65, quite similar to that expressed by the flow model. Plotting $\bar{R}$ against the void fraction also appears to eliminate the pressure parameter, at least for pressures up to 600 psi.

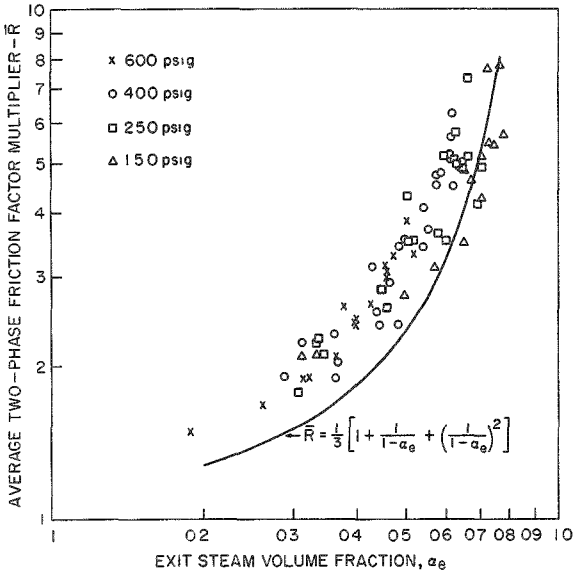

Fig. 4.4

Comparison of Argonne Data with Lottes Correlation

As mentioned above, the average two-phase friction multiplier displays a dependence upon the void fraction that is quite similar to the Lottes-Flinn correlation. On the other hand, this correlation does not exhibit a flow rate dependency that is apparently needed and it has been shown[35] that this correlation gives $\bar{R}$'s that are definitely too large at the higher void fractions.

Sher[36] reports a mass velocity effect on the local friction multiplier for boiling in vertical rectangular channels, 0.097 in. and 0.050 in. by 1.0 in., at 2000 psia, and presents his correlation in the form of a graph, Figure 4.5. The following method was suggested for applying the mass velocity parameter established at 2000 psia to lower pressures:

(1) Use the Martinelli-Nelson correlation to obtain the ratio of ϕ^2_{LO} at the pressure of interest to ϕ^2_{LO} at 2000 psia, as a function of x.

(2) Multiply the ordinate of Fig. 4.5 by this ratio for corresponding qualities to obtain a new family of curves.

(3) Integrate the curve of interest from zero to the exit quality to obtain the average value of the two-phase friction multiplier.

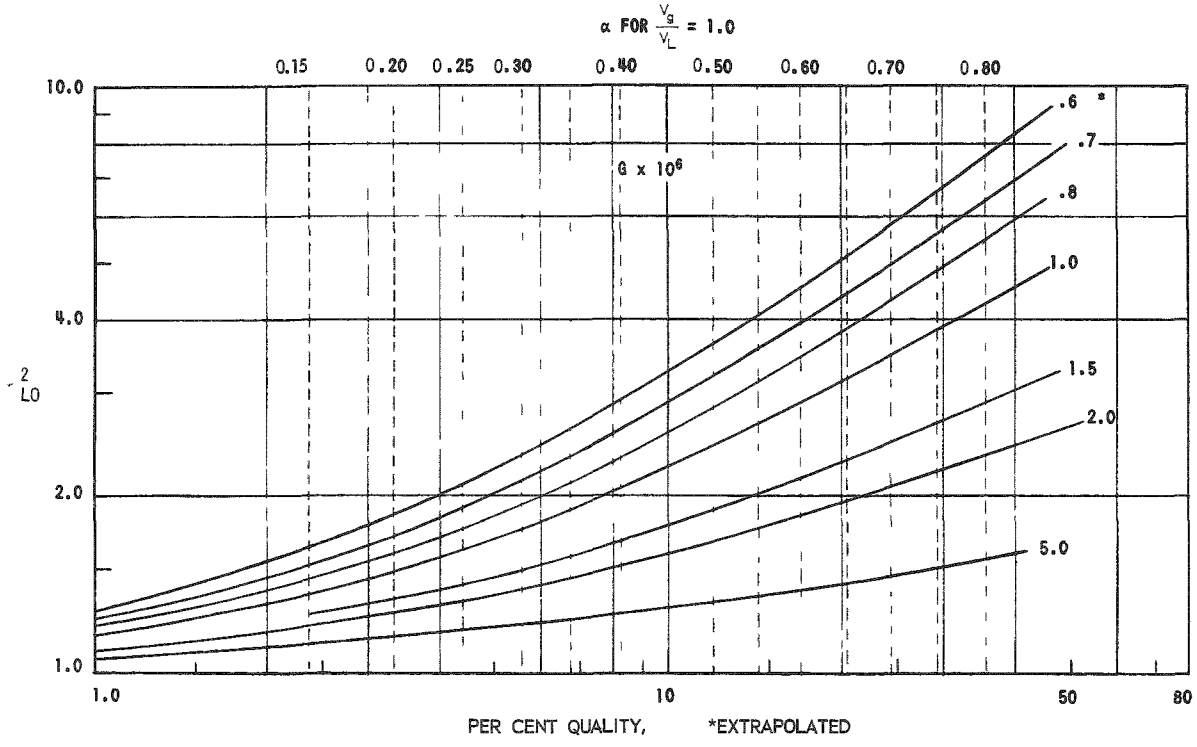

Fig. 4.5

Sher Two-Phase Pressure Drop Data

A comparison of this method with the Argonne data which was obtained at essentially a constant mass velocity of 0.6 x 10^6 lb/hr-ft^2, is shown in Fig. 4.6. It may be seen that Sher's mass velocity parameter is adequate for these low qualities and pressures and provides a better prediction of the data than does the Martinelli-Nelson correlation alone, Fig. 4.3.

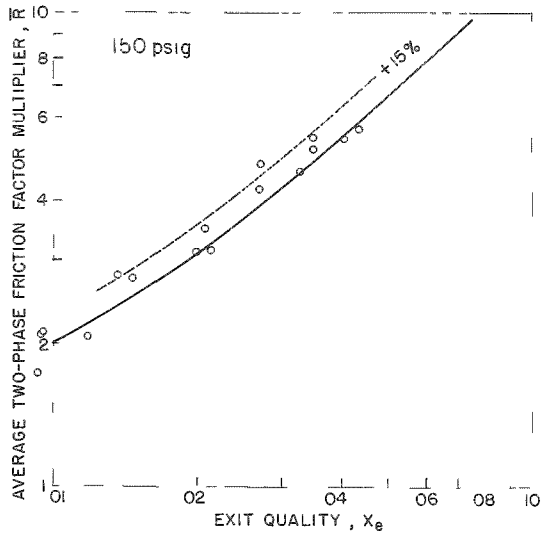

700-434-A

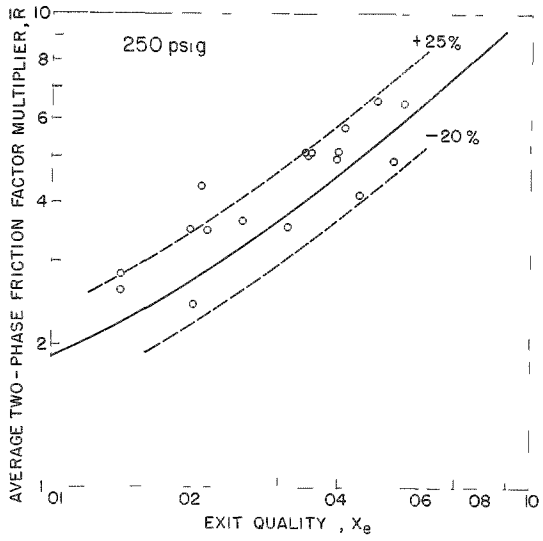

700-434-B

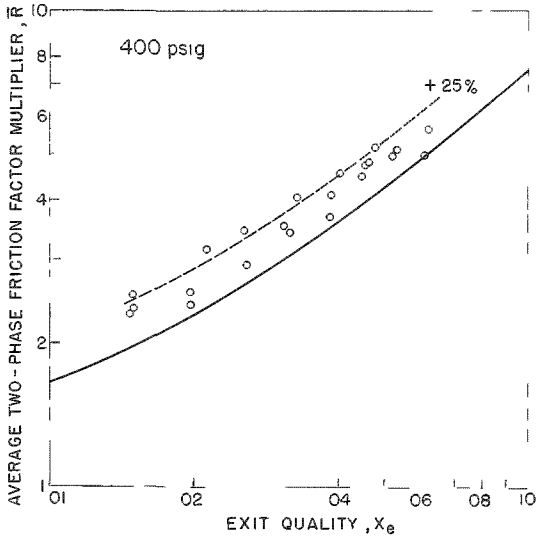

700-434-C

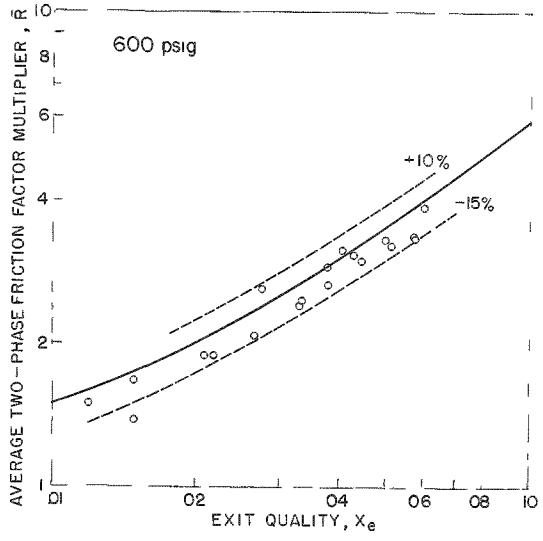

700-434-D

Fig. 4.6

Comparison of $\frac{1}{4}$ in. x 2 in. x 5 ft Channel Boiling Data with Sher-Martinelli Parameters. (G = 0.6 x 10^6 lb/hr - ft^2)

Based on the facts that, (1) two-phase friction exhibits a greater dependency on the void fraction than on the weight fraction, and

(2) the Martinelli-Nelson correlation corresponds to Sher's data for $G = 1 \times 10^6$ lb/hr-ft^2 at 2000 psia, the following alternate method has been proposed.(59)

(1) Obtain ϕ^2_{LO} from the Martinelli-Nelson curve, Fig. 4.2 for the pressure and qualities of interest.

(2) Convert Sher's correlation, Fig. 4.5, to a void fraction basis, assuming $V_g/V_L = 1$. At the void fraction of interest obtain the ratio of ϕ^2_{LO} at the mass velocity of interest to ϕ^2_{LO} at $G = 1 \times 10^6$ lb/hr-ft^2. Fig. 4.7 is a plot of this ratio vs void fraction.

(3) Multiply the Martinelli ϕ^2_{LO} by the ratio obtained from Sher's data, plot it as a function of channel length and integrate it to obtain the average friction multiplier, $\bar{R}$.

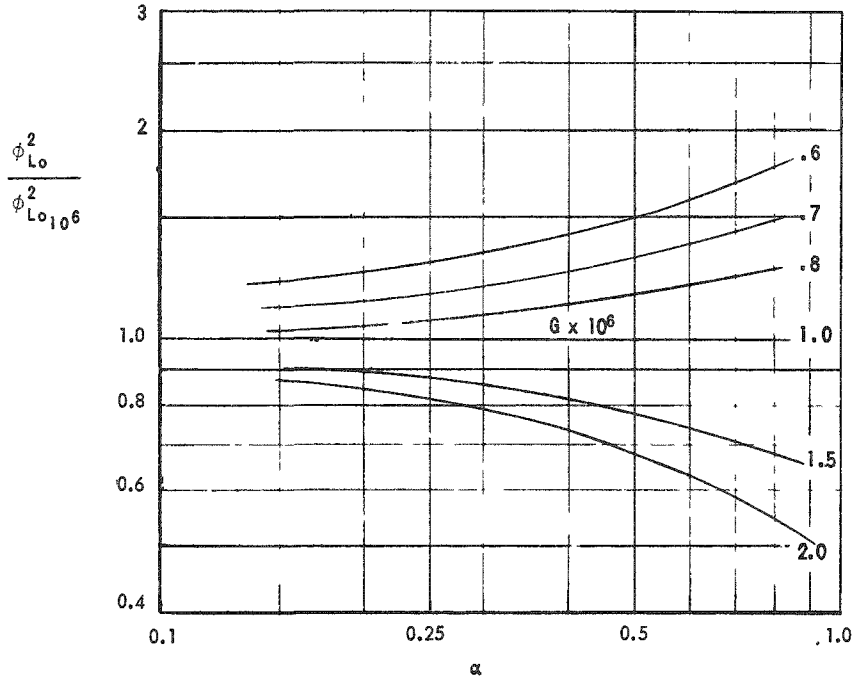

Fig. 4.7

Correction Factors Based on α from Sher Data Based on Slip = 1.0

Because of the lack of experimental data no recommendation can be made as to which of the two methods is the best; however, it is felt intuitively that the void fraction method is a more logical basis for extrapolating than is the weight fraction. The later method is the one presently recommended.

Several theoretical analyses are available for two-phase flow with vaporization.[66,69,70] In general, these correlations exhibit reasonable qualitative agreement with the Martinelli-Nelson correlation; however, their accuracy cannot be evaluated until more experimental boiling pressure drop data are available.

It is obvious that more boiling pressure drop data are necessary before accurate predictions of the pressure drop during boiling can be made. Even this may not be sufficient to solve the problem because of the inherent scatter in the frictional pressure drop data. This scatter is caused mainly by: inaccuracies in the void measurement which affect calculations of both the hydrostatic head and the acceleration pressure drop; and the inability to determine the true acceleration pressure drop component. This last factor presents the greatest obstacle against obtaining good boiling pressure drop data over a wide range of variables.

Leppert,[61] Schrock,[67] and Weatherhead (Argonne National Laboratory data)[71] have presented correlations of the sum of the frictional and acceleration pressure drop components. Schrock and Weatherhead show the data have less scatter when presented in this manner. Leppert could not find a mass velocity dependence. This suggests that the apparent mass velocity effect on frictional pressure drop may be partially or totally due to a mass velocity effect on the acceleration pressure drop which is caused by changing flow patterns. The difficulty with correlating the sum of the frictional and acceleration pressure drop components is that the friction pressure drop is a function of length while the acceleration pressure drop is independent of length, thus making it difficult to apply to other systems.

Martinelli and Nelson[59] have presented two equations for calculating the extremes of the acceleration pressure drop caused by vaporization of a two-phase mixture. For a homogeneous mixture (fog flow) the acceleration pressure drop will be a maximum and is expressed by

$$\Delta P_{acc} = \frac{G^2}{g_c}\left[(1 - x_e) + x_e\left(\frac{\rho_f}{\rho_g}\right) - 1\right]\frac{1}{\rho_f} \quad . \tag{4.21}$$

For two-phase flow in which the phases are completely separated and travel at different velocities (slip flow), the acceleration pressure drop is a minimum and is expressed by

$$\Delta P_{acc} = \frac{G^2}{g_c}\left[\frac{(1 - x_e)^2}{1 - \alpha_e} + \frac{x_e^2}{\alpha_e}\left(\frac{\rho_f}{\rho_g}\right) - 1\right]\frac{1}{\rho_f} \quad . \tag{4.22}$$

The true pressure drop probably lies somewhere between the two extremes. Since the acceleration term is quite often a large fraction of, or even greater

than, the frictional term, this uncertainty can cause considerable scatter in the frictional pressure drop data. Similarly the total pressure drop calculation will have this uncertainty even if the frictional pressure drop is known exactly.

The derivation of Eqs. (4.21) and (4.22) are based on the average velocities of the mixture and the phases, respectively. This implies that the momentum factor K_m, which is the ratio of the true momentum flux to the momentum flux evaluated at the average velocity, is approximately unity. For single phase flow K_m varies from 1 to 1.33. Since the velocity distributions in the two phases during slip flow are unknown and undoubtedly a function of flow pattern, the upper limit of the momentum factors are unknown and the factors, therefore, a function of the flow pattern. Experiments to measure the true momentum of the mixture would be most useful.

The hydrostatic head in a boiling channel is evaluated from

$$\Delta P_H = \left[\rho_f - \bar{\alpha}\,(\rho_f - \rho_g)\right] L_B \qquad (4.23)$$

where $\bar{\alpha}$ is the average void fraction. Evaluation of the void fraction is discussed in Section 3. Except for channels with very small equivalent diameters, the hydrostatic head is the major portion of the two-phase pressure drop during vertical flow. The uncertainties in evaluating the hydrostatic head are a function of the uncertainties in $\bar{\alpha}$.

5. Adiabatic Region

By far, the greatest majority of two-phase research work has been centered on adiabatic two-phase flow. This type of flow eliminates the large acceleration pressure drop term and it is also possible to use two-component mixtures, such as air-water, gas-oil, etc., thereby eliminating the need of a steam supply or heat source. Many of the available data are the result of research in the petroleum industry and in chemical engineering; fields that are truly interested in two-phase mixtures other than steam and water. A reasonable estimate is that more than ninety per cent of the available adiabatic, two-phase pressure drop data were obtained with mixtures other than steam-water. However, in the correlations and comparisons of data that have been reported, many investigators compare data obtained from different phase systems. The validity of these comparisons has yet to be substantiated.

More than eighty per cent of the available data have been obtained for horizontal flow, which eliminates the hydrostatic head. In all of the vertical flow data that have been surveyed, only one reference[17] reported steam-water data and this was at atmospheric pressure. Vertical flow, adiabatic, steam-water pressure drop data at various pressures are badly needed at this time.

The "standard" correlation of adiabatic, two-phase frictional pressure drop, against which most data and correlations are compared, is the Lockhart-Martinelli[64] correlation. The work of Lockhart and Martinelli consisted of a revision of a previous correlation by Martinelli and co-workers to make it applicable for the four types of two-phase flow that had been postulated; i.e., turbulent-turbulent, turbulent-viscous, etc. The basic postulates in the analysis were those mentioned in the discussion of the Martinelli-Nelson boiling pressure drop correlation in the previous section. The data used in the development were obtained from horizontal flow of air-water, air-oil, and air-benzene at pressures up to 52 psia.

The suggestion that two-phase pressure drop was strongly dependent upon flow patterns resulted from early work done with adiabatic, two-phase flow. Gazley and Bergelin, in a discussion of the Lockhart-Martinelli paper[64] were the first to suggest such a relation. Isbin[16] and Gresham[39] present summaries of most of the work that has been done in the observation and correlation of flow patterns, hence only the highlights will be discussed here.

Different flow patterns were observed as early as 1914. Several of the flow pattern correlations for horizontal flow have been referenced in the previous section on boiling pressure drop. Moen[72] has recently suggested modifications to Baker's and Kasiakova's correlations. Kosterin[73] reported that for horizontal flow the flow pattern was dependent upon the diameter of the pipe. He also reported that the entrance section had no effect on flow patterns in vertical and inclined pipes. Hoogendoorn[54] used Kosterin's type of correlation to show the effect of liquid viscosity and pipe diameter on the flow patterns for horizontal flow. The main effect of both variables was on the transition region between plug and slug flow. Govier[74,75] has shown a relation between vertical flow patterns and specific pressure drop regimes for various liquid flow rates and pipe diameters.

The Lockhart-Martinelli correlation has been shown by many investigators to be inadequate for specific horizontal flow patterns. In general, the correlation predicts too high for slug and plug flow and too low for annular and mist-annular flow. One of the more recent reports is that of Hoogendoorn.[54] It is an excellent piece of work based on atmospheric pressure, air-water and air-oil mixtures in horizontal pipes with inner diameters ranging from 24 mm to 140 mm. Hoogendoorn concludes that for horizontal flow the Lockhart-Martinelli correlation has three limitations; it cannot be used:

(a) for plug, slug or froth flow, if gas densities differ from that of air at atmospheric pressure,

(b) in the stratified and wave flow regions,

(c) in the mist-annular flow region.

He presents the following correlations,

(a) for plug, slug and froth flow

$$\Delta P_{TPF} = \Delta P_{LO}\left[1 + 230\left(\frac{m_g}{m_t}\right)^{0.84}\right]\left[0.00138\left(\frac{\rho_L}{\rho_g}\right)\right]^{\gamma} \qquad (4.24)$$

where

$$\gamma = 9.5\left(\frac{m_g}{m_t}\right)^{0.5} - 62.6\left(\frac{m_g}{m_t}\right)^{1.3}$$

for

$$\left(\frac{m_g}{m_t}\right) < 0.05 \quad ; \quad R_{E_{TP}} > 3000 \quad .$$

(b) For wave flow

$$\Delta P_{TPF} = C\left(\frac{m_g}{m_t}\right)^{1.45} \cdot \frac{1}{2}\,\frac{\Delta L}{D_e}\,\frac{m_t^2}{\rho_g} \qquad (4.25)$$

for

$$\left(\frac{m_g}{m_t}\right) < 0.8 \quad .$$

C depends mainly on pipe diameter and pipe roughness.

(c) For mist-annular flow

$$\Delta P_{TPF} = 0.12\,(m_g)^{-1/4} \cdot \frac{1}{2}\,\frac{\Delta L}{D_e}\,\frac{m_g^2}{\rho_g} \quad . \qquad (4.26)$$

Many objections have also been voiced about the Lockhart-Martinelli correlation because it does not recognize a flow rate effect. This effect has been reported in a number of different experiments[41,72,76,77] for horizontal flow.

Petrick[30] has reported a mass velocity effect on ϕ_L^2 for vertical flow, air-water, atmospheric pressure data which was limited to qualities up to 0.0043. The mass velocity was varied in two ways: (1) the mixture flow rate was varied for any given channel cross section, and (2) the mixture flow rate was held constant while the channel cross sections were varied. The mass velocity effect obtained by varying the

cross section was much more pronounced than that obtained by varying the flow rate, indicating that the geometry (or the effect that the geometry has on the flow pattern) may be of greater significance than the flow rate, at least for vertical flow. Moen[72] reports on a mass velocity effect for high pressure steam-water flow in horizontal pipes, but Isbin[17] could find no flow rate effect in vertical steam-water flow at atmospheric pressure. Similarly, Yaki[77] reported a mass velocity effect for horizontal flow but did not report such an effect[78] for vertical air-water flow. The only suggestion that could be found of a flow rate effect on Lockhart-Martinelli parameters for adiabatic, vertical two-phase pressure drop was reported by Dukler[79] for downward flow. This suggests that the flow rate effect may be pertinent only for horizontal flow.

A pipe diameter effect as reported by Govier[75] for vertical flow is also shown by Yaki's vertical flow[78] data and is suggested by Petrick's data.[30] Other investigators[53,54,77] have reported a diameter effect for horizontal flow.

Based on their annular flow model which postulates the increased friction is due to the increased local water velocity, Lottes and Flinn[19] suggest that the frictional pressure gradient ratio may be represented by

$$R = \left(\frac{1}{1-\alpha}\right)^2 \quad . \tag{4.27}$$

Richardson[22] found that his horizontal air-water flow data could be correlated by $R = (1/1-\alpha)^{1.75}$. Chisholm and Laird[80] found that for horizontal air-water flow $R = 0.8\,(1/1-\alpha)^{\beta}$ where $\beta = 1.75$ and 1.875 for smooth and galvanized pipe, respectively. Moen correlated his horizontal, steam-water data with Eq. (4.27) and found that the exponent varied from 1.6 to 2, depending upon flow rate.

Chenoweth and Martin[86] have proposed a correlation based on data from a number of sources for horizontal flow of various two-component mixtures at pressures up to 100 psia in pipe sizes from 0.6 to 3 in. in diameter. The correlation is presented in graphical form, Fig. 4.8, and represented all the data within ±50 per cent and 92 per cent of the data within ±35 per cent. Lester[82] compared steam-water data from 4- and 6-in. pipes with the correlation and found agreement within ±35 per cent.

Bertuzzi et al.[83] have also presented a correlation based on a large collection of horizontal, two-component data for pressures up to 55 psia and diameters of $\frac{1}{2}$ to 2 in. Their correlation represents the data with an algebraic deviation (bias) of 0.82 per cent and a standard deviation of 20.8 per cent. Both this correlation and the Chenoweth-Martin correlation reduce to the proper liquid pressure drop for all liquid flow and to proper gas pressure drop for all gas flow.

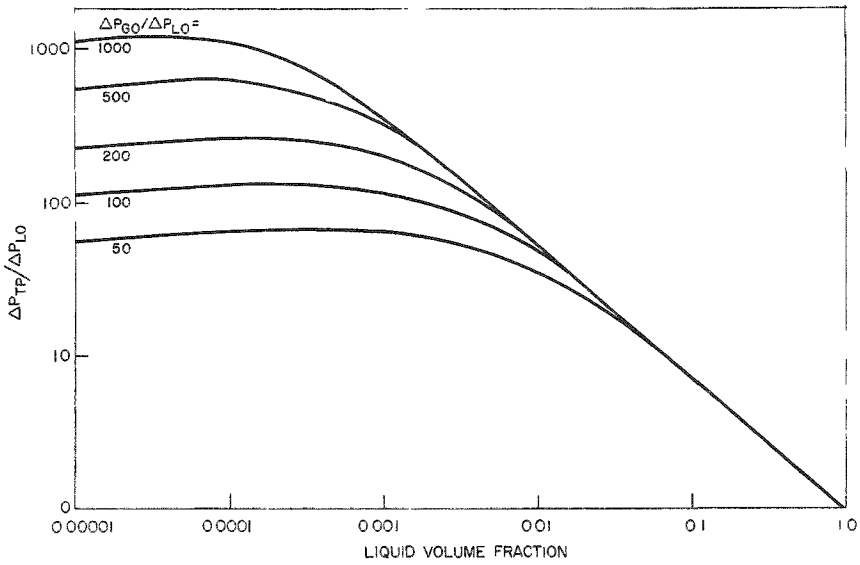

Fig. 4.8

Correlation for Turbulent Two-Phase Friction Pressure Drop in Horizontal Pipes

The effect of wall roughness on two-phase pressure drop has been reported by Chisholm and Laird(80) and Hoogendoorn.(54) Both reports were the result of atmospheric pressure, horizontal, air-water tests.

4.3. Conclusions

The state of the art, with respect to adiabatic, two-phase frictional pressure drop is adequately expressed in Bennett's conclusions.(37)

a. "There is no reliable method which can be applied to any system to predict flow patterns in two-phase flow.

b. "Two-phase pressure drops can be predicted in horizontal isothermal flow but the accuracy is not likely to be better than ±50 per cent. The method which has been mainly used is due to Lockhart and Martinelli.(53) Correlations due to Chenoweth and Martin(81) and Bertuzzi, Tek and Poettmann(83) may be an improvement but not radically so and await confirmation by other workers.

c. "Comparatively little work has been carried out on isothermal flow in vertical tubes with the additional complications of a hydrostatic head term.

d. "The hydrodynamics of two-phase flow therefore require a great deal more study in relation to all aspects."

5. CRITICAL HEAT FLUX AND BURNOUT

5.1. Introduction

For systems wherein heat is generated in a solid body and then transferred directly to a liquid or liquid-vapor coolant, the critical heat flux is defined as occurring at the transition from nucleate to film boiling and is characterized by a sharply defined increase in the temperature of the heat transfer surface. If the heat flux is sufficiently great, the resulting thermal excursion results in "burnout," physical destruction of the heat transfer surface. Although the two terms are commonly used interchangeably, "burnout" is a subjective occurrence that is frequently dependent upon such extraneous factors as material properties, pressure and/or thermal stresses, and corrosion rates and effects. Since the critical heat flux is normally the limiting condition for power and thermal design criteria, it is important that its magnitude and determining conditions be known with a minimum of uncertainty. Unfortunately, such is not the case. There is widespread disagreement regarding the applicability, magnitude, and effect of the several variables which have been associated with the determining conditions for the critical heat flux occurrence.

Despite the existence of much critical heat flux data which has appeared in recent years (and numerous correlations thereof), it is not possible at the present time to make authoritative pronouncements on the subject. For the purpose of making the most valid comparisons, the following discussion is limited to systems wherein there is the vertical up-flow of liquid or two-phase water in annuli or channels with uniform heat generation.

5.2. Effects on Magnitude

1. System Pressure

The pressure effect on the magnitude of the critical heat flux appears to be largely dependent upon the latent heat of vaporization (H_{fg}) and the specific volume of the vapor phase (V_g), both of which are pressure dependent properties of the coolant. For a system of fixed size and geometry operating at a fixed mass flow rate and containing liquid water at the bulk saturation condition (H_f) at the location of the critical heat flux occurrence, the effect of increasing system pressure is to increase the critical heat flux to a maximum value somewhere in the range of 600-1500 psia. This increase in the critical heat flux is presumed to be caused by the decreasing specific volume of the vapor phase which acts to decrease the thickness (and therefore the thermal resistance) of the boundary layer adjacent to the heat transfer surface. In the higher pressure range beyond the point of the maximum critical heat flux, the critical heat flux decreases continuously with increasing pressure. This decrease is believed to be caused by the decreasing value of the latent heat of vaporization and the resulting decrease in thermal energy transport from the boundary layer to the main body of the coolant.

Existing analytical correlations that express the effect of pressure on the critical heat flux, such as those of Kazakova,[84] Zuber and Tribus[85] Chang,[86] and Griffith[87] are basically dependent upon the latent heat of vaporization, the density of the vapor phase ($\rho_g = 1/v_g$), and a mass transport velocity term composed of varying combinations of the saturated coolant properties. Griffith's correlation also includes the effects of mass flow rate and coolant enthalpy in the subcooled and quality regions, being based on data for vertical channels. Empirical correlations which include the effect of pressure, particularly those of Green[88] and Silvestri,[89] show a peak critical heat flux in the range of 1200-1500 psia.

For subcooled water, the correlation of Jens and Lottes[8] for the case of liquid water flowing upward in vertical channels over the pressure range of 500-3000 psia is the most widely accepted. The pressure-dependent factors in this correlation show a well defined similarity to the latent heat of vaporization and the density of the vapor phase.

For the case of net steam generation, there is general agreement that the critical heat flux decreases with increasing pressure. Correlations for two-phase water in vertical rectangular channels at 2000 psia have been presented by Sonneman,[90] Bell,[91] Vanderwater,[92] Singh,[93] and Fauske,[94] all of which seem to be based on the same data, as are the correlations of Green[88] and Silvestri.[89]

2. Local Bulk Enthalpy

Critical heat flux data is usually presented as a function of the local bulk enthalpy of the coolant, or some equivalent thereof. For a constant pressure, the critical heat flux is primarily dependent upon the local bulk enthalpy, the critical flux decreasing with increasing enthalpy in the subcooled water and wet steam regions. However, the correlation of Griffith[87] shows a definite increase in critical heat flux in the wet steam region for pressures lower than 600 psia. There has been relatively little interest in this pressure range, and this finding appears to be unconfirmed.

3. Mass Flow Rate

In the usual presentation of critical heat flux as a function of local bulk enthalpy, the mass flow rate appears as a parameter. In the subcooled water region, there is general agreement that the critical heat flux increases with increasing mass flow rate, the rate of increase diminishing as the local bulk enthalpy approaches saturation. For the wet steam region, most correlations show a similar effect. However, the correlations of Bell,[91] and Sonneman[90] (both for 2000 psia), show a definite inversion of the mass flow rate effect in the quality region. Previously unpublished data at 2000 psia from ANL, shown in Fig. 5.1 is in agreement with this. Such a reversal of the mass flow rate effect, if it exists, is probably caused by a change in the two-phase flow regime.

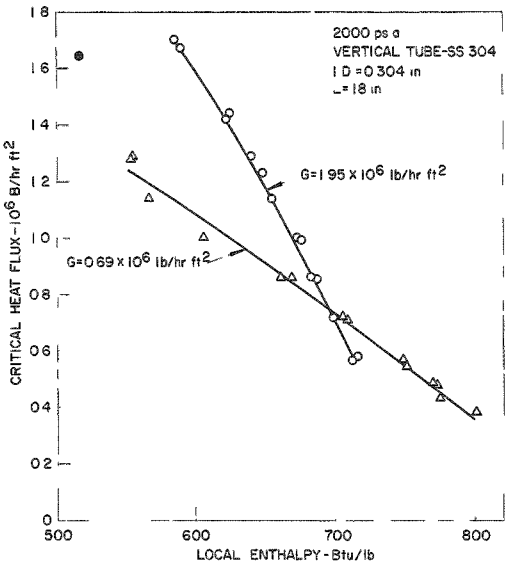

Fig. 5.1

Critical Heat Flux as Related to Mass Flow Rate

4. Flow Channel Size, Length and L/D Ratio

What, if any, effect these factors have upon the critical heat flux occurrence is a matter of considerable controversy. The correlation of Green[88] contains an L/D factor, while other correlations of the same data, Bell[91] and Silvestri,[89] contain only an equivalent diameter factor. Figure 5.2 presents additional 2000 psia data from ANL showing a decided diameter effect which decreases with increasing enthalpy. Comparison of data from two channels of the same diameter and different lengths (18 and 24 in.) showed no appreciable discrepancies.

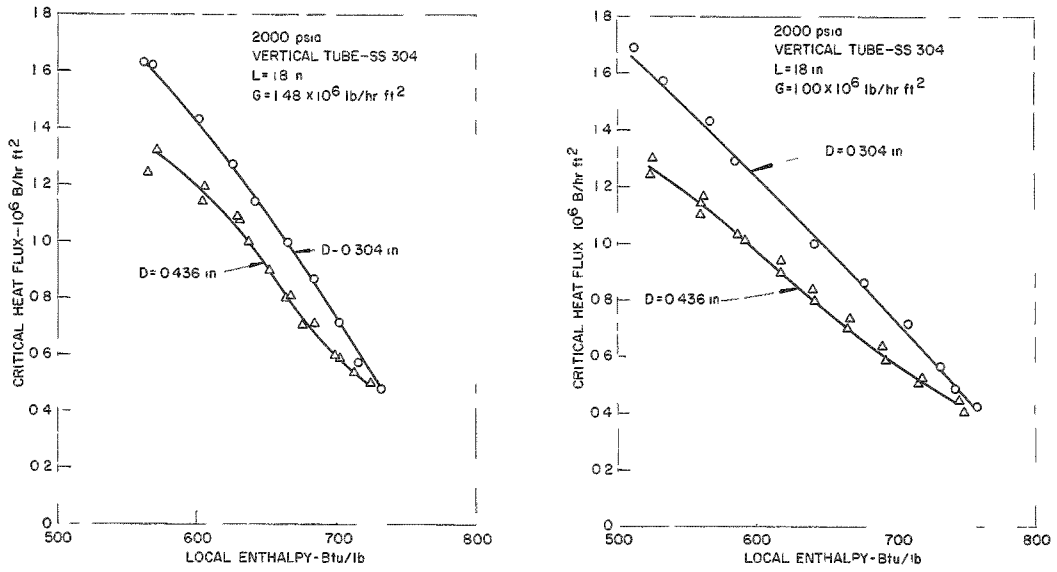

(a) (b)

Fig. 5.2

Critical Heat Flux as Related to Diameter

The effect of channel length is generally not considered as such in critical heat flux correlations, although inspection of data from many sources indicates that the critical heat flux reported decreases with increasing channel length. The often-discussed "effect of inlet subcooling" also appears in numerous presentations of data and is occasionally associated with length or L/D. For uniform heat generation the critical heat flux occurs at a highly localized and predictable location and, for any particular system, is readily reproducible. This indicates that the effect of channel length and inlet subcooling is only thermodynamically significant.

Levy,[95] in a presentation of critical heat flux data for natural convection in a vertical annulus at 1000 psia, states that the critical heat flux is preceded by hydrodynamic instability and is noticeably lower in magnitude than for the case of forced circulation. Levy further quotes Lowdermilk:[96] "...A very stable circuit with a high head pump leads to higher burnout heat fluxes than one with a low head pump." Lowdermilk[97] also reports marked variations in the magnitude of the critical heat flux in a low-pressure (15-100 psi) forced-circulation system due to flow instability caused by flow system characteristics external to the vertical tubular test section.

Figure 5.3 illustrates the flow instability preceding critical heat flux occurrence in a forced circulation system at 600 psia. The centrifugal circulating pump (Westinghouse Model 100-A) supplied a net head of approximately 90 psi for the 18 in. vertical tube with an L/D of 41. Lacking evidence to the contrary, this flow instability preceding the critical heat flux occurrence is presumed to be limited to the condition of net steam generation. If the instabilities cited by Levy and Lowdermilk, and illustrated by Fig. 5.3 are typical, it appears to preclude the determination of flow-quality criteria for the critical heat flux occurrence for the case of net steam generation. The critical design criterion in this case seems to be the hydrodynamic condition of flow and steam quality (or void-volume fraction) which determines flow instability, which applies to both forced and natural circulation systems.

5. Surface Condition

The small amount of data available indicate that a relatively rough surface finish, by providing numerically greater nucleation sites and/or greater surface turbulence, has a comparatively higher critical heat flux than is the case for a smooth polished finish. This may be deduced by comparing the bubble production from rough and smooth surface finishes in nucleate boiling photographs. Figure 5.4 shows data from a clean surface compared with later data from the same tube after repeated occurrence of the critical heat flux had produced a visibly corroded surface condition. Such an effect has only been noticed in the higher heat flux-local boiling ranges.

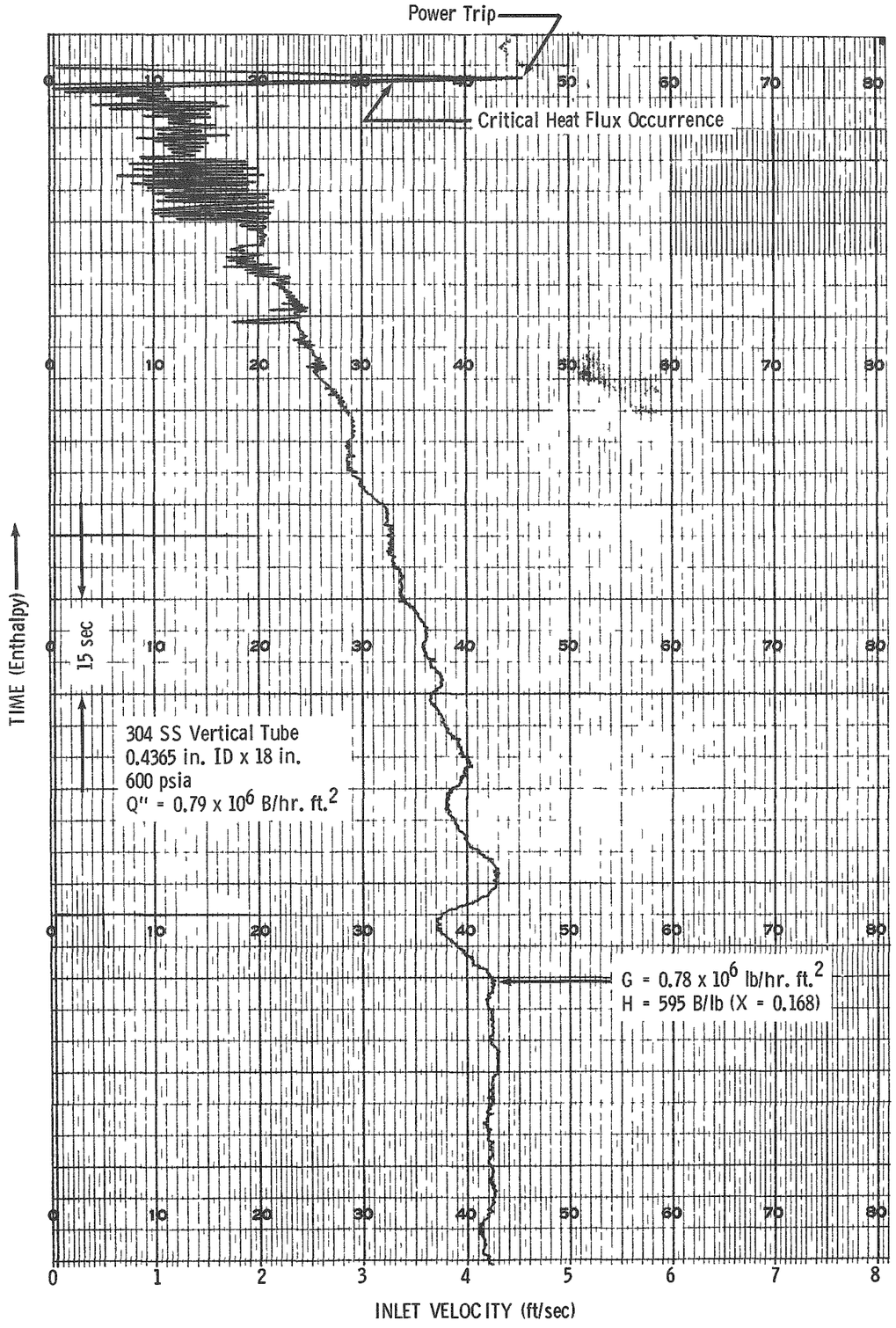

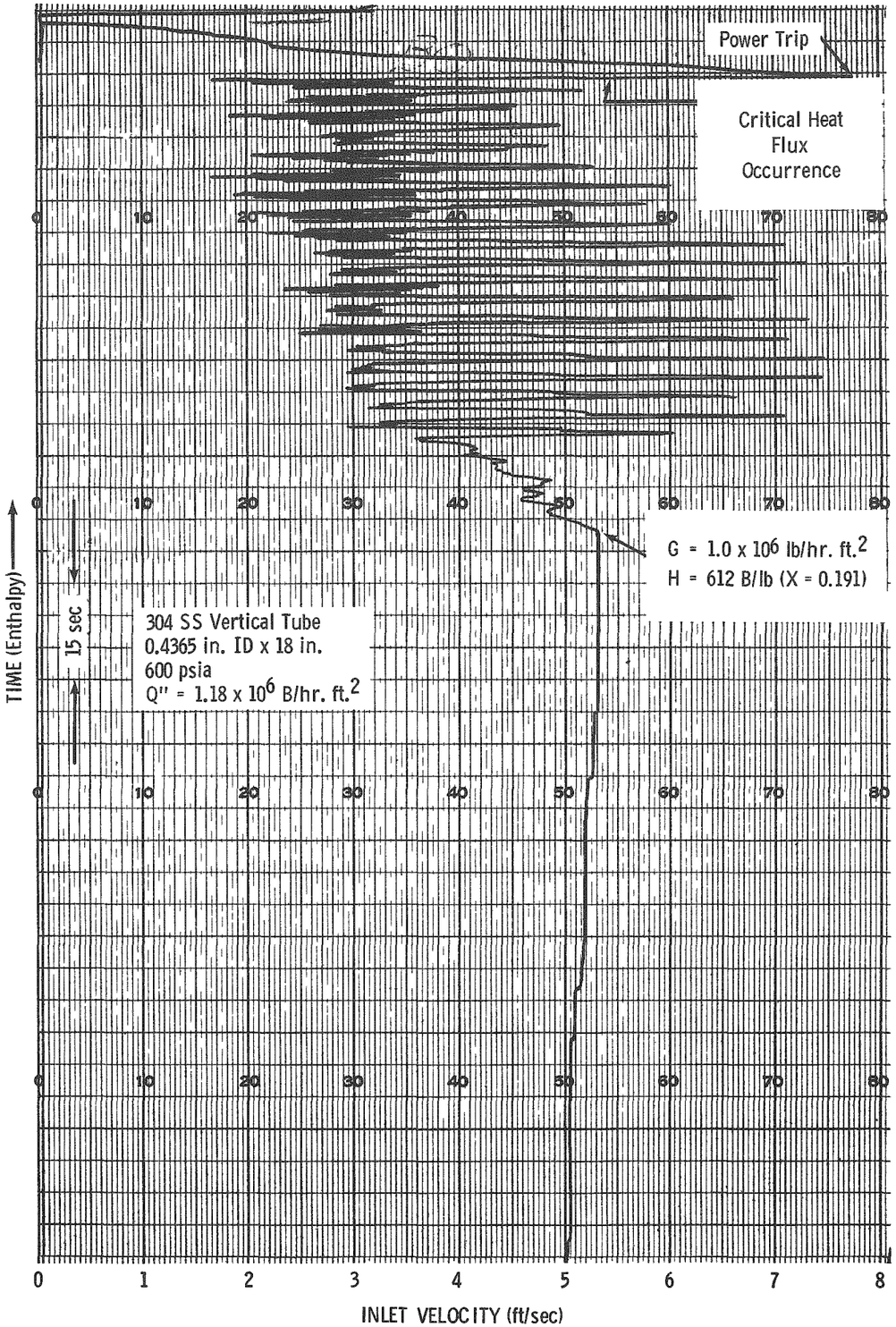

Fig. 5.3

Flow Instability Preceding Critical Heat Flux Occurrence

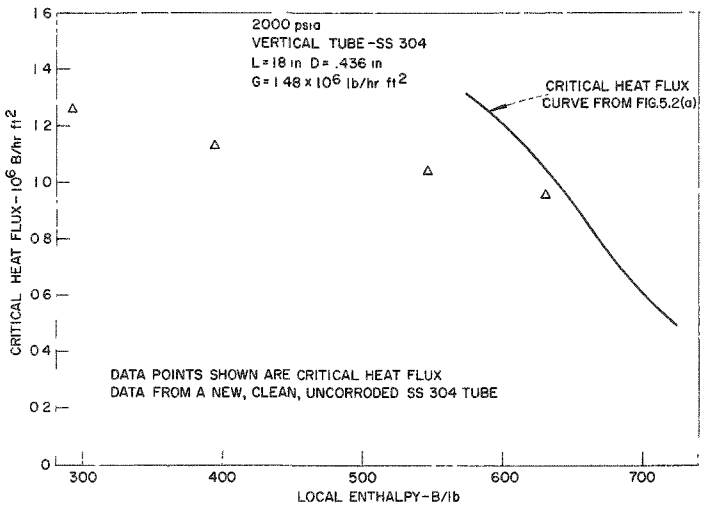

Fig. 5.4

The Effect of Increasing Surface Corrosion on Critical Heat Flux

6. Non-Uniform Heat Flux

A limited amount of data is available for the case of cosine and step-function heat generation at 2000 psia. Green(88) reports critical heat flux data for a modified cosine axial heat flux are the same as for uniform axial heat flux. Green(88) also reports that for a step-function ("hot spot") heat flux distribution, with a flux ratio of two, the critical heat flux is equal to or greater than that for uniform heat generation. ANL data are in agreement with this.

5.3 Conclusions and Recommendations

In view of the previous discussion, it is obvious that only the most general and qualitative recommendations can be made. For the case of subcooled water, the widely-accepted Jens and Lottes(8) equation seems to be the best available:

$$Q''_c = C\,(G)^m\,\Delta T_{sub}^{0.22} \text{ for } G \geq 1.0$$

where

Q''_c = critical heat flux in 10^6 Btu/hr ft^2
G = mass flow rate in 10^6 lb/hr ft^2
ΔT_{sub} = local subcooling $(T_{sat} - T_{bulk})$ - F
C, m are pressure dependent:

P psia	"m"	"C" (diam = 0.226 in.)	"C" (diam = 0.143 in.)
500	0.16	0.817	-
1000	0.275	0.626	0.915
1500	0.500	0.445	0.545
2000	0.725	-	0.300

The value of "C" appears to vary as the reciprocal diameter to the 0.8 power $\left(C \approx \frac{1}{D^{0.8}}\right)$ for the two diameters represented.

Because of recent evidence cited which indicates that flow instability rather than the critical heat flux should be the design criterion for the case of net steam generation, it is recommended that the existing literature be consulted for data from systems similar to the system of interest. Extreme caution should be used in seeking to apply steam quality critical heat flux data from forced circulation systems to the case of natural convection circulatory units. S. J. Green et al.[88] presents the latest and most complete compilation of pertinent data and correlations.

6. BOILING STABILITY

6.1. Introduction

There are several types of instability conditions connected with boiling. The first type is the instability associated with a liquid vapor interface, when the liquid is located above the vapor. Two other types are associated with boiling water reactors and reactor-simulating test loops which have both demonstrated unstable behavior under certain operating conditions. The first type of boiling stability is important in studying the nature of burnout or critical boiling heat flux. The second and third type, however, are considered to be of more importance for natural circulation boiling systems since flow instability usually appears at lower heat fluxes than the critical flux. Therefore, these discussions are limited to boiling flow stability problems as applied to natural circulation boiling systems and reactors. Reactor technology, in its present state, cannot predict either the dependence of the oscillation inception point or the frequency and amplitude of oscillation on operating conditions or design parameters. However, an experimental test program using both reactors and hydrodynamic test loops has shown certain trends in the dependence of oscillation on various parameters and conditions.

Analytical work using the above experimental data has been published. There is enough basic uncertainty of the cause and dependence of stability that models used as a basis for the published analytical work are useful only in predicting trends which can be compared with experimental data and in approximate extrapolation of the performance of an existing reactor to more stringent operating conditions. They do not give a consistent theoretical understanding of stability nor do they allow prediction of stability conditions in a reactor proposal during its design stages.

This discussion reviews the experimental program and analytical work associated with reactor and test loop stability.

6.2. Reactor Stability Experiments

The reactor stability experiments to date have been conducted using two distinct approaches: tests where the reactivity is increased in a step or ramp function and the response of reactor conditions (power, temperature) is recorded, and tests where the reactivity is harmonically oscillated and the resultant harmonic flux oscillation is measured.

Experiments using the first approach, i.e., a ramp or step reactivity input, include the Borax and Spert series of tests.

Borax[98-102] tests were of two types: (a) power excursion tests wherein, with the reactor running just critical, a large reactivity was inserted and the reactor was allowed to run for a predetermined time before automatically shutting down; (b) steady boiling tests, wherein the reactor was run at a given power level reached by steady increase in the reactivity. Typical traces taken during these tests are shown in Fig. 6.1. The results from these tests may be summarized as follows:

1. Power Excursions:

With low reactivity input there was a large initial power pulse followed by a drop in power as steam was formed to some low level about which power fluctuated randomly. With higher reactivity input there was a large initial power pulse followed by a power drop and then a series of smaller power pulses separated by low steady power. This type of response was called "chugging."

2. Steady Boiling Performance:

When the reactivity compensated by the steam was low, the reactor settled down to random fluctuations about a steady state after an initial power pulse.

At higher steam-compensated reactivity, the reactor settled back down to pulses of oscillations; i.e., a group of oscillations, then a relatively steady state until another group of oscillations appeared. As reactivity was increased, the oscillations increased in amplitude with less time between pulses until finally a state was reached with continuous oscillations of varying amplitude. With still higher reactivity the power pulses then went into an oscillation mode which after a time began to diverge.

The general effect of a pressure increase on all these tests was an increase in stability. Thus at a higher pressure level more reactivity could be compensated by the steam without loss of stability.

Borax IV[102,103] was different from the other Borax reactors in its fuel assembly material and design. Whereas the first three reactors had used aluminum-uranium alloy fuel elements with a corresponding large thermal conductivity, Borax IV used fuel pellets of mixed uranium oxide and thorium oxide having a low thermal conductivity. Borax IV, with these fuel elements, exhibited a greater degree of stability under similar conditions than did the other Borax reactors. These elements can apparently contribute to reactor stability under certain conditions. At the same time, however, they will increase the center fuel temperature and decrease the reactor protection against power excursions by increasing the time for steam to generate.

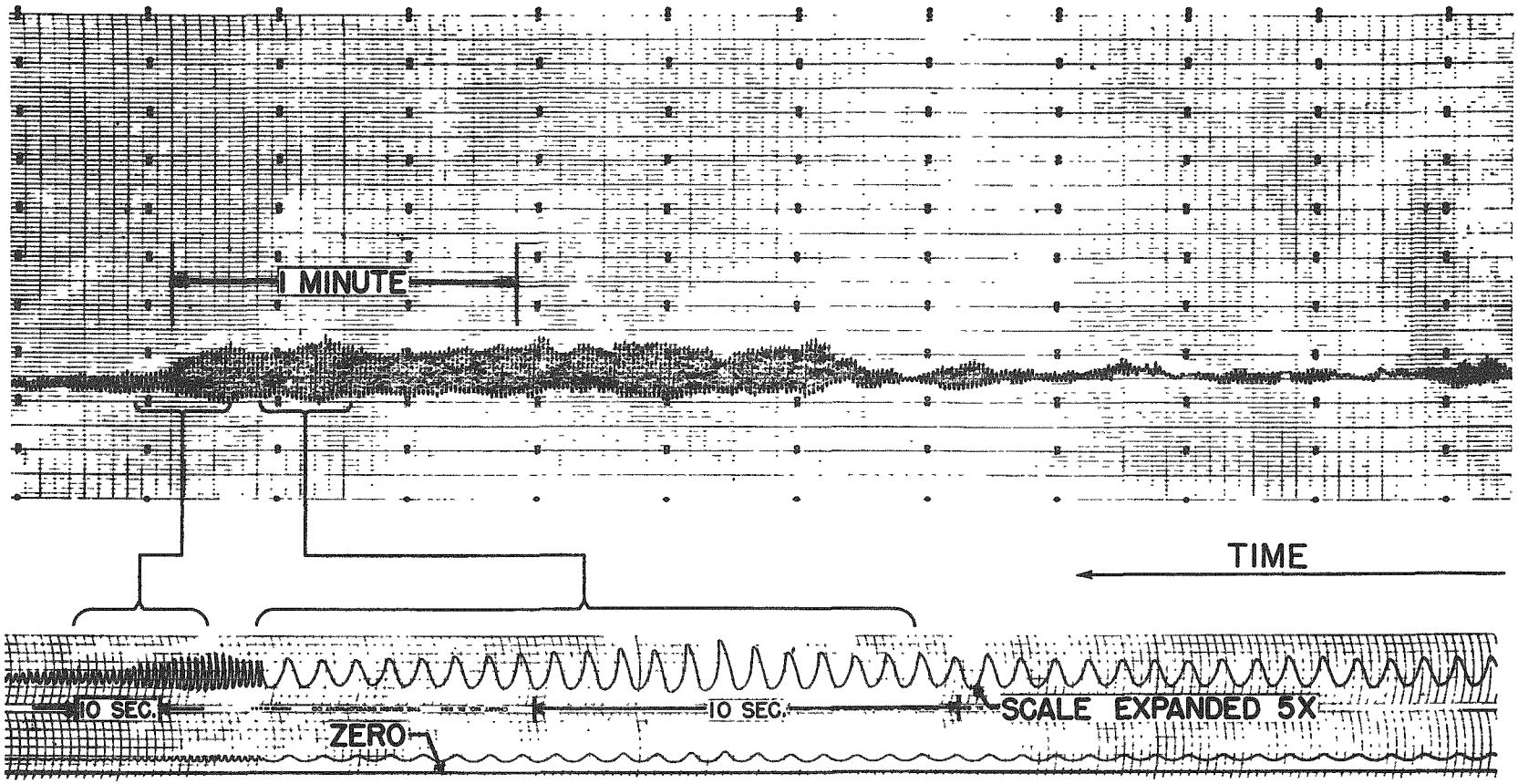

Fig. 6.1

Power Records of Oscillatory Boiling from Run 2, 10/22/53

201-593

The reactor was operating at an average power of 1100 kw at 130 psig, with 2.8% k_{eff} compensated by steam.

The upper record is from a Brown Electronik Recorder showing output of compensated ion chamber; zero is at bottom of chart.

The lower records are from a double pen brush recorder, expanding portions of the upper record as indicated. The lowest record includes the zero power line as indicated. The record just above expands the amplitude of oscillation by a factor of 5; the zero for this record is off the chart.

The Spert reactor tests[101,104-107] were similar to the steady boiling tests on Borax reactors. At the beginning of any particular test the reactor was running near critical; then the reactivity was increased at a linear rate to a predetermined point where control rod input of reactivity was stopped and subsequent reactor behavior observed. The Spert reactor and reactor test results were in many ways similar to the earlier Borax test. The Spert tests however included an attempt to demonstrate the stability dependence on various hydrodynamic effects.

The reactor tests were run with different water levels above the core, with different flow characteristics as produced by blocking off some of the flow channels, and with different surface tensions due to addition of detergent.

Figures 6.2a and 6.2b show two tests run with different water heights above the core but similar in other respects. These and other tests show an apparent increase in stability with decrease of water height above the core. As can be seen from these traces, however, the oscillations are large and random with reproducibility small. Thus the conclusions about water height are only qualitative and the slight quieting effect on the tests where detergent was added must be treated as questionable until more data supports it. There was no noticeable stability effect when some of the flow channels were blocked off.

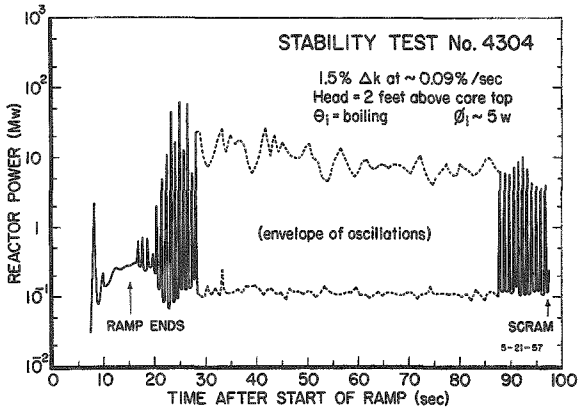

(a)
111-8891

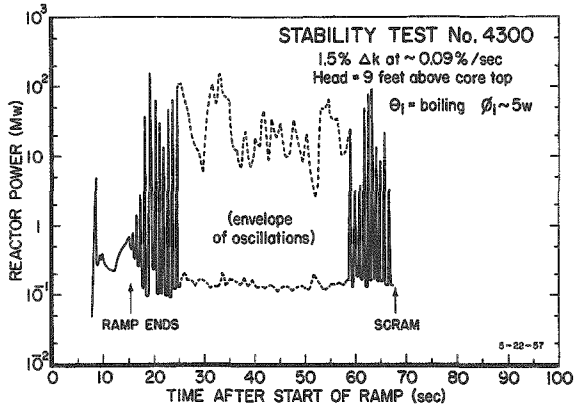

(b)
111-8890

Fig. 6.2

Stability Tests with Different Water Heights

The second approach to stability uses a harmonically oscillated reactivity input and compares this with the resultant oscillation in output power. By its nature this type of test is safer since the reactor does not reach a point of natural oscillation. On the other hand the tests are more difficult to perform and necessitate lengthy analysis.

This type of testing procedure has been used on EBWR,[108] Borax IV,[109] and Valecitos Boiling Water Reactor.[110]

Results of tests of the four Borax reactors, Spert Reactor, EBWR and VBWR represent all the experimental data on boiling water reactors and must be used as a basis for any boiling water reactor analysis.

6.3. Reactor Stability Analysis

The analytical work in this field has tended to follow the experimental separation into excursion tests, and transfer function measurements where the reactor was not subjected to self induced oscillations but was forced to oscillate by harmonically varying the reactivity input.

The Borax experiments as mentioned previously were parameter studies. There was very little analytical work done on the first three Borax reactor test results and on the excursion test results from Borax IV. A. J. Ulrich[111] investigated the heat transfer during power excursions on Borax II.

Some work has been done by the Ramo-Wooldridge Corporation in analytically predicting power transient results in the Spert I reactor.[112] In this analysis six equations relate initial excess reactivity, reactor power, excess reactivity, fuel plate temperature, steam volume in the core, volume of water expelled by heating at the fuel plate surface and throughout the volume of the water. These six equations, when combined with the reactor kinetic equations, form a closed set of non-linear differential equations.

When solved by a finite difference method using a digital computer these equations, including three adjustable constants, evidenced the same general trends as the Spert experimental data. These three constants, two of which are associated with voids and one with heat transfer, cannot presently be evaluated due to lack of knowledge of bubble dynamics and heat flow in transient boiling.

The equation set was also applied to special cases. When applied to the case of small oscillations where the power is represented by a particular trigonometric series, the result showed that the divergence of oscillations was partially dependent on the non-linear aspects of the equations. Stability predictions based on experimentally determined transfer functions would thus seem to be highly questionable.

The analysis of the forced oscillation tests has quite naturally followed a transfer function approach. Thus, in the analysis of the three reactors that have been subjected to forced oscillations (Borax IV, EBWR, VBWR) there is a heavy reliance on transfer functions.

In the analysis of the Borax IV tests,[109] a single loop feedback system with a single feedback transfer function was assumed. The feedback portion was assumed dependent on a void reactivity feedback k_0 and an effective average time constant, τ. H, the feedback transfer function, was evaluated from the experimental points and in turn furnished information on k_0 and τ. Both k_0 and τ followed expected trends with k_0 becoming more negative at higher powers as more reactivity was invested in voids, and τ becoming smaller as steam and heat transport times became smaller with higher flows. These first oscillations tests showed the practicality and value of such tests on boiling reactors and led to more extensive tests on EBWR and VBWR.

Eric Beckjord has attempted to analyze reactors using transfer functions for the equations representing the various individual processes.[113] This analysis uses no experimental data but rather uses a wholly theoretical approach.

The following effects are assumed to influence the stability of the core:

(1) Reactor kinetics
(2) Heat transfer using lumped parameter approach
(3) Steam voids (evaluated assuming a-f)

   a. Constant feed water flow
   b. Constant pressure
   c. Constant slip
   d. Constant water-steam equilibrium
   e. Axial flux proportional to full power
   f. No radial flux variation

(4) Steam flashing and condensation due to pressure variation
(5) Boiling boundary change due to pressure variation
(6) Boiling boundary changes caused by varying feed water flow rate
(7) Water density changes caused by temperature variation
(8) Void changes caused by water acceleration
(9) Hydraulic oscilllations

The prediction of stability from a wholly theoretical approach of this type is dependent on physical constants which are difficult to evaluate, questionable assumptions concerning little understood physical processes inside the reactor, and an assumed linearity in the differential equations. The resultant stability prediction, while valuable in showing trends, is too inaccurate for satisfactory design of a reactor.

DeShong and Lipinski[114] have analyzed the feedback transfer function results from the EBWR forced oscillation tests. The raw data from these tests were graphically handled to provide data smoothing. The resultant, measured feedback transfer function was considered during the formation of the model used in this analysis. The model thus formed differs from the theoretical model of Beckjord's analysis by inclusion of a time constant, apparently connected with the heat transfer process, which is evidenced in the experimental points. Also, DeShong and Lipinski did not find it necessary to include a hydraulic oscillation term.

Having defined a model, the experimental results were used to evaluate the model time constants at each operating condition. The extrapolation of the time constants was then used to estimate a point of instability. The results of this extrapolation indicated the reactor would become unstable at about 65 Mw. At 61.7 Mw, the point of feedwater pump capacity, the reactor flux record showed the reactor was on the verge of instability.

It was also found while conducting these tests that it is possible to estimate feedback transfer function at higher powers and given pressure by actual measurements at given power and lower pressure. Thus it is possible to estimate results measured at twice a given power density by measurements at the original power density and half the original pressure.

J. Thie[115] considered a smaller portion of the frequency range and analyzed a different model in this range than either Beckjord or DeShong and Lipinski. In the range considered this analysis results in six time constants; two associated with heat transport in non-boiling region, two associated with heat transport in the boiling region, one associated with average subcooled water transit time and one associated with average steam transit time. The results compare favorably with measured curves from EBWR This paper by Thie[115] also outlines a promising method of statistically analyzing the random power fluctuations of a reactor to furnish stability information about the reactor.

6.4. Test Loop Stability Experiments

Under certain operating conditions, with controlled variables (power, make-up water temperature, pressure) held constant, electrically heated natural circulation test loops are unstable. In the unstable region of operation many loop parameters exhibit oscillatory behavior. Experimental studies of this problem are currently under way at various research centers, but published information is rather limited.

Raymond Viskanta[116] investigated oscillatory characteristics of the Armadilla test loop.[19] This loop uses a one-shot gamma attenuation method[29] for measuring steam void fraction. Non-random fluctuations in the

output of this void measurement were used as a primary indication of instability; oscillations in the liquid level also indicated unstable behavior of the loop. The power at the inception of oscillations in the system was found at four pressures (75, 150, 250, 300 psig) with two additional variables considered, liquid level above the riser and flow restrictions in the downcomer crossover.

Liquid level above the riser had no discernible influence on stability. An increase in the flow restriction in the downcomer crossover had a definite stabilizing influence. The frequency of oscillation (determined by the void measurement, liquid level oscillations and oscillations in the pressure drop across the flow venturi in the downcomer) was constant regardless of the conditions of the loop.

A series of tests were conducted on the 2000 psia loop at Argonne National Laboratory[117] to find the inception of instability at different pressures with two geometries. The continuously recorded output of a differential pressure transducer connected across the venturi flow meter in the downcomer was used to determine the stability of each operating condition. (Fig. 6.3)

In an attempt to gain more insight into steady state equilibrium conditions around a known unstable point the 2000 psia test loop was run under forced circulation at conditions similar to the inception point with the results shown in Fig. 6.4. All of the points shown are forced circulation steady state runs with the same power, pressure and loop geometry as the natural circulation inception point. Each curve is drawn through all the points with one subcooling; the middle curve subcooling corresponds to that of the natural circulation point.

Some general conclusions can be drawn from the sum of Argonne National Laboratory natural circulation runs:

(1) Stability increases with pressure. (On the systems so far tested the increase of stable power with pressure was fairly linear.)
(2) Stability was influenced by geometry of the test section, riser and downcomer circuit. The general trend seems to be that an increase in the pressure drop in the two phase region of the flow loop decreases stability, while an increase in the pressure drop in the single phase region increases stability. As an example of these trends, a decrease in the riser size has little influence on driving head but greatly increases the friction in the two phase region and decreases peak stable power. A flow restriction in the crossover of the downcomer has a stabilizing influence.

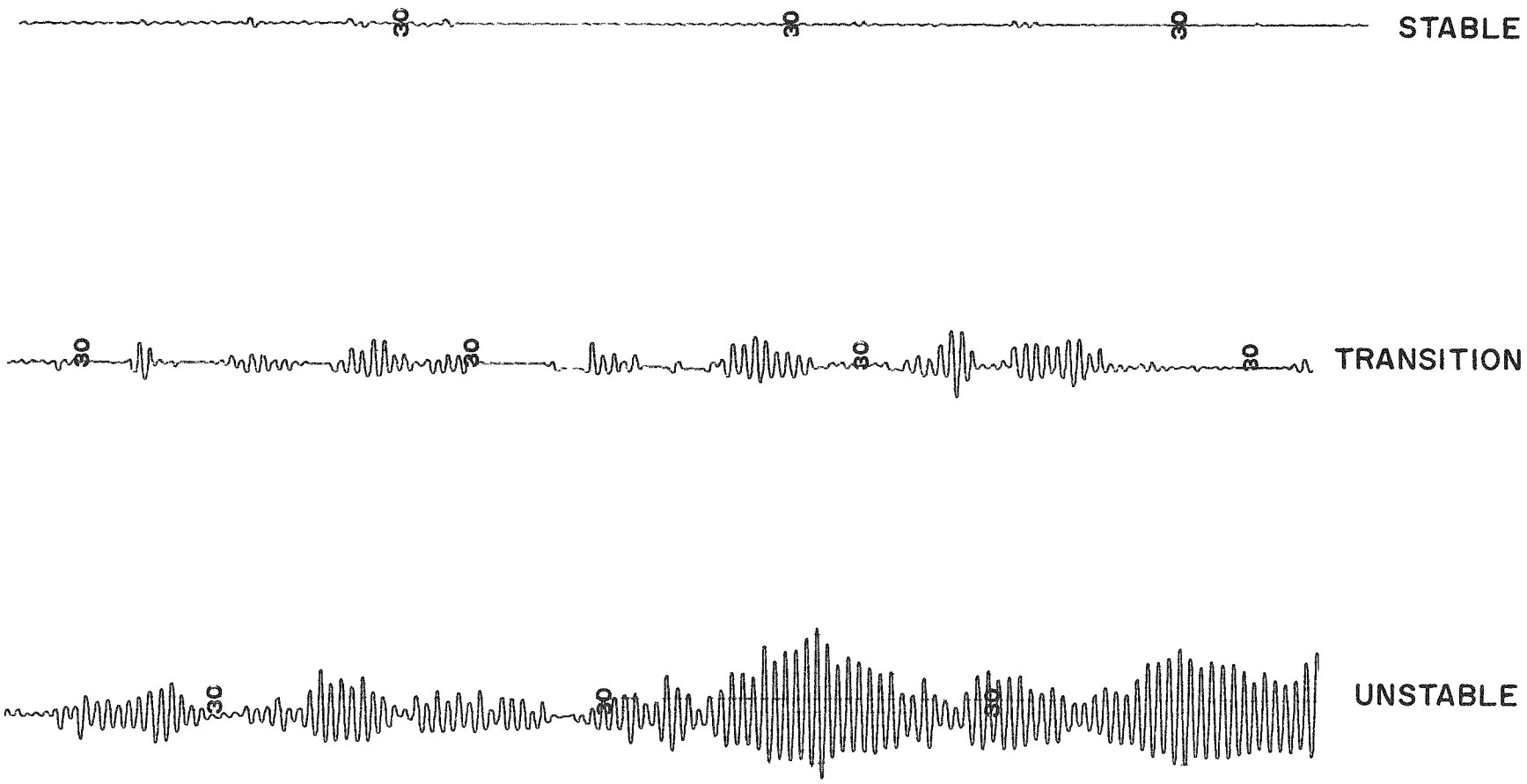

Fig. 6.3

Traces of Pressure Transducer Connected across Downcomer Venturi in 2000 psia Test Loop (1 in. dia. Heated Section and Riser)

111-8897

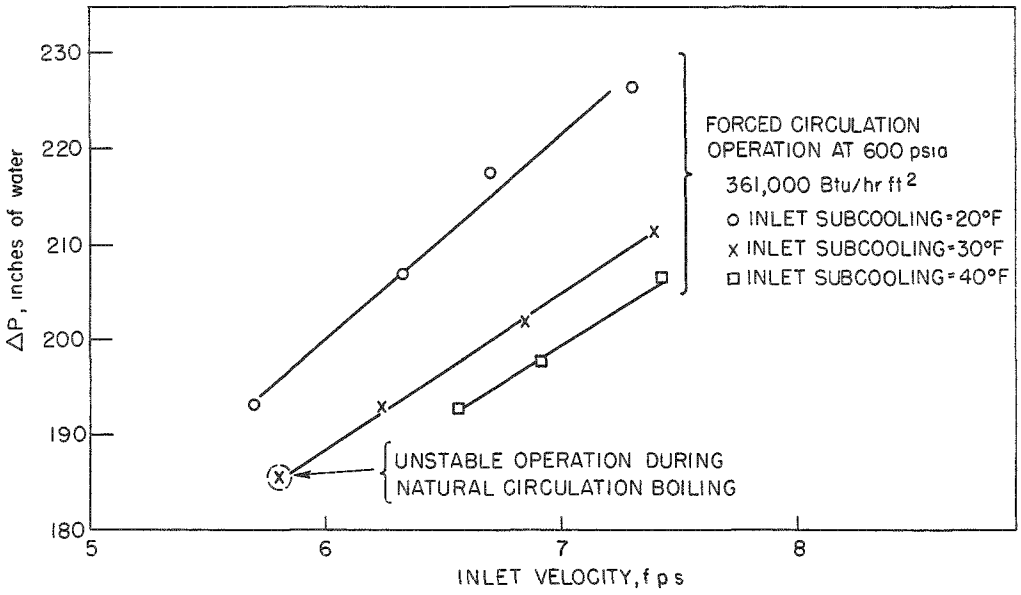

Fig. 6.4

Pressure Drop as a Function of Inlet Velocity for a 1 in. I.D. x 48 in. Vertical Pipe with a 1 in. I.D. x 10 ft High Chimney
111-8900

(3) Over the limited range of variation in the present equipment, the stability was independent of the liquid level above the riser.

(4) The period of oscillation did not vary much with variation of other parameters on one test loop.

The hydraulic test loop at the University of Minnesota[118,119] was a single loop with steam condensed while flowing as a two-phase mixture in the crossover. Loop geometry was invariant during the tests. No attempt was made to study the inception point of unstable flow; rather the tests were devoted to studying the loop performance while the loop was oscillating. The experimental information obtained from the loop was in the form of temperature and flow-rate-time traces as shown in Fig. 6.5. The period of oscillation was inversely proportional to the average flow rate. The period of oscillation was much longer (in the range of 50-200 sec) than those mentioned in available information from any other test loop.

Westinghouse is currently engaged in an experimental and theoretical program investigating flow stability in heated channels. This program was discussed at a Hydrodynamic Instability and Two-Phase Pressure Drop Session of the National Heat Transfer Conference held at Storrs, Connecticut during August of 1959. An abstract of this discussion[120] mentioned briefly the experimental apparatus, stating that stability was measured at a variety of conditions of inlet flow and subcooling at system pressures ranging from 600 to 1600.

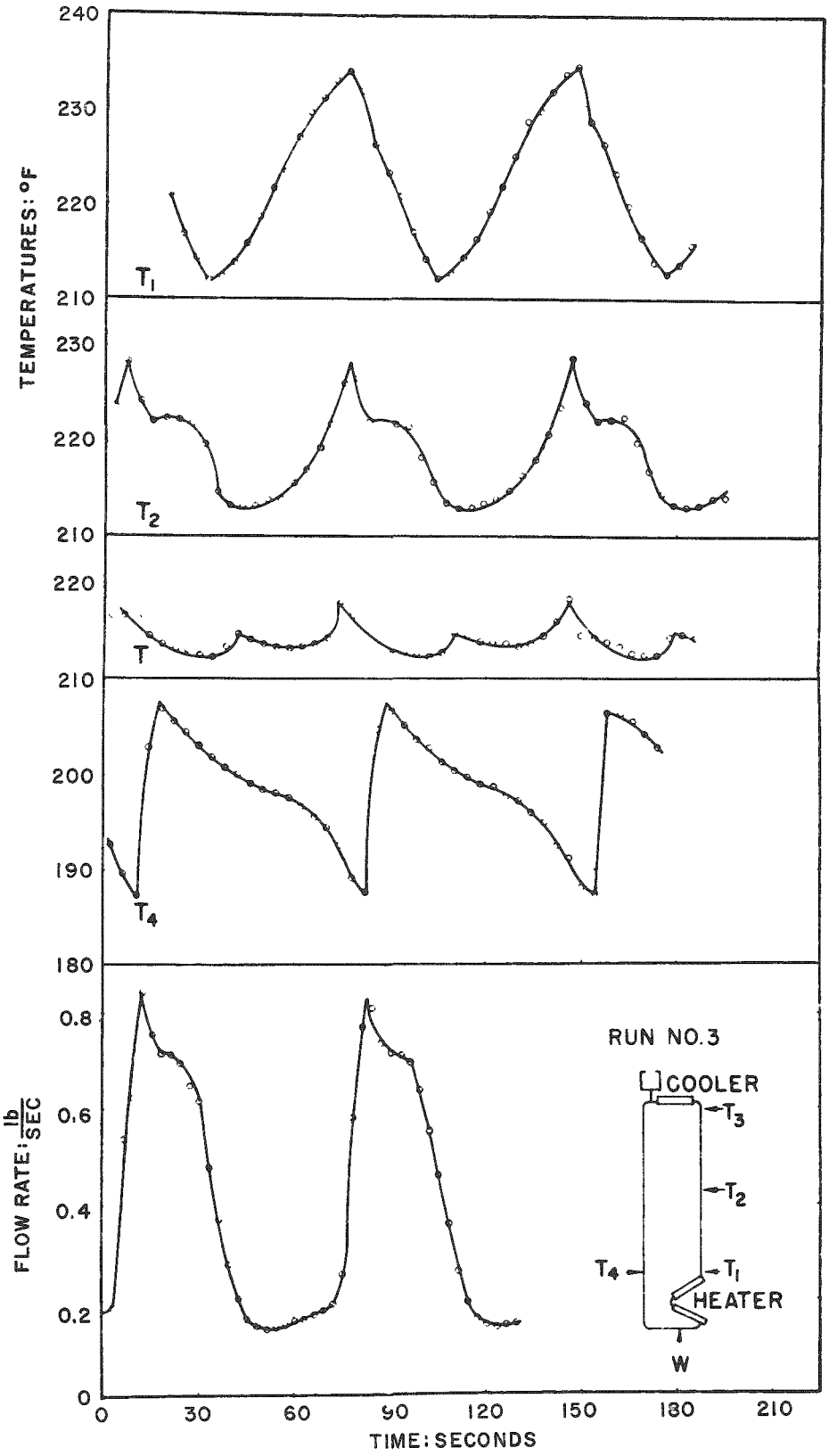

Fig. 6.5

Transient Temperature and Flow Behavior of a Hydraulic Test Loop, Run No. 3 - Q = 9.44 Btu/sec

111-8893

System parameters (plate temperatures, channel pressure drop, channel inlet flow rate) were measured by fast response transient instrumentation. Slides shown during the session gave experimental points on an exit quality versus fl/D basis where the f is a friction factor for two phase flow.

Ramo-Wooldridge has an atmospheric pressure test loop mocking up the Spert reactor. This loop is instrumented with an x-ray attenuation method for void measurement, a turbine meter for flow measurement and standard loop instrumentation for temperature and power.(121)

Using a ± 10% variation in pressure drop across the test section as the criterion of stability, General Electric ran stability and burnout tests on a natural circulation heated annular test loop with two geometries and control of inlet subcooling.(95) In addition to standard flow, temperature, pressure and liquid level measurements, four variables (ΔP across test section and downcomer orifice, temperature of inlet water and internal heater surface) were recorded on fast acting recorders (Fig. 6.6). Results from these tests are:

(1) Increased subcooling caused decreased stability.

(2) An increase in flow area caused by decreasing the center, heated portion of the annulus caused an increase in the total flow rate of the loop and a decrease in the stability. Note: For a given subcooling the larger flow area has a lower exit quality, thus a lower void fraction throughout the loop. With less driving head and less boiling length in the test section, the larger area test has less two-phase friction and more single-phase friction. At the same time the larger area system was more unstable.

(3) The effect of a restriction in the downcomer was to decrease total flow rate of the loop and to increase system stability.

Due to heat losses in the system it was impossible in most cases to operate at constant inlet subcooling on the rising portion of the velocity vs power curve.

The preceding experiments give a rather limited amount of experimental data to use when investigating the validity of any analytical approach to the problem. Specifically, the 2000 psia loop at Argonne, the Minnesota loop and the loop at General Electric gave time traces of system parameter oscillations showing frequency and amplitude of oscillation. In addition some general conclusions about stability effects can be drawn from the tests:

(1) Increased system pressure has a stabilizing influence.

(2) Additional flow resistance in the downcomer portion of the flow circuit has a stabilizing effect.

(3) Decreased subcooling has a stabilizing influence.

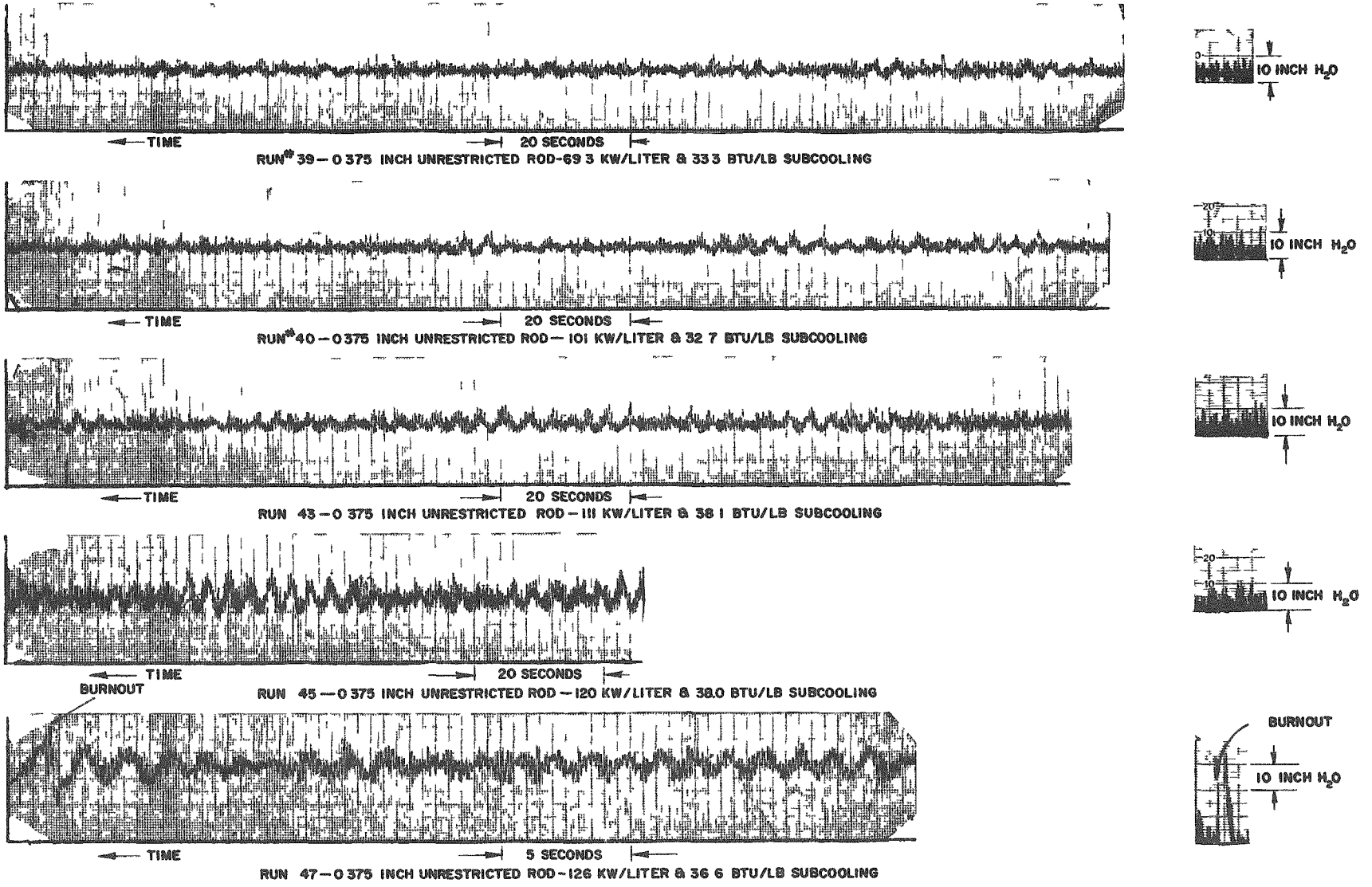

Fig 6 6a

Pressure Drop Traces as Power is Raised at Constant Inlet Subcooling

111-8892

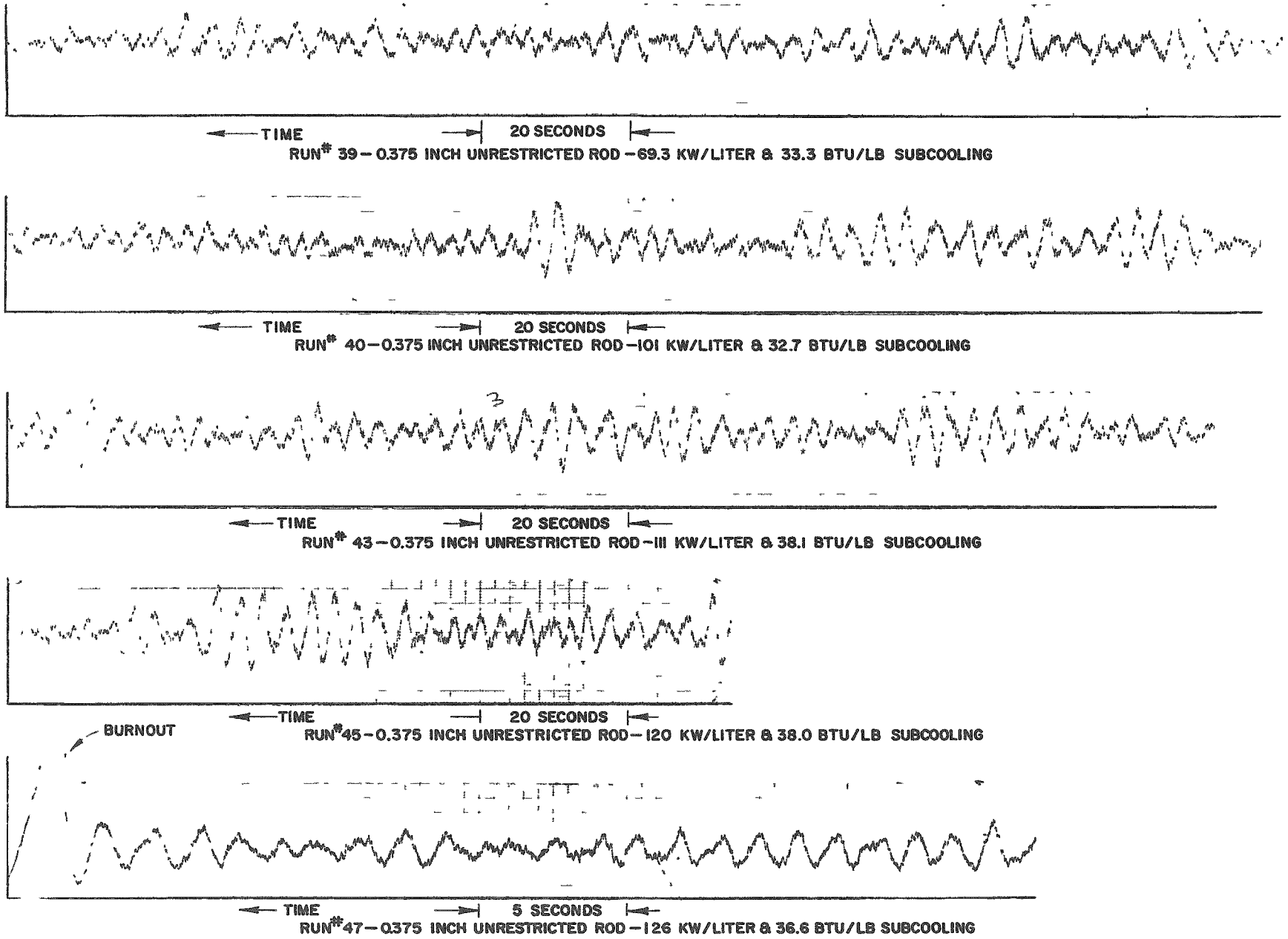

Fig. 6.6b

Flow Traces as Power is Raised at Constant Subcooling

111-8899

6.5 Test Loop Stability Analysis

The ability to predict the dependence of the inception point, frequency and amplitude of oscillations on system parameters is the goal of analytical work in this field. Two types of approaches have been used in previous and current attempts to analyze this problem. The first approach is that the general equations of the system, such as the energy, conservation of mass and momentum equations are solved with the resultant solution indicating the influence of system parameters on stability. The second approach is that some controlling phenomenon such as an extremum in the pressure drop vs flow rate curve is assumed the only phenomenon of importance, and system stability is evaluated by investigation of factors affecting this phenomenon.

Although the first method is obviously more general, the extra generality is accompanied by an increase in the complication of problem solution. The necessary simplifications for the solution of the general equations might mask the effect to be measured. If this is the case, the second approach will lead to more useful results. In the following portion of this discussion the two published approaches of the first type will be reviewed. In addition, a variety of single phenomenon which conceivably could cause oscillations will be considered. Where possible, the results of these analyses will be compared with experimental data.

Westinghouse[120,122] using the equations of continuity, energy and momentum obtained a transfer function between the mass flow rate and the heat flux. It was necessary, during the derivation of this transfer function, to assume:

(1) Parallel flow channels,
(2) Constant pressure drop across the channel,
(3) Constant inlet subcooling,
(4) Homogeneous flow model for calculating pressure drop.

The conditions of stability of this transfer function enables prediction of the frequency and exit quality for given hydrodynamic conditions in the tube. To be specific, two equivalent statements of the stability criterion are shown by the following equations, giving exit quality and exit enthalpy necessary for flow oscillations.

$$x_e = \frac{v_f}{v_{fg}} \left[\frac{fL}{D} + 1 + \frac{2x_e}{v_f/v_g + x} \right] \tag{6.1}$$

$$h_e = \frac{h_{fg}\, v_f}{v_{fg}} \left[\frac{fL}{D} + 1 + \frac{2x_e}{v_f/v_g + x} \right] + h_{sat} \tag{6.2}$$

The frequency ω_n is given by the equation:

$$\omega_n^2 = 2\,\frac{fV^2}{LD} + 4\,\frac{V}{L^2}\,(V_e - V_i) + \left(\frac{q}{L} - \frac{2V_e^2}{L^2} - \frac{fV}{2LD}\right)\frac{\rho_1}{\rho} \qquad (6.3)$$

or approximately:

$$\omega_n \approx \sqrt{\frac{f}{LD}}\;V \qquad (6.4)$$

Nomenclature in the above equations is standard, except as follows:

h_e - Enthalpy at channel exit

f - Two-phase friction factor

V - Coolant velocity at channel midpoint

V_i - Coolant velocity at channel inlet

V_e - Coolant velocity at channel exit.

Experimental verification of this model is claimed on the basis of correct prediction of experimental trends. Attempts to absolutely prove this model and most of the following analytical models are hampered by lack of knowledge of other aspects of two-phase hydrodynamics. Without adequate knowledge of relative velocity between phases, two-phase flow regimes and two-phase pressure drop, most of the analytical approaches which include these parameters can only be expected to predict trends. Lack of knowledge of two-phase friction factors[123] makes present verification of this model impossible. The slides, shown at the ASME Heat Transfer Conference, show the experimental data to fall considerably below the prediction and to fall about a line with a larger slope than predicted on a x_e vs fL/D graph.

E. H. Wissler also used a rather general approach in his thesis.[119] General energy, momentum and continuity equations were derived in vector notation including two phases with a discontinuous interface. These equations were applied to a model embodying the following assumptions:

(1) Steam and water are in equilibrium at any cross section.

(2) Each phase has a well defined cross sectional area at any position and time.

(3) Across its area each phase has a uniform velocity except a wall where velocity equals zero.

(4) Assumption three implies that the frictional force does no work on the fluid (thus no friction term in energy equation but friction force in momentum equation).

The resultant three equations were simplified by use of a defined mean density, mean velocity, mean energy, momentum transfer rate and energy transfer rate. The equations were then placed in a finite difference form, but since the finite difference equations would not converge, this approach was abandoned.

A one phase, open ended loop was analyzed using Laplace transforms and it was concluded:

(1) The oscillatory force must be generated in the riser.

(2) For oscillations to occur the fluid coefficient of expansion must exceed a certain value which is dependent on friction.

(3) Oscillation period equals fluid residence time in heater and riser.

From this analysis the conclusion was drawn that even in a two-phase, closed loop the period would be dependent on the geometry and the mean velocity.

This analysis was extended to a two-phase, closed loop and the resultant differential-difference equations when solved on an analog computer gave a time plot of flow rate with periods of oscillation roughly equivalent to experimental values.

The only quantitative values in this analysis dealt with periods of oscillation. No attempt was made to predict the inception point of instability.

The oscillations measured by Wissler are qualitatively and quantitatively different from those measured at General Electric and Argonne National Laboratory. Wissler's periods are long (50-200 sec) with steady amplitude and often non-symmetrical shapes. The other two loops show flow traces with two distinct periods; a short period (under 5 sec) and a longer period (50-100 sec). In general, these flow traces are quite similar to the power traces of oscillatory reactors.

In the second analytical approach to frequency prediction, Ray Viskanta[119] has considered the oscillation period and compared this to the period of natural oscillation of the hydraulic loop. Using LaGrangian equations of motion, a natural oscillation frequency of the two-phase test loop was calculated.[116] The calculated frequency, and the experimental frequency, from the Argonne National Laboratory test loop agreed very favorably. This approach, however, makes no assumptions to the underlying cause of instability and does not preclude the possibility that the good agreement obtained was due to chance.

Apparently, the first and most widely known analysis assuming the cause of unstable behavior to be a single phenomenon was the equation of unstable behavior with an extremum in the pressure drop, flow rate curve. Various papers using this approach have been published.(124-126)

As shown in Fig. 6.7 the power at which a decreasing pressure drop with increasing flow first becomes evident was thought to be the power where a given system becomes unstable.

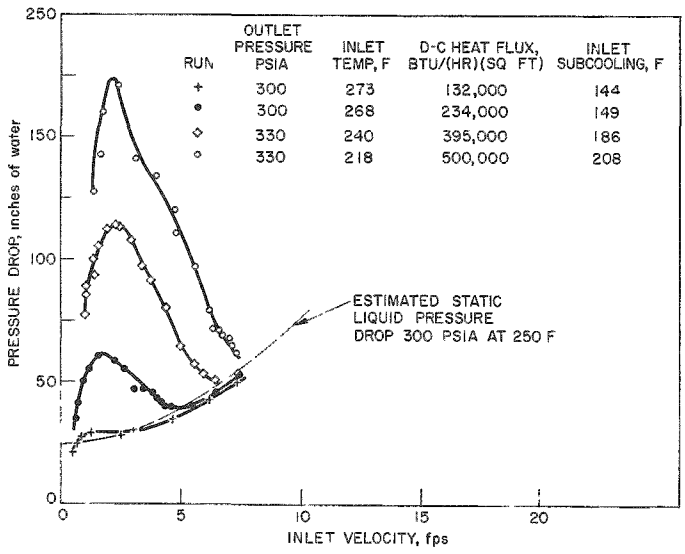

Fig. 6.7

Static Pressure Drop on a 0.174 in. I.D.
Stainless Steel AISI Type 347 Heated
Single Tube
111-8895

An early paper using this approach was published by M. Ledinegg.(124) In 1938, M. Ledinegg analyzed the pressure drop characteristics of a boiler tube in forced circulation by considering only friction and momentum pressure drop. For this particular case, the buoyancy effects and entrance losses were considered to be small compared to the friction and momentum pressure drop.

The friction pressure drop in the preheating zone was given as

$$\Delta P = \frac{f L_0 W^2}{2gDA^2 \rho_f} \tag{6.5}$$

and the mean density in the evaporating section was defined as the reciprocal of the mean specific volume

$$\frac{1}{\overline{\rho}} = \overline{v} = \frac{1}{L_t - L_0} \int_{L_0}^{L_t} v dL \quad . \tag{6.6}$$

Considering a uniform heat input, the steam flow weight ratio (pounds of steam flowing per pound of mixture flowing(is a linear function of length, so that

$$\overline{v} = \frac{1}{x_e} \int_0^{x_e} v dx \quad . \tag{6.7}$$

It was also assumed that the steam velocity was equal to the water velocity, so that $v = v_f + x v_{fg}$.

The mean specific volume is then

$$\overline{v} = \frac{1}{x_e} \int_0^{x_e} (v_f + x v_{fg}) dx = v_f + \frac{x_e}{2} v_{fg} \quad . \tag{6.8}$$

The boiling friction drop is

$$\Delta P = \frac{f W^2}{A^2 2 g D \rho_f} (L_t - L_0) \left[1 + \frac{x_e}{2} \frac{v_{fg}}{v_f} \right] \quad . \tag{6.9}$$

The acceleration or momentum pressure change may be found from a force balance to be

$$\Delta P = \frac{W^2 x}{A^2 \rho_f g} \left(\frac{v_{fg}}{v_f} \right) \quad . \tag{6.10}$$

Combining Eqs. (6.5), (6.6), (6.7), (6.9), and (6.10), the total pressure drop is

$$\Delta P = \frac{f W^2}{2 g D A^2 \rho_f} \left[L_0 + (L_t - L_0) \left(1 + \frac{x_e}{2} \frac{v_{fg}}{v_f} \right) \right] + \frac{W^2 x \, v_{fg}}{g A^2 \rho_f v_f} \quad . \tag{6.11}$$

From a heat balance of the boiler tube

$$Q = W \left[\Delta h + x h_{fg} \right] \quad , \text{ where } \Delta h = h_f - h_{in} \quad . \tag{6.12}$$

It is also noted that the relation between preheater length and total tube length is

$$L_0 = \frac{W \Delta h \, L_t}{Q} \quad . \tag{6.13}$$

Combining Eqs. (6.11), (6.12), and (6.13) and eliminating "x," yields a single pressure drop relation in terms of pressure, geometry, power and mass flow rate.

$$\Delta P = \frac{fL_t}{2_g D\rho_f A^2}\left[W^2\left(1 - \frac{\Delta h v_{fg}}{h_{fg}\, v_f}\right) + W\left(\frac{Q v_{fg}}{2h_{fg}\, v_f}\right) + \frac{W^3 \Delta h^2 v_{fg}}{2Q\, h_{fg}\, v_f}\right]$$

$$+\frac{WQv_{fg}}{\rho_f A^2 g h_{fg} v_f} - \frac{W^2 \Delta h v_{fg}}{\rho_f A^2 g h_{fg} v_f} \quad . \tag{6.14}$$

The condition for the onset of instability is defined mathematically as

$$\frac{d\Delta P}{dW} = 0 \quad .$$

If Eq. (6.14) is differentiated with respect to W, and the differential is set equal to zero, the result is a quadratic equation:

$$W^2 - \alpha W + \beta = 0 \tag{6.15}$$

where

$$\alpha = \frac{\frac{fL_t}{2gD}\left(\frac{2\Delta h v_{fg}}{h_{fg}} - 2v_f\right) + \frac{2\Delta h v_{fg}}{g\, h_{fg}}}{\frac{3\Delta h^2 v_{fg} fL_t}{4gDh_{fg}\, Q}} \tag{6.16}$$

and

$$\beta = \frac{\frac{v_{fg}\, Q}{h_{fg}}\left(\frac{fL_t}{4gD} + \frac{1}{g}\right)}{\frac{3\Delta h^2 v_{fg} fL_t}{4gDh_{fg}\, Q}} \quad . \tag{6.17}$$

The solution of Eq. (6.15) is

$$W = \frac{\alpha}{2} \pm \sqrt{\frac{\alpha^2}{4} - \beta} \quad . \tag{6.18}$$

For stable flow, the root expression is imaginary, and only one value of W is possible. For unstable flow, the root expression is real, and three values of W are possible for a given pressure drop. Under these conditions, a parallel flow arrangement of tubes would exhibit an unstable

condition; that is, some tubes would operate at flows different from neighboring tubes. It is also true that depending upon the shape of the ΔP versus W curve, some tubes may have flow rates changing as a function of time. The conditions that describe the onset of instability may then be defined as all cases for which

$$\alpha \geq 2\sqrt{\xi} \quad . \tag{6.19}$$

Referring to Eqs. (6.16) and (6.17), the condition is then

$$\Delta h \geq \frac{AB}{A + \frac{1}{g} - \sqrt{\frac{3}{2} A \left(\frac{1}{2} A + \frac{1}{g}\right)}} \tag{6.20}$$

where A is the geometry function

$$A = \frac{f L_t}{2gD} \tag{6.21}$$

and B is the pressure function

$$B = \left(\frac{v_f}{v_{fg}}\right) h_{fg} \quad . \tag{6.22}$$

Figure 6.8 shows Eq. (6.20) as a function of pressure and geometry. Several interesting conclusions can be drawn from Eq. (6.20) which are also evident from Fig. 6.8.

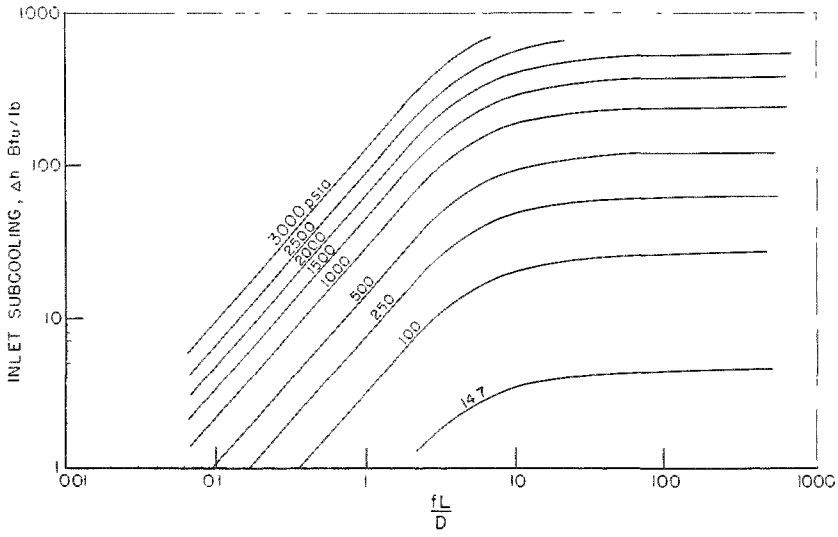

Fig. 6.8

Stability Criteria
(Ledinegg Analysis)
111-8898

(1) At low values of A, the amount of subcooling that can be tolerated is almost a linear function of A. The lines in Fig. 6.8 at low A have a slope of approximately unity.

(2) At high values of A, the amount of subcooling that can be tolerated is independent of geometry and has a limit

$$\Delta h \geq 7.46 \left(\frac{v_f}{v_{fg}} \right) h_{fg} \quad . \tag{6.23}$$

(3) At all conditions, the amount of subcooling that can be tolerated is directly proportional to B, which in turn is almost linear with pressure. Therefore, the tolerable subcooling is almost linear as a function of pressure (see Fig. 6.8).

The case of boiling in natural circulation with relatively short channels presents a different problem, since the buoyancy forces cannot be neglected. If the relative velocity of the steam is neglected (equal steam and water velocities) then the buoyancy term is:

$$\Delta P = \rho_f L_0 + \frac{L_t - L_0}{x_e \, v_{fg}} \ln \left(1 + \frac{x_e}{2} \frac{v_{fg}}{v_f} \right) \quad . \tag{6.24}$$

Equation (6.20) gives the lower limit of the buoyancy forces. The upper limit can be calculated assuming a linear change in density with length. For this case,

$$\Delta P = \rho_f L_0 + \left(\frac{\rho_f + \rho_e}{2} \right) \left(L_t - L_0 \right) \quad . \tag{6.25}$$

If either Eqs. (6.24) or (6.25) is added to Eq. (6.14) after eliminating "x," and the combined equation is differentiated with respect to W, an equation is obtained which is difficult to solve for the stability condition.

Although analysis leading to the stability criterion in Fig. 6.8 is based on a forced circulation system, the conclusions mentioned above seem to fit the experimental results for natural circulation stability tests.

The reason for this is not firmly established, but it may be argued that in the region of instability, the change in the buoyancy term which is a measure of the pumping head is not greatly affected by a change in mass flow rate, while the friction and momentum changes are greatly affected. Thus, the system acts as a forced circulation system with the constant driving head equal to the head of water, in the downcomer. It is

also interesting that the combination of Eq. (6.21) and conclusion (1) lead to a result quite similar to that of the Westinghouse analysis. (See Eq. 6.2). In this range, both approaches show some enthalpy (exit enthalpy in the Westinghouse approach, inlet enthalpy in the Ledinegg approach) at which the system goes unstable as a linear function of fL/D.

While all these results seem to lend credence to the basis for this model, the results of the forced circulation tests at Argonne National Laboratory (Fig. 6.4) show this is not the cause of the oscillations in the 2,000 psia loop. In these tests, pressure drop across the test section and riser, measured while the loop is operating in forced circulation with the same inlet subcooling and power as a natural circulation unstable run, show an increasing pressure drop with increasing flow rate.

The effect of power input on recirculation rate in a natural circulation system is shown in Fig. 6.9. Some investigators[127] have assumed this peak recirculation rate marks the last stable operating point and operation on the downward portion of the velocity curve is unstable.

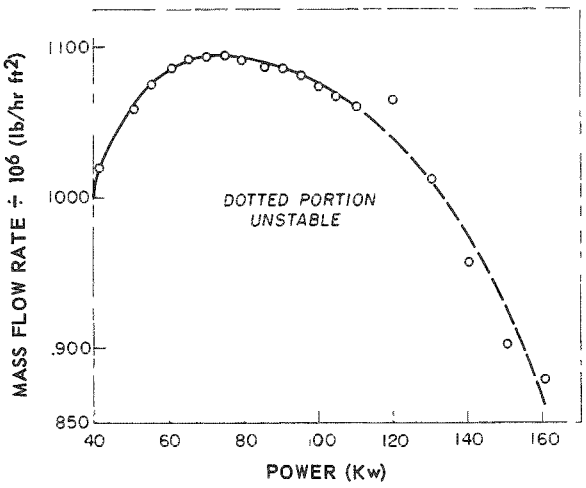

Fig. 6.9

Power vs Mass Flow Rate as Measured
on 2,000 psia Test Loop (1 in. dia.
Heated Section and Riser)
111-8894

It is instructive to again look critically at the flow oscillation traces from General Electric and Argonne National Laboratory tests. As previously mentioned, there is evident in both these traces two oscillation frequencies, a small period, continuous oscillation whose amplitude varies with a much larger period. While General Electric used as a criterion of instability the rather arbitrary point where pressure oscillations due to the continuous small period flow oscillations reach ± 10%, Argonne workers

have used variations in the larger period as a measurement of instability. The point at which the large period oscillations become definitely unstable is quite sensitive to system parameter changes. This should result in better reproducibility in experimental data than General Electric obtained in their published points.

Since General Electric always operated on the downward sloping portion of the velocity power curve and always had the random small period oscillations it might be possible that these oscillations show up after passing the maximum point of the curve and build up in amplitude as the system progressively deviated from this point. However, if differences in the longer period oscillations are used as a stability criterion the maximum point of the flow rate power curve would not correspond to inception of instability as systems have operated stably well past this point of the curve.

One of the models of instability mentioned by General Electric group considers static head potential energy. Quoting directly from GEAP 3215:[95]

> "A second model for vertical two-phase flow kinematics is based upon the potential energy of the static head. If a flow loop is operated in a condition of equilibrium, the steam velocity will exceed the water velocity by a particular amount, and a nearly uniform fraction of the channel volume will be occupied by steam. The natural circulation driving head is the steam volume fraction times the vertical height times the difference of water and steam densities. Now, if equilibrium is disturbed at the base of the loop by a change in heat addition, or a change in inlet water velocity, a different slip velocity is to be expected. As a consequence, the steam volume fraction will also change. In general, the steam volume fraction is not altered instantaneously across the riser, but changes progressively up the riser with the average velocity of flow. Consequently, the driving head changes, but the total effect is delayed by the fluid transit time up the riser. The general equation describing the model is

$$\frac{dV}{dt} + aV^2 + bV + \int_0^T f\,[Q,\ V\,(t-\tau)]\,d\tau - c = 0 \qquad (6.26)$$

where

V = inlet water velocity
T = fluid transit time across riser
f = volume fraction dependence on the inlet velocity and heat input
Q = function of heat input
a,b,c = loop friction loss and height parameters

"Conditions of instability can be derived from this equation which result in relations between a, b, f, and c. The fundamental period is approximately $\frac{3}{4}$ T. The instability can be controlled by increasing the loop pressure drop at the inlet or in the downcomer, which increases the value of a and b. Control may also be possible by increasing the riser pressure drop, but in some cases this course would affect the function of f, so that improvement would not necessarily result.

"Comparison of the measured loop period with the predicted value is satisfactory. The average riser fluid velocity is between 6 and 8 ft/sec; the riser height is 15 ft and hence the transit time is between 2 and $2\frac{1}{2}$ sec. The observed period is about 2 sec. The kinematics of this model, furthermore, are in general agreement with test results obtained in a natural circulation loop at the University of Minnesota.(118,128) The model has, however, a serious drawback. Unless the precise nature of the function f is known, the thresholds of instability with reference to heat input, loop pressure and inlet velocity cannot be predicted. Attempts to predict thresholds by means of slip velocity correlations, or correlations of steam volume fraction versus quality curves have not been successful to date. The model, therefore, leads to two alternative conclusions: either its kinematics are wrong, or the kinematics are right, and present knowledge of the mechanics of the two-phase flow is inadequate."

Again we are faced with the problem of insufficient proof due to lack of knowledge of two-phase hydrodynamics.

A second instability model proposed in the General Electric report is based on Levy's momentum equations for two-phase flow. Quoting the portion of the report which deals directly with this model:

"The third model to be considered is concerned with flow mechanics and flow pattern instability (129) It deals with the causes of instability rather than its propagation. It is based on equations derived by Levy.(130) His approach is to examine the energy transmitted by shear forces at the steam-water interface, and at the fluid-channel interface. When the shearing energy received by one fluid exceeds its ability to dissipate that energy at the channel wall, the excess appears in the form of eddies or slugs.

"For the momentum model of reference (130), the following equation is obtained:*

$$\frac{(dP/dy)_{LTP}}{(dP/dy)_0} = \frac{(dP/dy)_{TP}}{(dP/dy)_{LSP}} (1-x)^{1.75} - \frac{\rho_\ell - \rho_g}{(-dP/dy)_0} \alpha \sin \theta \qquad (6.27)$$

*Similar equations can be obtained for other steam slip relations.

where

$(dP/dy)_{LTP}$ = net pressure losses of water in two-phase flow (made up of losses at wall and interface)
$(dP/dy)_0$ = pressure loss for 100 percent water flow
$(dP/dy)_{TP}$ = two-phase pressure loss
$(dP/dy)_{LSP}$ = pressure loss for water flow alone
x = steam fraction by weight
ρ_ℓ = water density
ρ_g = gas density
α = steam void fraction
θ = inclination angle of channel from horizontal

Eddying occurs when the left hand side of the above equation is negative."

If the phenomenon of instability is really due to this eddying effect in the boundary layer it would seem a discontinuity should appear in the pressure drop characteristics of the two phase segment of the loop, as the loop approaches an unstable operating point. The series of forced circulation points taken at and near the instability inception point of the Argonne 2,000 psia loop fail to show any pressure drop discontinuity (Fig. 6.4).

Other models based on the idea of a change of two-phase flow regime would be faced with the same experimental fact and would seem to be invalid.

The results of some early experimental work done at Argonne National Laboratory showed it was possible in some systems to generate steam at a higher rate than could be removed in any steady flow state.

Figure 6.10 shows that for the given system, steam was generated at such a rate that steady flow is impossible under any conditions. The upper curve shows measured values of forced flow pressure drop which are all greater than 46 inches of water, which in the natural circulation case represents the available operating pressure differential. Such a power level would cause a chugging or pulsing flow. The characteristics of this type of flow are:

(1) violent expulsion of water by steam from the top or from both ends of the heated channel,
(2) re-entry of water into the empty channel; and then
(3) expulsion again, and then again
(4) re-entry, etc.

Although this phenomenon was apparently the cause of unstable behavior in this particular apparatus, it cannot be the general cause of unstable behavior in all loops as experimental results from the 2,000 psia loop do not show the discrepancy between forced circulation pressure drop and available natural circulation driving head at an unstable point (Fig. 6.4).

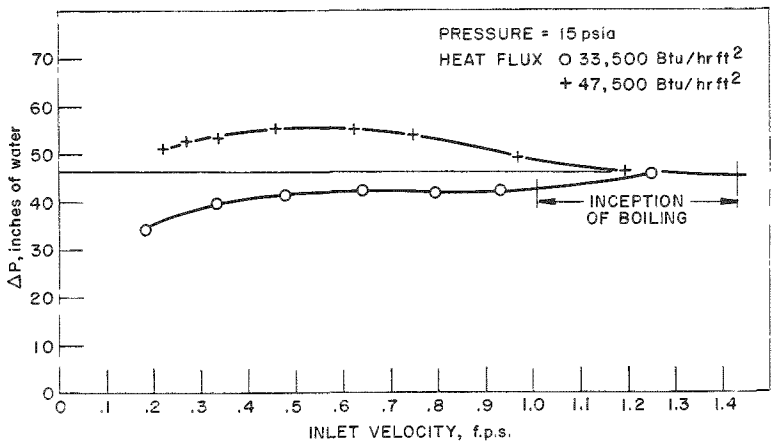

Fig. 6.10

Pressure Drop as a Function of Inlet Velocity
and Heat Flux for a 0.087 in. x 2.25 in. x
43 in. Vertical Channel
111-8896

Two more phenomena which could lead to unstable loop operation will be briefly mentioned.

Sonic velocity of a two-phase mixture becomes quite low under certain quality and pressure conditions.(131) It seems conceivable that some sort of a sonic velocity choking effect could become important at the operating conditions and velocity in a test loop.

Small, random, velocity fluctuations when combined with constant make-up water flow rate cause variations in downcomer density and subcooling. The effect of these subcooling variations on the driving head and pressure drop in the two-phase region should in turn cause another velocity fluctuation. The amplitude of the second velocity fluctuation would be dependent on the hydrodynamics of the two-phase system. It seems conceivable that at some power the hydrodynamics will be such that the feedback circuit (velocity to subcooling to velocity) will just reproduce the original velocity fluctuation, thus causing the loop to oscillate.

6.6. Stability Considerations in Reactor Design

The initial boiling reactors were designed as feasibility experiments. Based on early boiling experiments(132) which showed that large power densities were possible in a boiling reactor, the first Borax reactor was built to investigate the influence of boiling turbulence on reactor stability as well as other feasibility considerations. The experience gained from this reactor combined with information from further heat transfer and fluid flow experimental information was used as a basis for the design of the second Borax reactor.

This design procedure which has been quite generally followed has three important aspects.

(1) New reactors are designed similarly to earlier reactors so as to use experience gained from these reactors.

(2) The effects of changes on previous designs are roughly accounted for by parameter studies which indicate trends. Radical changes of an important nature may be experimentally checked on existing reactors or test loops before incorporation in large new reactors. As an example, the effects of elements with long thermal time constant was checked on Borax IV before EBWR was operated.

(3) A large factor of safety is included to account for variation.

The logical first step to a better design criterion for reactor stability is investigation of test loop stability. It seems doubtful that a reactor could operate stably where a test loop mock-up of the reactor is unstable though it is possible that the coupling between reactor steam voids and reactor power causes reactor instability at lower heat flux than the heat flux causing test loop instability.

Similarity of unstable flow traces in a natural circulation loop and unstable power traces in a reactor certainly points to a hydrodynamic basis for reactor instability.

Further credence is lent to the idea of the hydrodynamic basis of reactor stability by the operating experience of EBWR. Hydraulic loop tests on a system with geometry similar to the flow path in EBWR showed that an instability threshold existed at an exit void fraction of approximately 0.75. The exit void fraction in the maximum power EBWR fuel element at 61 Mw was estimated to be 0.70. EBWR approached both exit void fraction of 0.75 and unstable behavior of 61 Mw operation.

6.7. Conclusions

The experimental information in the field of reactor and test loop stability is sparse. Analytical procedures in this field are still in a preliminary state. This undeveloped state necessitates a large factor of safety in the stability considerations of proposed reactor design. The large factor of safety causes overdesign of reactors which are inherently limited in power removal by stability limitations. These limitations become more critical when an apparent connection between burnout and stability is noted.[133,95,117] A more precise method of prediction of stability is important to the future development of boiling water reactors.

7. CALCULATION PROCEDURES FOR BOILING SYSTEMS

7.1. Natural Circulation System Analysis

A natural circulation system is one in which fluid flow is derived through a density potential existing between vertical segments of the system, commonly referred to as the riser and downcomer. The density differential may be induced by a variety of methods, such as maintaining a sufficient temperature difference by heating or cooling one of the legs, etc.

Of particular interest with respect to boiling reactors is the system where sufficient heat is added to one leg to cause boiling of the fluid.

Analysis of such a natural circulation system is complicated by the interrelationship existing between various system parameters such as power, steam volume and weight fraction, circulation velocity, subcooling, etc., and plagued by inadequacy of information on two-phase flow concerning the relative velocity between the steam and water phases, fluids, etc. The basic research in the field of two-phase flow continues in an attempt to provide sufficient information on the above-mentioned problems that can be utilized in making a competent hydrodynamic analysis on natural circulation systems.

An analytical procedure for calculating the performance of a natural circulation system is presented, whose development was aided by comparing numerous data obtained from laboratory tests on natural circulation systems with varying geometries. The laboratory tests were required to establish the validity of a number of assumptions made in the analysis.

An analysis of a basic simple natural circulation system has been given by Lottes and Flinn.[19] However, the authors did not account for various riser heated section geometries which tend to complicate the problems considerably, nor did they account for the effect of subcooling which becomes increasingly important at higher pressures. Therefore, a very general analysis was made that could be applicable to the large majority of systems. The analysis for the natural circulation system is then modified for application in a forced circulation system.

1. Hydrodynamic Analysis

In a natural circulation system

$$\Sigma \Delta P = 0, \tag{7.1}$$

which states that the summation of the pressure drops, ΔP, around the closed loop, consisting of riser and downcomer, must be equal to zero. The total pressure drop over a differential length may be obtained as follows:

From a force or momentum balance,

$$\Sigma F_y = m \frac{dv}{dt} \quad . \tag{7.2}$$

Applying Eq. (7.2) over a differential pipe length depicted below,

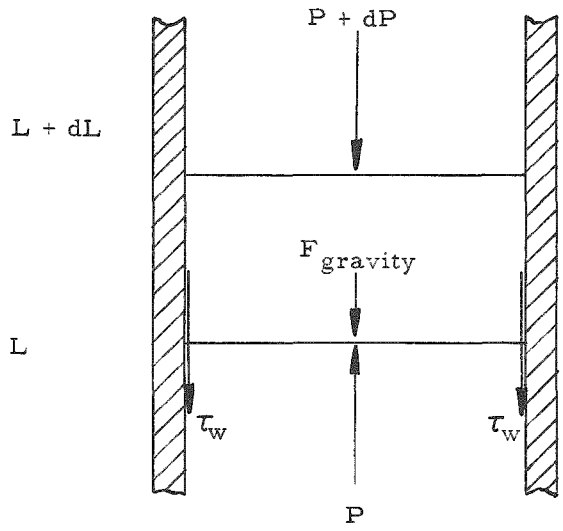

$$PA - A(P + dP) - A\rho dL\left(\frac{g}{g_c}\right) - \tau_w \pi D dL = m \frac{dv}{dt}$$

or

$$PA - PA - AdP - A\rho dL\left(\frac{g}{g_c}\right) - \tau_w \pi D dL = \rho \frac{AdL}{g_c} \frac{dv}{dt} \quad .$$

Simplifying

$$- dP - \rho dL\left(\frac{g}{g_c}\right) - \tau_w \frac{\pi D\, dL}{\frac{\pi D^2}{4}} = \rho \frac{dL}{g_c} \frac{dv}{dt} \quad .$$

By definition

$$\text{Friction factor} = F = \tau_w / \rho \frac{v^2}{2g} \quad .$$

Also, substituting $\frac{dL}{dt} = v$,

$$- dP - \rho dL \frac{g}{g_c} - 4F\rho \frac{v^2}{2g} \frac{dL}{D} = \rho \frac{vdv}{g_c}$$

or

$$- dP - \rho dL \frac{g}{g_c} - f\rho \frac{v^2}{2g} \frac{dL}{D} = \rho \frac{vdv}{g_c} \quad ,$$

where f is the Moody friction factor, and v is velocity.

The total pressure drop over a differential length therefore may be written as a summation of the frictional, hydrostatic head and acceleration components:

$$- dP_T = dP_f + dP_{head} + dP_{acc} \quad . \tag{7.3}$$

A basic natural circulation system is schematically illustrated in Fig. 7.1.

Fig. 7.1

Basic Natural Circulation System

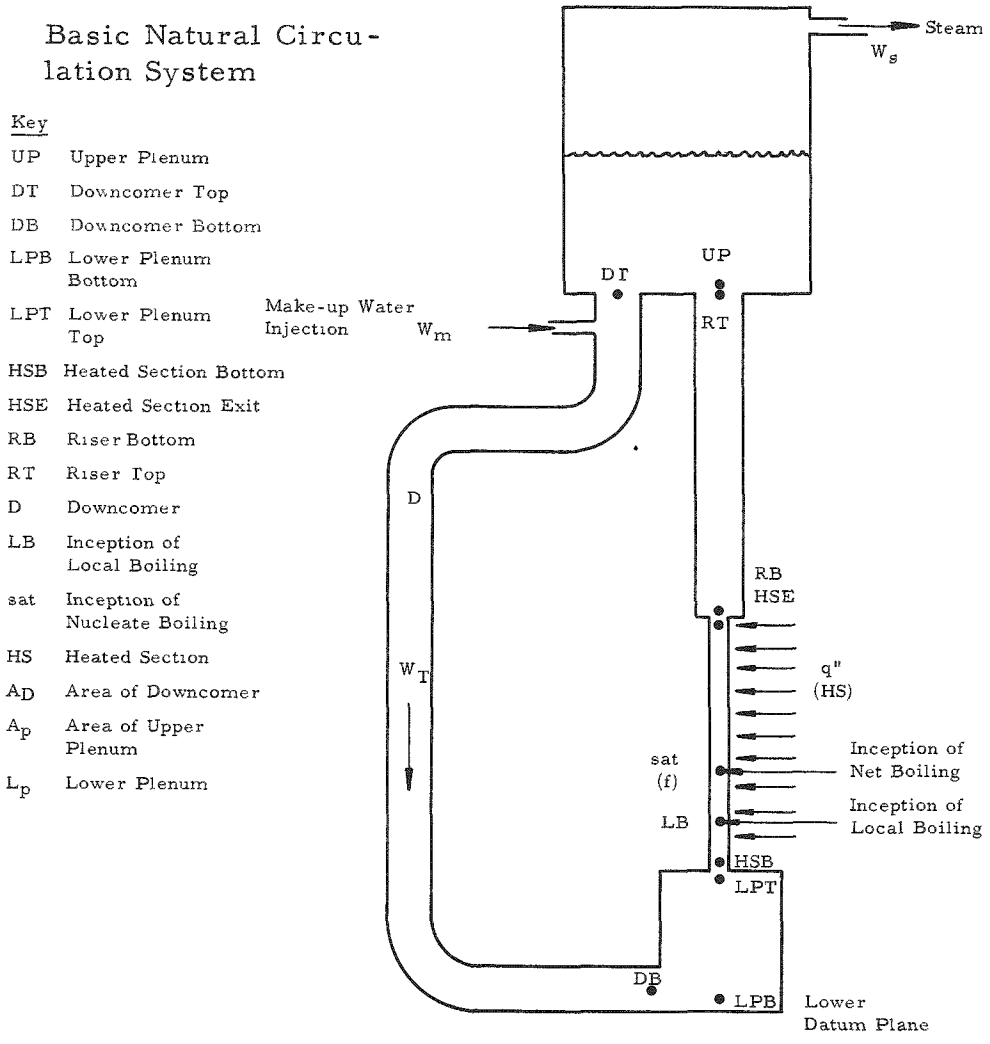

The system is broken down into various segments which lend themselves conveniently to analysis. Equation (7.3) is applied to each section individually and then a summation is made to satisfy Eq. (7.1). Starting at point UP (Fig. 7.1) the loop may be divided into the following sections:

(1) Contraction from Upper Plenum

$$-\int_{UP}^{DT} dP = \int_{UP}^{DT} dP_{Head} + \int_{UP}^{DT} dP_{acc} + \int_{UP}^{DT} dP_{Friction}$$

$$= \frac{g}{g_c}\rho_f \int_{UP}^{DT} dL + \int_{UP}^{DT} \rho_f \frac{v dv}{g_c} + \int_{UP}^{DT} dP_{Friction} \quad .$$

By definition for a contraction,

$$\int_{UP}^{DT} dP_{Friction} = K_{c_{UP}} \rho_f \frac{v^2_{DT}}{2g_c} \quad ,$$

so that

$$-\left[P\right]_{UP}^{DT} = \frac{g}{g_c}\rho_f \left[L\right]_{UP}^{DT} + \rho_f \left[\frac{v^2}{2g_c}\right]_{UP}^{DT} + K_{c_{UP}} \rho_f \frac{v^2_{DT}}{2g_c}$$

or, since $L_{DT} = L_{UP}$,

$$P_{UP} - P_{DT} = \rho_f \left[\frac{v^2_{DT}}{2g_c} - \frac{v^2_{UP}}{2g_c}\right] + K_{c_{UP}} \rho_f \frac{v^2_{DT}}{2g_c} \quad .$$

Simplifying, since $V_{UP} \ll V_{DT}$,

$$P_{UP} - P_{DT} = \rho_f \frac{v^2_{DT}}{2g_c}\left[1 + K_{c_{UP}}\right] \quad . \tag{7.4}$$

Also from the continuity equation

$$v_{DT} A_D \rho_{DT} = v_{sat} A_{HS} \rho_f \quad .$$

Thus

$$v^2_{DT} = v^2_{sat}\left(\frac{A_{HS}}{A_{DT}}\right)^2 \left(\frac{\rho_f}{\rho_{DT}}\right)^2 \quad .$$

Since $\rho_f = \rho_{DT}$,

$$v_{DT}^2 = v_{sat}^2 \left(\frac{A_{HS}}{A_D}\right)^2 \quad .$$

Equation (7.4) thus becomes

$$P_{UP} - P_{DT} = \frac{v_{sat}^2}{2g_c} \left(\frac{A_{HS}}{A_D}\right)^2 \rho_f \left[1 + K_{c_{UP}}\right]$$

or

$$P_{UP} - P_{DT} = \frac{v_{sat}^2}{2g_c} [N_1] \qquad (7.5)$$

where $N_1 \equiv (A_{HS}\ A_D)^2\ \rho_f\ (1 + K_{c_{UP}})$.

(2) Downcomer

$$-\int_{DT}^{DB} dP = \int_{DT}^{DB} dP_{Head} + \int_{DT}^{DB} dP_{acc} + \int_{DT}^{DB} dP_{Friction}$$

$$= \int_{DT}^{DB} \frac{g}{g_c}\ \rho_D\ dL + \int_{DT}^{DB} \rho_D\ \frac{v dv}{g_c} + \int_{DT}^{DB} f_D\ \rho_D\ \frac{v_D^2}{2g_c}\ \frac{dL}{D_D}$$

Integrating,

$$-\left[P\right]_{DT}^{DB} = \frac{g}{g_c}\ \rho_D\ \left[L\right]_{DT}^{DB} + \rho_D\ \left[\frac{v^2}{2g_c}\right]_{DT}^{DB} + f_D\ \rho_D\ \frac{v_D^2}{2g_c\ D_D}\ \left[L\right]_{DT}^{DB}$$

Since $v_{DB} = v_{DT} = v_D$,

$$P_{DT} - P_{DB} = -\rho_D \left[L_{DT} - L_{DB}\right] \frac{g}{g_c} + f_D \frac{\rho_D v_D^2}{D_D\ 2g_c} \left[L_{DT} - L_{DB}\right]$$

Substituting

$$v_D^2 = v_{sat}^2 \left(\frac{A_{HS}}{A_D}\right)^2 \left(\frac{\rho_f}{\rho_D}\right)^2 \quad ,$$

there is obtained

$$P_{DT} - P_{DB} = - \rho_D \left[L_{DT} - L_{DB} \right] \frac{g}{g_c} + f_D \frac{v_{sat}^2}{2g_c} \left(\frac{A_{HS}}{A_D} \right)^2 \left(\frac{(\rho_f)^2}{\rho_D D_D} \right) \left[L_{DT} - L_{DB} \right]$$

or

$$P_{DT} - P_{DB} = - \rho_D \left[L_{DT} - L_{DB} \right] \frac{g}{g_c} + \frac{v_{sat}^2}{2g_c} [N_2] \qquad (7.6)$$

with $N_2 \equiv f_D \, (A_{HS}/A_D)^2 \, (\rho_f^2/\rho_D \, D_D) \, (L_{DT} - L_{DB})$.

(3) Expansion from Downcomer to Lower Plenum

$$-\int_{DB}^{LPB} dP = \int_{DB}^{LPB} dP_{Head} + \int_{DB}^{LPB} dP_{acc} + \int_{DB}^{LPB} dP_{Friction}$$

$$= \int_{DB}^{LPB} \rho_D \frac{g}{g_c} dL + \int_{DB}^{LPB} \rho_D \frac{v dv}{g_c} + \int_{DB}^{LPB} dP_{Friction} .$$

As for the contraction, we define

$$\int_{DB}^{LPB} dP_{Friction} \equiv K_{E_{LPB}} \rho_D \frac{v_{DB}^2}{2g_c}$$

and, noting that $L_{LPB} = L_{DB}$,

$$- \left[P \right]_{DB}^{LPB} = \rho_D \left[\frac{v^2}{2g_c} \right]_{DB}^{LPB} + K_{E_{LPB}} \frac{v_{DB}^2}{2g_c} \rho_D$$

or

$$P_{DB} - P_{LPB} = \rho_D \left[\frac{v_{LPB}^2}{2g_c} - \frac{v_{DB}^2}{2g_c} \right] + K_{E_{LPB}} \frac{v_{DB}^2}{2g_c} \rho_D \quad .$$

Substituting

$$v_{LPB}^2 = v_{DB}^2 \left(A_D, A_{LP}\right)^2$$

and

$$v_{DB}^2 = v_{sat}^2 \left(\frac{A_{HS}}{A_D}\right)^2 \left(\frac{\rho_f}{\rho_D}\right)^2 \quad ,$$

there is obtained

$$P_{DB} - P_{LPB} = \frac{v_{sat}^2}{2g_c} [N_3] \tag{7.7}$$

with $N_3 \equiv (A_{HS}\ A_D)^2\ (/\ f\ \cdot\ D)^2 \left[\ \cdot\ D\ (A_D, A_{LP})^2 - \cdot\ D\ +\ K_{E_{LPB}}\right]$

(4) Lower Plenum

$$-\int_{LPB}^{LPT} dP = \int_{LPB}^{LPT} dP_{Head} + \int_{LPB}^{LPT} dP_{acc} + \int_{LPB}^{LPT} dP_{Friction}$$

$$= \int_{LPB}^{LPT} \frac{g}{g_c}\ \rho_D\ dL + \int_{LPB}^{LPT} /\ D\ \frac{v dv}{g_c}$$

$$+ \int_{LPB}^{LPT} f_{LPB}\ \rho D\ \frac{v^2\ dL}{2g_c\ D_{LP}} \quad .$$

Since there is no change in area, and hence fluid velocity, and the diameter of the lower plenum is so very large,

$$P_{LPB} - P_{LPT} = (g\ g_c)\ /\ D\ \left[L_{LPT} - L_{LPB}\right] \quad . \tag{7.8}$$

(5) Contraction from Lower Plenum

$$-\int_{LPT}^{HSB} dP = \int_{LPT}^{HSB} dP_{Head} + \int_{LPT}^{HSB} dP_{Friction} + \int_{LPT}^{HSB} dP_{acc}$$

$$= \int_{LPT}^{HSB} \frac{g}{g_c} \rho_D \, dL + \int_{LPT}^{HSB} dP_{Friction} + \int_{LPT}^{HSB} \rho_D \frac{v dv}{g_c} \quad .$$

Assuming $L_{LPT} = L_{HSB}$ and defining

$$\int_{LPT}^{HSB} dP_{Friction} = K_{c_{HSB}} \frac{v_{HSB}^2}{2g_c} \rho_D \quad ,$$

there is obtained

$$P_{LPT} - P_{HSB} = \rho_D \left[\frac{v^2}{2g_c} \right]_{LPT}^{HSB} + K_{c_{HSB}} \frac{v_{HSB}^2}{2g_c} \rho_D$$

$$= \rho_D \left[\frac{v_{HSB}^2}{2g_c} - \frac{v_{LPT}^2}{2g_c} \right] + K_{c_{HSB}} \frac{v_{HSB}^2}{2g_c} \rho_D \quad .$$

Substituting

$$v_{LPT}^2 = v_{HSB}^2 \, (A_{HS}/A_{LP})^2$$

and

$$v_{HSB}^2 = v_{sat}^2 \, (\rho_f/\rho_D)^2 \quad ,$$

there is obtained

$$P_{LPT} - P_{HSB} = \frac{\rho_f^2}{\rho_D} \frac{v_{sat}^2}{2g_c} \left[1 - \left(\frac{A_{HS}}{A_{LP}} \right)^2 + K_{c_{HSB}} \right]$$

or

$$P_{LPT} - P_{HSB} = \frac{v_{sat}^2}{2g_c} [N_4] \qquad (7.9)$$

with $N_4 \equiv (\rho_f^2/\rho_D) \left[1 - (A_{HS}/A_{LP})^2 + K_{c_{HSB}} \right]$.

2. Nonboiling Region

Since a large fraction of the nonboiling region may be in local boiling, the question immediately arises concerning the length of the local boiling region and the uncertainty in the distribution and magnitude of the local boiling voids. For the purpose of this analysis it is tacitly assumed that the local boiling voids adhere to the wall and therefore do not decrease the density of the fluid. The acceleration pressure drop due to the pressure of local boiling voids will be neglected here and incorporated into a total void acceleration pressure drop calculation in the boiling section.

The inception of local boiling and hence the length of the local boiling region can be estimated in the following manner. The wall temperature in the local boiling region is calculated using the Jens-Lottes equation:[8]

$$\Delta T_{sat} = 60 \left(\frac{q}{10^6}\right)^{0.25} e^{P/900}$$

and the value plotted on a temperature length graph as illustrated below.

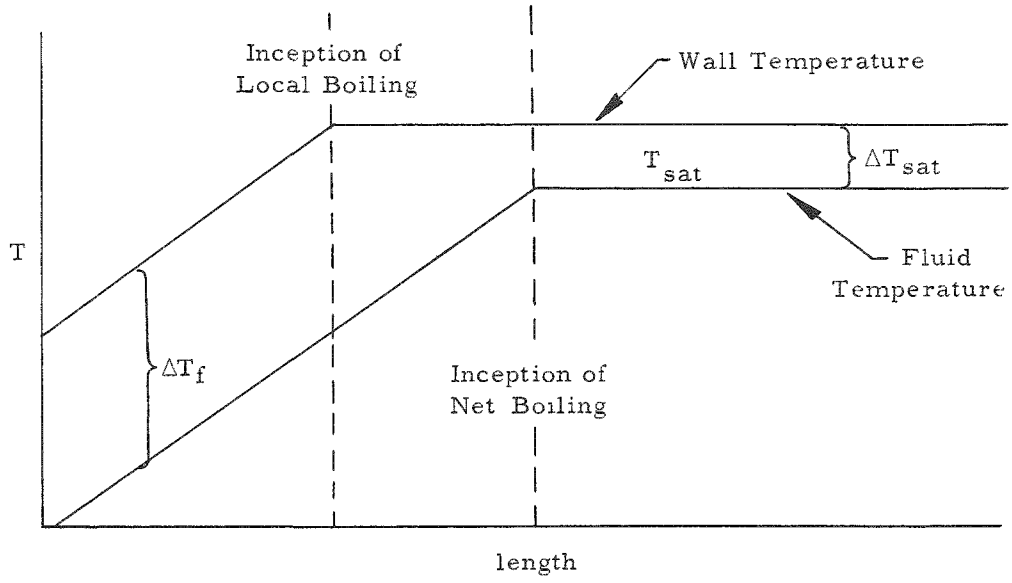

The wall temperature in the nonboiling region is then calculated by

$$T_w - T_f = q'' / h \quad ,$$

where h is given by the Colburn equation

$$h = 0.023 \frac{k}{D} (Re)^{0.8} (Pr)^{0.4} \quad .$$

The temperature in the nonboiling region is also plotted vs the channel length and the intersection of the two wall temperature profiles is designated as the inception of local boiling.

Having established the length of the local boiling region the total pressure drop across the nonboiling region can be computed in the following manner:

$$-\int_{HSB}^{sat} dP = \int_{HSB}^{sat} dP_{Head} + \int_{HSB}^{sat} dP_{acc} + \int_{HSB}^{LB} dP_{Friction}$$

$$+ \int_{LB}^{sat} dP_{Friction} = \int_{HSB}^{sat} \frac{g}{g_c} \rho \, dL + \int_{HSB}^{sat} \rho \frac{v dv}{g_c}$$

$$+ \int_{HSB}^{LB} f_{HS} \frac{v^2}{2g} \frac{\rho}{D_{HS}} dL + \int_{LB}^{sat} \bar{R}_{LB} f_{HS} \frac{v^2}{2g} \frac{\rho}{D_{HS}} dL$$

where $\bar{R}_{LB}$ = ratio of the local boiling pressure drop at the total flow rate,

$$\Delta P_{LB} / \Delta P_{SP} \quad .$$

It should be noted that the density ρ, friction factor f, and velocity v (indirectly) are functions of the temperature and hence length. However, for all practical purposes an average density, velocity and isothermal friction factor based on a mean temperature of the fluid in the various segments can be used for calculating the pressure drop due to friction and head loss unless extreme conditions are encountered, such as near the critical point. The acceleration integral can be expanded by substituting

$$G = \rho v = \text{constant}$$

and

$$dv = - \frac{G d\rho}{\rho^2} \quad .$$

Therefore,

$$-\int_{HSB}^{sat} dP = \frac{g}{g_c} \bar{\rho}_{NB} \int_{HSB}^{sat} dL - \frac{G^2}{g_c} \int_{HSB}^{sat} \frac{d\rho}{\rho^2} + \bar{\rho}_{NB} \bar{f} \frac{v_{NB}^2}{2g_c D_{HS}} \int_{HSB}^{LB} dL$$

$$+ \bar{\rho}_{LB} \bar{R}_{LB} \frac{\bar{f}_{LB} v_{LB}^2}{2g_c D_{HS}} \int_{LB}^{sat} dL \quad .$$

Simplifying

$$P_{HSB} - P_{sat} = \frac{g}{g_c} \bar{\rho}_{NB} (L_{sat} - L_{HSB}) + \frac{G^2}{g_c} \left[\frac{1}{\rho_f} - \frac{1}{\rho_{HSB}} \right]$$

$$+ \frac{\bar{\rho}_f^2}{\rho_{NB}} \frac{v_{sat}^2 \bar{f}}{2g_c D_{HS}} (L_{LB} - L_{HSB})$$

$$+ \frac{\rho^2}{LB} \bar{R}_{LB} \bar{f}_{LB} \frac{v_{sat}^2}{2g_c D_{HS}} (L_{LB} - L_{HSB})$$

or

$$P_{HSB} - P_{sat} = \frac{g}{g_c} (L_{sat} - L_{HSB}) \bar{\rho}_{NB} + \frac{v_{sat}^2}{2g_c} \left[N_5 + N_6 + N_7 \right] \quad . \tag{7.10}$$

3. Boiling Zone

A simplified analysis of the two-phase flow regime can be made by writing a force balance on a differential element in the boiling zone where there is a transfer of mass between the two phases, as depicted below.

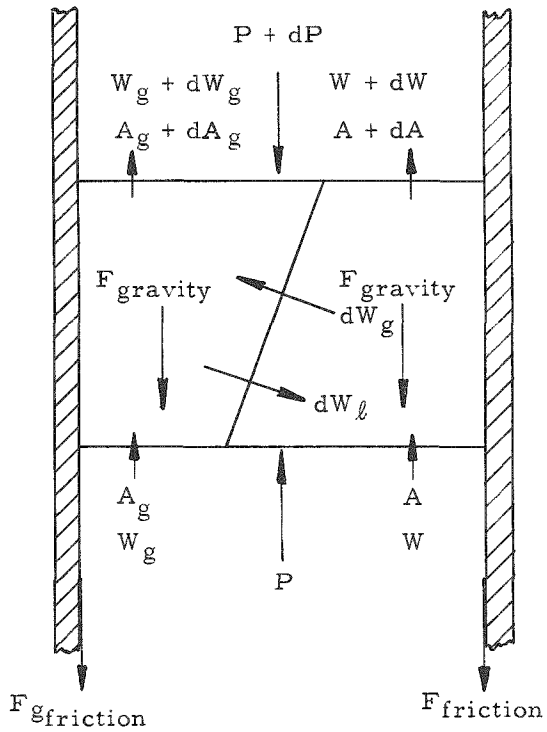

The assumptions made are:

(1) The pressure is constant across any plane normal to the direction of flow.

(2) The sum of the areas at a plane normal to the direction of flow occupied by the gas and liquid phase equals the total pipe area.

A force balance on the gas phase yields

$$PA_g - (P + dP)(A_g + dA_g) - dF_{fg} - (A_g\, dL\, \rho_g + dW_g)(g/g_c)$$

$$= (1/g_c)[(W_g + dW_g)(V_g + dV_g) - W_g\, V_g - dW_g V_\ell\,] \quad .$$

F_{fg} is defined as the force expended by the gaseous phase in overcoming friction. Simplifying,

$$PA_g - PA_g - P\,dA_g - A_g\,dP - dP\,dA_g - dF_{fg} - A_g\,dL\,\rho_g\,(g/g_c) + dW_g\,(g/g_c)$$

$$= (1/g_c)[W_g\,V_g + W_g\,dV_g + V_g\,dW_g + dW_g\,dVg - W_g\,V_g - V_\ell\;\; dW_g]$$

or, neglecting terms of second order,

$$-P\,dA_g - A_g\,dP - dF_{fg} - A_g\,dL\;\rho_g\,(g/g_c) - dW\,(g/g_c)$$

$$= (1/g_c)\,[W_g\,dV_g + V_g\,dW_g - V_\ell\;\; dW_g] \quad . \qquad (7.11)$$

Also, a force balance on the liquid phase gives

$$PA_\ell - (P+dP)(A_\ell + dA_\ell) - dF_{f\ell} - [A_\ell\,dL\,\rho_\ell + dW_\ell\,]\,(g/g_c)$$

$$= (1/g_c)\,[(W_\ell + dW_\ell)(V_\ell + dV_\ell) - V_\ell\,dW_\ell - W_\ell\;\; V_\ell\,] \quad .$$

Again $F_{f\ell}$ is defined as the force expended by the liquid phase in overcoming friction. Simplification yields

$$PA_\ell - PA_\ell - P\,dA_\ell - A_\ell\,dP - dP\,dA_\ell - dF_{f\ell} - A_\ell\,dL\rho_\ell\,(g/g_c) - (g/g_c)\,dW_\ell$$

$$= [W_\ell\;V_\ell + W_\ell\,dV_\ell + V_\ell\,dW_\ell + dW_\ell\,dV_\ell - V_\ell\,dW_\ell - W_\ell\;V_\ell\,]\,(1/g_c)$$

or

$$-P\,dA_\ell - A_\ell\,dP - dF_{f\ell} - A_\ell\,dL\rho_\ell\,(g/g_c) = [W_\ell\,dV_\ell\,](1/g_c) \quad . \qquad (7.12)$$

Summing Eqs. (7.1) and (7.12)

$$P(-dA_\ell - dA_g) - dP(A_g + A_\ell) - dF_{fg} - dF_{f\ell} - (g/g_c)\,dL(A_\ell \rho_\ell + A_g \rho_g)$$

$$+ dW_\ell (g/g_c) + dW_g (g/g_c) = (1/g_c)[W_\ell\, dV_\ell + V_\ell\, dW_\ell + W_g\, dV_g + V_g\, dW_g], \tag{7.13}$$

since

$$dA_\ell = -dA_g,\ A_g + A_\ell = A_p, \text{ and } dW_\ell = -dW_g \quad .$$

Further,

$$d(W_\ell\ V_\ell + W_g V_g) = [W_\ell\, dV_\ell + V_\ell\ dW_\ell + W_g\, dV_g + V_g\, dW_g](1/g_c) \quad ,$$

and

$$(dF_{fg} + dF_{f\ell}) = dP_{TPF}\, A_P$$

by definition, where dP_{TPF} is the two-phase frictional pressure drop loss. Accordingly Eq. (7.13) becomes

$$-dP\, A_p - dP_{TPF}\, A_p - (g/g_c)\,dL\,(A_\ell \rho_\ell + A_g \rho_g) = (1/g_c)\,d(W_\ell\ V_\ell + W_g V_g) \quad .$$

Dividing by A_p ,

$$-dP - dP_{TPF} - g/g_c\,(A_\ell/A_p\ \rho_\ell + A_g/A_p\ \rho_g)\,dL = \frac{d(W_\ell\, V_\ell + W_g\, V_g)}{g_c\, A_p} \tag{7.13a}$$

Defining $\alpha = A_g/A_p$,

$$(1 - \alpha) = A_\ell/A_p$$

and substituting into (7.13a);

$$-dP - dP_{TPF} - g/g_c\,[(1-\alpha)\rho\ell + \alpha\ \rho_g]\,dL = \frac{d(W_\ell\, V_\ell + W_g\, V_g)}{g_c\, A_p} \quad . \tag{7.14}$$

Applying Eq. (7.14) over the boiling length,

$$-\int_{sat}^{HSE} dP = \int_{sat}^{HSE} \frac{d(W_\ell V_\ell + W_g V_g)}{g_c A_p} + \int_{sat}^{HSE} dP_{TPF}$$

$$+ g/g_c \int_{sat}^{HSE} [(1 - \alpha)\rho_\ell + \alpha \rho_g]\, dL$$

or

$$P_{sat} - P_{HSE} = 1/g_c A_p \left[W_\ell V_\ell + W_g V_g\right]_{sat}^{HSE} + \left[\Delta P_{TPF}\right]_{sat}^{HSE}$$

$$+ \bar{\rho}_B \left[L\right]_{sat}^{HSE} \frac{g}{g_c} \quad ,$$

where

$$\bar{\rho}_B = \frac{\int_{sat}^{HSE} \rho dL}{L_{HSE} - L_{sat}} \quad .$$

Also defining

$$\bar{R} = \Delta P_{TPF}/\Delta P_{SPF}$$

as the ratio of the two-phase frictional pressure drop in the boiling zone to the single-phase pressure drop at the total flow rate,

$$\left[\Delta P_{TPF}\right]_{sat}^{HSE} = \bar{R}\, f_{HS}\, \rho_f \frac{v_{sat}^2}{2g_c} \frac{L_{HSE} - L_{sat}}{D_{HS}} \quad ,$$

so that

$$P_{sat} - P_{HSE} = \frac{1}{g_c A_p}\left[W_{\ell HSE} V_{\ell\, HSE} + W_{gHSE} V_{gHSE} - W_{\ell\, sat} V_{\ell sat} - W_{g_{sat}} V_{g_{sat}}\right]$$

$$+ \bar{R}\, f_{HS}\, \rho_f \frac{v_{sat}^2}{2g_c D_{HS}} (L_{HSE} - L_{sat}) + \bar{\rho}_B (L_{HSE} - L_{sat})$$

$$= \frac{1}{g_c A_p}\left[\frac{W_T(1 - x_e)(W_T)(1 - x_e)}{\rho_f(1 - \alpha_e) A_p} + \frac{x_e W_T(x_e W_T)}{\alpha_e A_p \rho_g} - W_T \frac{G}{\rho_f}\right]$$

$$+ \bar{\rho}_B (L_{HSE} - L_{sat}) + \bar{R}\, f_{HS}\, \rho_f \frac{v_{sat}^2}{2g_c} (L_{HSE} - L_{sat}) \quad .$$

Noting that $W_T / A_p = G$ and simplifying

$$P_{sat} - P_{HSE} = \left[\frac{(1 - x_e)^2}{(1 - \alpha_e)} \frac{1}{\rho_f} + \frac{x_e^2}{\alpha_e} \frac{1}{\rho_g} - \frac{1}{\rho_f}\right] \frac{G^2}{g_c} + \bar{\rho}_B (L_{HSE} - L_{sat})$$

$$+ \bar{R} \frac{f_{HS}}{D_{HS}} \rho_f \frac{v_{sat}^2}{2g_c} (L_{HSE} - L_{sat}) \quad .$$

The quantity $\left[\frac{(1 - x_e)^2}{(1 - \alpha_e)} \frac{1}{\rho_f} + \frac{x_e^2}{\alpha_e} \frac{1}{\rho_g} - \frac{1}{\rho_f}\right]$ is the acceleration multiplier, r, as defined by Martinelli and Nelson. Therefore,

$$P_{sat} - P_{HSE} = \frac{r G^2}{g_c} + \bar{R} \frac{f_{HS}}{D_{HS}} \frac{v_{sat}^2}{2g} \rho_f (L_{HSE} - L_{sat}) + \bar{\rho}_B (L_{HSE} - L_{sat})$$

or

$$P_{sat} - P_{HSE} = \frac{v^2}{2g_c} [N_8 + N_9] + \bar{\rho}_B (L_{HSE} - L_{sat}) \qquad (7.15)$$

4. Expansion or Contraction to a Riser

a. Expansion. The expansion for the two-phase fluid is treated in the same manner as for a single-phase fluid. Since only the overall pressure drop is desired, a force balance can be written across the expansion:*

$$M_g V_{g_{HSE}} + M_f V_{f_{HSE}} + P_{HSE} A_R = M_g V_{g_{RB}} + M_f V_{f_{RB}} + P_{RB} A_R \quad ;$$

$$P_{HSE} - P_{RB} = \frac{M_g}{A_R} (V_{g_{RB}} - V_{g_{HSE}}) + \frac{M_f}{A_R} (V_{f_{RB}} - V_{f_{HSE}}) \quad ;$$

$$V_{g_{RB}} = \frac{W_g}{\rho_g A_R \alpha_{RB}} = \frac{x_{HSE} \rho_f A_{HS} V_{sat}}{\rho_g A_R \alpha_{RB}} \quad ;$$

$$V_{g_{HSE}} = \frac{W_g}{\rho_g A_{HS} \alpha_{HSE}} = \frac{x_{HSE} \rho_f A_{HS} V_{sat}}{\rho_g A_{HS} \alpha_{HSE}} = \frac{x_{HSE} \rho_f V_{sat}}{\rho_g \alpha_{HSE}} \quad ;$$

* Personal Communication from F. Romie, American Standard Co.

$$V_{f_{RB}} = \frac{W_{f_{RB}}}{\rho_f A_R (1 - \alpha_{RB})} = \frac{(1 - x_{HSE}) \rho_f A_{HS} V_{sat}}{\rho_f A_R (1 - \alpha_{RB})} = \frac{(1 - x_{HSE})}{(1 - \alpha_{RB})} \frac{A_{HS}}{A_R} V_{sat}$$

$$V_{f_{HSE}} = \frac{W_{f_{HSE}}}{\rho_f A_{HS} (1 - \alpha_{HSE})} = \frac{(1 - x_{HSE}) \rho_f A_{HS} V_{sat}}{\rho_f A_{HS} (1 - \alpha_{HSE})} = \frac{(1 - x_{HSE})}{(1 - \alpha_{HSE})} V_{sat}$$

$$M_g = \frac{x_{HSE} W_T}{g} = \frac{x_{HSE} \rho_f A_{HS} V_{sat}}{g} \quad ;$$

$$M_f = \frac{(1 - x_{HSE}) W_T}{g} = \frac{(1 - x_{HSE}) \rho_f A_{HS} V_{sat}}{g} \quad ;$$

and

$$P_{HSE} - P_{RB} = \frac{x_{HSE} \rho_f A_{HS} V_{sat}}{g A_R} \left[\frac{x_{HSE} \rho_f A_{HS} V_{sat}}{\rho_g A_R \alpha_{RB}} - \frac{x_{HSE} \rho_f V_{sat}}{\rho_g \alpha_{HSE}} \right]$$

$$+ \frac{(1 - x_{HSE}) \rho_f A_{HS} V_{sat}}{g A_R}$$

$$\left[\frac{(1 - x_{HSE}) A_{HS} V_{sat}}{A_R (1 - \alpha_{RB})} - \frac{(1 - x_{HSE}) V_{sat}}{(1 - \alpha_{HSE})} \right] .$$

Substituting $A_{HS} A_R = \sigma$ and simplifying,

$$P_{HSE} - P_{RB} = \frac{\rho_f V_{sat}^2}{2g} 2\sigma$$

$$\left[x_{HSE}^2 \frac{\rho_f}{\rho_g} \left(\frac{\sigma}{\alpha_{RB}} - \frac{1}{\alpha_{HSE}} \right) + \left(1 - x_{HSE} \right)^2 \left(\frac{\sigma}{1 - \alpha_{RB}} - \frac{1}{1 - \alpha_{HSE}} \right) \right] . \tag{7.16}$$

A general equation for an expansion between any two risers (unheated flow channels) of areas A_i and A_{i+1} is

$$P_i - P_{i+1} = \frac{v_{sat}^2}{2g_c} 2\rho_f \frac{A_{HS}}{A_{i+1}} \left[\frac{x_{HSE}^2 \rho_f}{\rho_g} \left(\frac{A_{HS}}{A_{i+1}} \frac{1}{\alpha_{i+1}} - \frac{A_{HS}}{A_i} \frac{1}{\alpha_i} \right) + (1 - x_{HSE})^2 \left(\frac{A_{HS}}{A_{i+1}} \frac{1}{(1-\alpha)_{i+1}} - \frac{A_{HS}}{A_i} \frac{1}{(1-\alpha_i)} \right) \right] . \quad (7.17)$$

For $A_i = A_{HS}$ and $A_{i+1} = A_{RB}$,

$$P_i - P_{i+1} = \frac{v_{sat}^2}{2g_c} [N_{10}] \quad . \quad (7.18)$$

b. Contraction. The contraction is treated in an analogous manner but is more subject to question. A more rigorous treatment similar to the one made for a single-phase fluid is difficult because of uncertainties in energy balance for two-phase fluids and numerous questions concerning the vena contracta. Therefore a simplified approach was taken and the following assumptions were made:

(1) A vena contracta does not exist.

(2) The pressure is constant across plane 2, as depicted in the diagram below.

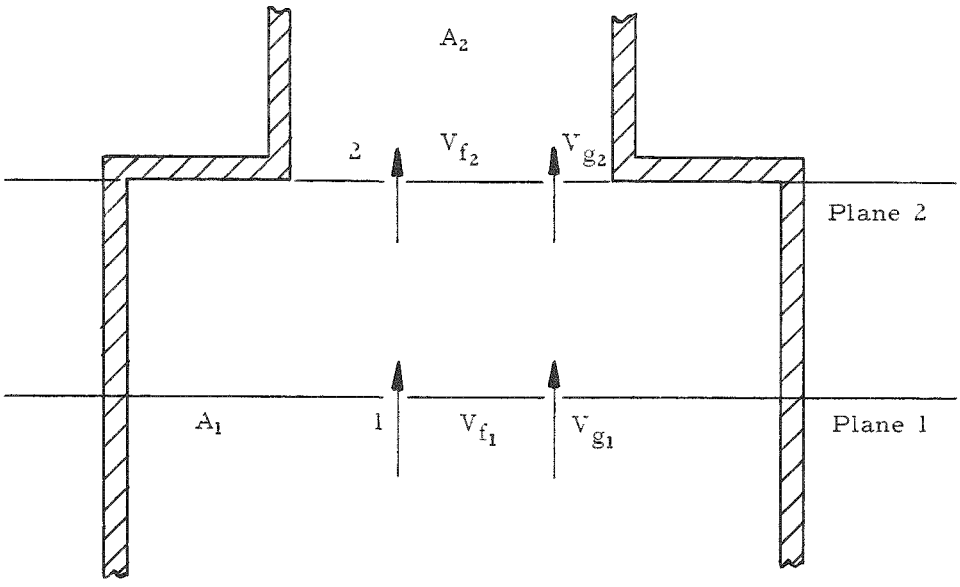

Writing a force balance as before

$$M_g V_g + M_\ell V_{\ell_1} + P_1 A_1 = M_g V_{g_2} + M_\ell V_{\ell_2} + P_2 A_1$$

or

$$P_{HSE} - P_{RB} = \frac{M_g}{A_{HS}} \left(V_{g_{RB}} - V_{g_{HSE}} \right) + \frac{M_\ell}{A_{HS}} \left(V_{\ell_{RB}} - V_{\ell_{HSE}} \right) \quad .$$

Substituting for the velocity, etc., and simplifying,

$$P_{HSE} - P_{RB} = f \frac{v_{sat}^2}{2g} (2) \left[x_{HSE}^2 \frac{\nu_f}{\nu_g} \left(\frac{A_{HS}}{A_R \gamma_{RB}} - \frac{1}{\gamma_{HSE}} \right) + (1 - x_{HSE})^2 \left(\frac{A_{HS}}{A_R (1 - \gamma_{RB})} - \frac{1}{1 - \gamma_{HSE}} \right) \right] \tag{7.19}$$

This is identical to Eq. (7.16). Therefore, Eq. (7.17) is a general equation for both an expansion or a contraction from the heated section. The general equation for any contraction is

$$P_i - P_{i+1} = \frac{v_{sat}^2}{2g_c} (2\nu_f) \left(\frac{A_{HS}}{A_{i+1}} \right) \left[x_{HSE}^2 \frac{\nu_f}{\nu_g} \left(\frac{A_{HS}}{A_{i+1}} \frac{1}{(\alpha_{i+1})} - \frac{A_{HS}}{A_i} \frac{1}{\alpha_i} \right) + (1 - x_{HSE})^2 \left(\frac{A_{HSE}}{A_{i+1} (1 - \gamma_{i+1})} - \frac{A_{HS}}{A_i (1 - \gamma_i)} \right) \right] \tag{7.19a}$$

As a result the pressure drop for a series of expansions and contractions can be written as

$$\Sigma \Delta P_i = \frac{v_{sat}^2}{2g_c} \Sigma N_{10} \quad . \tag{7.20}$$

c. Riser

$$-\int_{RB}^{RT} dP = \int_{RB}^{RT} dP_{Head} + \int_{RB}^{RT} dP_{acc} + \int_{RB}^{RT} dP_{Friction} \quad .$$

Since there is no change in voids in the adiabatic riser section,

$$\int_{RB}^{RT} dP_{acc} = 0$$

and

$$-\int_{RB}^{RT} dP = \int_{RB}^{RT} \rho_R \, dL + \int_{RB}^{RT} R \, f_R \frac{v_R^2}{2g_c} \rho_f \frac{dL}{D_R} \quad ,$$

where R is defined as $\Delta P_{TPF} / \Delta P_{SPF}$ in the riser. Then

$$\left[P\right]_{RT}^{RB} = \rho_R \left[L\right]_{RB}^{RT} + R\, f_R \frac{v_{sat}^2}{2g_c}\left(\frac{A_{HS}}{A_R}\right)^2 \frac{\rho_f}{D_R} \left[L\right]_{RB}^{RT}$$

and

$$P_{RB} - P_{RT} = \rho_R (L_{RT} - L_{RB}) + R\, f_R \frac{v_{sat}^2}{2g_c}\left(\frac{A_{HS}}{A_R}\right)^2 \frac{\rho_f}{D_R} (L_{RT} - L_{RB})$$

or

$$P_{RB} - P_{RT} = \rho_R (L_{RT} - L_{RB}) + \frac{v_{sat}^2}{2g_c} [N_{11}] \quad . \tag{7.21}$$

5. Expansion into Upper Plenum

The expansion into the upper plenum is given by Eq. (7.7).

Summing Eqs. (7.5), (7.6), (7.7), (7.8), (7.9), (7.10), (7.15), 7.17), and (7.21) to satisfy Eq. (7.1) and simplifying,

$$\frac{v_{sat}^2}{2g} [N_1 + N_2 + N_3 + N_4 + N_5 + N_6 + N_7 + N_8 + N_9 + \Sigma N_i + N_{11}]$$

$$- \rho_D (L_{DT} - L_{DB}) + \rho_D [L_{LPT} - L_{LPB}] + \rho_{NB} (L_{sat} - L_{HSB})$$

$$+ \overline{\rho}_B (L_{HSE} - L_{sat}) + \rho_R (L_{RT} - L_{RB}) = 0 \quad . \tag{7.22}$$

Since

$$(L_{DT} - L_{DB}) = L_{RT} - L_{LPB} \quad ,$$

then

$$L_{DT} - L_{DB} = (L_{LPT} - L_{LPB}) + (L_{sat} - L_{HSB}) + (L_{HSE} - L_{sat}) + (L_{RT} - L_{RB}) \quad . \tag{7.23}$$

Substituting Eq. (7.23) into Eq. (7.22) and simplifying,

$$\frac{v_{sat}^2}{2g}\left[N_1 + N_2 + N_3 + N_4 + N_5 + N_6 + N_7 + N_8 + N_9 + \Sigma N_i + N_{11}\right]$$

$$= (\rho_D - \overline{\rho}_{NB})(L_{sat} - L_{HSB}) + (\rho_D - \overline{\rho}_B)(L_{HSE} - L_{sat})$$

$$+ (\rho_D - \rho_R)(L_{RT} - L_{RB}) \quad . \tag{7.24}$$

Defining and substituting,

$L_{sat} - L_{HSB} = L_{NB}$ = nonboiling length,

$L_{HSE} - L_{sat} = L_B$ = boiling length,

$L_{RT} - L_{RB} = L_R$ = riser length,

$L_{DT} - L_{DB} = L_D$ = downcomer length,

$\Sigma L_{Ri}(\rho_D - \rho_{Ri}) = L_R(\rho_D - \rho_R)$,

and

$$\Sigma N_{Ri} = N_{11} \quad ,$$

Equation (7.24) becomes, for systems that may have a series of risers with varying diameters,

$$\frac{v_{sat}^2}{2g} = \frac{L_{NB}(\rho_D - \overline{\rho}_{NB}) + L_B(\rho_D - \overline{\rho}_B) + \Sigma L_{Ri}(\rho_D - \rho_{Ri})}{N_1 + N_2 + N_3 + N_4 + N_5 + N_6 + N_7 + N_8 + N_9 + \Sigma N_i + \Sigma N_{11}} \quad . \tag{7.25}$$

The individual N terms in Eq. (7.25) may be classified in the following manner:

$$N_1 = \rho_f\left(\frac{A_{HS}}{A_D}\right)^2\left[1 + K_{c_{UP}}\right]$$ = acceleration of the fluid from the upper plenum to downcomer and frictional resistance at contraction.

$$N_2 = f_D\left(\frac{L_D}{D_D}\right)\left(\frac{\rho_f^2}{\rho_D}\right)\left(\frac{A_{HS}}{A_D}\right)^2$$ = frictional resistance in downcomer.

$$N_3 = \frac{\rho_f'}{\rho_D}\left(\frac{A_{HS}}{A_D}\right)^2\left[\left(\frac{A_D}{A_{LP}}\right)^2 - 1 + K_{E_{LPB}}\right]$$ = deceleration of fluid and frictional losses at the expansion from the downcomer to lower plenum.

$$N_4 = \frac{\rho_f^2}{\rho_D}\left[1 - \left(\frac{A_{HS}}{A_{LP}}\right)^2 + K_{c_{HSB}}\right]$$

= acceleration of fluid and frictional losses at the contraction from lower plenum to the heated section.

$$N_5 = 2\rho_f\left[\frac{\rho_{HSB} - \rho_f}{\rho_{HSB}}\right]$$

= acceleration of fluid in nonboiling length due to density change with temperature.

$$N_6 = \frac{\rho_f^2}{\rho_{NB}}\left(\frac{f_{HS}}{D_{HS}}\right)(L_{NB})$$

= frictional resistance in the non-boiling segment of the heated section.

$$N_7 = \frac{\rho_f^2}{\rho_{LB}}(\bar{R}_{LB})\left(\frac{f_{HS}}{D_{HS}}\right)(L_{LB})$$

= frictional resistance in the local boiling segment of the heated section.

$$N_8 = 2\,(r)(\rho_f)^2$$

= acceleration of fluid due to formation of steam voids in the heated channel.

$$N_9 = \rho_f(\bar{R})\left(\frac{f_{HS}}{D_{HS}}\right)(L_B)$$

= frictional resistance in the boiling segment.

$$N_{10} = 2\rho_f\left(\frac{A_{HS}}{A_{i+1}}\right)\left\{x_{HSE}^2\frac{\rho_f}{\rho_g}\left(\frac{A_{HS}}{(A_{i+1})(\alpha_{i+1})} - \frac{A_{HS}}{(A_i\alpha_i)}\right) + (1 - x_{HSE})^2\left(\frac{A_{HS}}{(A_{i+1})(1-\alpha_{i+1})}\,\frac{A_{HS}}{A_i(1-\alpha_i)}\right)\right\}$$

= total pressure drop due to an expansion or contraction.

$$N_{11} = R\,f_R\left(\frac{A_{HS}}{A_R}\right)^2\frac{\rho_f}{D_R}\,L_R$$

= frictional loss in the adiabatic risers.

The various factors in Eq. (7.25), such as R, $\bar{R}_B$, $\bar{R}_{LB}$, ρ_B, V_g/V_f, etc., can be obtained from empirical correlations or by analytical means as discussed previously.

7.2. Forced Circulation System Analysis

The basic analysis presented for the natural circulation system applied equally to the forced circulation system with slight modification. The pump in the forced circulation system must overcome the frictional and acceleration losses in the loop plus the differential hydrostatic head

between the downcomer and riser section. The differential head in the loop is a negative quantity since the downcomer density is greater than the riser density. Equation (7.25) can therefore be rewritten as

$$W_P = \frac{v^2}{2g_c \rho_D} [N_1 + - - - + N_1 + - - - N_{pc}]$$

$$- \left[\left(1 - \frac{\bar{\rho}_{NB}}{\rho_D} \right) L_{NB} + \left(1 - \frac{\bar{\rho}_R}{\rho_D} \right) L_B + \Sigma \left(1 - \frac{\rho_{Ri}}{\rho_D} \right) L_{Ri} \right] ,$$

where W_P is the pump work requirement (based on the downcomer density), $N_1 + - - - N_1 - - -$ are defined by Eq. (7.25), and N_{PC} is the number of velocity heads lost in the pump circuit exterior to the reactor.

7.3. Comparison of Analyses with Laboratory Data

The validity of the analyses and the assumptions made therein was checked by comparing the calculation procedure with performance test data obtained from laboratory loops. These tests were run on a basic natural circulation loop in which the riser geometry was varied to introduce contractions and expansion into the flow circuit. A series of runs was made for each geometry at various pressures and powers. The power was increased for each set of runs until hydrodynamic instability ensued.

The laboratory loop used for these performance tests is schematically illustrated in Fig. 7.2. The geometries studied were a one-inch diameter heated section, 4 feet in length, with risers $\frac{3}{4}$, 1 and 2 in. in diameter.

The performance of each of the geometries studied was precalculated, using the methods outlined in the previous section. The calculated recirculation velocity was plotted as a function of the exit steam volume fraction of the heated section, as shown in Figs. 7.2 to 7.9.

It should be noted that there is some question concerning the absolute value of the measured steam volume fraction due to instrumentation difficulties which were discovered after completion of the testing program. This probable error applies only to the data for the 1-in. and $\frac{3}{4}$-in. riser geometries. The measured velocities are correct and therefore the trend of the data is also essentially accurate. The only change that could result would be to shift the data to the right on the abscissa. In spite of the probable error in the data, some interesting observations can be made from each of the three geometries studied.

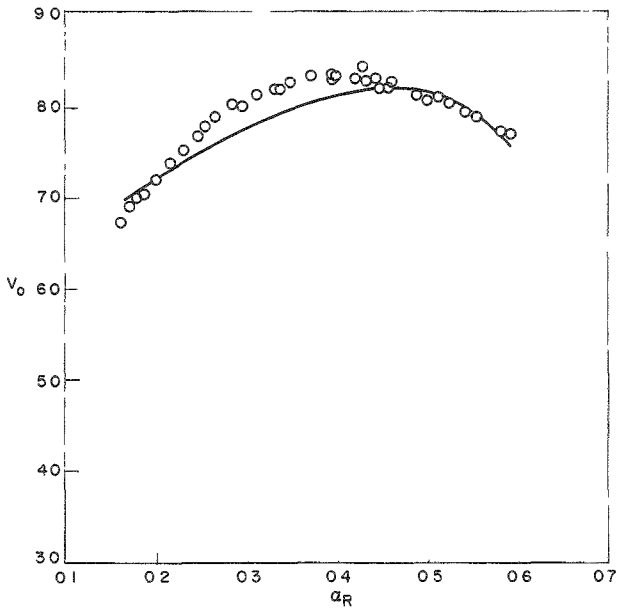

Fig. 7.2

Comparison of the Predicted and Measured Performance of a Natural Circulation System. 2-in. Riser; 600 psig.

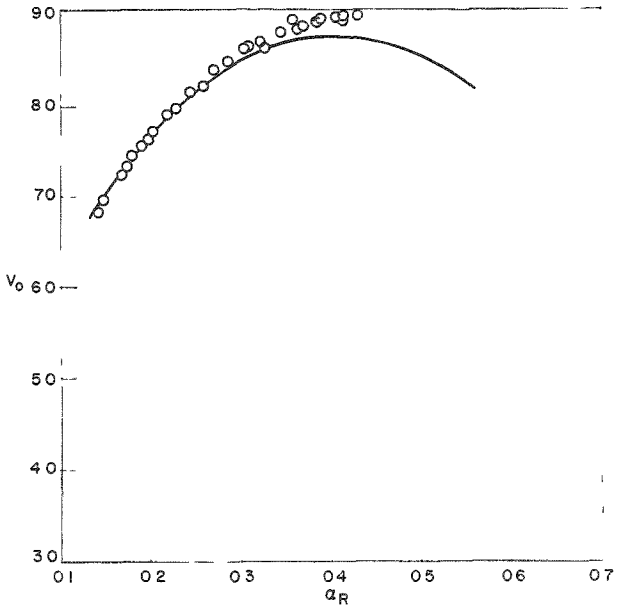

Fig. 7.3

Comparison of the Predicted and Measured Performance of a Natural Circulation System. 2-in. Riser; 1000 psig.

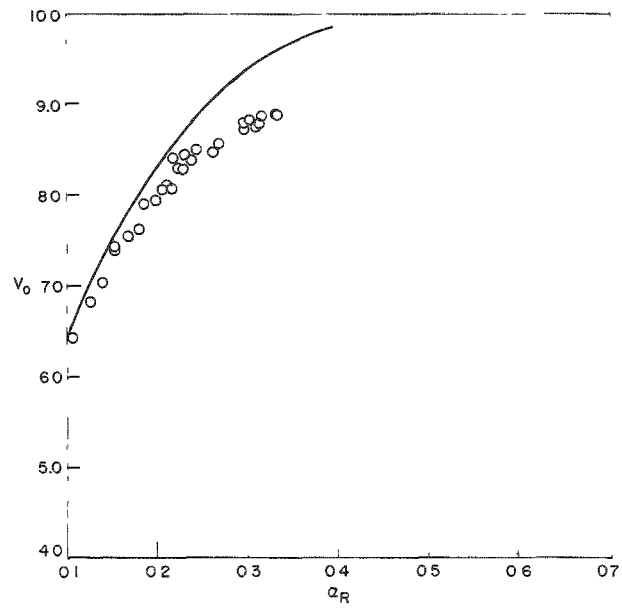

Fig. 7.4

Comparison of the Predicted and Measured Performance of a Natural Circulation System. 2-in. Riser; 1500 psig.

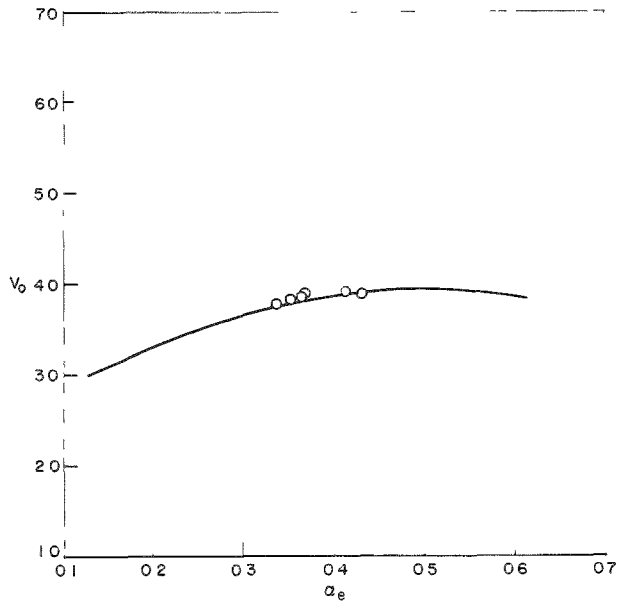

Fig. 7.5

Comparison of the Predicted and Measured Performance of a Natural Circulation System. 3/4-in. Riser; 600 psig.

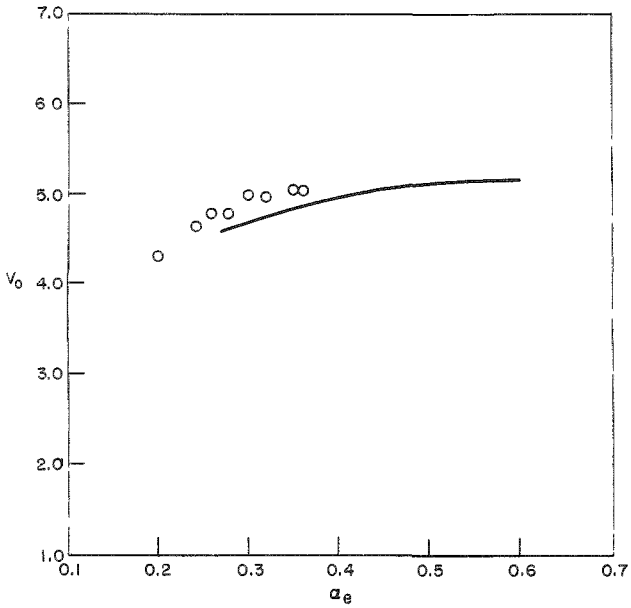

Fig. 7.6

Comparison of the Predicted and Measured Performance of a Natural Circulation System. 3/4-in. Riser; 1000 psig.

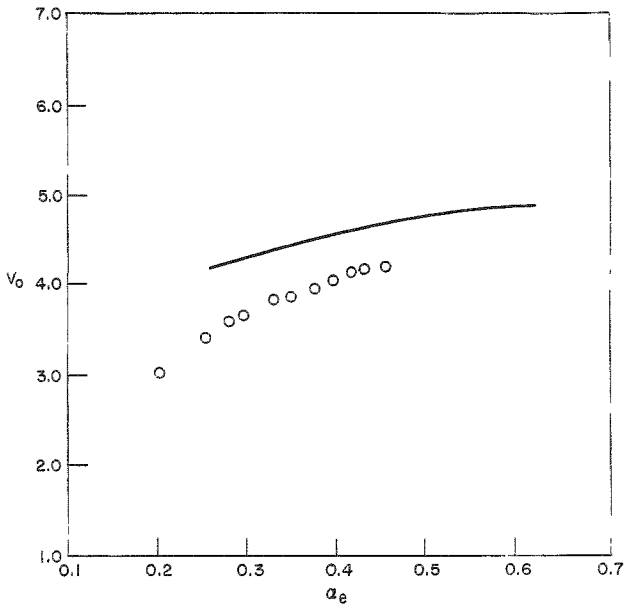

Fig. 7.7

Comparison of the Predicted and Measured Performance of a Natural Circulation System. 3/4-in. Riser; 1500 psig.

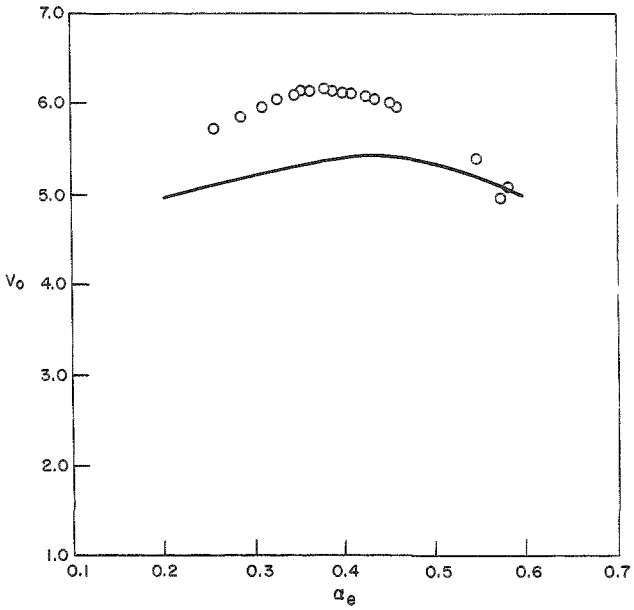

Fig. 7.8

Comparison of the Predicted and Calculated Performance of a Natural Circulation System. 1-in. Riser; 600 psig.

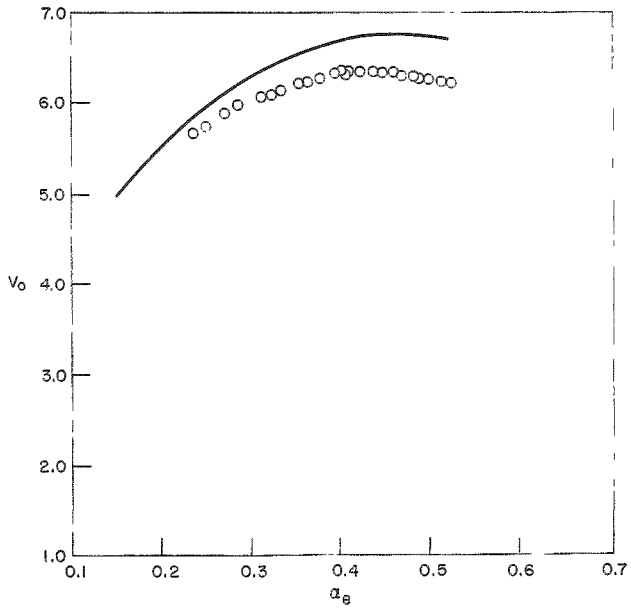

Fig. 7.9

Comparison of the Predicted and Measured Performance of a Natural Circulation System. 1-in. Riser; 1000 psig.

1. Two-inch Diameter Riser

In a boiling system the acceleration pressure drops due to the system geometry, and the formation of steam voids in the boiling section represent a large fraction of the pressure drop due to friction and acceleration of the fluid. For the three geometries studied, the acceleration pressure drops accounted for a substantial percentage of the combined pressure drops. Also, the percentage of the pressure drop due to acceleration of the fluid generally increased as the void level increased. Therefore the amount of pressure recovery occurring at the expansions must be accounted for in the hydrodynamic analysis in order to accurately predict the performance. If zero recovery is assumed, the calculated recirculation velocity will be too low; if total recovery is assumed, the calculated velocity is too high. This was borne out by the data.

As can be seen in Figs. 7.2 to 7.4, the laboratory data check the calculated performance very well for the three pressures studied. The use of the momentum balance for calculating the pressure recovery across an expansion therefore appears to be validated.

2. Three-fourths-inch Riser Geometry

In addition to the acceleration pressure drop due to the contraction from the lower plenum and formation of steam voids, an additional acceleration pressure drop occurs at the contraction from the 1-in. heated section to the $\frac{3}{4}$-in. riser. The system is rather unique, however, because for all practical purposes the acceleration pressure drops must be regarded as irrecoverable; it is assumed that there is no pressure recovery. This can be attributed to the fact that the expansion into the upper plenum involves a very large change of area. Thus, as for a single-phase fluid, the entire fluid velocity head can be lost; that is, ΔP across the expansion approaches zero. This was actually borne out by measurement. Two static pressure taps were placed at the expansion into the upper plenum, one in the riser and the other just above the riser exit in the upper plenum. In all instances the measured pressure drop was zero or very slightly positive.

Although the data check the calculated performance very well, as shown in Figs. 7.5 to 7.7, the validity of using a momentum balance across the contraction from the 1-in. pipe to the $\frac{3}{4}$-in. riser cannot be completely established. The frictional pressure drops are very high, especially for the $\frac{3}{4}$-in. riser, and as a result even though the acceleration pressure drop is substantial, it is not the dominant loss. Therefore any error made in calculating the frictional losses would be reflected in the magnitude of the pressure drop across the contraction. If we assume that the absolute frictional pressure drops are essentially correct (as they are thought to be, however), a momentum balance across a contraction appears to yield satisfactory estimates of the pressure drop.

3. One-inch Riser

For this geometry the two-phase frictional pressure drop is the dominant loss in the system. Therefore the comparison of the data with the calculated performance tends to demonstrate the validity of the method used for calculating the two-phase friction factor. As discussed previously, the acceleration pressure drop due to void formation and the contraction from the lower plenum can be treated as irrecoverable.

As can be seen from Figs. 7.8 and 7.9, there is good agreement between data and calculations. The data could not be obtained over a wider range of voids because of the onset of instability.

From the comparisons given above, the validity of the calculation procedure presented appears to be established. Perhaps the major uncertainties remaining concern the contraction of a two-phase mixture and the two-phase friction factors over wide mass velocity ranges and pressures. These problems are under study currently.

8. THERMAL HYDRAULIC DESIGN PROCEDURES FOR BOILING WATER REACTORS

8.1. Introduction

In order to realize economic nuclear power the desirability of incorporating certain design objectives becomes readily apparent, if the desired goal is to be realized. A few of the objectives that the boiling water reactor designer might seek are:

(a) optimization of specific power and power density in the core;

(b) optimization of in-core fuel residence time;

(c) optimization of power density per unit void;

(d) high fuel conversion ratio;

(e) employment of circulation of the core coolant;

(f) use of internal gravity vapor-liquid separation;

(g) use of low enrichment fuel;

(h) use of ceramic (UO_2) rather than metallic fuel;

(i) to obtain the highest neutron economy possible by elimination of unnecessary core, structural material, etc.

Unfortunately, a substantial degree of incompatibility exists between the various objectives. Basically, the incompatibility stems from conflicting physics and engineering requirements and, as a result, the reactor design which evolves generally represents a compromise between the physics thermodynamics and hydraulics design objectives. However, in arriving at the compromise design a number of design parameters are usually taxed to their limits. The result is that in many instances either one or several of these parameters or design criteria actually establishes the limits of reactor performance. Therefore, before a calculation procedure for reactor core analysis is presented, a brief discussion of a few of the major design parameters or criteria of boiling water reactors is given. An attempt is made to point out how these criteria affect reactor design and ranges and conditions under which they may tend to become limiting. The calculation procedure is then illustrated by a sample core analysis.

8.2. Boiling Water Reactor Design Criteria

1. Moderator-to-Fuel Ratio

The moderator-to-fuel ratio is perhaps the most important reactor design parameter because of its immediate impact on core physics and because it essentially represents the bridge between physics and engineering. Establishing the moderator-to-fuel ratio of a reactor, as one might

suspect, is the area of greatest conflict between the engineer and physicist because of the incompatibility of the most desirable objectives of each.

From an engineering viewpoint it is desirable to have a large moderator-to-fuel ratio to obtain a large equivalent diameter of the core coolant flow channel. This is especially true for the natural-circulation boiling water reactor, since the major hydrodynamic resistance exists within the core. As the moderator-to-fuel ratio decreases, the recirculation velocity also decreases due to the increased frictional resistance within the core. As a result, the reactor power, and hence performance, drops, since the reactor power is essentially proportional to the recirculation velocity for a fixed amount of reactivity tied up in steam voids.

Also, as the moderator-to-fuel ratio is decreased, the coolant power density increases. As a result, the core recirculation flow rate must be increased if the same mean core steam volume fraction is to be maintained. The moderator-to-fuel ratio could eventually be lowered to a point where it would be impossible to obtain the desired coolant flow rate by natural convection and, as a result, forced circulation of the coolant would have to be employed. On the other hand, if the moderator-to-fuel ratio is increased too far, the maximum heat flux becomes very large and either the fuel centerline temperature becomes excessive or the critical maximum heat flux is reached.

From a physics viewpoint, the moderator-to-fuel ratio strongly influences a number of important core design criteria such as fuel cycle costs, reactor stability, etc. The effect of the moderator-to-fuel ratio on the reactor physics can be seen by a superficial examination of the factors of the criticality equation for a bare, enriched, water-moderated reactor:

$$k_{eff} = \frac{\eta f \epsilon p}{1 + (L^2 + \tau)B^2} \quad .$$

Of particular interest are the terms f and p, the thermal utilization and the resonance escape probability, which are related to the moderator-to-fuel ratio as follows:

$$f \approx \frac{1}{k_1 + k_2(M/F)}$$

and

$$p \approx \frac{1}{f_1(M/F)/f_2(M/F)} \quad ,$$

where $f_2(M/F)$ changes more rapidly than $f_1(M/F)$.

As can be seen, increasing the moderator-to-fuel ratio lowers the thermal utilization and increases the resonance escape probability. If this trend is carried too far, the thermal utilization decreases faster than the increase of the resonance escape probability and the enrichment of the core would have to be increased. Decreasing the moderator-to-fuel ratio will eventually lead to a required increase in enrichment due to the reverse effect. As a result there is an optimum moderator-to-fuel ratio for a minimum fuel enrichment.

The enrichment, however, is but one of several factors which must be considered in evaluating the fuel cycle costs. The number of fuel rods in the core increases as the moderator-to-fuel ratio decreases, since the fuel rod diameter is usually fixed independently by the limiting centerline temperature. Increasing the number of fuel pins increases the fuel fabrication costs. However, as the moderator-to-fuel ratio is decreased, the resonance escape probability decreases and hence the conversion ratio increases. The production of additional fissionable material enhances the fuel burnup (MWD/ton) considerably. The fuel burnup can also be increased by adding enrichment. This, however, must be weighed against the increased cost and the lowering of the conversion ratio.

The fuel lifetime and fuel inventory are also strongly affected by the moderator-to-fuel ratio. The characteristics of a reactor system having a high moderator-to-fuel ratio are a low fuel inventory, low fuel burnup, high average heat flux, low fuel lifetime (if no excess enrichment is added), high specific power, and low coolant power density system. The low moderator-to-fuel core on the other hand will have a longer fuel lifetime, higher fuel burnup, higher coolant power density, lower average heat flux, high fuel inventory and a low specific power. All of these factors must be studied and weighed.

The effect of the moderator-to-fuel ratio on the reactor stability and safety must also be evaluated. The boiling water reactor must be designed with a negative power coefficient of reactivity due to formation of steam voids within the core; that is, as the water moderator is expelled from the core, the reactivity must decrease. It should be noted, however, that a very large negative void coefficient is not desirable either. If the negative void coefficient is too large, reactor instability can result due to the self-regulating feedback control characteristic of the system.

The magnitude of the negative void coefficient will depend upon the moderator-to-fuel ratio and the core buckling. There is a range of moderator-to-fuel ratio where the effects of the variation of the resonance escape probability (p) and the thermal utilization (f) on the core reactivity will essentially cancel each other. As a result, the core buckling can then be set so that the void coefficient will be negative due to void formation and the resultant neutron exchange. In general, the lower the water-to-metal ratio, the more negative the void coefficient becomes.

To establish this moderator-to-fuel ratio, all the various factors affecting both the engineering and physics requirements of the core must be thoroughly investigated. Only then can a compromise on the moderator-to-fuel ratio be reached.

2. Critical Maximum Heat Flux (Burnout)

A major uncertainty in boiling reactor design is the prediction of the critical heat flux. The critical heat flux is defined as the transition from nucleate to film boiling and is marked by a sharply defined increase in the temperature of the heat transfer surface. If the heat flux is sufficiently great, the resulting thermal excursion results in physical destruction of the heat transfer surface. "Burnout" is a term usually used interchangeably with critical heat flux, although it is sometimes used to denote the point of actual failure. Since the first usage is a misnomer and the second subject to such extraneous variables as material properties, pressure and/or thermal stresses, and corrosion rates and effects, "burnout" is an ambiguous and ill-defined term.

The critical heat flux and the determining conditions thereof have been of considerable interest for at least a decade, and numerous experimental investigations have been made. However, no correlations of net boiling "burnout" have been developed to describe adequately its relationships with all various system parameters. The burnout heat flux is a function of the mass velocity, mixture enthalpy, system pressure, and possibly such additional factors as surface condition, geometry, etc. Much of the work that has been done to date on the critical heat flux problem has been summed up and reviewed in WAPD-188.[134] One of the most important conclusions listed in this report is that for nonuniform axial flux distribution the critical flux may not occur at either the point of maximum heat flux or maximum mixture enthalpy (exit condition). Thus in the boiling water reactor where highly skewed axial power distributions have been measured, the core exit condition cannot be used for establishing the burnout limits. The entire channel must be analyzed and the local heat fluxes and fluid conditions compared with existing burnout data and correlations to establish the burnout point. As the critical pressure is approached, the critical maximum flux decreases and the net boiling length in the core approaches zero. At very high pressures, the power peak will therefore occur in a region of local or subcooled boiling. It is also possible that, even though the critical maximum flux is exceeded, a true burnout need not necessarily occur, providing the film boiling coefficient is large enough. Recent film boiling data have shown that the temperature rise accompanying the departure from nucleate boiling is not excessive for heat fluxes of $q < 200{,}000$ Btu. Thus in a boiling water reactor which uses the oxide as fuel and stainless steel as cladding it may be possible to operate in the film boiling region under certain conditions. However, more such data are needed at heat fluxes of the order of magnitude existing in reactors (150,000 to 450,000 Btu/hr ft^2) and at comparable mass velocities.

In evaluating the probable burnout point in a boiling water reactor operating with natural circulation of the coolant, consideration must also be given to the stability of the system. When a system is hydrodynamically unstable, this departure from nucleate boiling can occur at lower value of heat flux than the value obtained under forced circulation for identical conditions. This is demonstrated in Fig. 8.1, which shows a trace of the recirculation velocity and the point of burnout for a natural-circulation system which became hydrodynamically unstable. The estimated burnout heat flux under forced-circulation conditions is ~700,000 Btu/hr ft^2, whereas the burnout occurred at a flux of ~560,000 Btu/hr ft^2. However, the fact that the system is hydrodynamically unstable does not preclude a burnout at any heat flux. Unfortunately, there is practically no information available on natural circulation burnout or the effect of instability on burnout.

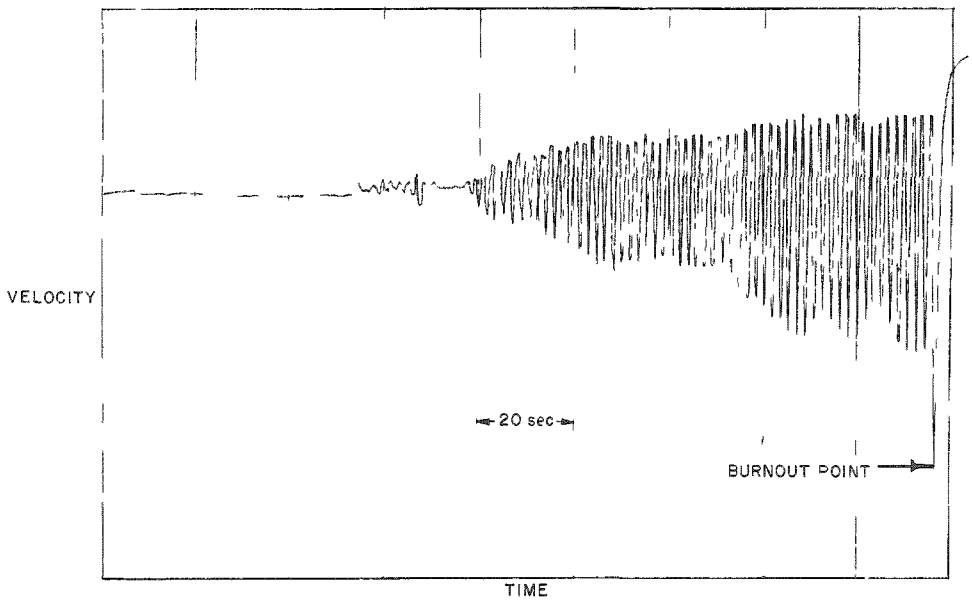

Fig. 8.1

Velocity As a Function of Time for a Natural Circulation Burnout

3. Vapor-Liquid Separation

In a reactor, such as EBWR, where steam is withdrawn directly from the reactor vessel, a reactor power is ultimately reached where the vapor-liquid separation problem becomes so acute that excessive moisture carryover and steam carryunder occur, adversely affecting reactor operation. The present trend of increasing the power and operating pressure of boiling water reactors has caused vapor-liquid separation to become one of the major problems in boiling water reactor plant engineering.

Knowledge concerning the mechanism and various factors influencing the separation of steam from steam-water mixtures in reactor vessels or in separate steam drums is quite incomplete. As a result of lack of information, sizing of the reactor vessel and internals with any degree of confidence becomes difficult at best.

The little information that has been reported has appeared in the English and Russian literature. However, the experimental data obtained by different techniques are in some cases inconsistent, and the given equations do not predict correctly the fraction of moisture carried by the steam for certain ranges of steam loads and pressures.

In a natural-circulation boiling water reactor of the EBWR type the vapor-liquid separation problem can be divided into the following parts: (1) liquid carryover in the effluent steam; (2) steam carryunder in the downcomer; (3) effectiveness of liquid makeup water injection and the rapidity of steam quenching thereafter; (4) transport of steam through stagnant steam-water mixtures (vapor holdup above core).

The problem of carryunder of entrainment of steam in the liquid in a natural vapor-separation system is a major one in either a natural or forced convection system. The entrainment of the steam in the liquid in the downcomer is in general a function of the downcomer velocity and system pressure. In a natural-circulation system any entrainment that may occur in the downcomer adversely affects reactor operation, since the recirculation is reduced and this in turn lowers the reactor power. There is practically no information available that could be used for estimating the amount of carryunder that could be expected under normal reactor conditions.

The carryunder problem in a forced-circulation system could be just as severe. In general, the velocities are somewhat greater in such a system, both in the core and the downcomer. The entrainment of the steam into the suction lines of the pump could decrease the NPSH to a point where pump cavitation problems could become serious, depending on the condition of the makeup water and point of injection.

The seriousness of the steam carryunder problem will be determined by the rapidity with which the entrained steam bubbles are quenched and, of course, by the amount of steam entrained. It is conceivable that the entrained steam bubbles are not collapsed immediately because of insufficient mixing in the downcomer; as a result the steam would be carried a considerable distance before condensing. This will, to a large degree, be dependent on the mode of makeup water injection. The makeup water injection ring must be designed so that the makeup water is distributed evenly across and around the entire downcomer to insure fast, thorough mixing. Should substantial quantities of steam carryunder occur, the net driving

head for natural circulation would be reduced. A reduction in net driving head would in turn reduce the recirculation flow rate and increase the core steam volume fraction.

In a closed reactor vessel the mixture-vapor interface of a two-phase fluid depends upon the initial water level and upon the steam void content (power level in a reactor system). The voids that are formed in the reactor core and riser and entrained in the downcomer displace an equal volume of water, which causes an increase in the mixture height. The water level above the riser is, in turn, further expanded by the vapor flowing through it, which creates a stagnant two-phase mixture or "bed." The final height of the two-phase mixture is a function of the superficial steam velocity (based on vessel diameter) and water content above the riser. Thus, for a given initial water level at saturation (with no voids present) the expansion of the two-phase "bed" increases with increasing power because of the higher superficial steam velocity and the increased water content which was expelled from the region below the riser.

The height of the two-phase mixture cannot be obtained by purely analytical means. Recourse must be made to experimental data on vapor holdup through stagnant beds of water. Unfortunately, no data exist for flow of steam through stagnant water at 600 psi in large vessels. However, such data are available on air-water systems at atmospheric pressure and in vessels up to 36 inches in diameter.[135] Additional data have been reported by Behringer[134] for steam flowing through water in a 2-in. pipe at various pressures up to 600 psi. This data tended to check the work of Zmola[135] and serve as a basis of extrapolation of the air-water data to higher pressures for the large diameter vessels.

Calculations of the height of the vapor-mixture interface have been made for EBWR at 40 Mw and tend to explain the increase in carryover actually measured at that power level, since they show that the interface would have been very close to the steam ring at these powers.

Additional data on the transport of vapors through low-velocity water at the higher pressures must be obtained before optimum vessel sizes can be chosen.

The problem of entrainment of liquid with the steam will also influence strongly the sizing of the reactor vessel. Data in the Russian literature indicate that the entrainment is not a function of the superficial velocity alone but also of dome height; that is the liquid entrainment is a function of the steam dome volume. The superficial steam velocity is known to affect primary vapor separation through its effect on the steam "disengaging height" at the interface. The steam disengaging height is defined as the length required for the transition from the steam-water mixture to steam of constant quality. The existence of this zone, which probably results from the expulsion of liquid droplets by the disengaging steam

at the vapor-liquid interface, has been demonstrated in EBWR (see Fig. 8.2). As can be seen, the disengaging height increases with increasing superficial steam velocity and hence reactor power. Therefore the minimum steam dome height for effective primary natural vapor-liquid separation must exceed the disengaging height.

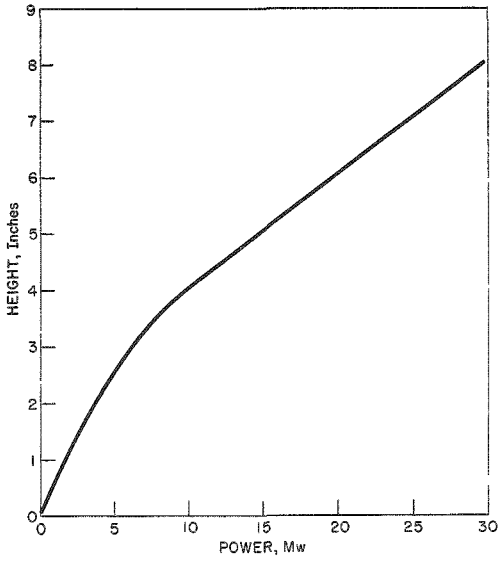

Fig. 8.2

Disengaging Height (Interface Thickness) as a Function of Power in EBWR

It can be seen that sizing of the pressure vessel and, in fact, the actual reactor design depend to a very large degree on the vapor-liquid separation problem. If the primary vapor-liquid separation cannot be achieved within the reactor vessel, recourse must be made to external separation means such as steam drums, etc.

4. Reactor Geometry; Natural vs Forced Circulation

Recirculation of the coolant through the reactor core can be achieved by either natural or forced convection. Proper selection of the mode of operation can be made only after a careful evaluation of the limitations imposed by reactor design parameters, such as reactor geometry, minimum flow-rate requirements, vapor separation, reactor stability, etc.

In a natural-convection system the recirculation flow rates that can be obtained are determined primarily by the system geometry. More specifically, the hydraulic diameters, relative flow areas and heights of the core, riser and downcomer are the controlling factors. Employment of natural circulation, therefore, tends to impose limitations upon the geometry that can be used. In a forced-circulation system the reactor geometry is not usually a major factor, providing the necessary pump head and capacity requirements do not exceed feasible limits.

Natural-circulation flow rates can be as high or higher than flows normally associated with a forced-circulation system. Laboratory tests on a natural-circulation loop showed that recirculation velocities up to 10 ft/sec could readily be obtained. Basically the system consisted of a heated section, a 4-ft long pipe of 1-in. diameter, and a 2-in. diameter riser, 8 ft long. The flow rates usually associated with forced circulation are in the range of 8-12 ft/sec.

Natural-circulation velocities can be increased either by enlarging the core coolant channel hydraulic diameter and relative flow areas of the riser and downcomer or by adding riser height. A natural-circulation system featuring a riserless core or heated section yields recirculation velocities which are generally quite low, about 2-4 ft/sec. However, by adding riser height of large hydraulic diameters, the net natural-circulation driving head is increased without introducing additional flow resistance. As a result the recirculation velocity can readily be increased.

An important reactor design parameter which can influence the selection of either natural or forced circulation is the vapor-separation problem. As mentioned previously, in a closed reactor vessel a power level is ultimately reached where the separation problem becomes acute and excessive moisture carryover and carryunder occurs which adversely affect reactor operation. When this point is reached, it is usually necessary to resort to external separation methods, such as the use of steam drums. Such a system has an excellent natural-circulation potential, since the basic design readily lends itself to incorporation of adequate riser height to obtain the desired performance. However, the effect of high risers on reactor stability is unknown at present. It is a well known fact that maintenance of flow equilibrium in a multi-riser system is a critical problem.

Reactor stability considerations will also have a direct bearing on the selection of the type of circulation. Laboratory tests have shown that natural-circulation stability is a function of system geometry, pressure, and exit steam volume fraction of the heated channel. These tests have shown that there is apparently a threshold value of the exit steam volume fraction beyond which hydrodynamic instability occurs. This relationship is also a function of pressure; as the system pressure increases, the system will become unstable at a lower value of the exit steam volume fraction, but at a higher power density.

Hydrodynamic stability is strongly affected by the system geometry. Placement of restrictions in the downcomer tends to increase the stability of the system; that is, the threshold value of the exit steam volume fraction increases at the inception of instability.

A series of tests which were run to study the effect of riser geometry showed that, for a system where riser flow area was one-half that of the test section, hydrodynamic instability was observed at a power density of 120 kw/l at 600 psi; the inlet section velocity was approximately 4 ft/sec. By comparison, stable operation was obtained at a power level of 350 kw/l for the riser geometry of twice the flow area of the test section. The recirculation velocity in this instance was 8 ft/sec.

It should be noted that, in general, natural-circulation systems are hydrodynamically stable over wide ranges of conditions, and from information gained recently it appears that the stability of such systems can be improved considerably by proper design. More information is needed, however, especially on high riser systems of large hydraulic diameter and of varying relative flow areas to the core.

Forced-convection systems with multiple flow channels are also subject to hydrodynamic instabilities which result from parallel channel effects. These effects are due to possible variations in the resistance of each channel while they are being maintained at a fixed pressure differential common to all. As a result, orificing of the individual channels is required to eliminate the possibility of flow fluctuations occurring. This is a much discussed subject, but little laboratory information is available.

In the final analysis, the merits of a natural-circulation or forced-circulation system must be subject to economic comparison. The initial capital investment and maintenance of the external pump loops of the forced-circulation system must be weighed against the cost of the much more simplified but possibly more limited natural-circulation system.

8.3. Design Procedure for Boiling Water Reactors

A design procedure which may be used in a boiling water reactor design study is outlined below. It should be recognized that the method of approach suggested is but one of a number that can be followed. A design procedure will, in fact, evolve during the design study and will be governed by the objectives and type of reactor under study. The sole purpose of this outline is to illustrate the various calculation procedures generally used in boiling water reactor design analysis.

1. Establish the design objective. The design objectives usually are many and varied, such as (a) a specified total power, (b) the maximum power that can be obtained from a given size of pressure vessel, (c) a certain core power density, (d) achieving vapor-liquid separation within the reactor vessel, (e) natural or forced circulation, etc.

2. Conduct a general parametric study of the various design parameters such as coolant channel hydraulic diameter, riser length, core diameter and height, mean core steam volume fraction, moderator-to-fuel ratio, structure-to-fuel ratio, etc. The purpose of this study would be to establish feasible limits on the various design parameters which would satisfy the design objectives. The thermal hydraulic portion of the study is tied to the core physics and fuel element design by the following equations:

$$nD_R^2 = \frac{D_c^2}{(M/F) + (S/F) + 1} \tag{8.1}$$

$$D_e = \left[D_c^2 - nD_R^2\left(1 + \frac{S}{F}\right)\right] \Big/ nD_R \tag{8.2}$$

$$P_R = n\pi D_R L_c q_c'' / 3.413 \times 10^6 \tag{8.3}$$

$$T_{\mathfrak{L}\,max} = T_{sat} + R_{max}/avg\ q_c''\left(\frac{D_R}{4k_R} + \frac{1}{h_c} + \frac{t_c}{k_c} + \frac{1}{h_B}\right) \quad . \tag{8.4}$$

These equations can be plotted in graphical form, as shown in Fig. 8.3. Such graphs can readily be used in a parametric study. Preliminary estimates of the core recirculation flow rate, steam volume fraction, power density, etc., can be obtained from generalized "average channel" calculations, which can be made rather quickly. The inherent assumptions in such an analysis are (1) a constant axial heat input, and, (2) the overall performance characteristics of the core can be estimated by an analysis of the average channel (based on power density). Although these assumptions are subject to much question, the calculated performance by the average channel method will not vary very greatly from a detailed analysis unless radical departures from ordinary reactor geometries are encountered.

The following procedure and equations can be used for the thermal hydraulic calculations:

$$P.D._{kw/l} = P_R(1000)/l_c A_{coolant}(28.3) \tag{8.5}$$

where 28.3 converts cu ft to liters. The cross-sectional flow area is related to the moderator to fuel ratio as follows:

$$A_{coolant} = \frac{\pi D_c^2}{4} - \frac{n\pi D_R^2}{4}\left[1 + \frac{S}{F}\right] \quad . \tag{8.6}$$

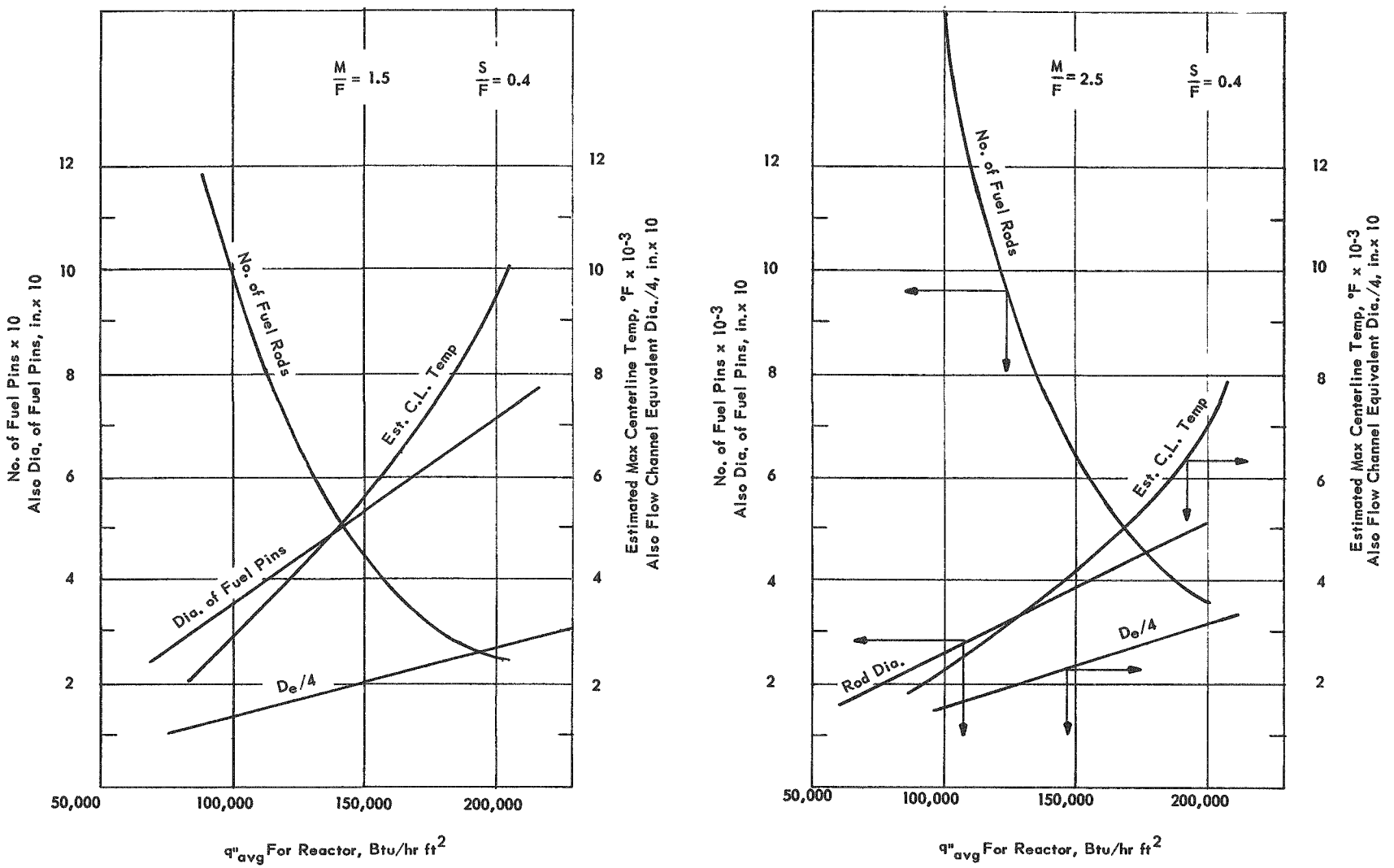

Fig. 8.3

Relationships between Various Reactor Design Parameters

Therefore,

$$P.D._{kw/L} = \frac{P_R(1000)}{L_c(28.3)\left(\frac{\pi D_c^2}{4} - \frac{n\pi D_R^2}{4}\left[1 + \frac{S}{F}\right]\right)} \quad . \tag{8.7}$$

The average coolant power density is also related to the hydraulics of the system. From a heat balance on the boiling section of the average channel with a uniform heat input,

$$Q = W_T x_e h_{fg} = V A_{coolant} \rho_l x_e h_{fg} \quad . \tag{8.8}$$

Converting to power density in kw/L,

$$P.D._{kw/L} = \frac{Q(3600)}{3413\, A_{coolant} L_B(28.3)} = \frac{V \rho_l x_e h_{fg}}{(28.3)\frac{L_B}{L_c}(L_c)}\left(\frac{3600}{3413}\right)$$

and

$$P.D._{avg\ kw/L} = \frac{V x_e \rho_l h_{fg}}{\frac{L_B}{L_c}(L_c)}\,(0.0374) \quad . \tag{8.9}$$

Equating Eq. (8.5) and (8.9),

$$V = 948\, P_R L_B / L_c A_{coolant} x_e \rho_l h_{fg} \quad . \tag{8.10}$$

Eq. (8.10) merely defines the relationship between the recirculation velocity, core geometry and power. The recirculation velocity, V, is also, however, a function of the hydraulic characteristic of the system. The relationship between the velocity and the system geometry is given by Eq. (7.25):

$$\frac{V^2}{2g} = \frac{L_{nB}(\rho_D - \bar{\rho}_{NB}) + L_B(\rho_D - \bar{\rho}_B) + \Sigma_{R_i}(\rho_D - \rho_{R_i})}{N_1 + \cdots + N_g + \Sigma N_i + \Sigma N_{R_i}} \tag{8.11}$$

where

$$N_1 = \rho_f\left(\frac{A_{HS}}{A_D}\right)^2\left[1 + K_{c_{UP}}\right] = \text{acceleration of the fluid from the upper plenum to downcomer and frictional resistance at contraction.}$$

$$N_2 = f_D\left(\frac{L_D}{D_D}\right)\left(\frac{\rho_f}{\rho_D}\right)\left(\frac{A_{HS}}{A_D}\right)^2 = \text{frictional resistance in downcomer.}$$

$$N_3 = \frac{\rho_f^2}{\rho_D}\left(\frac{A_{HS}}{A_D}\right)^2\left(\frac{\rho_f}{\rho_D}\right)^2\left[\left(\frac{A_D}{A_{LP}}\right)^2 - 1 + K_{E_{LPB}}\right]$$ = deceleration of fluid and frictional losses at the expansion from the downcomer to lower plenum

$$N_4 = \frac{\rho_f^2}{\rho_D}\left[1 - \left(\frac{A_{HS}}{A_{LP}}\right)^2 + K_{C_{HSB}}\right]$$ = acceleration of fluid and frictional losses at the contraction from lower plenum to the heated section.

$$N_5 = 2\rho_f\left[\frac{\rho_{HSB} - \rho_f}{\rho_{HSB}}\right]$$ = acceleration of fluid in nonboiling length due to density change with temperature.

$$N_6 = \frac{\rho_f^2}{\rho_{LB}}\left(\frac{f_{HS}}{D_{HS}}\right)\left(L_{NB}\right)$$ = frictional resistance in the nonboiling segment of the heated section.

$$N_7 = \frac{\rho_f^2}{\rho_{LB}}\left(\bar{R}_{LB}\right)\left(\frac{f_{HS}}{D_{HS}}\right)\left(L_{LB}\right)$$ = frictional resistance in the local boiling segment of the heated section.

$$N_8 = 2(r)(\rho_f)^2$$ = acceleration of fluid due to formation of steam voids in the heated channel.

$$N_9 = \rho_f(\bar{R})\left(\frac{f_{HS}}{D_{HS}}\right)\left(L_B\right)$$ = frictional resistance in the boiling segment.

$$N_{10} = 2\rho_f\left(\frac{A_{HS}}{A_{i+1}}\right)\left[x_{HSE}^2\left\{\frac{\rho_f}{\rho_g}\frac{1}{(\alpha_{i+1})} - \frac{A_{HS}}{A_i}\frac{1}{\alpha_i}\right\}\right.$$

$$\left. + \left(1 - x_{HSE}\right)^2\left\{\frac{A_{HS}}{A_{i+1}}\frac{1}{(\alpha_i + 1)} - \frac{A_{HS}}{A_i\alpha_i}\right\}\right]$$ = total pressure drop due to an expansion or contraction.

$$N_{11} = Rf_R\left(\frac{A_{HS}}{A_R}\right)^2\frac{\rho_f}{D_R}L_R$$ = frictional loss in the adiabatic risers.

Thus the thermodynamic and hydraulic Eqs. (8.10) and (8.11), which describe the behavior of the average channel, must be solved simultaneously. The unknowns in the equation can be obtained as follows:

The coolant cross sectional flow area, $A_{coolant}$, can be estimated from Eq. (8.6) if a fuel element design and core layout has not been decided upon.

The two-phase friction factor multipliers $\overline{R}$ and R can be obtained from the literature or by the methods suggested in Section 7.

The acceleration pressure drop multiplier, r, is

$$r = \left[\frac{(1 - x_e)^2}{1 - \alpha_e} + \frac{x_e^2}{\alpha_e}\frac{\rho_f}{\rho_g} - 1\right]\frac{1}{\rho_f} \quad . \tag{8.12}$$

The mean density in the boiling segment may be found as a function of pressure, slip ratio, and exit steam volume fraction. For the preliminary analysis of this type, the assumption is made that the slip ratio is constant along the heated length and that there is a uniform heat input.

$$\overline{\rho}_B = 1 - \frac{1 - (\rho_g/\rho_f)}{1 - \psi}\left\{1 - \left[\frac{1}{\alpha_e(1 - \psi)} - 1\right]\ln\left[\frac{1}{1 - \alpha_e(1 - \psi)}\right]\right\} \quad , \tag{8.13}$$

where

$$\psi \equiv \frac{V_g}{V}\frac{\rho_g}{\rho_1} \quad .$$

The two-phase mixture density in an adiabatic riser section is simply

$$\rho_{R_i} = (1 - \alpha_{R_i})\rho_f + \alpha_{R_i}\rho_g \quad . \tag{8.14}$$

The change in voids due to a geometry change may be estimated from the following semi-empirical equation:

$$\alpha_2 = \frac{1}{\frac{(1/\alpha_1 - 1)}{(A_1/A_2)N} + 1} \tag{8.15}$$

where N is the slope of the slip ratio vs water velocity plot as discussed in Section 7.

The mixture quality, X, is related to the steam volume fraction, α, by the slip ratio V_g/V_l through the continuity equation. At any plane normal to the fluid flow in a channel,

$$W_g/W_f = xW_T/(1 - x)W_T = \rho_g A_g V_g/\rho_l A_l V_l \quad .$$

Introducing

$$A_g = \alpha A_T$$

and

$$A = (1 - \alpha)A_T \quad ,$$

and simplifying,

$$x = \frac{1}{1 + \rho_l/\rho_g \dfrac{(1/\alpha - 1)}{V_g/V_l}} \quad . \tag{8.16}$$

The boiling length ratio may be obtained from an overall heat balance on a boiling channel

$$Q_T = W_T \left[h_f - h_i + x_e h_{fg}\right] = W_g \left[h_f - h_M + h_{fg}\right] \quad .$$

Inspection of the above equation will reveal that

$$Q_B/Q_T = h_{fg}/(h_f - h_M + h_{fg}) \quad . \tag{8.17}$$

This ratio is therefore dependent only on pressure and feedwater injection temperature.

For a uniform heat input,

$$Q_B/Q_T = L_B/L_T = h_{fg}/(h_g - h_M) \quad . \tag{8.18}$$

A direct solution of Eq. (8.10) and (8.11) is not possible, since Eq. (8.11), describing the hydraulic characteristics of the system, is implicit in velocity V. The procedure generally used for solving these equations is as follows. The solution is found by an iterative process.

(1) Assume a value of exit steam volume fraction, α_e.

(2) Estimate a value of the slip ratio (using the correlations presented in the previous section) and calculate the quality, using Eq. (8.16).

(3) Calculate the boiling length from Eq. (8.18).

(4) Solve the flow Eq. (8.11).

(5) Re-evaluate the slip ratio and recalculate the quality if necessary. Repeat process until solution converges.

(6) Calculate the velocity, using Eq. (8.10) and the quality calculated in step 2.

(7) If the velocity calculated in step 6 equals the velocity calculated in step 4, the desired solution has been obtained. If the two velocities are not equal, a new value of the exit steam volume fraction must be assumed and the entire procedure repeated until the velocities become equal.

Such an analysis is carried out for a series of differing reactor geometries of varying core flow equivalent diameters, core height, riser height, etc., and a series of curves of the type shown in Fig. 8.4 is obtained. Such curves are very useful in that they yield quick estimates of reactor performance for a great number of possible reactor designs. Preliminary sizing of the pressure vessel can also be carried out at this point since the total recirculation flow rates, core voids, etc., can be obtained.

The total recirculation flow rate is

$$W_T = A_{coolant} V \rho_1 \quad .$$

The downcomer is generally sized so that it will have a negligible pressure drop due to friction and low enough velocity so that excessive carryunder of steam is not obtained. A thermal shield analysis is then made to establish the thickness. Combining these factors, the diameter of the vessel can be set. The height of the vessel is established by allowing sufficient length on the lower plenum, core, riser, and primary internal vapor separation, if desired. The required vessel height above the riser is a function of the reactor power, initial saturated zero-power water level, pressure, etc., as discussed previously in the section on vapor-separation problems.

3. Select several of the most probable final designs and then make detailed physics, engineering and thermal-hydraulic calculations to arrive at the final design. The calculation procedure for a detailed core analysis is much more complex, due to the additional complicating factors of constant inlet subcooling across the core and the axial and radial power distribution within the core.

In such an analysis, the following unknowns are to be determined: (1) the core inlet subcooling, (2) total recirculation flow rate, (3) velocity profile across the core, (4) mean core steam volume fraction, (5) axial and radial steam volume fraction profiles, (6) axial and radial mixture quality profile, (7) boiling length profile across the core.

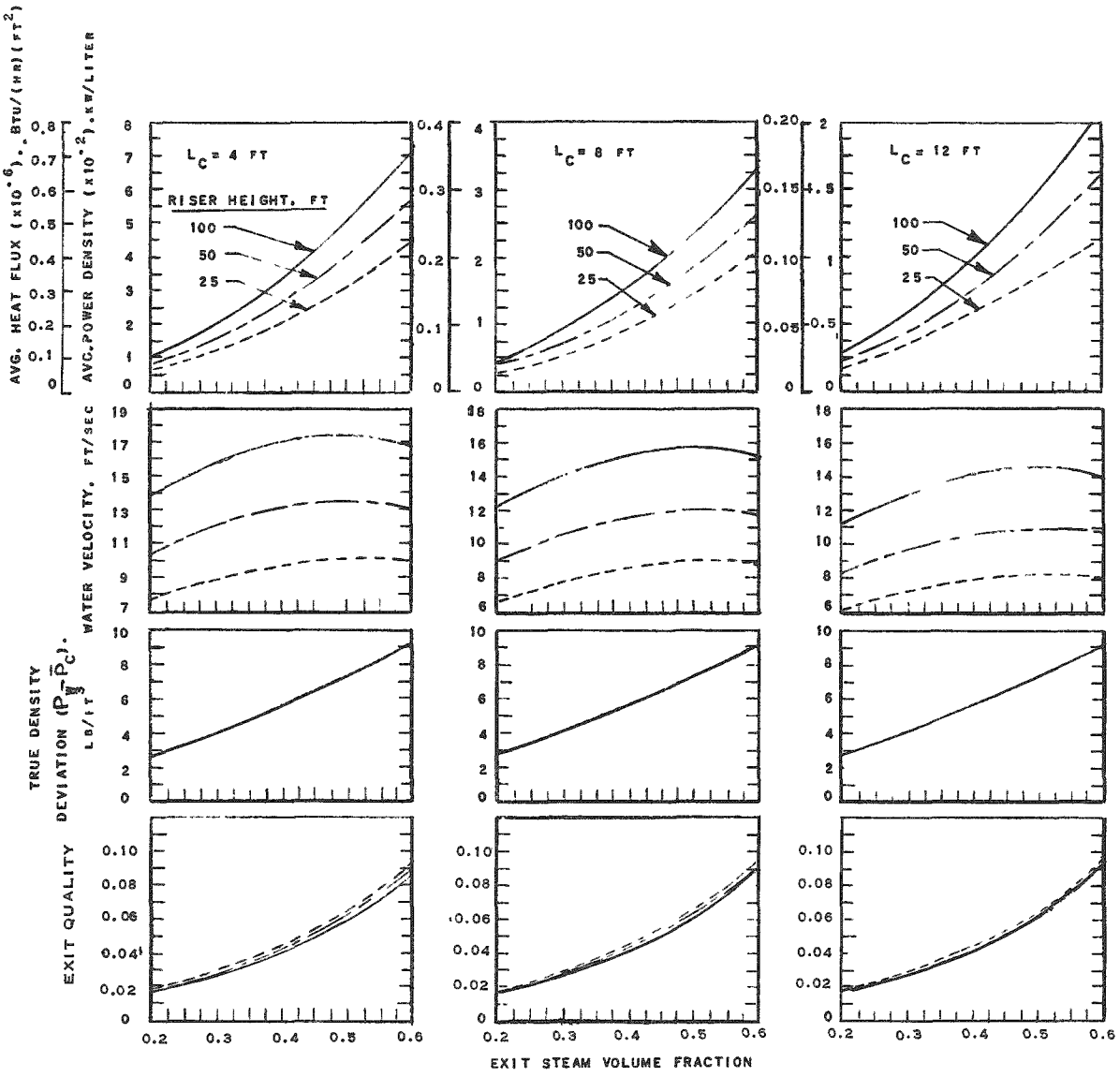

Fig. 8.4

Effect of Riser Height and Exit Steam Volume Fraction on Performance of Natural Circulation Boiling Reactors; D_e = 0.5 in.; D_R = 1 in.; P = 1000 lb/in.^{2}

These factors are a function of the axial and radial core power distributions. The power distribution, however, in turn is a function of the system hydraulics, since it is a function of the steam volume fraction distribution within the core. The core physics and hydrodynamics are coupled together by this interrelationship.

A procedure that can be followed for a core analysis is as follows:

(1) Assume a radial and an axial power distribution and calculate the power density distribution.

(2) Assume a velocity profile across the core.

(3) Calculate the total recirculation flow rate, W_T:

$$W_T = \rho_f \int_0^R V_r dA; \quad = \rho_f \int_0^R V_r 2\pi r dr; \quad = 2\pi\rho_f \int_0^R V_r r dr$$

(4) Calculate the core inlet subcooling by a heat balance at the top of the downcomer where the make-up water is injected:

$$W_m h_m + (1 - \bar{x}_e) W_T h_f = W_T h_i \quad .$$

Since $W_m = W_S = \bar{x}_e W_T$,

$$\bar{x}_e W_T h_m + (1 - \bar{x}_e) W_T h_f = W_T h_1$$

or

$$h_i = \bar{x}_e h_m + (1 - \bar{x}_e) h_f \quad .$$

(5) Select a number of points (channels) at appropriate core radii for analysis and determine the power release from step 1. More points should be selected near the outer region of the core because (1) the power distribution usually varies more markedly near the core periphery and (2) the velocity profile must be established more accurately since the greatest percentage of the total coolant flow occurs at the outer region of the core.

(6) Calculate the exit mixture quality for each of the points (or channel) selected for study by a heat balance using the assumed velocity profile from step 2.

$$P.D._{kw/L} = 0.0374\, V_r \rho_f (h_f - h_i - x_e h_{fg})/L_c \quad .$$

(7) Calculate the exit steam volume fraction profile using the mixture qualities in step 6. Also estimate the steam volume fraction in the various risers. The steam volume fraction is calculated by the following equation:

$$\frac{V_g}{V_l} = \left(\frac{x}{1 - x}\right)\left(\frac{1 - \alpha}{\alpha}\right)\frac{\rho_l}{\rho_g} \quad .$$

The slip ratio may be obtained from the slip ratio correlations presented in the previous section.

(8) Calculate the boiling length for the various channels under study by the following relationships:

$$\frac{Q_{NB}}{Q_T} = \frac{(h_f - h_i)}{(h_f - h_i) + x_l h_{fg}}$$

and

$$Q_B/Q_T = 1 - Q_{NB}/Q_T \quad .$$

A plot of Q/Q_T vs the core length, L_c, can be obtained by integrating the power distribution. The point at which boiling begins is where

$$Q/Q_T = Q_{NB}/Q_T \quad .$$

(9) Calculate the recirculation velocity by the flow Eq. (8.11) at the selected points on the core radius.

(10) Compare the recirculation velocity profile obtained from step 9 with the one initally assumed in step 2. If the profiles are the same, the performance of the core has been established. If the profiles are not the same, steps 2-10 must be repeated until agreement is reached.

(11) After the calculation has been completed, the assumed power distributions must be recalculated using the new steam volume fraction profile. If the new power distribution does not check the one in step 1, the entire procedure must be repeated.

Alternate methods of solution can be used. For instance, a subcooling could have initially been assumed and then the velocity profile calculated. The solution would iterate on the subcooling instead.

To illustrate the procedure for analyzing a natural-circulation boiling water reactor, consider the proposed operation of EBWR (Experimental Boiling Water Reactor) at 100 Mw.[59] Fig. 8.5 lists the dimensions to be used in the calculation and indicates the relationship of the various riser sections.

	Area	D_e
Plate elements	0.0580 ft^2	0.0573 ft
Spike elements	0.0591 ft^2	0.0417 ft

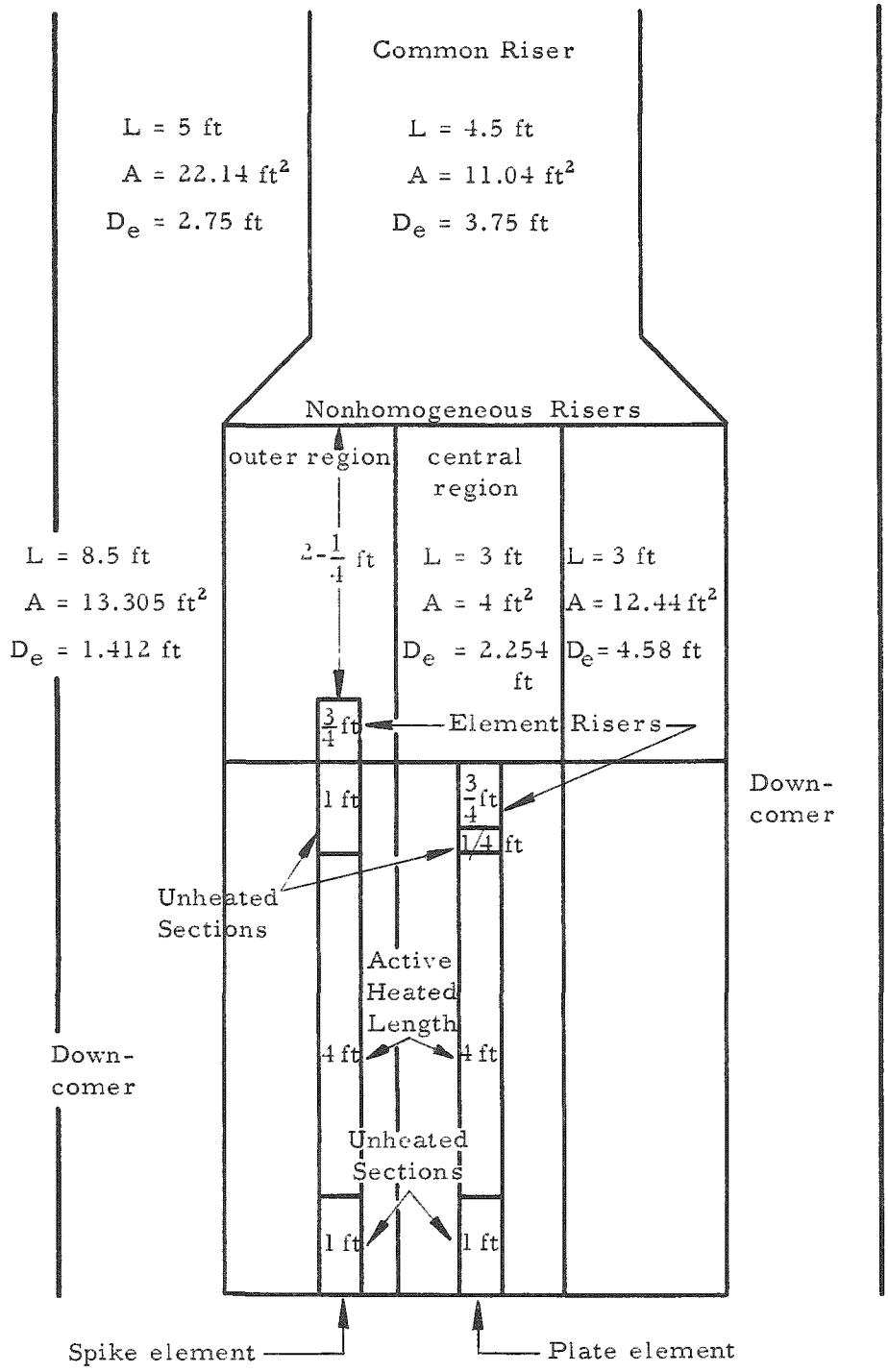

Fig. 8.5

Proposed EBWR Operation at 100 Mw

There are two types of fuel elements in the core. In the central region (i.e., the region in which the elements feed the central portion of the non-homogeneous riser) there are 32 plate-type elements. Grouped around these elements are 28 rod-type elements with a higher enrichment, called spike elements. The spike elements feed into the outer (also called annular) portion of the non-homogeneous riser. Around the spike elements are grouped 87 more plate-type elements, completing the core.

Element	Number	Area per Element	Total Area
Plate - central	32	0.0580 ft^2	1.856 ft^2
Spike	28	0.0591 ft^2	1.655 ft^2
Plate - outer	87	0.0580 ft^2	5.046 ft^2
			8.557 ft^2

The average power per element is

$$Q_{avg} = \frac{100 \text{ Mw}}{147 \text{ elements}} \times 3.413 \times 10^6 \frac{\text{Btu}}{\text{hr Mw}} = 2.322 \times 10^6 \frac{\text{Btu}}{\text{hr}} .$$

A graphical integration of the radial power distribution indicates that 26.24% of the power is generated in the central region. The operating pressure is 600 psia, and makeup water is fed to the reactor at 100°F. Thus, the total steam flow is

$$W_S = \frac{\text{Power}}{h_g - h_{in}} = \frac{3.413 \times 10^8}{1203.2 - 68.0} = 3.007 \times 10^5 \text{ lb/hr} .$$

The steam flow to the central nonhomogeneous riser is

$$W_{s_C} = 0.2624 \times 3.007 \times 10^5 = 0.7890 \times 10^5 \text{ lb/hr} .$$

The steam flow to the outer annular region is

$$W_{s_A} = (3.007 - 0.789) \times 10^5 = 2.218 \times 10^5 \text{ lb/hr} .$$

A velocity profile for the entire core is assumed as a basis for calculation. Assume the velocity in the spike elements is 5.4 ft/sec and the velocity in the plate-type elements is everywhere 7 ft/sec.

The flow rates of the regions are then calculated.

W_c = central fluid flow = ρAV

= 49.75 lb/ft^3 x 1.856 ft^2 x 7 ft/sec x 3.6 x 10^3 sec/hr

= 2.327 x 10^6 lb/hr .

$$W_A = \text{annular fluid flow} = \rho A_{spike} V_{spike} + \rho A_{plate} V_{plate}$$

$$= 49.75 \times 1.655 \times 5.4 \times 3.6 \times 10^2 + 49.75 \times 5.046 \times 7 \times 3.6 \times 10^3$$

$$= 7.927 \times 10^6 \text{ lb/hr} \quad .$$

The total core flow rate is thus

$$W_T = 1.0254 \times 10^7 \text{ lb/hr} \quad .$$

The net quality in the common riser is

$$x = W_S/W_T = 0.0293 \quad .$$

The quality in the central riser is

$$x_C = W_{s_C}/W_C = 0.0339 \quad .$$

The quality in the outer riser is

$$x_A = W_{s_A}/W_S = 0.0280 \quad .$$

The subcooling is calculated by

$$h_{in} = (1 - x)h_f + xh_m$$

$$= 0.9707 \times 471.6 + 0.0293 \times 68 = 459.8 \text{ Btu/lb} \quad .$$

Thus,

$$\Delta h_{sub} = 471.6 - 459.8 = 11.8 \text{ Btu/lb} \quad .$$

This value of subcooling is assumed to remain constant across the entire core.

The void fraction in the various regions is calculated by

$$\alpha = \left[1 + \frac{\rho_g}{\rho_f} \frac{V_g}{V_f} \frac{(1 - x)}{x}\right]^{-1} \quad .$$

Thus, the void fractions in the various regions are:

Central riser

$$\alpha_{R_2} = \left[1 + \frac{1.89}{38.3} \times \frac{0.9661}{0.0339}\right]^{-1} = 0.416$$

Outer riser

$$\alpha_{R_2} = \left[1 + \frac{1.87}{38.3} \times \frac{0.9720}{0.0280}\right]^{-1} = 0.371$$

Tapered region of common riser

$$\alpha_R = \left[1 + \frac{1.82}{38.3}\,\frac{0.9707}{0.0293}\right]^{-1} = 0.388$$

Common riser

$$\alpha_{R_3} = \left[1 + \frac{1.59}{38.3}\,\frac{0.9707}{0.0293}\right]^{-1} = 0.536 \quad .$$

Vessel above common riser

$$\alpha_V = \left[1 + \frac{2.10}{38.3}\,\frac{0.9707}{0.0293}\right]^{-1} = 0.355 \quad .$$

The previously discussed Eq. (8.11) for computing natural-circulation velocity as applied to this system is

$$\frac{V_0^2}{2g} = \frac{a + b + c_1 + c_2 + c_3}{N_{1_1} + N_{1_2} + N_2 + N_3 + N_{4_1} + N_{4_2} + N_{4_3} + N_6 + N_7 + N_8 + N_{9_1} + N_{9_3} + N_{9_4}} \quad .$$

The significances of the terms of the equation as applied to this problem will be dealt with explicitly below and the values will be calculated. The analysis of a system as complicated as this one can be simplified by treating the terms related to external users and downcomers separately from the terms related to the elements. This is because the pressure differential between the entrance to an element at the lower plenum and the exit from an element at the end of the element portion of riser into the nonhomogeneous riser must be the same for all elements of the same length feeding the same nonhomogeneous riser.

Thus, by rearranging terms so that

$$\frac{V_0^2}{2g}\left[N_{1_1} + N_{1_2} + N_{4_2} + N_{4_3} + N_{9_3} + N_{9_4}\right] - c_2 - c_3 = a + b + c_1$$

$$-\frac{V_0^2}{2g}\left[N_2 + N_3 + N_{4_1} + N_6 + N_7 + N_8 + N_{9_1}\right] \quad ,$$

the left side of the equation contains terms related to the external risers and downcomers, whereas the right side of the equation contains terms related to the interior of an element.

The pressure differentials through various elements are compared to the pressure differentials through the external risers and downcomers. The velocities in the elements are adjusted until the pressure differentials agree.

The pressure differentials in the external risers and downcomers are

$$\Delta P_I = \frac{\overline{V}_0^2}{2g}\left[N_{1_1} + N_{1_2} + N_{4_2} + N_{4_3} + N_{9_3} + N_{9_4}\right] - c_2 - c_3$$

where $\overline{V}_0$ is the average velocity of the elements feeding a given external riser, for the velocity distribution originally assumed.

The significances of the various terms are listed, and the calculation is illustrated for the central riser section. In the calculations of hydrostatic head the common riser is assumed to be 1.5 feet shorter than its actual length, to account for steam carryover and allow for possible shortening of the riser.

(1) Friction loss, in lb_m/ft^3, in upper portion of downcomer

$$N_{1_1} = f_{D_1}\left(\frac{L_{D_1}}{D_{D_1}}\right)\left(\frac{\rho_f^2}{\rho_D}\right)\left(\frac{A_C}{A_{D_1}}\right)^2$$

$$= (0.00905)\left(\frac{5}{2.75}\right)\left(\frac{49.75^2}{50.25}\right)\left(\frac{8.557}{22.14}\right)^2$$

$$= 0.12 \quad .$$

(2) Friction loss in lower portion of downcomer

$$N_{1_2} = f_{D_2}\left(\frac{L_{D_2}}{D_{D_2}}\right)\left(\frac{\rho_f^2}{\rho_D}\right)\left(\frac{A_C}{A_{D_2}}\right)^2$$

$$= (0.0093)\left(\frac{8.5}{1.412}\right)\left(\frac{49.75^2}{50.25}\right)\left(\frac{8.557}{13.305}\right)^2$$

$$= 1.14 \quad .$$

(3) Friction loss in nonhomogeneous riser

$$N_{4_2} = f_{R_2} R_{R_2}\left(\frac{L_{R_2}}{D_{R_2}}\right)\left(\frac{A_C}{A_{R_2}}\right)^2 \rho_f$$

$$= (0.009)\,(6.00)\left(\frac{3.00}{2.254}\right)\left(\frac{1.856}{4.00}\right)^2 (49.75) = 0.77 \quad .$$

(4) Friction loss in common riser

$$N_{4_3} = f_{R_3} R_{R_3} \left(\frac{L_{R_3}}{D_{R_3}}\right)\left(\frac{A_C}{A_{R_3}}\right)^2 \rho_f$$

$$= (0.0078)(4.00)\left(\frac{4.5}{3.75}\right)\left(\frac{8.557}{11.04}\right)(49.75)$$

$$= 1.12 \quad .$$

(5) Expansion from common riser into vessel above

$$N_{9_3} = 2\rho_f\left(\frac{A_C}{A_V}\right)\left[x^2 \frac{\rho_f}{\rho_g}\left(\frac{A_C}{A_V \alpha_V} - \frac{A_C}{A_{R_3}\alpha_{R_3}}\right)\right.$$

$$\left. + (1-x)^2\left(\frac{A_C}{A_V(1-\alpha_V)} - \frac{A_C}{A_{R_3}(1-\alpha_{R_3})}\right)\right]$$

$$= 2(49.75)\left(\frac{8.557}{32.28}\right)\left[(0.0293)^2\,(38.3)\right.$$

$$\left(\frac{8.557}{33.28 \times 0.355} - \frac{8.557}{11.04 \times 0.536}\right) + (0.9707)^2$$

$$\left.\left(\frac{8.557}{33.28 \times 0.645} - \frac{8.557}{11.04 \times 0.464}\right)\right] = -31.24 \quad .$$

(6) Contraction loss from nonhomogeneous riser into common riser

$$N_{9_4} = 2\rho_f\left(\frac{A_C}{A_R}\right)\left[x^2 \frac{\rho_f}{\rho_g}\left(\frac{A_C}{A_{R_3}\alpha_{R_3}} - \frac{A_C}{A_R \alpha_R}\right)\right.$$

$$\left. + (1-x)^2\left(\frac{A_C}{A_{R_3}(1-\alpha_{R_3})} - \frac{A_C}{A_R(1-\alpha_R)}\right)\right]$$

$$= 2(49.75)\left(\frac{8.557}{16.44}\right)\left[(0.0293)^2(38.3)\left(\frac{8.557}{11.04 \times 0.536} - \frac{8.557}{16.44 \times 0.388}\right)\right.$$

$$\left. + (0.9707)^2\left(\frac{8.557}{11.04 \times 0.464} - \frac{8.557}{16.44 \times 0.612}\right)\right]$$

$$= 40.15 \quad .$$

(7) Hydrostatic head in nonhomogeneous riser

$$C_2 = (\bar{\rho}_D - \bar{\rho}_{R_2}) L_{R_2}$$

$$= (50.25 - 29.59)\, 3 = 61.98 \text{ lb}_m/\text{ft}^2 \quad .$$

(8) Hydrostatic head in common riser

$$C_3 = (\rho_D - \rho_{R_3}) L_{R_3}$$

$$= (50.25 - 30.95)\, 3 = 57.90 \text{ lb}_m/\text{ft}^2 \quad .$$

The summation of the n terms is 12.06, so that

$$(\bar{V}_0^2/2g) \sum N = (49.00/64.34)(12.06) = 9.18 \quad .$$

The total pressure differential through the risers and downcomers is thus

$$\Delta P_I = -110.70 \text{ lb}_f/\text{ft}^2 \quad .$$

The same type of analysis is used to find ΔP_I for the spike elements and the outer plate-type elements. The results are:

spike

$$\Delta P_I = -91.63 \text{ lb}_f/\text{ft}^2$$

plate, outer

$$\Delta P_I = -105.43 \text{ lb}_f/\text{ft}^2 \quad .$$

The pressure differential through individual elements is now calculated. Six points in the core were selected to obtain the velocity profile. The points were radii of 10, 25, 40, 50, 60, and 70 cm. The radial power distribution shown in Fig. 8.6 was used to obtain the power at each point. Consider a point at radius 10 cm, to illustrate the calculation. The power of an element at radius 10 cm is

$$Q_r = \left(\frac{Q_r}{Q_{avg}}\right) Q_{avg} = (1.085)(2.322 \times 10^6) = 2.519 \times 10^6 \text{ Btu/hr} \quad .$$

Several iterations on velocity will be necessary in order to find the correct velocity for an element. As a first assumption, $V_0 = 7$ ft/sec will be selected. Thus, the fluid flow rate for an element at radius 10 cm is

$$W = \rho A V = (49.75)(0.0580)(7.0)(3.6 \times 10^3) = 72.716 \text{ lb/hr.}$$

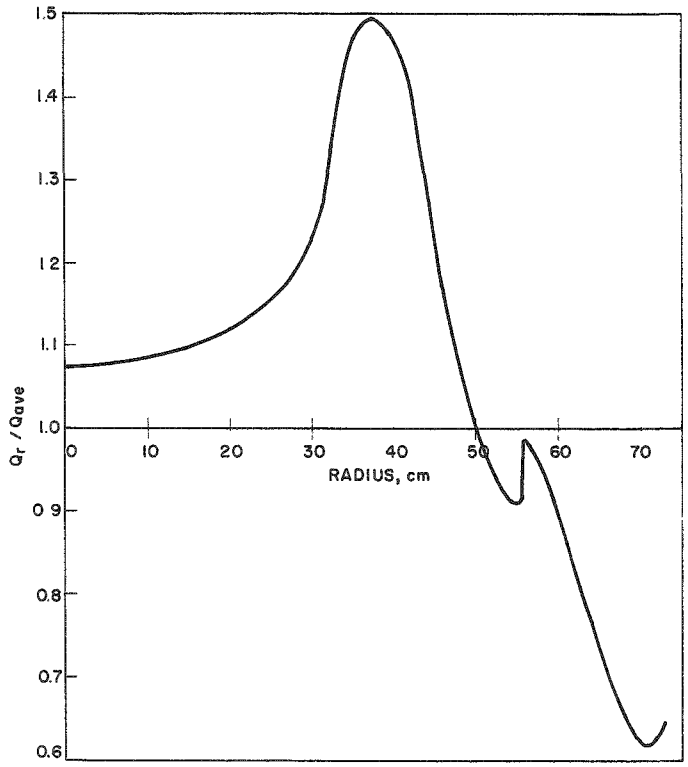

Fig. 8.6

EBWR 100-Mw Radial Power Profile

The power required to bring the subcooled liquid to saturation is

$$Q_{NB} = W\Delta h_{sub} = (72{,}716)(11.8) = 0.858 \times 10^6 \text{ Btu/hr} \quad .$$

The nonboiling and boiling lengths of the element are now found by using Fig. 8.7, a plot of the fraction of total power along the axial length of the element.

$$Q_{NB}/Q_r = 0.858 \times 10^6/2.519 \times 10^6 = 0.341 \quad .$$

Thus, the nonboiling length is

$$L_{NB} = 30.4 \text{ cm} = 0.997 \text{ ft}$$

and the boiling length is

$$L_B = 3.003 \text{ ft} \quad .$$

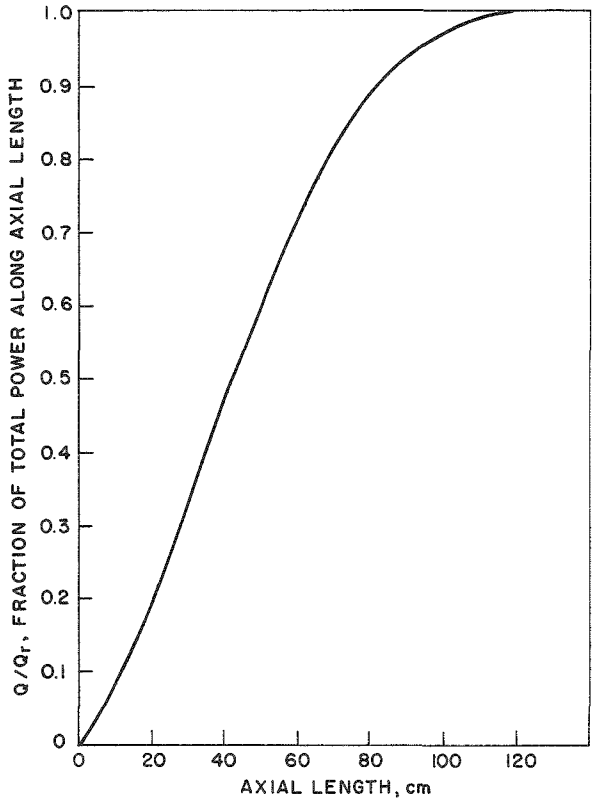

Fig. 8.7

EBWR 100-Mw Axial Power Profile

The average density in the boiling region is found by selecting a number of equally spaced points along the boiling length, determining by Fig. 8.7 the fraction of total power generated up to each point, subtracting from that the fraction of the power used in the nonboiling length to reach saturation, thereby determining the quality at the point, by which the slip can be obtained so as to calculate the void fraction at the point, and thus obtaining the density at each point. The average of these densities along the boiling length is the average boiling density. This procedure must be used because the axial power distribution is not of a simple shape.

This calculation will be illustrated for the last point in the element. Here, all the power has been generated so

$$Q/Q_r = 1.000 \quad .$$

Thus,

$$(Q-Q_{NB})/Q_r = 1.000 - 0.341 = 0.659 \quad .$$

The quality is

$$x = \frac{Q_B}{Wh_{fg}} = \frac{Q - Q_{NB}}{Wh_{fg}} = \frac{Q_r}{Wh_{fg}}\left(\frac{Q - Q_{NB}}{Q_r}\right)$$

$$= \frac{2.519 \times 10^6}{(72{,}716)(731.6)} (0.659) = 0.0312 \quad .$$

Thus, the void fraction in the element riser is

$$\alpha = \left[1 + \frac{1.50}{38.3} \times \frac{0.9688}{0.0312}\right]^{-1} = 0.451 \quad .$$

The density at the last point and in the element riser is

$$\rho = (1 - \alpha)\,\rho_f + \alpha\rho_g = 0.549 \times 49.75 + 0.451 \times 1.3$$

$$= 27.90 \quad .$$

The same type of calculation for other points along the boiling length yields the average boiling density

$$\bar{\rho}_B = 33.39 \quad .$$

The pressure differential in the elements are

$$\Delta P_{II} = a + b + c_1 - (V_0^2/2g)\left[N_2 + N_3 + N_{4_1} + N_6 + N_7 + N_8 + N_{9_1}\right] \quad ,$$

where V_0 is the velocity assumed for the iteration. The significances of the various terms are listed, and the calculation is illustrated, using the 7 ft/sec velocity at radius 10 cm for which the previous terms were calculated.

(1) Friction loss, in lb_m/ft^3, in nonboiling section of element

$$N_2 = f_C\,(L_{NB}/D_C)(\rho_f^2/\rho_{NB})$$

$$= (0.0146)\left(\frac{1 + 0.997}{0.0573}\right)\left(\frac{49.75^2}{50.00}\right)$$

$$= 25.20 \quad .$$

(Note: 1 foot of unheated element added to L_{NB}).

(2) Friction loss in boiling section of element

$$N_3 = f_C\bar{R}\,(L_B/D_C)\,\rho_f$$

$$= (0.0146)(2.04)\left(\frac{0.25 + 3.003}{0.0573}\right)(49.75)$$

$$= 84.11 \quad .$$

(Note: 0.25 ft of unheated element added to L_B).

(3) Friction loss in element portion of riser

$$N_{4_1} = f_{R_1} R_{R_1} (L_{R_1}/D_C) \rho_f$$

$$= (0.0146)(3.43)(0.75/0.0573)(49.75)$$

$$= 32.61 \quad .$$

(4) Acceleration from top of lower plenum into heated element

$$N_6 = \rho_f^2/\rho_D = 49.72^2/50.25 = 49.25 \quad .$$

(5) Acceleration in nonboiling region

$$N_7 = 2\rho_f(\bar{\rho}_D - \rho_f)/\bar{\rho}_D$$

$$= 2(49.75)(50.25 - 49.75)/50.25 = 0.99 \quad .$$

(6) Acceleration due to void formation

$$N_8 = 2\rho_f \left[\frac{(1-x)^2}{(1-\alpha)} + \frac{x^2}{\alpha}\frac{\rho_f}{\rho_g} - 1\right]$$

$$= 2(49.75)\left[\frac{(0.9688)^2}{0.549} + \frac{(0.0312)^2}{0.451}(38.3) - 1\right]$$

$$= 78.80 \quad .$$

(7) Expansion from element riser into nonhomogeneous riser

$$N_{9_1} = 2\rho_f \left(\frac{A_C}{A_{R_2}}\right)\left[x^2 \frac{\rho_f}{\rho_g}\left(\frac{A_C}{A_{R_2}\alpha_{R_2}} - \frac{A_C}{A_{R_i}\alpha_{R_1}}\right)\right.$$

$$\left. + (1-x)^2\left(\frac{A_C}{A_{R_2}(1-\alpha_{R_2})} - \frac{A_C}{A_{R_1}(1-\alpha_{R_1})}\right)\right]$$

$$= 2(49.75)\left(\frac{1.856}{4.00}\right)\left[(0.0312)^2 (38.3)\left(\frac{1.856}{4.00 \times 0.416} - \frac{1.856}{1.856 \times 0.451}\right)\right.$$

$$\left. + (0.9688)^2\left(\frac{1.856}{4.00 \times 0.584} - \frac{1.856}{1.856 \times 0.549}\right)\right] = -48.89 \quad .$$

(8) Hydrostatic head in nonboiling section

$$a = (\bar{\rho}_D - \bar{\rho}_{NB}) L_{NB}$$

$$= (50.25 - 50.00)(1 + 0.997) = 0.50 \text{ lb}_m/\text{ft}^2 \quad .$$

(9) Hydrostatic head in boiling section

$$b = (\bar{\rho}_D - \bar{\rho}_B) L_B$$

$$= (50.25 - 33.39)(0.25 + 3.003) = 54.85 \text{ lb}_m/\text{ft}^2 \quad .$$

(10) Hydrostatic head in element riser

$$c_1 = (\bar{\rho}_D - \rho_{R_1}) L_{R_1}$$

$$= (50.25 - 27.90)(0.75) = 16.76 \text{ lb}_m/\text{ft}^2 \quad .$$

The summation of the n terms is 222.07, so that

$$(V_0^2/2g) \Sigma N = (49.00/64.34)(222.07) = 169.12 \quad .$$

The total pressure differential through the element is

$$\Delta P_{II} = -97.01 \text{ lb}_f/\text{ft}^2 \quad .$$

Thus,

$$\Delta P_I - \Delta P_{II} = -110.70 + 97.01 = -13.69 \text{ lb}_f/\text{ft}^2 \quad .$$

The assumed velocity was, therefore, slightly low. Assuming $V_0 = 7.5$ ft/sec would yield $\Delta P_I - \Delta P_{II} = 0.98$. Plotting $\Delta P_I - \Delta P_{II}$ against V_0 for several iterations yields $V_0 = 7.47$ ft/sec at radius 10 cm.

This procedure is applied to the other core radii selected to obtain the following velocity profile:

Radius, cm	V_0, ft/sec
10	7.47
25	7.43
40	3.85
50	7.45
60	7.46
70	7.51

This velocity profile is plotted in Fig. 8.8.

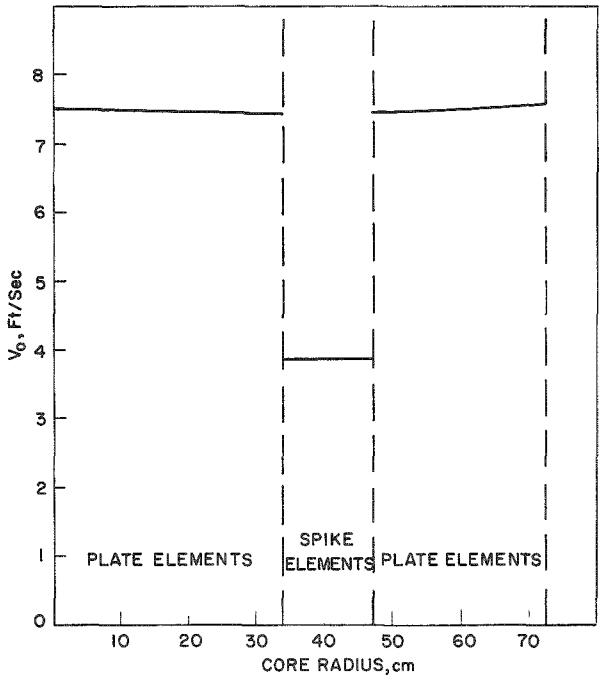

Fig. 8.8

EBWR 100-Mw Radial Velocity Profile

A more complicated velocity profile would require a graphical integration of the velocity over the core to obtain the average velocities of the regions. In this case, however, it is sufficient to estimate them from the plot. In the central region $\overline{V}$ = 7.44 ft/sec; in the spike region $\overline{V}$ = 3.85 ft/sec; and in the outer plate region $\overline{V}$ = 7.48 ft/sec. Thus, the flow rates for the core regions can be calculated as was done for the originally assumed velocity profile:

$$W_C = 2.473 \times 10^6 \text{ lb/hr}$$

$$W_A = 7.901 \times 10^6 \text{ lb/hr}$$

$$W_T = 1.0374 \times 10^6 \text{ lb/hr} \quad .$$

The quality for this flow is

$$x = (3.007 \times 10^5)/1.0374 \times 10^7 = 0.0290 \quad .$$

The subcooling is

$$h_{sub} = 459.9$$

or

$$\Delta h_{sub} = 11.7 \text{ Btu/lb} \quad .$$

Since the originally assumed velocity profile yielded a subcooling of Δh = 11.8 Btu/lb, the calculated velocity profile is quite accurate. Another velocity profile would need to be assumed and the calculation procedure repeated if the subcoolings did not agree.

9. REFERENCES

1. B. R. Mead, F. E. Romie, and A. G. Guibert, "Proceedings of Heat Transfer and Fluid Mechanics Institute," Stanford, California, p. 209 (1951).
2. W. M. Rohsenow, and J. A. Clark, "A Study of the Mechanism of Boiling Heat Transfer," Trans. ASME, 73, p. 609 (1951).
3. F. C. Gunther, "Photographic Study of Surface-Boiling Heat Transfer to Water with Forced Convection," Trans. ASME, 73, p. 115 (1951).
4. W. H. McAdams, "Heat Transmission," 3rd Edition (1954).
5. W. M. Rohsenow, "A Method of Correlating Heat-Transfer Data for Surface Boiling of Liquids," Trans. ASME 74, p. 969 (1952).
6. H. K. Forster, et al., "Dynamics of Vapor Bubbles and Boiling Heat Transfer," A.I.Ch.E. Journal, 1, p. 531 (1955).
7. A. S. Perkins and J. W. Westwater, "Measurement of Bubbles Formed in Boiling Methanol," A.I.Ch.E. Journal, 2, p. 471 (1956).
8. W. H. Jens and P. A. Lottes, "Analysis of Heat Transfer Burnout, Pressure Drop, Density Data for High Pressure Water," ANL-4627 (May 1, 1951).
9. J. F. Mumm, "Heat Transfer to Boiling Water Forced Through a Uniformly Heated Tube," ANL-5276 (November 1954).
10. L. A. Bromley, "Heat Transfer and Stable Film Boiling," Chemical Engineering Progress, 46, p. 221 (1950).
11. J. A. Robertson, et al., "Behavior of Uranium Dioxide as a Reactor Fuel," Proceedings of the Second United Nations International Conference on the Peaceful Uses of Atomic Energy, Geneva, 6, p. 655 (1958).
12. K. Berg, et al., "Thermal Conductivity of UO_2," Proceedings of the Second United Nations International Conference on the Peaceful Uses of Atomic Energy, Geneva, 7, p. 691 (1958).
13. R. C. Martinelli and D. B. Nelson, "Prediction of Pressure Drop during Forced-Circulation Boiling of Water," Trans. ASME, 78, p. 695-702 (1948).
14. C. E. Dengler, Sc.D. Thesis in Chemical Engineering, Massachusetts Institute of Technology (1952).
15. K. D. Eddy, M.S. Thesis, University of Minnesota (1954).
16. H. S. Isbin, R. H. Moen, and D. R. Mosher, "Two-phase Pressure Drops," AECU-2994 (November 1954).

17. H. S. Isbin, N. C. Sher, and K. C. Eddy, "Void Fraction in Two-phase Steam-Water Flow," A.I.Ch.E. Journal, 3, p. 136-142 (1957).

18. H. C. Larson, Ph.D. Thesis, University of Minnesota (1958).

19. P. A. Lottes, and W. S. Flinn, "A Method of Analysis of Natural Circulation Boiling Systems," Nuclear Science and Engineering (December 1956).

20. W. H. Cook, "Boiling Density in Vertical Rectangular Multichannel Sections with Natural Circulation," ANL-5621 (1956).

21. J. F. Marchaterre, "The Effect of Pressure on Boiling Density in Multiple Rectangular Channels," ANL-5522 (1956).

22. B. L. Richardson, "Some Problems in Horizontal Two-phase, Two-component Flow," ANL-5949 (December 1958).

23. T. A. Hughes, "Steam-Water Mixture Density Studies in a Natural Circulation High-pressure System," Babcock and Wilcox Company, Research Center, Alliance, Ohio, Report No. 4.

24. J. Asyee, Ph.D. Thesis, Technical University of Delft, Holland.

25. K. Schwartz, "Investigations of Density Distribution. Water and Steam Velocities. as Well as Pressure Loss in Vertical and Horizontal Flow up Boiler Tubes," VDK-Forschungsheft 445B, 1 (1954).

26. W. A. Gresham, P. A. Foster, and R. J. Kyle, "Review of the Literature on Two-phase (Gas-Liquid) Fluid Flow in Pipes," Interim Report No. 1 Project A-186, Engineering Experimental Station of the Georgia Institute of Technology (June 1955).

27. R. Masnovi, "Literature Survey of Two-phase Flow," University of Pittsburgh (May 1, 1957).

28. M. Petrick, and B. S. Swanson, "A Radiation-Attenuation Method of Measuring Density of Two-phase Fluid," Review of Scientific Instruments, 29, p. 1079 (1958).

29. H. H. Hooker and F. G. Popper, "A Gamma-ray-attenuation Method for Void Fraction Determination in Steam-Water Mixtures," ANL-5766 (November 1958).

30. M. Petrick, "Investigation of Two-phase Air-Water Flow Phenomena," ANL-5787 (1958).

31. R. A. Egen, D. A. Dingee, and J. W. Chastain, "Vapor Formation and Behavior in Boiling Heat Transfer," BMI-1163 (1957).

32. P. Griffith, J. A. Clark, and W. M. Rohsenow, "Void Volumes in Subcooled Boiling System," Paper No. 58-HT-19, Presented at the ASME-AIChE Joint Heat Transfer Conference, Chicago, Illinois (August 18-21, 1958).

33. D. G. Poletavkin, and N. A. Shapkin, "Teploenergetika," 5, No. 4, p. 54-58 (1958).

34. C. P. Costello, "Local Boiling Effects on Density and Pressure Drop," Technical Report No. 3, Nuclear Technology Laboratory, Stanford University (1960).

35. B. M. Hoglund, R. W. Weatherhead and T. R. Epperson, "Two-phase Pressure Drop in a Natural Circulation Boiling Channel," ANL-5760 (August 1961).

36. H. C. Sher, "Estimation of Boiling and Non-Boiling Pressure Drop in Rectangular Channels at 2000 psia," WAPD-TH-300 (March 1957).

37. J. A. Bennett, "Two-Phase Flow in Gas-Liquid Systems - A Literature Survey," AERE CE/R 2497 (1958).

38. D. A. Charvonia, "A Review of the Published Literature Pertaining to the Annular, Two-phase Flow of a Liquid and a Gaseous Medium in a Pipe," Purdue University Jet Propulsion Center, Report No. TM-58-1 (November 1958).

39. W. A. Gresham, P. A. Foster and R. J. Kyle, "Review of the Literature on Two-phase Gas-Liquid Fluid Flow in Pipes," W.A.D.C. Technical Report 55-422 (Part I) (June 1955).

40. W. Struiver, "Two-phase Fluid Flow Literature Review and Programme," Technical Note No. 89, Dominion Laboratory, Dept. of Scientific and Industrial Research, New Zealand (July 1955).

41. R. Jenkins, "Two-phase, Two-component Flow of Water and Air," M.S. Thesis, University of Delaware (September 1947).

42. L. F. Moody, "Friction Factor for Pipe Flow," Trans. ASME, 66, p. 671 (1944).

43. W. M. Kays, "Loss Coefficients for Abrupt Changes in Flow Cross Section with Low Reynolds Number Flow in Single and Multiple Tube Systems," Trans. ASME, 72, p. 1067 (1950).

44. E. N. Sieder, and G. E. Tate, "Heat Transfer and Pressure Drop of Liquids in Tubes," Industrial Engineering Chemistry, 28, p. 1429 (1936).

45. B. S. Petukhov, and G. E. Muchnik, Soviet Physics-Technical Physics, Vol. 2, No. 5, p. 996-1000, (a translation of the Journal of Technical Physics, 27, No. 5) (1957).

46. F. Kreith and M. Summerfield, "Heat Transfer to Water at High Flux Densities with and without Surface Boiling," Trans. ASME, 71, No. 7, p. 805 (1949).

47. R. G. Deissler, "Analysis of Turbulent Heat Transfer, Mass Transfer, and Friction in Smooth Tubes at High Prandtl and Schmidt Numbers" N.A.C.A. Report 1210 (1955).

48. J. B. Reynolds, "Local Boiling Pressure Drop," ANL-5178 (March 1954).

49. H. F. Buchberg, F. Romie, R. Lipkis, and M. Greenfield, Proceedings of the Heat Transfer and Fluid Mechanics Institute, Stanford, California (1951).

50. R. R. Rohde, Personal communication.

51. R. J. Weatherhead, "Reactor Engineering Division Quarterly Report, Section II, April 1-June 30, 1955," ANL-5471, p. 89-93 (1955).

52. G. E. Alves, "Concurrent Liquid-Gas Flow in a Pipe-line Contactor," Chemical Engineering Progress, 50, p. 449 (1954).

53. O. Baker, "The Design of Pipe Lines for the Simultaneous Flow of Oil and Gas," The Oil and Gas Journal, 53, p. 185 (1954).

54. C. J. Hoogendoorn, "Gas-Liquid Flow in Horizontal Pipes," Chemical Engineering Science, 9, p. 205-217 (1959).

55. L. Krasiakova, lu., Zhurnal Tekh Fiziki, 22, No. 4 p. 656 (1952).

56. B. K. Kozlov, "Forms of Flow of Gas-Liquid Mixtures and Their Stability Limits in Vertical Tubes," Zhurnal Tekh Fiziki, 24, No. 12 p. 2285-2288 (1954).

57. W. C. Galegar, W. B. Stovall and R. L. Huntington, "More Data on Two-phase Vertical Flow," Petroleum Refiner, 33, No. 11, p. 208-211 (1954).

58. J. W. Hoopes, "Flow of Steam-Water Mixtures in a Heated Annulus and Through Orifices," A.I.Ch.E. Journal, 3 p. 268-275 (1957).

59. P. A. Lottes, M. Petrick, and J. F. Marchaterre, "Lecture Notes on Heat Extraction from Boiling Water Power Reactors," ANL-6063 (October 1959).

60. W. H. Jens, and P. A. Lottes, "Two-phase Pressure Drop and Burnout Using Water Flowing in Round and Rectangular Channels," ANL-4915 (October 1952).

61. G. Leppert, M. Jakob, and J. B. Reynolds, "Pressure Drop During Forced Circulation Boiling," Chemical Engineering Progress Symposium Series, No. 18, 52, p. 29-36 (1956).

62. D. H. Weiss, "Pressure Drop in Two-phase Flow," ANL-4196 (October 1952).

63. R. C. Martinelli, L. M. K. Boelter, T. H. M. Taylor, E. G. Thomsen and E. H. Morrin, "Isothermal Pressure Drop for Two-phase, Two-component Flow in Horizontal Pipe," Trans. ASME, 66, 2, p. 139-151 (1944).

64. R. W. Lockhart and R. C. Martinelli, "Proposed Correlation of Data for Isothermal Two-phase, Two-component Flow in Pipes," Chemical Engineering Progress, 45, No. 1, p. 39-48 (January 1949).

65. W. F. Davidson, P. H. Hardie, C. G. Humphreys, A. A. Markson, A. R. Mumford and T. Ravese, "Studies of Heat Transmission Through Boiler Tubing at Pressures from 500-3000 Pounds," Trans. ASME, 65, p. 553 (1943).

66. S. Levy, "Steam Slip-Theoretical Prediction from Momentum Model," ASME Paper No. 59-HT-15, Third National Heat Transfer Conference, August 9-12, 1959, Storrs, Connecticut.

67. V. E. Schrock and L. M. Grossman, "Local Pressure Gradients in Forced Convection Vaporization," Nuclear Science and Engineering, 4, No. 3, p. 245-250 (1959).

68. R. P. Stein, J. W. Hoopes, M. Markels, W. A. Selke, A. J. Bendler and C. F. Bonilla, "Pressure Drop and Heat Transfer to Nonboiling and Boiling Water in Turbulent Flow in an Internally Heated Annulus," Chemical Engineering Symposium Series No. 11, 50, p. 115-126 (1954).

69. S. G. Bankoff, "A Variable-Density Single-Fluid Model for Two-phase Flow with Particular Reference to Steam-Water Flow," ASME Paper No. 59-HT-7, Third National Heat Transfer Conference, Storrs, Connecticut, August 9-12, 1959.

70. J. C. Westmoreland, "Prediction of the Pressure Loss and Density Factors for Two-phase Annular Flow with or without Heat Generation," KAPL-1792 (Feb. 1, 1957).

71. R. J. Weatherhead, Personal communication.

72. R. H. Moen, "Pressure Drop in Two-phase Flow," Ph.D. Thesis, Department of Chemical Engineering, University of Minnesota (August 1956).

73. S. I. Kosterin, "An Investigation of the Influence of Diameter and the Altitude of a Pipe on the Hydraulic Resistances and on the Structure of Flow of a Gas-Liquid Mixture," Izvestiia-Akademiia Nauk, SSRR-Otdelenie, 1864 (July-December 1949).

74. G. W. Govier, B. A. Radford, and J. S. C. Dunn, "The Upwards Vertical Flow of Air Water Mixtures - Pt. I " The Canadian Journal of Chemical Engineering, p. 58-70 (August, 1957).

75. G. W. Govier, and W. L. Short, "The Upward Vertical Flow of Air-Water Mixtures Pt. II," The Canadian Journal of Chemical Engineering p. 195-202 (October 1958).

76. H. A. Johnson and A. H. Abou-Sabe, "Heat Transfer and Pressure Drop for Turbulent Flow in Air-Water Mixtures in a Horizontal Pipe," Trans. ASME, 74, 977 (1952).

77. Sakae Yaki and Yasuo Kato, "Fundamental Studies on Horizontal Pipe Reactor, (1) Flow Patterns and Pressure Drops of Gas-Liquid Mixture Through Horizontal Pipes," Chemical Engineering (Japan), 18, p. 2-15 (1954).

78. Sakae Yaki and Teiji Sasaki, "Studies on Vertical Pipe Reactor, (II) Flow Pattern, Hold-up and Pressure Drop in Gas-Liquid Two-phase Flow Through Vertical Pipes," Chemical Engineering (Japan) 17, p. 216-223 (1953).

79. A. E. Duckler, "An Investigation of Pressure Drop for Isothermal Two-phase Film Flow in a Vertical Tube," M.S. Thesis, University of Delaware (1949).

80. D. Chisholm, and A. D. K. Laird, "Two-phase Flow in Rough Tubes," ASME Paper No. 57-SA-11, Semi-Annual Meeting, San Francisco, California (June 1957).

81. J. M. Chenoweth and M. W. Martin, "Turbulent Two-phase Flow," Petroleum Refiner, 34, No. 10, p. 151-155 (October 1955).

82. G. W. Lester, "Correlation of Two-phase Pressure Drop Measurements for Steam-Water Mixtures in a 4.06 in. Diameter and a 6.06 in. Diameter Horizontal Pipeline," AERE CE/M 217 (1958).

83. A. F. Betuzzi, M. R. Tek and F. H. Poettman, "Simultaneous Flow of Liquid and Gas Through Horizontal Pipe," Journal of Petroleum Technology (January 1956).

84. E. A. Kazakova, "The Influence of Pressure on the First Crisis in Boiling Water from a Horizontal Surface," published in "Problems of Heat Transfer with a Change of Phase," G.E.I., Moscow (1953).

85. N. Zuber and M. Tribus, "Further Remarks on the Stability of Boiling Heat Transfer," AECU-3631 (1958).

86. Y. P. Chang, "A Theoretical Analysis of Heat Transfer in Turbulent Convection," AECU-3551 (1956).

87. P. Griffith, "The Correlation of Nucleate Boiling Burnout Data," ASME Paper No. 57-HT-21 (1957).

88. S. J. Green, et al., "Forced-Convection Heat Transfer Burnout Studies for Water in Rectangular Channels and Round Tubes at Pressures Above 500 psia," WAPD-188 (October 1958).

89. M. Silvestri, et al., "A Critical Survey of the Literature on Burnout Studies with Wet Steam," Energia Nucleare, 6, 637-660 (1959).

90. G. Sonneman, "Correlation of Burnout Data," WAPD-TH-160 (1956).

91. D. W. Bell, "Correlation of Burnout Heat Flux Data at 2000 psia," Presented at ANS (June 1959).

92. R. G. Vanderwater, "An Analysis of Burnout in Two-phase, Liquid-Vapor Flow" PhD. Thesis, University of Minnesota (1956).

93. S. P. Singh, "Burnout in Steam-Water Flow at 2000 psia," Ph.D. Thesis, University of Minnesota (1958).

94. H. K. Fauske, "Analysis of Burnout in Two-phase Flow," Ph.D. Thesis, University of Minnesota (1959).

95. S. Levy and E. S. Beckjord, "Hydraulic Instability in a Natural Circulation Loop with Net Steam Generation at 1000 psia," GEAP-3215 (1959).

96. W. H. Lowdermilk, "Boiling Burnout with Stable Flow in Tubes," Presented at Working Session of National Heat Transfer Conference, Chicago (1958).

97. W. H. Lowdermilk, "Investigation of Boiling Burnout and Flow Stability for Water Flowing in Tubes," NACA-TN-4382 (1958).

98. J. R. Dietrich and D. C. Layman, "Transient and Steady State Characteristics of a Boiling Reactor, The BORAX experiments, 1953," ANL-5211 (February, 1954).

99. Argonne Staff, "Experimental Investigation of the Self-Limitation of Power During Reactivity Transients in a Subcooled Water-Moderated Reactor," ANL-5323 (1954).

100. J. R. Dietrich, "Experimental Determinations of the Self-Regulation and Safety of Operating Water-Moderated Reactor," P/481, First International Conference on Peaceful Uses of Atomic Energy, Geneva (1955).

101. S. G. Forbes, F. Schroeder, and W. Nyer, "Instability in the SPERT-I Reactor, Preliminary Report," IDO-16309 (October 1956).

102. B. Maxon, O. Schulze, J. Thie, "Reactivity Transients and Steady State Operation of a Thoria-Urania Fueled Boiling Reactor (BORAX IV)," ANL-5733 (1958).

103. O. A. Schulze, "BORAX IV: Preliminary Report on the Present Series of Experiments with Oxide Fuels," TID-7535 (May 1957).

104. W. E. Nyer, et al., "Experimental Investigations of Reactor Transient," IDO-16285 (April 1956).

105. T. R. Wilson, "An Engineering Description of the SPERT-I Research Facility," IDO-16318 (June 1957).

106. W. E. Nyer and S. G. Forbes, "SPERT Program Review," IDO-16415 (September 1957).

107. F. Schroeder, "Stability Tests with the SPERT-I Reactor," IDO-16383 (July 1957).

108. J. A. DeShong, Jr., "Power Transfer Functions of EBWR Obtained Using a Sinusoidal Reactivity Driving Function," ANL-5798 (December 1957).

109. J. M. Harrer, et al., "Performance Evaluation of Direct Cycle Boiling Water Nuclear Power Plants Based on Recent EBWR and BORAX Data," P/2379, Second International Conference on Peaceful Uses of Atomic Energy, Geneva, 9, 264 (1958).

110. E. Beckjord, et al., "Operation of a High Performance Light Water Boiling Reactor", P/1923, Second International Conference on Peaceful Uses of Atomic Energy, Geneva 9, 455 (1958).

111. A. J. Ulrich, "Results of Recent Analysis of BORAX-II Transient Experiments," ANL-5532 (April 1956).

112. H. C. Corben et al., "Theory of Power Transients in the SPERT-I Reactor," IDO-16434 (January 1958).

113. E. S. Beckjord, "Dynamic Analysis of Natural Circulation Boiling Water Power Reactors," ANL-5799 (March 1958).

114. J. A. DeShong, Jr., and W. C. Lipinski, "Analysis of Experimental Power-Reactivity Feedback Transfer Functions for a Natural Circulation Boiling Reactor," ANL-5850 (July 1958).

115. J. A. Thie, "Theoretical Reactor Statics and Kinetics of Boiling Reactors," P/638, Second International Conference on Peaceful Uses of Atomic Energy, Geneva, 11, 440 (1958).

116. R. Viskanta, Personal communication.

117. G. Rezek, Personal communication.

118. E. H. Wissler, H. S. Isbin, and N. R. Amundson, "The Oscillatory Behavior of a Two-Phase Natural Circulation Loop," AICHE Preprint No. 59 (1955).

119. E. H. Wissler, "The Transient Behavior of a Two-Phase Natural Convection Loop," PhD Thesis, University of Minnesota (June 1958).

120. E. R. Quandt, "The Analysis and Experimental Measurement of Parallel Channel Flow Oscillations," WAPD-T-1004.

121. W. P. Ball, D. B. Langmuir, and R. W. Wright, "X-Ray Measurement of Time Varying Steam Void Fraction in a Thin Water Channel," RW-RL-137.

122. E. R. Quandt, "Analysis of Parallel Channel Transient Response and Flow Oscillations," WAPD-AD-TH-489 (April 1959).

123. B. Hoglund, Personal communication.

124. M. Ledinegg, "Unstabiltat der Stomong bei Naturlichem und Zwangsumlauf, Die Warme," p. 891-898 (1938).

125. W. K. Woods, "Qualitative Analysis of Pressure Drop During In-Pile Boiling," HW-31157 (March 1954).

126. H. Chilton, "A Theoretical Study of Stability in Water Flow Through Heated Passages," J. Nuclear Energy, 5 (1957).

127. J. Asyee, "Summary of an Experimental Investigation on the Heat-Removal of the First Fuel-Charge of the HBWR," Halden Internal Report HIR-11 (May 1959).

128. C. D. Alstad, H. S. Isbin, and N. R. Amundson, "The Transient Behavior of Single Phase Natural Circulation Water Loop Systems," ANL-5409 (1956).

129. S. Levy, "Preliminary Predictions of Flow Pattern Instability in Two-Phase Flow," GEAP-3126 (1959).

130. S. Levy, "Steamslip-Theoretical Prediction from Momentum Model," ASME Paper No. 59-HT-15.

131. H. S. Isbin, J. E. Moy and A. J. R. DaCruz, "Two-Phase Steam Water Critical Flow," A.I.Ch.E. Journal, 3, No. 3, p. 361-365 (September 1957).

132. P. A. Lottes, et al., "Experimental Studies of Natural Circulation Boiling and Their Application to Boiling Reactor Performance," P/1983, Second International Conference on Peaceful Uses of Atomic Energy, Geneva, 7, 784 (1958).

133. R. P. Stein, "Flow Instability Burnout in a Simulated Reactor Fuel Channel" Presented during Hydrodynamic Instability and Two-phase Pressure Drop Session of Natural Heat Transfer Conference, Storrs, Connecticut (August 1959).

134. P. Behringer, "Velocity in Rise of Steam Bubbles in Boiler Tubes," Verein deutscher Inginieure Forschungsheft, 4 (1934).

135. P. C. Zmola, R. V. Bailey, et al., "Transport of Gases Through Liquid-Gas Mixture," Tulane University and Oak Ridge National Laboratory, unpublished.

10. NOMENCLATURE

Section					Description
2	3	4	7	8	
A					Area, ft^2
				$A_{coolant}$	Total cross-sectional area of coolant
			A_p		Area of Pipe
		B(subscript)			Bulk
				B^2	Buckling
C_p					Specific heat of liquid, BTU/lb °F
		C_p			Specific heat, BTU/lb °F
C_{sf}					Coefficient in Eq. (2.3)
			D		Equivalent Diameter
D					Pipe Diameter
		D-B (subscript)			Based on Dittus - Boelter heat transfer equation
				D_c	Core diameter (Feet or inches?)
D_e		D_e			Equivalent diameter, ft
				D_e	Mean equivalent diameter of flow channel
D_0					Outer diameter, ft
				D_r	Diameter of fuel rod (Inches?)
		F(subscript)			Friction
			F_{fg}		Force expended by gas phase in overcoming friction
			F_{fl}		Force expended by liquid phase in overcoming friction
			F_y		Force of the y'th variety
			G		Mass flow rate
G					Mass flow rate, $lb_m/hr\ ft^2$
	G				Mass flow rate, lb mixture/hr ft^2
		G			Mass velocity, lb/ft^2-sec
		H(subscript)			Hydrostatic
		Heat(subscript)			Heating
		K			Expansion or contraction loss coefficient, dimensionless
			K_c		Contraction coefficient
			K_E		Expansion coefficient
		K_m			Momentum correction factor, dimensionless
L	L	L			Length, feet
				L*	Diffusion length
			L		Length
	L_B			L_B	Boiling length
		LB(subscript)			Local boiling
				L_c	Core height or length
	L_{NB}			L_{NB}	Non-boiling length

NOTE: Sections 1, 5, and 6 are self explanatory.

Section					Description
2	3	4	7	8	
		LO (subscript)			Based on liquid phase at total mixture flow rate
		GO (subscript)			Based on gas phase at total mixture flow rate
	L_t				Total length
				L_T	Total heated length
				M/F	Volumetric ratio of moderator to fuel
				N	Slope of plot of slip ratio vs water velocity
	Nu				Nusselt number
	P	P			Pressure, psia
			P		Pressure
P					Pressure, lb_f/ft^2
				P_R	Total reactor power
	Pr	PR	Pr		Prandtl number
				P.D.$_{kw/l}$	Power density in kw/liter
				Q	Power
				Q_{avg}	Average power per fuel element
	Q_B			Q_B	Heat input to boiling section
				Q_{NB}	Heat input to non-boiling section
				Q_r	Power of fuel element at radius r
	Q_t			Q_t	Total heat input
				$R, \overline{R}$	Two-phase friction factor multipliers
		R			Ratio of two-phase frictional pressure gradient to liquid phase frictionless pressure gradient, based on total mixture flow rate, dimensionless
				$R_{max/avg}$	Ratio of maximum to average heat flux in core
	R_e	R_E	Re		Reynolds number
		R_q			Ratio of actual heat flux to heat flux required to induce local boiling just at the channel exit, dimensionless
				S/F	Volumetric ratio of structure (fuel cladding, control rods, superstructure, etc.) to fuel
T		T	T		Temperature, °F
				$T_{\mathbb{C}max}$	Maximum fuel rod centerline temperature in core
		TPF (subscript)			Two-phase friction
				T_{sat}	Saturation temperature
			T_w		Wall temperature
				V	Recirculation velocity
			V		Velocity ft/sec
				$\overline{V}$	Average velocity
	V_f				Water velocity, ft/sec
	V_g		V_g		Steam or gas velocity, ft/sec

Section					Description
2	3	4	7	8	
				V_g/V_l	Slip ratio
			V_ℓ		Velocity of liquid phase
	V_0				Superficial velocity (defined as G/ρ_f) ft/sec
				$\overline{V_0}$	Average velocity of elements feeding a given external riser
				V_r	Axial flow velocity at radius r
				W	Fluid flow rate
				W_A	Annular fluid flow
				W_c	Central fluid flow
			W_g		Weight flow of gas
			W_ℓ		Weight flow of liquid
				W_m	Flow rate of makeup water
				W_s	Total steam flow
				W_{s_A}	Steam flow rate to outer annular region
				W_{s_c}	Total steam flow to control non-homogeneous riser
				W_T	Total recirculation flow rate
				X	Mixture quality
a					Coefficient in Eq. (2.25), BTU/hr ft F
		acc(subscript)			Acceleration
b					Coefficient in Eq. (2.25), BTU/hr ft F^2
	e (subscript)				Base of natural logarithm
		e(subscript)			Exit
		f	f		Moody friction factor
			F		Fanning friction factor, dimensionless
				f	Thermal utilization
		f(subscript)			Saturated liquid
				$f_1 f_2$	Arbitrary functions
g					Acceleration of gravity, 4.17 (10^8) ft/hr^2
		g(subscript)			Gas; saturated vapor
			g		Acceleration of gravity
g_c					Conversion factor, 4.17 (10^8) lb_m ft/hr^2 lb
h		h			Turbulent convective heat transfer coefficient, BTU/hr - ft^2 - °F
			h		Enthalpy
				h_B	Boiling heat transfer coefficient
h_b					Boiling coefficient, BTU/hr ft^2 F
				h_c	Contact resistance between cladding and fuel
h_c					Condensing coefficient, BTU/ hr ft^2 F
				h_f	Enthalpy of saturated liquid

Section					Description
2	3	4	7	8	
h_{fg}				h_{fg}	Latent heat of vaporization, BTU/lb
				h_g	Enthalpy of saturated vapor
				h_i	Enthalpy of water at inlet to the core
				h_{in}	Enthalpy of inlet water
				h_M, h_m	Enthalpy of makeup water
		in(subscript)			Inlet
		iso(subscript))			Isothermal
k			k		Thermal conductivity, BTU/hr ft F
				k_c	Thermal conductivity of cladding
				k_{eff}	Effective multiplication factor
k_f					Thermal conductivity of liquid, BTU/hr ft F
k_V					Thermal conductivity of vapor, BTU/hr ft F
				$\overline{k}_R$	Estimated mean heat conductivity of fuel rod
				k_1, k_2	Arbitrary constants
			m		Mass
		m			Superficial mass velocity, Kg/m^2-sec
				n	Number of fuel rods in core
				p	Resonance escape probability
p_1					Vapor pressure at saturation lb_f/ft^2
p_v					Vapor pressure at maximum superheat, lb_f/ft^2
q			q	q	Power, BTU/hr
q"		q"	q"	q"	Heat flux, BTU/hr ft^2
q'''					Power density, BTU/hr ft^3
				q''_c	Average heat flux in core
r				r	Radius, ft
			r		Acceleration multiplier of Martinelli and Nelson
		sub(subscript)			Subcooling
		t(subscript)			Total
			t		Time
t					Temperature
				t_c	Cladding thickness
vf(subscripts)					Specific volume of fluid, ft^3/lb
v_{fg}					Specific volume of vaporization, ft^3/lb
		w(subscript)			Wall
x					Wall thickness, ft
	x				Quality, lb steam/lb mixture
		x			Ratio of gas flow rate to total flow rate, dimensionless
				x_A	Quality in outer riser

Section					Description
2	3	4	7	8	
	x_c				Quality at inception of local boiling
				x_c	Quality in central riser
			x_e	x_e	Quality at exit
				$\overline{x_e}$	Average exit mixture quality
	x_{tt}	x_{tt}			Parameter of Martinelli
	α	α	α	α	Steam volume fraction; void fraction
		α_e		α_e	Exit steam volume fraction
		ΔP		ΔP	Pressure differential
				ΔP_I	Total pressure differential through risers and downcomers
				ΔP_{II}	Pressure differential in fuel elements
ΔT, T_x, $T_w - T_{sat}$					Heating surface temperature minus saturation temperature, °F
		$(\Delta T_{sub})_o$			Subcooling at point where local boiling starts, °F
	ΔT_{sat}				Wall superheat, $T_{wall} - T_{saturation}$
					Fast fission factor
		ϵ/D			Roughness ratio, dimensionless
θ					Angle
		ΔT			Temperature difference, °F
μ					Viscosity, lb_m ft-hr
		μ			Viscosity, lb ft-sec
μ_f					Viscosity of liquid, lb_m/ft-hr
ρ		ρ	ρ	ρ	Density, lb_m ft^3
				ρ_B	Average boiling density
				ρ_D	Density in downcomer
				ρ_f	Density of saturated liquid
	ρ_f				Density of liquid, lb ft^3
	ρ_g			ρ_g	Density of gas, lb/ft^3
				ρ_s	Density of saturated liquid
				ρ_{NB}	Average density in non-boiling section
				ρ_{R_i}	Two-phase density mixture; local riser density
σ					Surface tension of liquid-vapor interface, lb_f/ft
				τ	Fermi Age
			τ_w		Shear stress
		ϕ_{Ltt}			Square root of the ratio of the two-phase frictional pressure gradient if the liquid alone were flowing in the pipe, dimensionless
		ϕ^2_{Lo}			Ratio of two-phase frictional pressure gradient to liquid phase frictional pressure gradient, based on the total mixture flow rate, dimensionless (same as "D" R)